Effective Hamiltonians beyond the Leading Order and their Applications

Thesis presented by

Laura Reina

for the degree of Doctor Philosophiae

supervisor: Prof. G. Martinelli

S.I.S.S.A. – I.S.A.S.

Elementary Particle Sector

academic year 1991 - 92

October 12, 1992

to H.

Contents

Introduction

Quark mixing and CP-violation are two important subjects of the Standard Model physics and might suggest the presence of new physics beyond it. Among the reasons which might justify the interest in the physics of CP-violation and flavour mixing, the possibility to probe the perturbative and non-perturbative theoretical consistence of the model and to investigate the physics of heavy flavours are maybe the most important ones.

At higher order in perturbation theory strong and electro-weak interactions are present both at short and at long distances. Many physical quantities can be theoretically computed and experimentally measured with great accuracy, testing the reliability of the whole theory to a great extent. On the other hand, more precise theoretical predictions will permit the determination of a larger number of the unknown parameters of the Standard Model. The physics of CP-violation and quark-mixing, in particular, is related the top quark physics. In absence of a direct determination of its mass and couplings, we have here a real possibility for their indirect determination. Indeed, even though absent at the typical scale of weak decays, heavy flavours can be present in loops as virtual corrections, i.e. when higher orders in the perturbative calculation of given physical quantities are considered. Radiative corrections are generally suppressed by powers of the strong or electro-magnetic coupling constant. Nevertheless, heavy quarks as the top quark, can give relevant contributions, because large logarithms of their mass are present in the renormalization procedure.

K-meson and B-meson systems are the natural framework where the physics of quark mixing and CP-violation is studied. Flavour-mixing and CP-violating weak decays are described by Effective Hamiltonians of the form:

$$\mathcal{H}_{eff} = \sum_i C_i(\mu) O_i(\mu)$$

where the product of currents present in the true hamiltonian is expanded through the OPE (Operator Product Expansion), at a scale μ, as a sum over a given set of operators $\{O_i(\mu)\}$ with suitable Wilson coefficients $\{C_i(\mu)\}$. The short and long distance parts of the problem factorize into the Wilson coefficients and the operators respectively. In the evaluation of physical amplitudes, the Wilson coefficients are treated perturbatively, while the matrix elements of the effective operators $\{O_i\}$ are derived with non-perturbative techniques. In this thesis we will focus on the perturbative part of the problem only. On the non-perturbative side, we will only use, when necessary,

the main results coming from lattice calculations . In the final numerical analysis, in particular, we will use lattice results, which have already reached a level of reliability such as to be useful for physical applications.

The previous Effective Hamiltonian can be computed at scale $\mu \simeq m_b$ (for B-meson physics) or $\mu \simeq m_s$ (for K-meson physics) using the standard RG (Renormalization Group) techniques. The Wilson coefficient evolution obeys a particular RGE (Renormalization Group Equation), derived from the scale-independence of the global Effective Hamiltonian. The solution of the RGE for the Wilson coefficients can be given in different approximations in perturbation theory: LLA (Leading Logarithms Approximation), NLO (Next-to-Leading Logarithms Approximation), etc. There are several reasons which require the calculation of the NLO solution for a given Effective Hamiltonian. Besides the more general ones (consistent utilization of Λ_{QCD} in different contexts; justification of the "running" values of the quark masses used at different scales, etc.), the real point is that heavy flavour-dependence is strictly speaking a NLO effect as we will explain in great detail in Chapt.2. In the case of Effective Hamiltonians for K- and B-physics the implementation of the RG formalism gives rise to a strong m_t-dependence, which would not be present in the LLA form of the hamiltonian.

In the framework of K- and B-physics, two main classes of weak processes are studied with respect to flavour-mixing and CP-violation:

- $\Delta F = 2$ mixing $\longrightarrow$ indirect CP-violation,
- $\Delta F = 1$ decays $\longrightarrow$ direct CP-violation,

where F denotes either b- or s-flavour. The Effective Hamiltonian for $\Delta F = 2$ mixing processes involves four-quark vertex operators only (see fig.(2.1). It has been studied first in the LLA for small and large values of the top mass and finally determined up to NLO for large values of the top mass [15]. The two loop anomalous dimension matrix was originally computed in [5] in the DRED (Dimensional Reduction) regularization scheme and subsequently reproduced in ref. [13] in the NDR (Naive Dimensional Reduction) and HV (t'Hooft-Veltman) schemes. It belongs as to say to the "*past*" of perturbative calculation in the field of CP-violation and flavour mixing. The NLO knowledge of $\mathcal{H}_{eff}^{\Delta F=2}$ allows a good theoretical determination of the ϵ and of the x_d mixing parameters for neutral K- and neutral B-system respectively.

On the other hand, direct CP-violation in weak non-leptonic decays of K- and B-meson is governed by the $\Delta F = 1$ Effective Hamiltonian. The LLA evolution of the $\Delta F = 1$ Effective Hamiltonian have been studied both in presence of QCD corrections only and in presence of QCD+QED corrections [30, 24, 41]. The renormalization procedure involves here a much larger number of operators, listed in (1.45). Below the m_t-threshold for $\Delta B = 1$-decays or below the m_c-thresholds for $\Delta S = 1$-decays, due to the failure of GIM mechanism new operators arises besides the usual four-quark ones. They are the so called "Penguin"-operators corresponding to diagrams as the one in fig.(1.7) or (2.2), with a gluon (QCD-penguins) or a photon (QED-penguins) running in the wavy line. Penguin operators present some striking features:

- they are one-loop effective operators which are in principle suppressed by a power of the coupling constant. Nevertheless their matrix elements might be large and their contribution to some physical quantities is determinant;
- they have a strong m_t-dependence;
- they are greatly influenced by QED corrections [10, 24, 41], because the matrix elements of QED-penguin operator are greatly enhanced with respect to the QCD-penguin ones.
- their evolution is strongly modified by NLO corrections.

In the present thesis the evolution of the $\Delta F = 1$ Effective Hamiltonian is computed at the NLO in QCD corrections and at LO in the QED ones. We have studied the vertex+penguin two-loop renormalization mixing and computed the two-loop anomalous dimension matrix. This can be called the "*present*" of perturbative calculations in the physics of CP-violation and flavour-mixing. A complete calculation is still missing in literature, while in ref. [16] the pure QCD case was treated. The present calculation add a very important piece of knowledge to the theoretical description of K- and B-meson physics and we believe that many interesting phenomenological implementation will be possible. At the same time, it would be extremely important to have a clear theoretical picture of the problem, whenever the non-perturbative techniques were improved.

The thesis consists of four chapters. Chapt.1 summarizes the physics of flavour mixing and CP-violation in the three generation Standard Model. General comments are made about the indirect determination of the unknown top parameters. The discussion is finally restricted to K- and B-systems. Next, the detailed calculation of the NLO evolution of the Effective Hamiltonian for $\Delta F = 1$ weak decays is given in Chapt.2 and Chapt.3. First the general formalism for the NLO evolution of the Wilson coefficients in presence of QCD and QED corrections is derived. Then we discuss initial conditions for the evolution of the coefficient functions, the origin and the dynamics of operator mixing and the final results for the anomalous dimension matrix. The analytic aspects of the calculation are given in Chapt.3, where we will describe the most important techniques and the results. Chapt.4 is devoted to numerical applications of the analytic results, with an outlook to the possible future implementation in the physics of CP-violation and flavour mixing.

Chapter 1

Quark-mixing, CP-violation and the unknown parameters of the Standard Model

1.1 Introduction

In this chapter the main aspects of quark-mixing and CP-violation in the three generation Standard Model (SM) will be summarized. This sector of the SM physics is extremely important for the determination of some unknown parameters of the SM itself.

Quark-mixing is an extremely wide subject and I will not be exhaustive about. I will introduce and discuss only those aspects which are the background for the work that will be developed and detailed in the following chapters.

A part from the Higgs sector, some important and still unknown parameters of the SM are related to the physics of the top quark, mainly its mass (m_t) and couplings. For the obvious reason that the top quark has not been discovered yet, a direct determination of both its mass and couplings is not available. However, the Effective Hamiltonian (EH) formalism gives us the opportunity to derive "indirect" estimates and bounds of the still missing parameters. It is the physics of K- and B-mesons (mainly their CP-violating weak decays) which plays a fundamental role in this respect. On the other hand, when the top will be discovered in present or future experiments, the same physics would become an important test of the SM itself.

In Section 1.2 quark-mixing and CP-violation in the three generation SM are briefly summarized and related to specific K- and B-processes. Sections 1.3 and 1.4 will give some more details about K- and of B-physics.

Some general comments are in order at this point.

- m_t

  In K- or B-meson weak decays, physical amplitudes have no explicit m_t-dependence at the tree level. At high energy scales (above the top threshold), the top quark appears in loops and its contribution is very important in CP-violating decays.

  Let us briefly explain why the top contribution becomes so relevant. The top is active only at very large scales, while a generic weak decay usually involves much lower scales. At low scales the physics of a given weak process is described by Effective Hamiltonians (EH) of the form:

$$\mathcal{H}_{eff} = \sum_i C_i(\mu) O_i(\mu) \tag{1.1}$$

  where $\{O_i(\mu)\}$ is a given set of local operators and $\{C_i(\mu)\}$ the corresponding set of Wilson coefficients in the Operator Product Expansion (OPE) evaluated at scale μ. Below the M_W threshold[1], the top quark is integrated out and we would not expect any dependence on its mass anymore. On the contrary, a strong m_t-dependence appears in the initial conditions for the evolution of the coefficient functions.

  The coefficients $C_i(\mu)$ can be computed perturbatively and their evolution from a scale of order $O(M_W)$ (where perturbation theory applies) to the low energy scale μ is given by the solution of the Renormalization Group (RG) equations. The m_t-dependence arises as a loop effect (when the top quark is present in loops) in the evaluation of the initial conditions for the evolution of the coefficients from M_W to μ. We may write that:

$$\vec{C}(\mu) = \vec{C}(M_W, m_t, M_X)\hat{U}(M_W, \mu) \tag{1.2}$$

  where M_W, m_t and M_X are the heaviest masses in the theory[2] (X being a generic heavy particle, f.i. a physical Higgs in some extension of the SM, etc.), and $\hat{U}(M_W, \mu)$ the evolution matrix from M_W to μ scales.

  The m_t-dependence of $\vec{C}(M_W)$ should be computed referring to a particular weak process. A large number of virtual processes have been computed and the m_t-dependence of their Effective Hamiltonians is known. They allow to fix the correct m_t-dependence of the initial conditions for different weak processes in terms of some basic analytic functions. We list in table (1.1) some weak decays and mixings (for K- and B-mesons) together with the basic functions which have been introduced to describe them. The main processes have been originally computed by Inami and Lim [34] and successively updated by Flynn and Randall [24]. Very recently a complete analysis appeared in a paper by Buras et al.

[1] To simplify we assume $M_W \simeq m_t$. We will comment on that later on.

[2] Again we will assume $M_X \simeq M_W$, as for the top mass.

[14, 16], where the small-m_t and large-m_t behaviour, the gauge-dependence and the scaling properties of the functions given in Table (1.1) are studied. The initial conditions for the Coefficient Function in (1.2) are computed in terms of the updated set of these so called "Inami-Lim functions". Here following we give their explicit m_t dependence:

$$
\begin{aligned}
S(x_t) &= x_t\left[\frac{1}{4}+\frac{9}{4}\frac{1}{(1-x_t)}-\frac{3}{2}\frac{1}{(1-x_t)^2}\right]+\frac{3}{2}\left[\frac{x_t}{x_t-1}\right]^3\ln x_t \\
B(x_t) &= \frac{1}{4}\left[\frac{x_t}{1-x_t}+\frac{x_t\ln x_t}{(x_t-1)^2}\right] \\
C(x_t) &= \frac{x_t}{8}\left[\frac{x_t-6}{x_t-1}+\frac{3x_t+2}{(x_t-1)^2}\right] \\
D(x_t) &= -\frac{4}{9}\ln x_t+\frac{-19x_t^3+25x_t^2}{36(x_t-1)^3}+\frac{x_t^2(5x_t^2-2x_t-6)}{18(x_t-1)^4}\ln x_t \\
D'(x_t) &= -\frac{(8x_t^3+5x_t^2-7x_t)}{12(1-x_t)^4}\ln x_t+\frac{x_t^2(2-3x_t)}{2(1-x_t)^4}\ln x_t \\
E(x_t) &= -\frac{2}{3}\ln x_t+\frac{x_t^2(15-16x_t+4x_t^2)}{6(1-x_t)^4}\ln x_t+\frac{x_t(18-11x_t-x_t^2)}{12(1-x_t)^3} \\
E'(x_t) &= -\frac{x_t(x_t^2-5x_t-2)}{4(1-x_t)^3}+\frac{3}{2}\frac{x_t^2}{(1-x_t)^4}\ln x_t \\
X(x_t) &= \frac{x_t}{8}\left[\frac{x_t+2}{x_t-1}+\frac{3x_t-6}{(1-x_t)^2}\ln x_t\right] \\
Y(x_t) &= \frac{x_t}{8}\left[\frac{x_t-4}{x_t-1}+\frac{3x_t}{(x_t-1)^2}\ln x_t\right] \\
Z(x_t) &= -\frac{1}{9}\ln x_t+\frac{18x_t^4-163x_t^3+259x_t^2-108x_t}{144(x_t-1)^3} \\
&\quad +\frac{32x_t^4-38x_t^3-15x_t^2+18x_t}{72(x_t-1)^4}\ln x_t
\end{aligned}
\tag{1.3}
$$

where $x_t = m_t^2/M_W^2$. For future discussions, it is important to give the large-x_t behaviour of the basic functions in (1.3):

$$
\begin{aligned}
&S(x_t)\,, C(x_t) \propto x_t\ ,\ \ D(x_t)\propto \ln x_t\ , \\
&B(x_t)\,, E(x_t)\,, D'(x_t)\,, E'(x_t) \propto \text{const}
\end{aligned}
\tag{1.4}
$$

A power-like or logarithmic dependence on a large m_t may have important consequences in the SM predictions for many weak processes. Appearing as a loop-effect in the initial conditions for the evolution of the coefficient function, it could in principle justify by itself a NLO calculation.

- *Top quark couplings*

  In the SM with three generations, the Cabibbo-Kobayashi-Maskawa (CKM) matrix is responsible for quark-mixing and its matrix elements fix the couplings

Weak Process	*Related Functions*
$B^0-\bar{B}^0$ mixing	$S(x_t)$
$K \to \pi\nu\bar{\nu}$, $B \to K\nu\bar{\nu}$, $B \to \pi\nu\bar{\nu}$	$X(x_t)$
$K \to \mu\bar{\mu}$, $B \to l\bar{l}$	$Y(x_t)$
$K_L \to \pi^0 e^+ e^-$	$Y(x_t), Z(x_t)$, $E(x_t)$
$K \to \pi\pi$: ϵ'	$S(x_t)$, $X(x_t)$, $Y(x_t)$, $Z(x_t)$, $E(x_t)$
$B \to K^*\gamma$	$D'(x_t)$, $E'(x_t)$
$B \to Ke^+e^-$	$Y(x_t)$, $Z(x_t)$, $E(x_t)$, $E'(x_t)$

Table 1.1: Basic functions governing the m_t-dependence of various weak amplitudes

between quarks and charged vector bosons. The mixing matrix depends also on complex phases (one for three generations) responsible for CP-violation. Thus, on one hand CP-violation can be extremely helpful in "hunting" those couplings of the top quark which are still poorly known. On the other hand non-leptonic and semi-leptonic weak decays are of fundamental importance in this respect. Virtual processes could also give informations about hidden sectors of the theory, provided we control with sufficient precision the theoretical predictions. This could become relevant in the present and future determination of new physics beyond the SM. From the analysis of weak decays and the comparison with the experimental informations at hand, we can get an indirect determination of the t-couplings. We will see in section 1.2 how many different physical processes, whose amplitudes:

$$\begin{aligned} &A_1(m_t, CKM, \ldots) \\ &A_2(m_t, CKM, \ldots) \\ &\ldots \end{aligned} \tag{1.5}$$

depend on m_t and on the CKM matrix parameters can cooperate to a combined determination of both m_t and t-couplings.

We conclude this brief introduction with a classification of different K- and B-processes:

- $\Delta F = 2$ processes $\longrightarrow$ box diagrams
- $\Delta F = 1$ processes $\longrightarrow$ vertex and penguins diagrams

where F is a generic flavour (see fig.(1.4) and (1.6)).

$\Delta F = 2$ processes belong, as to say, to the "*past*" of perturbative calculations: they have been computed to NLO (Next-to-Leading Order) and their Effective Hamiltonians have been proved to be quite stable under perturbative corrections up to this order [15]. On the other hand, the interest of the present study is in $\Delta F = 1$ processes and, in this contest, we have computed the NLO Effective Hamiltonian. Contrary to the $\Delta F = 2$ case, a big enhancement for some coefficients of the EH is found at NLO. This fact, together with the large number of physical processes described by the $\Delta F = 1$ EH, makes the subject extremely interesting.

1.2 Quark mixing and the Unitary Triangle

In this section the main features of quark-mixing in the SM framework are recalled, together with the description of CP-violation in terms of the Unitary Triangle (UT).

It is well known that in the SM only neutral currents are both flavour and helicity-conserving, while charged currents are only helicity-conserving and mix up- to down-type quarks. This mixing is defined through the CKM matrix, a unitary matrix which relates quark weak current eigenstates to mass eigenstates. In the three generation SM this matrix is parametrized by three angles and one complex phase. It's just this complex phase the only responsible for CP-violation in the SM: again we see the deep connection existing between CP-violation and quark couplings.

Many different parametrization of the CKM matrix have been proposed and used during years. Here are the most important ones:

- the Kobayashi and Maskawa parametrization [39]

$$\mathbb{V} = \begin{pmatrix} c_1 & -s_1 c_3 & -s_1 s_3 \\ s_1 c_2 & c_1 c_2 c_3 - s_2 s_3 e^{i\phi} & c_1 c_2 s_3 + s_2 c_3 e^{i\phi} \\ s_1 c_2 & c_1 s_2 c_3 + c_2 s_3 e^{i\phi} & c_1 s_2 s_3 - c_2 c_3 e^{i\phi} \end{pmatrix} \tag{1.6}$$

- The Particle Data Group or "*standard*" parametrization [44]

$$\mathbb{V} = \begin{pmatrix} c_{12} c_{13} & s_{12} c_{13} & s_{13} e^{-i\delta} \\ -s_{12} c_{23} - c_{12} s_{23} s_{13} e^{i\delta} & c_{12} c_{23} - s_{12} s_{23} s_{13} e^{i\delta} & s_{23} c_{23} \\ s_{12} s_{23} - c_{12} c_{23} s_{13} e^{i\delta} & -s_{12} c_{23} - s_{12} c_{23} s_{13} e^{i\delta} & c_{23} c_{13} \end{pmatrix} \tag{1.7}$$

Considering the smallness of the mixing angles, one can also introduce for practical purposes a "reduced" form of the mixing matrix, obtained by expanding all the matrix elements in the small parameter

$$\lambda = |\mathbb{V}_{us}| = 0.221 \pm 0.002 \tag{1.8}$$

up to $O(\lambda^4)$:

- The *original* Wolfenstein parametrization [59, 60]

$$\mathbb{V} = \begin{pmatrix} 1-\frac{\lambda^2}{2} & \lambda & A\lambda^3(\rho - i\eta) \\ -\lambda & 1-\frac{\lambda^2}{2} & A\lambda^2 \\ A\lambda^3(1-\rho-i\eta) & -A\lambda^2 & 1 \end{pmatrix} \tag{1.9}$$

- The *modified* Wolfenstein parametrization [59, 60]

$$\mathbb{V} = \begin{pmatrix} 1-\frac{\lambda^2}{2} & \lambda & A\lambda^3\sigma e^{-i\delta} \\ -\lambda & 1-\frac{\lambda^2}{2} & A\lambda^2 \\ A\lambda^3(1-\sigma e^{i\delta}) & -A\lambda^2 & 1 \end{pmatrix} \tag{1.10}$$

The relation between the two Wolfenstein parametrizations is simply given by:

$$\rho = \sigma\cos\delta \ , \ \eta = \sigma\sin\delta \tag{1.11}$$

It's interesting to note that [35] CP-violation effects result always proportional to:

$$J_{CP} = \mathrm{Im}(\mathbb{V}_{cb}\mathbb{V}_{us}\mathbb{V}^*_{ub}\mathbb{V}^*_{cs}) \tag{1.12}$$

J_{CP} is a universal quantity: it does not depend on the parametrization and on the phase convention. Due to the smallness of the mixing angles involved, J_{CP} results to be of $O(\lambda^6) \sim 10^{-3}$ and this fixes the order of magnitude of CP-violation in the SM. In other words, CP-violation in the SM framework turns out to be "naturally" small.

We should stress that the two Wolfenstein parametrizations in (1.9) and (1.10) are expansions in the small λ parameter. The order given in (1.9) and (1.10) could also not be adequate for accurate calculations. For instance, in the evaluation of CP-violation from (1.12) a higher order of the expansion is required in order to have a non zero J_{CP}. On the other hand, J_{CP} may also be defined in terms of different elements of the CKM matrix:

$$J_{CP} = \mathrm{Im}(\mathbb{V}_{ud}\mathbb{V}_{tb}\mathbb{V}^*_{ub}\mathbb{V}^*_{td}) \tag{1.13}$$

and in this case the $O(\lambda^3)$ expansion would be enough. Any consistent check of CP-violation would require in any case the evaluation of both (1.12) and (1.13).

The unitarity of the CKM mixing matrix provides a very powerful and intuitive way to describe the pattern of CP-violation, for given parameters and physical inputs. Indeed, from the CKM matrix, being a (3×3) matrix, nine unitarity relations of the form:

$$\begin{aligned} \sum_i \mathbb{V}_{ij}\mathbb{V}^*_{ik} &= \delta_{jk} \\ \sum_i \mathbb{V}_{ji}\mathbb{V}^*_{ki} &= \delta_{jk} \end{aligned} \tag{1.14}$$

can be derived, for i, j and k running over quark flavours. It is easy to convince oneself that six of the previous relations defines a triangle in the complex plane. Among them, the most interesting case to our purpose is the following one:

$$\mathbb{V}_{ud}\mathbb{V}^*_{ub} + \mathbb{V}_{cd}\mathbb{V}^*_{cb} + \mathbb{V}_{td}\mathbb{V}^*_{tb} = 0 \tag{1.15}$$

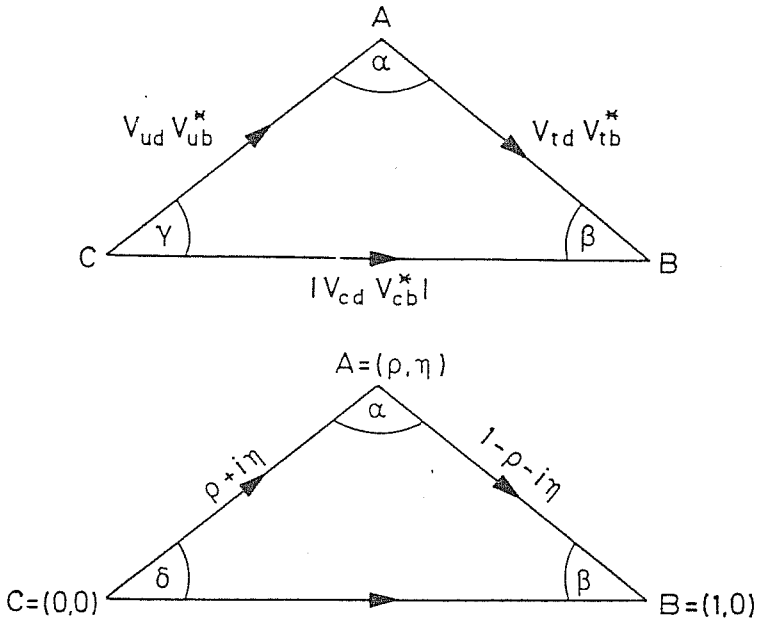

Figure 1.1: Unitarity Triangle

because it involves some not well-known couplings like $\mathbb{V}_{ub}$ and $\mathbb{V}_{td}$. It defines the triangle shown in figure (1.1), specialized to the case :

$$\mathbb{V}_{ud} \simeq 1 \ , \ \mathbb{V}_{tb} \simeq 1 \ , \ \mathbb{V}_{cd}, \mathbb{V}_{cb} \ \ real \tag{1.16}$$

and its area is related to the measure of CP-violation by:

$$|J_{CP}| = 2 \cdot A_{\triangle} \tag{1.17}$$

Obviously the shape of the UT does not depend on the parametrization chosen. The choice of the parametrization can only affect the position of the UT in the complex plane. The lengths of its sides are given by moduli of elements of the CKM matrix, therefore by physical quantities. In order to see the importance of the angles of the UT, which in fact fix the shape of the triangle itself, we chose a given parametrization, f.i. the Wolfenstein ones (original or modified). It is common in literature to rescale the sides of the UT by $|\mathbb{V}_{cd}\mathbb{V}_{cb}| = A\lambda^3$. In this case the vertices of the UT become:

$$\begin{aligned} A &= \left(\frac{\mathrm{Re}\mathbb{V}_{ub}}{|\mathbb{V}_{cd}\mathbb{V}_{cb}|}, \frac{-\mathrm{Im}\mathbb{V}_{ub}}{|\mathbb{V}_{cd}\mathbb{V}_{cb}|} \right) = (\rho, \eta) \\ B &= (1,0) \\ C &= (0,0) \end{aligned} \tag{1.18}$$

as shown in figure (1.1), and the angles have the following expressions:

$$\sin 2\alpha = \frac{2\eta(\eta^2+\rho^2-\rho)}{(\rho^2+\eta^2)((1-\rho)^2+\eta^2)} = \frac{2\sin\delta(\sigma-\cos\delta)}{1+\sigma^2-2\sigma\cos\delta}$$

$$\begin{aligned} \sin 2\beta &= \frac{2\eta(1-\rho)}{(1-\rho)^2+\eta^2} = \frac{2\sigma \sin\delta(1-\sigma\cos\delta)}{1+\sigma^2-2\sigma\cos\delta} \\ \sin 2\gamma &= \frac{2\rho\eta}{\rho^2+\eta^2} = \sin 2\delta \end{aligned} \tag{1.19}$$

Most important:

$$\begin{aligned} \mathbb{V}_{ub} &= |\mathbb{V}_{ub}|e^{-i\gamma} \\ \mathbb{V}_{td} &= |\mathbb{V}_{td}|e^{-i\beta} \\ \gamma &= \delta \end{aligned} \tag{1.20}$$

that is: γ is just the CP-violating complex phase in the CKM matrix and γ and β are directly related to the phases of $\mathbb{V}_{ub}$ and $\mathbb{V}_{td}$, the less known elements of the matrix.

Many decays or mixing amplitudes in K- or B-physics can be expressed as functions of $\sin\phi$ or $\cos\phi$, for $\phi = \alpha, \beta$ or γ, or as functions of the ratios:

$$\begin{aligned} R_b &= \frac{|\mathbb{V}_{ub}|}{|\mathbb{V}_{us}\mathbb{V}_{cb}|} = \sqrt{\rho^2+\eta^2} = \sigma \\ R_t &= \frac{|\mathbb{V}_{td}|}{|\mathbb{V}_{us}\mathbb{V}_{ts}|} = \sqrt{(1-\rho)^2+\eta^2} = \sqrt{1+\sigma^2-2\sigma\cos\delta} \end{aligned} \tag{1.21}$$

They coincide exactly with the lengths of sides AC and AB of the UT and in the (ρ,η) plane they describe two circles centered in C and B respectively.

In figure (1.2) all the informations we have from K-physics and B-physics are summarized in an "ideal" way, where any process contributes with a single curve. This is clearly not the case: we should have a band instead of a curve for each contribution, but the aim of the picture is just to remind the interest of the phenomenology involved in the problem.

Figure (1.2) can be read as follows: from the experimental knowledge of λ and A ($|\mathbb{V}_{ub}/\mathbb{V}_{uc}|$) parameters in the Wolfenstein parametrization, we can estimate the radius R_b:

$$R_b = \frac{1}{\lambda}\left|\frac{\mathbb{V}_{ub}}{\mathbb{V}_{cb}}\right| \tag{1.22}$$

with:

$$\begin{aligned} A &= \lambda^{-2}|\mathbb{V}_{cb}| = 0.085\left[\frac{|\mathbb{V}_{cb}|}{0.041}\right] \\ \lambda &= 0.22 = |\mathbb{V}_{us}| \\ R_b &\sim 0.59 \pm 0.18 \end{aligned}$$

and $|\mathbb{V}_{cb}|$ from semi-leptonic B-meson decays.

Then the ϵ parameter of CP-violation in the $K^0 - \bar{K}^0$ mixing gives an hyperbola in the (ρ,η) plane (whose position can vary greatly depending also on non-perturbative

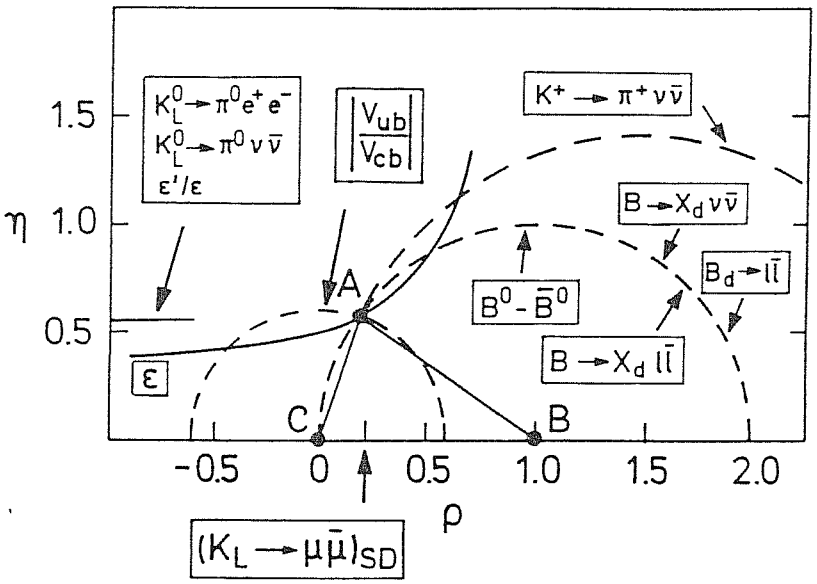

Figure 1.2: UT in the (ρ, η) plane

inputs), which could intersect the circle of radius R_b into two points. $B^0 - \bar{B}^0$ mixing, through the x_d parameter, fixes A to lie on a circle of radius R_t, centered in B. Hence the position of A in the (ρ, η) plane is determined and further ambiguities in the dependence from m_t can be constrained or even removed by using other physical inputs, like the ϵ' parameter or rare semileptonic K- and B-decays.

1.3 K-physics

We will focus mainly on CP-violation in the K-system. At the end we will only give some details about rare K-decays, an open field where many studies are going on.

About the first subject, we can investigate CP-violation in the K-system on two fronts:

- "*indirect*" CP-violation → "ϵ- *parameter*":CP-violation in the $K^0 - \bar{K}^0$ mass matrix;
- "*direct*" CP-violation → "ϵ'-*parameter*": CP-violation in the direct $K \to 2\pi$ transitions.

as illustrated in fig.(1.3).

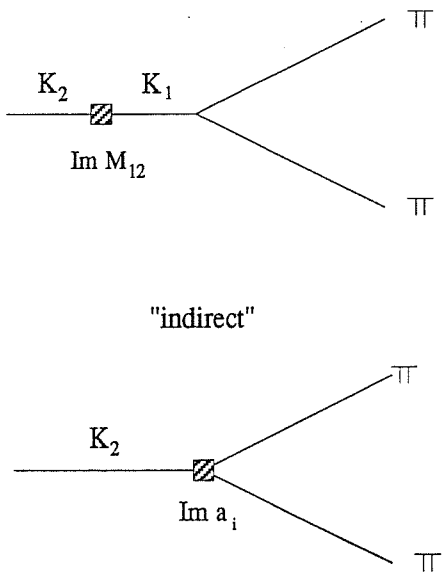

Figure 1.3: "*Indirect*" and "*direct*" CP-violation.

We will introduce now the main formalism and characteristics for the two previous parameters: ϵ and ϵ'.

(1) ϵ parameter

With three quark generations, the indirect CP-violation in the $K^0 - \bar{K}^0$ mass matrix is given by the following expression:

$$\begin{aligned} \epsilon &= \frac{\exp i\frac{\pi}{4}}{\sqrt{2}\Delta M}(\mathrm{Im}M_{12} + 2\xi \mathrm{Re}M_{12}) \\ &\simeq \frac{\exp i\frac{\pi}{4}}{\sqrt{2}}\left(\xi + \frac{\mathrm{Im}M_{12}}{\Delta M}\right) \end{aligned} \tag{1.23}$$

where

$$\xi = \frac{\mathrm{Im}A_0}{\mathrm{Re}A_0} \ , \qquad \text{with} \qquad \langle \pi\pi(I=0)|\mathcal{H}_w|K\rangle = A_0 e^{i\delta_0} \ , \tag{1.24}$$

is only a very small correction. ΔM is the mass difference between K_L and K_S, the two physical kaon mass-eigenstates, (experimentally: $\Delta M = 3.5 \cdot 10^{-15}$ GeV) and M_{12} is the dispersive part of the off-diagonal elements of the $K^0 - \bar{K}^0$ mixing mass-matrix:

$$M_{12} = \langle \overline{K}_0 | \mathcal{H}_{eff}^{|\Delta S|=2} | K_0 \rangle \tag{1.25}$$

At lowest order in weak interactions, there are two box-diagrams (see fig.(1.4)) which contribute to the $|\Delta S| = 2$ amplitude and similarly for any other $|\Delta F| = 2$ process (F =flavour) (e.g., the B_0–$\overline{B}_0$ mixing).

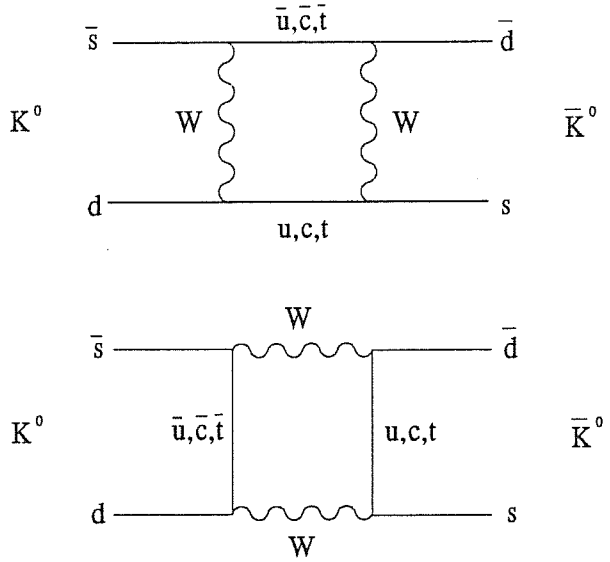

Figure 1.4: Two possible box-diagrams for the $K^0 - \bar{K}^0$ mixing.

At low energy scales and in the absence of QCD corrections, they reduce to the following effective hamiltonian, originally computed by Inami and Lim [34]:

$$\mathcal{H}_{eff}^{|\Delta S|=2} = = \frac{G_F^2}{16\pi^2} M_W^2 (\bar{d}\gamma_L^\mu s)^2 \left\{ \lambda_c^2 S(x_c) + \lambda_t^2 S(x_t) + 2\lambda_c \lambda_t S(x_c, x_t) \right\} \tag{1.26}$$

where:

- G_F is the Fermi coupling constant,
- $\gamma_L^\mu = \gamma^\mu(1-\gamma_5)$,
- λ_q's are related to the CKM matrix element by

$$\lambda_q = V_{qi}^* V_{qf} \tag{1.27}$$

  where 'i' and 'f' are the labels of the initial and final states respectively (for example, $i = s$ and $f = d$ in the K_0–$\overline{K}_0$ mixing case),
- $x_q = m_q^2/M_W^2$,
- the functions $S(x_i)$ and $S(x_i, x_j)$ are the so-called *Inami-Lim* functions [34], obtained from the calculation of the basic box-diagram. We already gave their expressions and large m_t behaviour in section 1.1, eq.(1.3) and (1.5).

The evaluation of the $\Delta F = 2$ EH at higher order in perturbation theory requires two main observations:

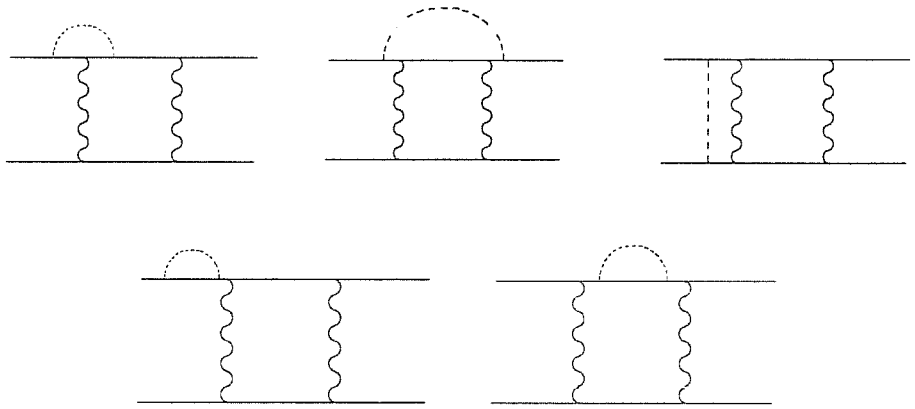

Figure 1.5: One loop QCD corrections to the box diagrams: the dashed line is a gluon.

i) the only operator appearing, under QCD corrections and renormalization mixing, in the x_t-dependent part of the EH is a four-fermion operator of O^+-type [4, 27, 5, 15]. Thus one needs only to compute, to a given order (f.i. LO or NLO) the anomalous dimension of a four-fermion vertex operator without mixing. The other terms in the EH require some more elaboration, but they are also not so relevant as the x_t-dependent one.

ii) the initial conditions for the coefficient functions at scale M_W are given at the tree level by the Inami-Lim functions $S(x_i)$ and $S(x_i, x_j)$; while at the one loop level they are given by the computation of one-loop QCD corrections to the box diagrams in fig.(1.4). The hard calculation of diagrams in fig.(1.5) is found in ref.[21, 15].

The first calculations of the effective $\Delta F = 2$ amplitude considered only the case of a small m_t in the LO approximation [30, 57, 56, 46]. The most definite paper among the LO approximation ones has been the classical paper by Gilman and Wise [30], where all the theoretical details of the problem were clarified.

By then, the experimental bounds on m_t made the possibility of a large m_t more and more reliable. Many different analysis of the effective $\Delta F = 2$ hamiltonian appeared in literature [14, 25, 36, 37, 26]. A more refined calculation, for large m_t and at the NLO has been completed by Buras et al. in ref.[15] for the only case of the purely x_t-dependent part. In ref.[15] it is shown that the NLO effective hamiltonian for K_0–$\overline{K}_0$ mixing, as well as for any other $\Delta F = 2$ process, is of the form:

$$\mathcal{H}_{eff}^{|\Delta S|=2} = \frac{G_F^2}{16\pi^2} M_W^2 (\bar{d}\gamma_L^\mu s)^2 \left\{ \lambda_c^2 \eta_1 S(x_c) + \lambda_t^2 \eta_2 S(x_t) + 2\lambda_c \lambda_t \eta_3 S(x_c, x_t) \right\} \tag{1.28}$$

The EH in (1.28) has the same form as in the small m_t case, because QCD corrections factorize to a large extent also in the large m_t case .

B_K	*Method*	*Reference*
0.33	Chiral Perturbation Theory	[23]
0.39 ± 0.10	Hadronic Sum Rules	[48, 49, 52]
0.58 ± 0.16	QCD Sum Rules	[22]
0.70 ± 0.10	$1/N$	[8, 29]
0.77 ± 0.07	Lattice	[38]
0.88 ± 0.20	Lattice	[28]
0.92 ± 0.03	Lattice	[12]
1.03 ± 0.07	Lattice	[9]

Table 1.2: B_K values obtained with different approach

From the EH in (1.28), we can derive the amplitude M_{12}:

$$M_{12} = \frac{G_F^2}{12\pi^2} M_W^2 B_K f_K^2 m_K \left\{ \lambda_c^2 \eta_1 S(x_c) + \lambda_t^2 \eta_2 S(x_t) + 2\lambda_c \lambda_t \eta_3 S(x_c, x_t) \right\} \quad (1.29)$$

and finally:

$$|\epsilon|_{\xi=0} = C_\epsilon B_K A^2 \lambda^6 \eta \left\{ \eta_3 S(x_c, x_t) + \eta_2 S(x_t)[A^2\lambda^4(1-\rho)] - \eta_1 S(x_c) \right\} \quad (1.30)$$

where

$$C_\epsilon = \frac{G_F^2 f_K^2 m_K M_W^2}{6\sqrt{2}\pi^2 \Delta M} \sim 4 \cdot 10^{-4} \quad (1.31)$$

Here, B_K is a factor which is inserted to take into account all the possible deviations from the vacuum insertion approximation in the evaluation of the $\langle \bar{K}^0 | (\bar{d}\gamma_L^\mu s)^2 | K^0 \rangle$ matrix element ($B_K = 1$ corresponding to an exact vacuum insertion approximation). The value of B_K is the main theoretical uncertainty and a very large spread in the theoretical estimates is reported in literature, as one can see from table (1.2). B_K is the renormalization group invariant B-factor, defined as :

$$B_K = B_K(\mu) \left[\alpha_{QCD}(\mu)\right]^{-2/9} \quad (1.32)$$

The QCD corrections η_i depends both on the definition of B_K and on the definition of quark masses. Choosing for m_i the running masses $m_i(m_i^*)$ and for B_K the definition in (1.32), the values of η_2 and η_3 can be taken to be fairly stable with respect to the variation of m_c, m_b, m_t and Λ_{QCD}. The same is not strictly true for η_1, but since the charm contribution is small, this does not significantly affect the final predictions. The typical values for the η_i parameters are:

$$\eta_1 = 0.85 \ , \ \eta_2 = 0.57 \ , \ \eta_3 = 0.36 \quad (1.33)$$

corresponding to: $m_c = 1.4$ GeV, $m_b = 4.6$ GeV, $m_t = 140$ GeV and $\Lambda_{QCD} = 200$ MeV. For very large m_t the second term in eq. (1.28) dominates. The most important result of the analysis of ref.[15] has been to state that the perturbative approach in the effective hamiltonian formalism is completely justified, because the EH results to be quite stable under higher order perturbative corrections.

Finally, using the experimental value of ϵ:

$$|\epsilon_{exp}| = (2.258 \pm 0.018) \cdot 10^{-3} \tag{1.34}$$

we can cast eq.(1.30) in the form

$$|\epsilon|_{\xi=0} = C_\epsilon B_K A^2 \lambda^6 \eta \left\{ \eta_2 S(x_t) A^2 \lambda^4 (1-\rho) - K \right\} \tag{1.35}$$

where

$$K = \eta_3 S(x_c, x_t) - \eta_1 S(x_c) \tag{1.36}$$

For ϵ fixed at its experimental value, Eq.(1.35) defines a hyperbola in the (ρ, η) plane, as it is shown in fig.(1.2).

(2) ϵ' parameter

The direct CP-violation parameter of the K-system appears in $\Delta S = 1$ non-leptonic decays and can be written as:

$$\epsilon' = -\frac{\omega}{\sqrt{2}} \xi (1 - \Omega) e^{i\phi} \tag{1.37}$$

where

$$\omega = \frac{\mathrm{Re}A_2}{\mathrm{Re}A_0} \ , \ \xi = \frac{\mathrm{Im}A_0}{\mathrm{Re}A_0} \ , \ \Omega = \frac{1}{\omega} \frac{\mathrm{Im}A_2}{\mathrm{Im}A_0} \tag{1.38}$$

with $\phi = \pi/2 + \delta_2 - \delta_0$ and A_i and δ_i defined by:

$$e^{i\delta_i} A_i = \langle \pi\pi (I = i) | \mathcal{H}_{eff}^{|\Delta S|=1} | K \rangle \tag{1.39}$$

It is convenient to introduce the ratio ϵ'/ϵ which has the advantage to be practically independent of phases. The experimental results for this quantity are:

$$\mathrm{Re}\left(\frac{\epsilon'}{\epsilon}\right) = \begin{cases} (2.3 \pm 0.7) \cdot 10^{-3} & NA31 \\ (0.6 \pm 0.7) \cdot 10^{-3} & E731 \end{cases} \tag{1.40}$$

Theoretically the ratio ϵ'/ϵ has the form:

$$\frac{\epsilon'}{\epsilon} = \frac{\omega}{\sqrt{2}} \frac{1}{|\epsilon|} \xi (1 - \Omega) \tag{1.41}$$

For some of the quantities appearing in eq.(1.41) we can use their experimental value:

$$\omega \simeq 0.045 \ , \ \mathrm{Re}A_0 \simeq 3,3 \cdot 10^{-7} \ GeV \tag{1.42}$$

the remaining amplitudes are computed in the EH formalism. The generic hamiltonian is given by:

$$\mathcal{H}_{eff}^{|\Delta S=1|} = \sum_i C_i(\mu) Q_i(\mu) \tag{1.43}$$

The complete basis of operators entering the EH when QCD corrections are taken into account is now much more complicated than in the ϵ-case and is given by:

$$\begin{aligned}
Q_1 &= (\bar{s}_\alpha d_\beta)_{(V-A)} (\bar{u}_\gamma u_\delta)_{(V-A)} \cdot \delta_{\alpha\beta} \otimes \delta_{\gamma\delta} \\
Q_2 &= (\bar{s}_\alpha d_\beta)_{(V-A)} (\bar{u}_\gamma u_\delta)_{(V-A)} \cdot \delta_{\alpha\delta} \otimes \delta_{\gamma\beta} \\
Q_{3,5} &= (\bar{s}_\alpha d_\beta)_{(V-A)} \sum_{q=u,d,s} (\bar{q}_\gamma q_\delta)_{(V\mp A)} \cdot \delta_{\alpha\beta} \otimes \delta_{\gamma\delta} \\
Q_{4,6} &= (\bar{s}_\alpha d_\beta)_{(V-A)} \sum_{q=u,d,s} (\bar{q}_\gamma q_\delta)_{(V\mp A)} \cdot \delta_{\alpha\delta} \otimes \delta_{\gamma\beta} \\
Q_{7,9} &= \frac{3}{2} (\bar{s}_\alpha d_\beta)_{(V-A)} \sum_{q=u,d,s} e_q (\bar{q}_\gamma q_\delta)_{(V\pm A)} \cdot \delta_{\alpha\beta} \otimes \delta_{\gamma\delta} \\
Q_{8,10} &= \frac{3}{2} (\bar{s}_\alpha d_\beta)_{(V-A)} \sum_{q=u,d,s} e_q (\bar{q}_\gamma q_\delta)_{(V\pm A)} \cdot \delta_{\alpha\delta} \otimes \delta_{\gamma\beta}
\end{aligned} \tag{1.44}$$

where $_{(V\pm A)}$ index indicates the chiral structure, i.e.:

$$(\bar{q}_i q_j)_{(V\pm A)} \equiv \bar{q}_i \gamma^\mu (1 \pm \gamma_5) q_j \tag{1.45}$$

while $\delta_{\alpha\beta}\otimes\delta_{\gamma\delta}$ and $\delta_{\alpha\delta}\otimes\delta_{\gamma\beta}$ distinguish two different colour-structures, corresponding to the two possible contractions on the colour indices. Different operators are obtained by different combination of Dirac- and colour-structures.

The technical construction of the NLO Effective Hamiltonian for $\Delta S = 1$ transitions will be considered in detail in Chapt.2 and Chapt.3. Here we will only justify the presence of so many operators, generated by weak and strong interactions.

At the tree level we have only one four-fermion vertex operator: Q_2. At the one-loop level this operator mixes under renormalization (QCD corrections) not only with its Fierz conjugate operator Q_1, but also with QCD "penguin" operators, $Q_3, \ldots, Q_6$, due to the diagram in fig.(1.6). First only strong penguin diagrams were considered. Then, it was realized that, even though suppressed by the smaller coupling, EW penguins, i.e. γ-penguins and Z^0-penguins (see fig.(1.6) and (2.4), could have been important in the expression of ϵ'/ϵ. In particular, electro-magnetic corrections survive also below the M_W-threshold and new penguin operators $O_7, \ldots, O_{10}$ are generated. The matrix elements of O_7 and O_8 ($8_L \times 8_R$ of $SU(3)_L \times SU(3)_R$) do not vanish in the chiral limit and give important contributions. These new EW penguin operators mix with QCD-vertex and penguin operators, giving a final (10×10) anomalous dimension matrix.

It was found [10, 24] that for small m_t EW-penguins corrections to ϵ'/ϵ have the same sign as the QCD-penguin ones, increasing ϵ'/ϵ. On the contrary, for large m_t their contribution reverses sign and tends to cancel the effect of QCD-penguins, thus decreasing ϵ'/ϵ. For very high values of m_t it can even become negative.

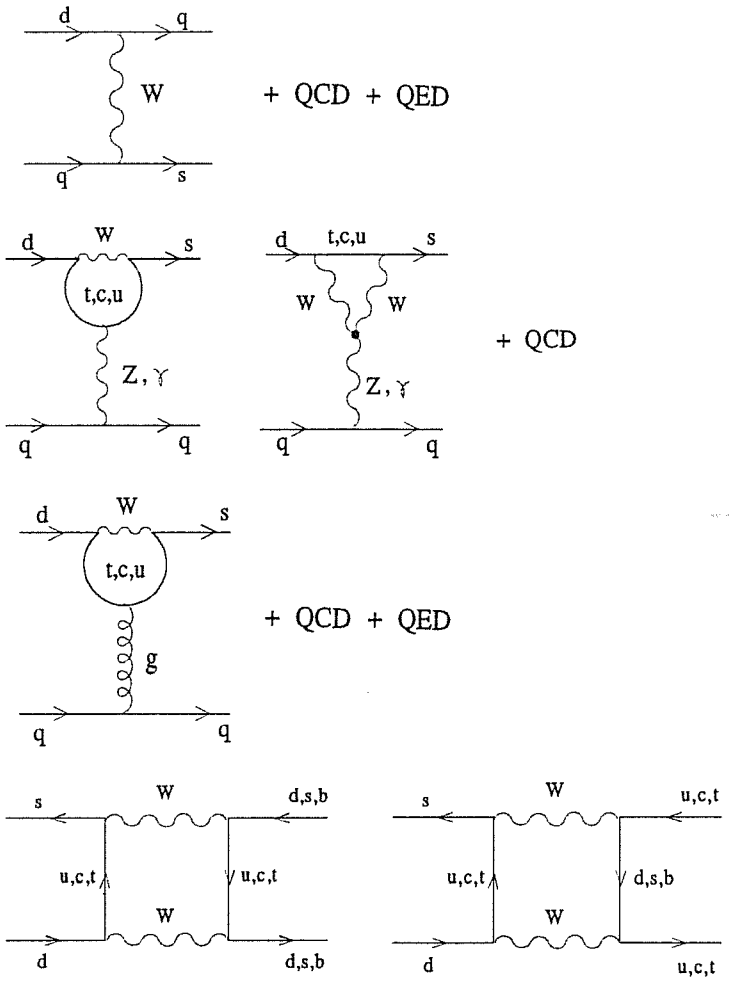

Figure 1.6: All the contributions to the $\Delta S = 1$ Hamiltonian in the Full Theory.

For large m_t also Z^0-penguins and W-box diagrams shown in fig.(1.6), which enter only the coefficient function at the initial scale M_W, contribute, decreasing the value of ϵ'/ϵ.

A non negligible contribution comes also from isospin breaking terms (in the quark masses), while only minor corrections are due to other combination of operators.

The expression of ϵ'/ϵ is usually given factorizing the contribution of the leading QCD penguin operator, Q_6, and including in Ω all the other terms:

$$\frac{\epsilon'}{\epsilon} \propto y_6\langle Q_6\rangle_0 \left[1-\bar{\Omega}\right] \tag{1.46}$$

and

$$\bar{\Omega} = \Omega_{\eta+\eta'} + \Omega_{EWP} + \Omega_8 + \Omega_{27} + \Omega_P \tag{1.47}$$

$\Omega_{\eta+\eta'}$ being the isospin-breaking term in the quark masses, represented by $\pi^0\eta\eta'$ mixing and the other terms being defined as :

$$\begin{aligned}
\Omega_{EWP} &= \frac{1-\sqrt{2}\omega}{\omega}\left[\frac{y_7\langle Q_7\rangle_2 + y_8\langle Q_8\rangle_2}{y_6\langle Q_6\rangle_0}\right] \\
\Omega_8 &= -\left[\frac{y_1\langle Q_1\rangle_0 + y_2\langle Q_2\rangle_0}{y_6\langle Q_6\rangle_0}\right] \\
\Omega_{27} &= \frac{1}{\omega}\left[\frac{(y_1+y_2)\langle Q_2\rangle_2}{y_6\langle Q_6\rangle_0}\right] \\
\Omega_P &= -\left[\frac{y_3\langle Q_3\rangle_0 + y_5\langle Q_5\rangle_0}{y_6\langle Q_6\rangle_0}\right]
\end{aligned} \tag{1.48}$$

$y_1 \ldots y_8$ are coefficient functions of the related operators.

We observe that the m_t influence is clearly a NLO effect, because it enters the initial conditions for the penguin operators at one-loop. Previous analyses have been performed by including one-loop initial condition for the coefficient functions (in order to have the m_t-dependence), but using the one-loop anomalous dimension matrix in the evolution equation. Even though this may be numerically the main effect, there is a perturbative inconsistency in this procedure. The authors of ref.[14] motivated this choice because of the presence of a renormalization scheme-independent part in the coefficient functions at the M_W-scale, but this does not remove the previous inconsistence. Their analysis had a great impact, because they pointed out the relevance of EW penguins, etc. Nevertheless, for consistency the calculation of the two-loop anomalous dimension is mandatory. This is precisely what we compute in this thesis. Analogous results have been obtained by the group of Buras et al. in Munich.

(3) Rare K-meson decays

We mention here for completeness some important semi-leptonic and leptonic rare K-meson decays, where a calculation of the EH beyond the leading order

may have an important phenomenological impact. We will not treat them in detail, because it is beyond the argument of this thesis. Nevertheless, since they are related to the determination of m_t or t-couplings, we will give the expression of some branching ratios.

- $K^+ \to \pi^+ \nu\bar{\nu}$

  This decays receives contributions both from box- and penguin-diagrams. Its branching ratio can be written as:

$$B(K \to \pi^+ \nu\bar{\nu}) = 4.67 \cdot 10^{-11} A^4 [X(x_t)]^2 \left[\eta^2 + \frac{2}{3}(\bar{\rho}_0^e - \rho)^2 + \frac{1}{3}(\bar{\rho}_0^\tau - \rho)^2)\right] \tag{1.49}$$

  where

$$\bar{\rho}_0^i = 1 - \frac{P_0^i \lambda^{-5}}{A^2 X(x_t)} \tag{1.50}$$

  and P_0^i represents the charm contribution, for $i = e, \mu, \tau$. $X(x_t)$ is given in (1.3). This expression clearly determines a circle in the complex (ρ, η) plane as we can see in fig.(1.2). As all the other inputs we have from K-physics, this branching ratio alone is not enough to fix neither m_t nor $|\mathbb{V}_{td}|$.

- $K^{0}{}_L \to \pi^0 \nu\bar{\nu}$

  The main contribution, as before, comes from box and penguins diagrams. The branching ratio is found in literature to be of the form:

$$B(K_L \to \pi^0 \nu\bar{\nu}) = 1.94 \cdot 10^{-10} \left[\eta^2 A^4\right] X^2(x_t) \tag{1.51}$$

  where $X(x_t)$ is given in (1.3) and, due to the absence of charm contribution, a better analysis is possible.

- $K_L \to \mu\bar{\mu}$

  It has been measured experimentally:

$$B(K_L \to \mu\bar{\mu})_{SD} = \begin{cases} (8.4 \pm 1.1) \cdot 10^{-9} & (E137) \\ (7.64 \pm 0.5 \pm 0.4) \cdot 10^{-9} & (E791) \end{cases} \tag{1.52}$$

  where the index "SD" stays for "short distance", because this is only a part of the whole branching ratio. From theoretical computations one has:

$$B(K_L \to \mu\bar{\mu})_{SD} = 1.71 \cdot 10^{-9} A^4 [Y(x_t]^2 [\rho_0 - \rho] \tag{1.53}$$

  where $Y(x_t)$ is given in (1.3) and again mainly box and penguins diagrams contribute.

- $K_L \to \pi^0 e^+ e^-$

  This decays consists of a direct as well as of an indirect CP-violation part, plus a CP-conserving part. Very recently some indications appeared that the

direct CP-violating part dominates. In spite of the very complex analysis, it is possible to cast the final result in a quite simple form:

$$B(K_L \to \pi^0 e^+ e^-)_{CPdir} = 0.32 \cdot 10^{-10} \eta^2 A^4 I(x_t) \tag{1.54}$$

where

$$\begin{aligned} I(x_t) \;=\; & \Big[P_0(K_L \to \pi^0 e^+ e^-) + (Y(x_t) - 4\sin^2\theta_W Z(x_t)) + \\ & P_E E(x_t)\Big]^2 + Y^2(x_t) \end{aligned} \tag{1.55}$$

$Y(x_t)$, $Z(x_t)$ and $E(x_t)$ are given in (1.3) and the charm contribution turns out to be irrelevant.

The above branching ratios may put constraints on the allowed regions of the (ρ, η) plane, because of their sensitivity to the short distance structure of the theory, in particular to the top quark mass.

1.4 *B*-physics

Due to the fact that B-physics involves all the generations of quarks, CP-violation appears not only as loop-effect, but also at the tree-level. For this reason the CP-violation scenario in the B-system is much richer. We can have CP-violation whenever in a given weak amplitude the complex phase of the CKM matrix appears. This happens in:

- $\Delta B = 2$ transitions : $B^0 - \bar{B}^0$-mixing;
- $\Delta B = 1$ transitions : B-decays;
- $\Delta B = 0$ transitions : final state strong interactions.

$\Delta B = 2$ transitions only take place in the *neutral* B-system. $B^0 - \bar{B}^0$-mixing is the most rich source of CP-violation for the B-system. In the B^0-decay to a final state f indeed, due to the mixing two different paths are possible:

$$B^0 \to B^0 \to f \quad \text{or} \quad B^0 \to \bar{B}^0 \to f \tag{1.56}$$

where CP-violation can be originated both by the phase in the $B^0 - \bar{B}^0$ mixing and by the different phases in $B^0 \to f$ and $\bar{B}^0 \to f$. Thus, CP-violation can be present even if the two decays $B^0 \to f$ and $\bar{B}^0 \to f$ are CP-conserving.

On the other hand, $\Delta B = 1$ decays can give origin to CP-violation observables only if combined with either $B^0 - \bar{B}^0$ mixing or final state strong interactions. We will see an example of that in discussing the main features of the measurable asymmetries of the B-system.

Finally, $\Delta B = 0$ cannot be a source of CP-violation by themselves, but only coupled to $\Delta B = 1$ or $\Delta B = 2$ processes.

In the same spirit of the previous section, we will recall some important features about:

- $x_{d,s}$ parameters of $B^0 - \bar{B}^0$ mixing
- $\Delta B = 1$ decays and asymmetries.

Finally, not concerned with CP-violation physics, we will recall some of the most interesting rare B-decays, to explain the last curves appearing in fig.(1.2).

(1) $B^0 - \bar{B}^0$-mixing

The description of $B^0 - \bar{B}^0$ mixing is strictly analogous to the one of $K^0 - \bar{K}^0$ mixing: both are $\Delta F = 2$ processes that can be described by a four-fermion operator EH at low scales. The formalism we have seen in section 1.3 is still valid and we have only to account for the differences arising in the CKM sector. B^0–$\bar{B}^0$-mixing is computed at the lowest order in weak interaction referring to the box diagrams in fig.(1.4), with external states $(\bar{b}s)(\bar{s}b)$ or $(\bar{b}d)(\bar{d}b)$ respectively. The presence of the b-quark greatly enhances the coupling with the t-quark running in the internal propagators. All the couplings in the box diagram are now of the same order and the contribution from the top-quark dominates. As we will see in a while, it is possible to give approximate expression for the B^0-system mixing parameter just because the top contribution is indeed largely predominant.

First of all, let us introduce the mixing parameter $x_{d,s}$[3] defined as:

$$x_{d,s} \equiv \frac{(\Delta M)_{B_{d,s}}}{\Gamma} = C_{B_{d,s}} \eta_{QCD} S(x_t) |\hat{\mathbb{V}}_{t(d,s)}|^2 \qquad (1.57)$$

where $(\Delta M)_{B_{d,s}}$ is the mass difference between the mass eigenstates of the $(B^0 - \bar{B}^0)_{B_{d,s}}$ system respectively and $\Gamma = 1/\tau_{B_{d,s}}$, with $\tau_{B_{d,s}}$ being the B-meson life-time. The previous formula (1.57) derives from the general expression for the $\Delta F = 2$ EH in (1.26) or (1.28) as it was the case for the ϵ-parameter expression. $S(x_t)$ is here the usual Inami-Lim function for the $\Delta F = 2$ EH, explicitly given in (1.3). η_{QCD} summarize all the short distance QCD corrections to the box-diagram, both at LO and NLO. The NLO full computation is given in ref. [15] where it has been shown that the NLO result is almost scale-independent, if $\bar{m}_t(m_t)$ is taken. η_{QCD} is to a good approximation given by:

$$\eta_{QCD} \simeq 0.55 \qquad (1.58)$$

[3]Up to now only the mixing in the B_d-system has been isolated. On the other hand, the global mixing in the B-system, to which both B_d and B_s contribute, has been observed.

f_{B_d}	*Method*	*Reference*
184 ± 7	F E S R	[50]
190 ± 50	QCD Sum Rules	[45]
220 ± 25	QCD Sum Rules	[7]
205 ± 40	Lattice	[1]
205 ± 20	Lattice	[53]
155 ± 15	Relativistic Quark Model	[17]
233 ± 35	QCD Inspired Models	[19]

Table 1.3: Values of f_{B_d} obtained in different non perturbative approaches.

The constant $C_{B_{d,s}}$ factorizes all the dependences on masses, non-perturbative parameters and the $B_{d,s}$ life-time, namely:

$$C_{B_{d,s}} = \tau_{B_{d,s}} \frac{G_F^2}{6\pi^2} m_b M_W^2 (B_{B_{d,s}} f_{B_{d,s}}^2) \tag{1.59}$$

where $B_{B_{d,s}}$ and $f_{B_{d,s}}^2$ are the analogous of the B_K and f_K factors for the K-system. Both $B_{B_{d,s}}$ and $f_{B_{d,s}}^2$ originate in the approximate evaluation of the matrix elements of the operator $(\bar{b}d)(\bar{d}b)$ or $(\bar{b}s)(\bar{s}b)$ between B^0 and $\bar{B}^0$ states. The major source of uncertainty is the hadronic matrix element of four-fermion operator and various non-perturbative approaches to their evaluation have been proposed and developed. The general belief is that $B_{B_d} \approx 1$, while many different values for f_{B_d} can be found in literature. We report the present status of f_{B_d} in Table(1.3), where for each method only the most updated results are given. Present analyses generally consider $\sqrt{B_{B_d}} f_{B_d}$ in the range:

$$160 \text{ MeV} \leq \sqrt{B_{B_d}} f_{B_d} \leq 240 \text{ MeV} \tag{1.60}$$

In particular, the first indication of a quite large value for f_{B_d} came from the lattice approach and recently QCD sum rules seem to confirm it. Assuming lattice results, some interesting previsions on the pattern of CP-violation in the three family SM have been presented in ref. [43]. In ref. [43] a large value of f_{B_d} is related through the the expression of x_d itself, to a positive cosine of the γ-angle in the UT, i.e. to a large value of $(\sin 2\beta)$, being β the homonymous angle in the UT. That is seen as a positive indication for a large CP-violation in B-system asymmetries, quite interesting from the experimental point of view.

We finally remember that the accounted experimental value for x_d, measured by ARGUS, CLEO and LEP and is:

$$x_d = 0.67 \pm 0.10 \tag{1.61}$$

and this last one, compared to the theoretical determinations at hand can be inserted in many different CP-violation analysis and can add a further piece to the comprehension of fig.(1.2). Indeed, the experimental knowledge of x_d constrains the vertex A of the UT to lie on a circle of radius R_t centered in the vertex $B = (0,1)$. The expression of the radius R_t derived from x_d is approximately given by:

$$R_t = 1.85\sqrt{x_d}\frac{1}{A}\left[\frac{1.28\,\text{ps}}{\tau_{b_d}}\right]^{1/2}\left[\frac{200\ \text{MeV}}{\sqrt{B_{B_d}f_{B_d}^2}}\right]x_t^{-0.38} \tag{1.62}$$

where A is the one of the Wolfenstein parametrization: $A = \lambda^{-2}|\hat{\mathbb{V}}_{cb}|$, $x_t = m_t^2/M_W^2$, and the experimental value of $\tau_{B_d} = 1.28\,\text{ps}$ has been taken.

The intersection between the circle of radius R_t from B^0–$\bar{B}^0$-mixing, the circle of radius R_b from the experimental measurement of $|\hat{\mathbb{V}}_{ub}|/|\hat{\mathbb{V}}_{cb}|$ and the hyperbola of the K-system ϵ-parameter, for fixed values of the top mass m_t fixes the position of the A-vertex univocally, giving a given unique set of the three UT angles (α,β,γ). Obviously this refers only to the ideal situation in which both the theoretical errors on B_{B_d} and f_{B_d} and the experimental errors on R_b, i.e. $\hat{\mathbb{V}}_{cb}$, on x_d and τ_{B_d} had been reduced to be very small. Otherwise we should let all our uncertain quantities varying in a suitable theoretical+experimental range. Each curve would thus be a band in the (ρ,η)-plane and we could only select regions in the plane itself. Nevertheless, any improvement both on the theoretical and the experimental side, moving towards a restriction of the allowed regions in the (ρ,η) plane, could also fix some limits on m_t or $|\hat{\mathbb{V}}_{td}|$.

Finally one should remember that the knowledge of x_s, not yet experimentally available, would represent a great improvement in this direction, because the ratio:

$$\frac{x_d}{x_s} = \frac{|\hat{\mathbb{V}}_{td}|^2}{|\hat{\mathbb{V}}_{ts}|^2}(1 + \text{flavour symmetry breaking effects}) \tag{1.63}$$

does not depend on m_t and on any non-perturbative parameter and $|\hat{\mathbb{V}}_{ts}| \simeq |\hat{\mathbb{V}}_{cb}|$. The determination of $|\hat{\mathbb{V}}_{td}|$ would be much better and the result much better employed in the combined analysis of picture (1.2). Up to now this last feature is still in the ballpark of future promises.

(2) $\Delta B = 1$ decays and asymmetries.

Let us consider first the case of the neutral B-system, where both $\Delta B = 2$ and $\Delta B = 1$ CP-violation is present. The description of the charge B-system will be simply obtained by turning off the mixing.

In the $B^0-\bar{B}^0$-system, due to the mixing, the time evolution of initially pure B^0 and $\bar{B}^0$ states [31] is given by:

$$\begin{aligned} |B^0(t)\rangle &= g_+(t)|B^0\rangle + e^{i\phi_M} g_-(t)|\bar{B}^0\rangle \\ |\bar{B}^0(t)\rangle &= e^{-i\phi_M} g_-(t)|B^0\rangle + g_+(t)|\bar{B}^0\rangle \end{aligned} \tag{1.64}$$

where the time-dependent coefficient are:

$$\begin{aligned} g_+(t) &= \exp\left(-\frac{\Gamma_t}{2} - imt\right)\cos\frac{\Delta mt}{2} \\ g_-(t) &= i\exp\left(-\frac{\Gamma_t}{2} - imt\right)\sin\frac{\Delta mt}{2} \end{aligned} \tag{1.65}$$

where the mixing is described by the mass difference Δm and by the phase ϕ_M.

In order to account for the decay of B^0 and $\bar{B}^0$ into final CP-conjugate states f and $\bar{f}$ one has to introduce four amplitudes:

$$\begin{aligned} A(f) &\equiv A(B^0 \to f) = A_1\exp(i\phi_1) + A_2\exp(i\phi_2) \\ \bar{A}(f) &\equiv A(\bar{B}^0 \to f) = \bar{A}_1\exp(i\bar{\phi}_1) + \bar{A}_2\exp(i\bar{\phi}_2) \\ A(\bar{f}) &\equiv A(B^0 \to \bar{f}) = \bar{A}_1\exp(-i\bar{\phi}_1) + \bar{A}_2\exp(-i\bar{\phi}_2) \\ \bar{A}(\bar{f}) &\equiv A(\bar{B}^0 \to \bar{f}) = \bar{A}_1\exp(-i\bar{\phi}_1) + \bar{A}_2\exp(-i\bar{\phi}_2) \end{aligned} \tag{1.66}$$

where CP-violation is expressed by the phases ϕ_1 and ϕ_2, while A_1 and A_2 depend on non CP-violating parameters of the CKM matrix, final state strong interactions and hadronic matrix elements.

From these amplitudes, one can derive [31] the time-dependent decay rates in the following form:

$$\begin{aligned} \Gamma(f,t) &= \Gamma(B^0(t) \to f) = |A(f)|^2\exp[-i\Gamma t] \\ &\quad \left[\cos^2(\frac{\Delta mt}{2}) + |\xi|^2\sin^2(\frac{\Delta mt}{2}) - \mathrm{Im}\xi\,\sin(\Delta mt)\right] \\ \bar{\Gamma}(f,t) &= \Gamma(\bar{B}^0(t) \to f) = |\bar{A}(f)|^2\exp[-i\Gamma t] \\ &\quad \left[|\xi|^2\cos^2(\frac{\Delta mt}{2}) + \sin^2(\frac{\Delta mt}{2}) + \mathrm{Im}\xi\,\sin(\Delta mt)\right] \\ \Gamma(\bar{f},t) &= \Gamma(B^0(t) \to \bar{f}) = |\bar{A}(\bar{f})|^2\exp[-i\Gamma t] \\ &\quad \left[|\bar{\xi}|^2\cos^2(\frac{\Delta mt}{2}) + \sin^2(\frac{\Delta mt}{2}) + \mathrm{Im}\bar{\xi}\,\sin(\Delta mt)\right] \\ \bar{\Gamma}(\bar{f},t) &= \Gamma(\bar{B}^0(t) \to \bar{f}) = |\bar{A}(\bar{f})|^2\exp[-i\Gamma t] \\ &\quad \left[\cos^2(\frac{\Delta mt}{2}) + |\bar{\xi}|^2\sin^2(\frac{\Delta mt}{2}) - \mathrm{Im}\bar{\xi}\,\sin(\Delta mt)\right] \end{aligned} \tag{1.67}$$

where ξ and $\bar{\xi}$ are defined as:

$$\xi = e^{i\phi_M}\frac{\bar{A}(f)}{A(f)} \quad , \quad \bar{\xi} = e^{-i\phi_M}\frac{A(\bar{f})}{\bar{A}(\bar{f})} \tag{1.68}$$

In the case of charged B-mesons no decay to a common state is possible and we are left with only two possible decay rates:

$$\Gamma(B^- \to f) = |A(B^- \to f)|^2 \quad , \quad \Gamma(B^+ \to \bar{f}) = |A(B^+ \to \bar{f})|^2 \tag{1.69}$$

From the previous expressions some very interesting *asymmetries* can be constructed, measuring the amount of CP-violation in the B-system. They are direct measurements of the differences: $\Gamma(f,t) \neq \bar{\Gamma}(\bar{f},t)$, $\Gamma(\bar{f},t) \neq \bar{\Gamma}(f,t)$ and $\Gamma(B^- \to f) \neq \Gamma(B^+ \to \bar{f})$. In particular, three of these physical asymmetries are of particular experimental relevance:

- The time-dependent asymmetry:

$$R_1(f,t) \equiv \frac{\Gamma(B^0(t) \to f) - \Gamma(\bar{B}^0(t) \to f)}{\Gamma(B^0(t) \to f) + \Gamma(\bar{B}^0(t) \to f)} \tag{1.70}$$

- The time-integrated asymmetry:

$$R_2(f,t) \equiv \frac{\int_0^\infty [\Gamma(B^0(t) \to f) - \Gamma(\bar{B}^0(t) \to f)]dt}{\int_0^\infty [\Gamma(B^0(t) \to f) + \Gamma(\bar{B}^0(t) \to f)]dt} \tag{1.71}$$

- the charged meson asymmetry:

$$R_3(f) \equiv \frac{\Gamma(B^- \to f) - \Gamma(B^+ \to \bar{f})}{\Gamma(B^- \to f) + \Gamma(B^+ \to \bar{f})} \tag{1.72}$$

Using the previous expressions for the decay rates, R_1, R_2, and R_3 can be given as function of ξ, $\bar{\xi}$ and the physical amplitudes.

Therefore, the real task will be to provide a formalism in which these amplitudes can be computed. This is exactly the formalism of EH, which will be the argument of the next chapter. We will provide here only the final result in order to get the physics of the problem. It turns out that $\Delta B = 1$-decays can be described by an EH containing both vertex and penguin operators (see section (1.3). The vertex operators involved result to be:

$$\begin{array}{ll} O_2^{(1)} = (\bar{b}c)_{(V-A)}(\bar{c}s)_{(V-A)} & O_2^{(5)} = (\bar{b}c)_{(V-A)}(\bar{u}d)_{(V-A)} \\ O_2^{(2)} = (\bar{b}u)_{(V-A)}(\bar{u}s)_{(V-A)} & O_2^{(6)} = (\bar{b}c)_{(V-A)}(\bar{u}s)_{(V-A)} \\ O_2^{(3)} = (\bar{b}c)_{(V-A)}(\bar{c}d)_{(V-A)} & O_2^{(7)} = (\bar{b}u)_{(V-A)}(\bar{c}s)_{(V-A)} \\ O_2^{(4)} = (\bar{b}u)_{(V-A)}(\bar{u}d)_{(V-A)} & O_2^{(8)} = (\bar{b}u)_{(V-A)}(\bar{c}d)_{(V-A)} \end{array} \tag{1.73}$$

and the penguin ones:

$$O_3^s = (\bar{b}s)_{(V-A)}(\bar{u}u + \bar{c}c + \bar{d}d + \bar{s}s + \bar{b}b)_{(V-A)} \tag{1.74}$$

$$O_3^d = (\bar{b}d)_{(V-A)}(\bar{u}u + \bar{c}c + \bar{d}d + \bar{s}s + \bar{b}b)_{(V-A)} \tag{1.75}$$

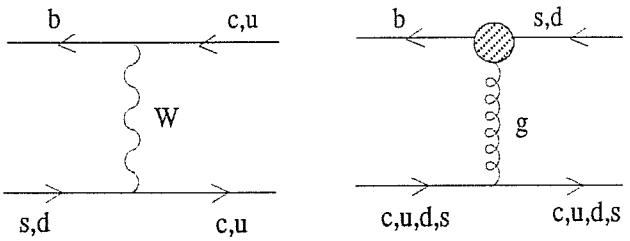

Figure 1.7: Vertex and Penguin diagrams corresponding to CP-violating $\Delta B = 1$ decays.

They appear in the EH with suitable wilson coefficients and they evolve and mix under the RG as we will detail in the section 2.1. Their two-loop anomalous dimension calculation on the other side is explained in section 2.2 and in chapter3.

The previous operators correspond to different described by the two cases reported in fig.(1.7). The decay classification has been very carefully studied in ref. [16] and we avoid to report it here, because of its technicality. Our aim here is only to stress how in the framework of Effective Field Theory a complete description of the physics of $\Delta B = 1$ is available and we can apply it directly to the study of the asymmetry problem, a very wide and promising field for the understanding of CP-violation.

(3) Rare B-decays.

As in the case of K-physics, we will summarize here the branching ratios of some of the most interesting rare B-decays. Our aim will be only to point out how they can be relevant in the (ρ, η) plot of fig.(1.2). Again, as in B^0–$\bar{B}^0$-mixing, the t-dependent contribution dominates and sometimes this simplify the analytical calculations. Moreover, non-perturbative effects are expected to be less important then in K-physics.

- $B \to X_s \sum \nu\bar{\nu}$

  This decay is analogous to the $K \to \pi\nu\bar{\nu}$ decay seen in the summary of the rare K-decays. It corresponds indeed to the elementary transition $b \to s\nu\bar{\nu}$, as well as the other one was related to the $s \to d\nu\bar{\nu}$ one. Moreover, here the charm contribution is completely irrelevant and the only contribution comes from W-box diagrams and Z^0-penguin diagrams. It receives some contributions from Z^0 magnetic penguin too, but they can be safely neglected. The branching ratio is proportional to the only $X(x_t)$ Inami-Lim function and given in its explicit dependence on m_t as:

$$B(B \to X_s \sum \nu\bar{\nu}) = 2.19 \cdot 10^{-5}[X(x_t)]^2 = 3.5 \cdot 10^{-5} \left[\frac{m_t}{140 \text{ GeV}}\right]^{2.36} \quad (1.76)$$

  where $X(x_t)$ is given in (1.3). Our real interest is in the $B(B \to X_d \sum \nu\bar{\nu})$ branching ratio, expected to be of $O(10^{-6} - 10^{-5})$, because it would give $|\hat{\mathbb{V}}_{td}|$.

- $B \to X_s e^+ e^-$

  This time we have to compare with the $K_L \to \pi^0 e^+ e^-$ decay and observe again that the decay is now completely top-dominated. Also in this case Z^0 magnetic penguin contributions can be neglected. NLO corrections have been calculated [18] and the final expression for the amplitude reads is a complicate expression of $Y(x_t)$, $Z(x_t)$, $E(x_t)$, $E'(x_t)$ and $D'(x_t)$. The branching ratio is expected to be of the order:

$$\begin{aligned} B(B^0 \to X_s e^+ e^-) &= (1-2)\cdot 10^{-5} \\ B(B^0 \to X_s \mu^+ \mu^-) &= (6-8)\cdot 10^{-6} \end{aligned} \tag{1.77}$$

  and similarly for the X_d-case in which again we are interested.

- $B^0 \to l\bar{l}(l = e, \mu, \tau)$

  This decays has its analogous in the $K_L \to \mu\bar{\mu}$ one, but where charm contribution and long-distance contribution be neglected. A direct calculation is possible in this case and it gives:

$$B(B \to l\bar{l}) = K \cdot |\hat{\mathbb{V}}_{tb}\hat{\mathbb{V}}^*_{ts}|^2 Y(x_t)^2 \tag{1.78}$$

  where

$$K = \tau_{B_s} \frac{G_F^2}{2\pi} \left(\frac{\alpha_e}{4\pi}\right)^2 \frac{1}{\sin^4 \vartheta_W} f_B^2 m_l^2 m_B \sqrt{1 - \frac{m_l^2}{m_B^2}} \tag{1.79}$$

  The same expression holds for the B_d case with $|\hat{\mathbb{V}}_{ts}|$ substituted by $|\hat{\mathbb{V}}_{td}|$, but unfortunately its magnitude is expected to be about ten times smaller.

Chapter 2

Effective Hamiltonian formalism for weak amplitudes: NLO formulation

2.1 General Discussion

Weak interactions are characterized by the presence of a wide range of physical mass scales, from m_t (the mass of the top quark, $200 \leq m_t \leq 100$ GeV) to M_W (the mass of the charged vector boson, $M_W \sim 80$ GeV) till m_b (the mass of the b-quark, ~ 4.5 GeV), m_c (the mass of the c-quark, ~ 1.5 GeV) or m_s, m_d, m_u (the masses of the light quarks, $\sim 100 - 0$ MeV). This offers the opportunity to describe weak processes occurring at low energy in terms of Effective Hamiltonians (EH).

In the EW+QCD theory, besides the fundamental couplings, we find new, effective local interactions which originate as one-loop effects from the elementary couplings of the theory. These low energy effective vertices, appearing as one-loop effects, are suppressed by $O(\alpha)$ or $O(\alpha_s)$ coefficients (where α and α_s are the EW and the QCD coupling constant respectively). Nevertheless, they can be enhanced by other effects, such as QCD-radiative corrections, etc. (see below).

In order to see how these vertices are originated, one has only to consider a given weak process at low-energy, where all the heavier degrees of freedom have been integrated out. Thus, besides the well-known four-fermion Fermi interaction (see fig.(2.1)), we can find also FCNC (Flavour Changing Neutral Current) effective vertices, cf. fig.(2.2), or box vertices, cf. fig.(2.3).

These vertices do not introduce new parameters: they depend only on the CKM matrix elements and on quark masses. This last feature emphasizes their importance: they are an indirect but powerful way to investigate the effects of heavy quarks or new physics. These effective vertices are the basis of the physics of FCNC (Flavour Changing Neutral Currents).

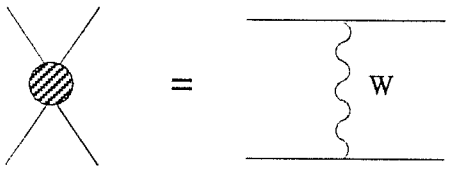

Figure 2.1: Effective four-fermion interaction.

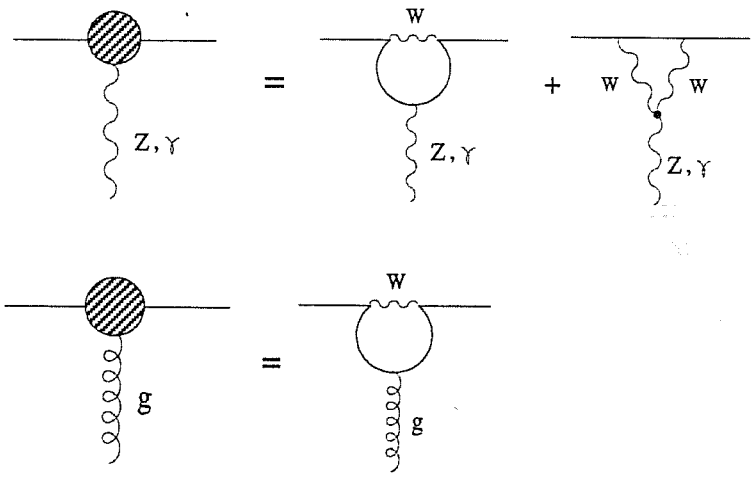

Figure 2.2: Effective penguin vertices.

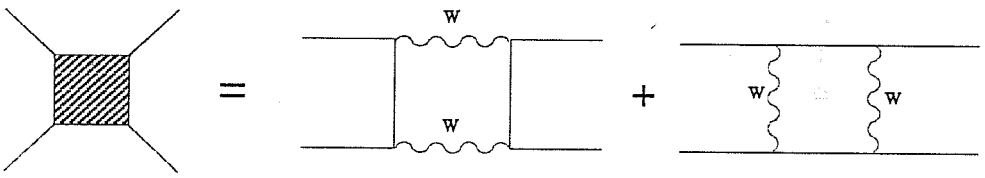

Figure 2.3: Effective box vertices.

Generally speaking, the EH ($\mathcal{H}_{eff}$) which describes a given weak process at a scale μ consists of the product of two weak currents. Through OPE, $\mathcal{H}_{eff}$ can be expanded over an operator basis $\{O_i\}$ for given coefficients C_i in a standard way:

$$\mathcal{H}_{eff} = \frac{G_F}{\sqrt{2}} \sum_i C_i O_i \tag{2.1}$$

The physical amplitude relative to the weak decays of a given meson (K, B,...) will be of the form:

$$\langle F|\mathcal{H}_{eff}|I\rangle = \frac{G_F}{\sqrt{2}} \sum_i C_i \langle F|O_i|I\rangle \tag{2.2}$$

where F and I represent the final and the initial state respectively. The simple form of $\mathcal{H}_{eff}$ has an enormous importance from many points of view.

- First of all, the OPE in terms of local operators and Wilson coefficient functions give us the possibility of separating the perturbative contributions to the amplitude from the non-perturbative ones.

  The non-perturbative part consists of the matrix elements of the operators $\{O_i\}$. This part is presently more difficult to evaluate and it still demands for improvements on the theoretical side.

  On the other hand, the Wilson coefficients C_i can be computed perturbatively in a systematic way. We will discuss in great detail the perturbative evaluation of the coefficient functions besides the Leading Order and the interplay between strong and EW interactions effects. QCD-corrections are known to modify the Wilson coefficients by a sensible amount. This is in particular true for non-leptonic weak decays, where gluons can be exchanged between both the quark weak currents.

- From $\mathcal{H}_{eff}$ one can obtain scale independent physical results: the μ-scale dependence cancels between operators and coefficients. Thus, one has the freedom of choosing the scale at which coefficients and operators match, depending on the physical problem of interest ($O(1\text{ GeV})$, $O(m_c)$, $O(m_b)$ for K-, D- or B-decays respectively). Different scales will correspond to different operator sets, which will reproduce the correct physics when matched by suitable coefficients.

- Finally, the presence in the theory of very different mass scales implies not only the possibility of an effective field theory formulation, but also the appearance of very large logarithms in the theory itself, as $\log \frac{M_W^2}{\mu^2}$, $\log \frac{m_t^2}{\mu^2}$, etc. The usual perturbative expansion needs to be improved, i.e. logarithms as $\log \frac{M_W^2}{\mu^2}$ need to be resummed to all orders in α_s (in a given approximation for α_s: LO, NLO, etc.). This is achieved by RG (Renormalization Group) techniques, keeping in mind the μ-independence of $\mathcal{H}_{eff}$ mentioned above.

  We will see in detail how this works up to NLO and give the general expression of the RG-improved coefficients at whatever "perturbative" (≥ 1 GeV) scale.

In the following we will explain the details of the basic formalism for the scale evolution of the Wilson coefficients. The problem will be developed in three main steps, where we will consider:

Step 1 : the case of an EH given by a single local operator, with only QCD radiative corrections;

Step 2 : the case of an EH expressed in terms of a complete basis of local operators $\{O_i\}$, with only QCD radiative corrections;

Step 3 : the case of the EH at **Step 2**, with also QED radiative corrections switched on.

Step 1

Let us consider the case of an EH defined by a single operator with coefficient function:

$$C\left(\frac{Q^2}{\mu^2}, \alpha_s\right) \tag{2.3}$$

where we have given the explicit dependence on the following quantities:

- α_s, the strong coupling constant;
- μ^2, the renormalization subtraction mass scale (fixed scale);
- Q^2, the generic scale.

The coefficients are taken to be dimensionless.

The scale independence of the EH provides the following RG equation for the coefficient function[1]:

$$\left\{-\frac{\partial}{\partial t} + \beta(\alpha)\frac{\partial}{\partial \alpha} - \bar{\gamma}(\alpha)\right\} C(t, \alpha) = 0 \tag{2.4}$$

where $\beta(\alpha)$ is the QCD β-function, defined by:

$$\beta(\alpha) = \frac{\partial \alpha}{\partial \ln \mu^2} = -\frac{\partial \alpha}{\partial t} \qquad \left(t = \ln \frac{Q^2}{\mu^2}\right) \tag{2.5}$$

and, $\bar{\gamma}(\alpha)$ is determined in terms of the anomalous dimensions of the operator related to the coefficient and of the weak current as:

$$\bar{\gamma}(\alpha) = \gamma(\alpha) - 2\gamma_J \tag{2.6}$$

[1] we drop the index $_s$ in the first two steps, since there we are concerned only with QCD corrections: α will mean α_s everywhere and the same convention will old for all the other "strong" quantities involved.

Beyond the leading order the anomalous dimension of the weak current is in general not zero, depending on the renormalization scheme.

Both $\beta(\alpha)$ and $\bar{\gamma}(\alpha)$ have a perturbative expansion of the form:

$$\beta(\alpha) = -b\alpha^2(1 + b'\alpha + \cdots) \tag{2.7}$$

and

$$\bar{\gamma}(\alpha) = \bar{\gamma}^{(0)}\alpha + \bar{\gamma}^{(1)}\alpha^2 + \cdots \tag{2.8}$$

where

$$b = \frac{11N - 2N_f}{12\pi} \quad , \quad b' = \frac{1}{(4\pi)^2 b}\left[\frac{34}{3}N^2 - \frac{13}{3}NN_f + \frac{N_f}{N}\right] \tag{2.9}$$

The solution of the (2.4) has the familiar form:

$$C(t,\alpha) = C(0,\alpha(t))\exp\left\{\int_\alpha^{\alpha(t)} \frac{\bar{\gamma}(\alpha')}{\beta(\alpha')}d\alpha'\right\} \tag{2.10}$$

where $\alpha(t)$ is the running coupling constant at the scale Q^2 and α is the running coupling constant at scale μ^2. $C(0,\alpha(t))$ is the initial condition for the evolution of the coefficient function and it has the following series expansion:

$$C(0,\alpha) = 1 + C^{(1)}\alpha + \cdots \tag{2.11}$$

It is clear that, starting from (2.7), (2.8) and (2.11), we can expand at a given order the solution of the Renormalization Group equation (2.4).

We now give some more details on this point. From the perturbative expansion of $\beta(\alpha)$, one can derive different expressions of the running QCD coupling constant, in different approximations, at one- or two-loop order.

- In the LLA (Leading Logarithm Approximation) the term b' is neglected and one has:

$$\alpha(t) \simeq \frac{\alpha}{1 + b\alpha t} = \frac{1}{b\ln(Q^2/\Lambda^2)} \tag{2.12}$$

where the momentum scale Λ, the QCD scale parameter, is defined by:

$$\Lambda = \mu\exp\left(-\frac{1}{2b\alpha}\right) \tag{2.13}$$

or

$$\ln\frac{\mu^2}{\Lambda} = \frac{1}{b\alpha} \tag{2.14}$$

QCD asymptotic freedom is evident in the behaviour of $\alpha(t)$.

LLA means in fact that only terms of the form $(\alpha t)^n$ are kept at each order n in perturbation theory. In presence of large logarithms in the theory these terms are not negligible, because we work in the limit:

$$\begin{aligned} \alpha &\ll 1 \\ \alpha t &\simeq (\alpha t)^n \simeq 1 \end{aligned} \tag{2.15}$$

- The NLO (Next to Leading Order logarithms) expression of the running coupling constant is obtained by including b' too. In this case:

$$\alpha(t) = \alpha_0(t)\left[1 + b'\alpha_0(t)\ln\frac{\alpha_0(t)}{\alpha} + O(\alpha_0^2(t))\right] \tag{2.16}$$

where $\alpha_0(t)$ is the LLA expression for α_s, or:

$$\begin{aligned}\alpha(t) &= \alpha_0(t)\left[1 - b'\alpha_0(t)\ln\ln\frac{Q^{2\,2}}{\Lambda} + O(\alpha_0^2(t))\right] = \\ &= \frac{1}{b\ln(Q^2/\Lambda^2)}\left[1 - \frac{b'}{b}\frac{\ln\ln(Q^2/\Lambda^2)}{\ln(Q^2/\Lambda^2)} + O(\alpha_0^2(t))\right]\end{aligned} \tag{2.17}$$

and

$$\ln\frac{\mu^2}{\Lambda^2} = \frac{1}{b\alpha} + \frac{b'}{b}\ln(b\alpha) \tag{2.18}$$

In the NLO approximation, not only terms of the form $(\alpha t)^n$ but also terms of the form $\alpha(\alpha t)^n$ are retained. They are usually smaller than the LLA contributions, but not negligible. The NLO contributions play an important role in the definition of several physical quantities, as explained in the introduction.

The evolution equation for the coefficient, eq.(2.4) combined with the expansions (2.7) and (2.8) results in the following NLO expression:

$$C(\alpha,t) = (1 + C^{(1)}\alpha)\left[\frac{\alpha}{\alpha(t)}\right]^{\gamma^{(0)}/b}\left\{1 + \frac{\alpha - \alpha(t)}{\pi}R + \cdots\right\} \tag{2.19}$$

where

$$\left[\frac{\alpha}{\alpha(t)}\right]^{\gamma^{(0)}/b} \tag{2.20}$$

represents the resummation of the leading logarithm corrections, while

$$R = \frac{\pi}{b}\left[\bar{\gamma}^{(1)} - bC^{(1)} - b'\gamma^{(0)}\right] \tag{2.21}$$

and the NLO expression for α in (2.16) is used.

We still have to determine the initial conditions for the coefficient function in (2.11). In the LLA the initial condition for the coefficient function is given by the tree level result, $C^{(0)}$. At NLO we need to evaluate the one-loop term $C^{(1)}$ of the coefficient expansion. $C^{(1)}$ is obtained by matching (at a given order) the full theory (with W, t-quark, etc.) with the effective one, where heavy degrees of freedom have been integrated out. The matching is improved at one-loop on finite parts of different amplitudes. In order to obtain consistent results the same renormalization scheme used in the whole NLO calculation has to be used.

The contribution of the full theory will be of the form $T\left(M_W^2/-p^2,\alpha\right)$ and the one of the effective theory of the form $A\left(-p^2/\mu^2,\alpha\right)$. The coefficient function $C\left(M_W^2/\mu^2,\alpha\right)$ will match the two scales. By definition:

$$T\left(\frac{M_W^2}{-p^2},\alpha\right) = C\left(\frac{M_W^2}{\mu^2},\alpha\right) A\left(\frac{-p^2}{\mu^2},\alpha\right) \tag{2.22}$$

In particular:

$$\begin{aligned} T\left(\frac{M_W^2}{-p^2},\alpha\right) &= \left[1+\frac{\alpha}{4\pi}\left(-\frac{1}{2}\gamma^{(0)}\ln\frac{M_W^2}{-p^2}+\tilde{T}\right)\right] O \\ C\left(\frac{M_W^2}{\mu^2},\alpha\right) &= \left[1+\frac{\alpha}{4\pi}\left(-\frac{1}{2}\gamma^{(0)}\ln\frac{M_W^2}{\mu^2}+C^{(1)}\right)\right] \\ A\left(\frac{-p^2}{\mu^2},\alpha\right) &= \left[1+\frac{\alpha}{4\pi}\left(-\frac{1}{2}\gamma^{(0)}\ln\frac{-p^2}{\mu^2}+\tilde{A}\right)\right] O \end{aligned} \tag{2.23}$$

where O is the operator in the EH and the explicit dependence on the different mass scales is shown. The logarithmic terms match each other and the analogous matching should be satisfied by the finite parts, i.e.:

$$C^{(1)} = \tilde{T} - \tilde{A} \tag{2.24}$$

This ends up with case of a single operator Effective Theory.

Step 2

The case of a single operator is quite useful to fix the main ideas. More often however one has to deal with much more complicated operator bases. We will see now how **Step 1** can be generalized to the case of a multi-operator basis. We will have a vector of coefficient functions $\vec{C}(t,\alpha)$ and a matrix of anomalous dimensions $\hat{\vec{\gamma}}(\alpha)$. Using a *vectorial* formalism, we can give the Effective Hamiltonian in the form:

$$\mathcal{H}_{eff} = \vec{O}^T(t)\vec{C}(t) \tag{2.25}$$

where $\vec{C}(t)$ and $\vec{O}(t)$ are the vectors of the coefficient functions and of the operators respectively and $\vec{C}(t)$ includes also the dependence on $\alpha(t)$. The RG eq.(2.4) in the matrix case reads:

$$\left\{-\frac{\partial}{\partial t}+\beta(\alpha)\frac{\partial}{\partial\alpha}-\hat{\vec{\gamma}}(\alpha)\right\}\vec{C}(t,\alpha)=0 \tag{2.26}$$

where $\hat{\vec{\gamma}}(\alpha)$ has a perturbative expansion in α analogous to the one in (2.8) and, as before, $\hat{\vec{\gamma}}(\alpha)$ means $(\hat{\gamma}(\alpha)-2\hat{\gamma}_J)$. If the anomalous dimension matrix is not diagonal, each non-diagonal elements $\hat{\vec{\gamma}}_{ij}(\alpha)$ expresses the mixing under renormalization between operator O_i and operator O_j. The generic solution of (2.26) is now given by:

$$\begin{aligned} \vec{C}(t,\alpha) &= T_\alpha \exp\left\{-\int_\alpha^{\alpha(t)} d\alpha' \frac{\hat{\vec{\gamma}}^T(\alpha')}{\beta(\alpha')}\right\}\vec{C}[\alpha(t)] \\ &= \hat{\mathbb{E}}[\alpha,\alpha(t)]\vec{C}[\alpha(t)] \end{aligned} \tag{2.27}$$

where

$$\vec{C}[\alpha(t)] = \vec{C}(0, \alpha(t)) \tag{2.28}$$

T_α denotes an ordered expansion over the coupling constants with an increasing coupling when going from the right to the left. This turns out to be the case, because $\hat{\vec{\gamma}}(\alpha)$ is now a matrix and:

$$\left[\hat{\vec{\gamma}}(\alpha_1), \hat{\vec{\gamma}}(\alpha_2)\right] \neq 0 \quad \text{for} \quad \alpha_1 \neq \alpha_2 \tag{2.29}$$

Explicitly, T_α-product means:

$$\begin{aligned} & T_\alpha \exp\left\{\int_\alpha^{\alpha(t)} d\alpha' \frac{\hat{\vec{\gamma}}^T(\alpha')}{\beta(\alpha')}\right\} = \qquad (2.30) \\ = \; & 1 + \int_\alpha^{\alpha(t)} d\alpha' \frac{\hat{\vec{\gamma}}^T(\alpha')}{\beta(\alpha')} + \int_\alpha^{\alpha(t)} \int_\alpha^{\alpha'} d\alpha' d\alpha'' \frac{\hat{\vec{\gamma}}^T(\alpha')}{\beta(\alpha')} \frac{\hat{\vec{\gamma}}^T(\alpha'')}{\beta(\alpha'')} + \cdots = \\ = \; & \exp\left[\frac{\hat{\gamma}^{(0)T}}{b} \ln \frac{\alpha}{\alpha(t)}\right] + \int_\alpha^{\alpha(t)} d\alpha' \exp\left[\frac{\hat{\gamma}^{(0)T}}{b} \ln \frac{\alpha'}{\alpha(t)}\right] \left(-\frac{\hat{\vec{\gamma}}^{(1)T}}{b}\right) \exp\left[\frac{\hat{\gamma}^{(0)T}}{b} \ln \frac{\alpha}{\alpha'}\right] \end{aligned}$$

to the required accuracy.

In order to find a solution for the evolution matrix:

$$\hat{\mathbb{E}}[\alpha(t), \alpha] = T_\alpha \exp\left\{\int_\alpha^{\alpha(t)} d\alpha' \frac{\hat{\vec{\gamma}}^T(\alpha')}{\beta(\alpha')}\right\} \tag{2.31}$$

let us introduce a matrix $\hat{\mathbb{V}}(\alpha)$ s.t.

$$\hat{\mathbb{E}}[\alpha(t), \alpha] = \hat{\mathbb{V}}[\alpha(t)] \hat{\mathbb{E}}^{(0)}[\alpha(t), \alpha] \hat{\mathbb{V}}^{-1}[\alpha] \tag{2.32}$$

where:

$$\hat{\mathbb{E}}^{(0)}[\alpha(t), \alpha] = \exp\left\{\frac{\hat{\gamma}^{(0)T}}{b} \ln \frac{\alpha}{\alpha(t)}\right\} \tag{2.33}$$

is the LLA evolution matrix. By comparison, differenziating the right hand side of (2.31) and (2.32) with respect to $\alpha(t)$, we get:

$$\frac{\partial \hat{\mathbb{V}}[\alpha(t)]}{\partial \alpha(t)} + \frac{1}{\alpha(t)} \left[\frac{\hat{\gamma}^{(0)T}}{b}, \hat{\mathbb{V}}[\alpha(t)]\right] = \left(\frac{\hat{\vec{\gamma}}^T(\alpha(t))}{\beta(\alpha(t))} + \frac{\hat{\gamma}^{(0)T}}{b} \frac{1}{\alpha(t)}\right) \hat{\mathbb{V}}[\alpha(t)] \tag{2.34}$$

Using the perturbative expansion of $\hat{\vec{\gamma}}^T(\alpha)$ and $\beta(\alpha)$ and writing $\hat{\mathbb{V}}[\alpha(t)]$ as:

$$\hat{\mathbb{V}}[\alpha(t)] \simeq \hat{\mathbb{I}} + \frac{\alpha(t)}{4\pi} \hat{\mathbb{V}}^{(1)} \tag{2.35}$$

we finally get:

$$\hat{\mathbb{V}}^{(1)} + \left[\frac{\hat{\gamma}^{(0)T}}{b}, \hat{\mathbb{V}}^{(1)}\right] = 4\pi \left(-\frac{\hat{\vec{\gamma}}^{(1)T}}{b} + \hat{\gamma}^{(0)T} \frac{b'}{b}\right) \tag{2.36}$$

The solution of eq. (2.36) will define the matrix $\hat{\mathbb{V}}^{(1)}$, which summarizes the NLO corrections to the evolution matrix for the coefficient function. In fact:

$$\hat{\mathbb{E}}[\alpha(t),\alpha] = \left(\hat{\mathbb{I}} + \frac{\alpha(t)}{4\pi}\hat{\mathbb{V}}^{(1)}\right)\hat{\mathbb{E}}^{(0)}[\alpha(t),\alpha]\left(\hat{\mathbb{I}} - \frac{\alpha}{4\pi}\hat{\mathbb{V}}^{(1)}\right) \tag{2.37}$$

In order to find a solution we have still the freedom of choosing a suitable operator basis. It is common in literature and useful in calculation to chose the basis which diagonalize $\hat{\gamma}^{(0)T}$. If $\hat{\mathbb{U}}$ is the matrix which diagonalize $\hat{\gamma}^{(0)T}$:

$$\hat{\gamma}_D^{(0)} == \hat{\mathbb{U}}^{-1}\hat{\gamma}^{(0)T}\hat{\mathbb{U}} \tag{2.38}$$

we will denote the other transformed matrices as:

$$\hat{\mathbb{G}}^{(1)} = \hat{\mathbb{U}}^{-1}\hat{\gamma}^{(1)T}\hat{\mathbb{U}} \tag{2.39}$$

and

$$\hat{\mathbb{W}}^{(1)} = \hat{\mathbb{U}}^{-1}\hat{\mathbb{V}}^{(1)}\hat{\mathbb{U}} \tag{2.40}$$

The LLA evolution matrix results automatically diagonalized:

$$\begin{aligned}\hat{\mathbb{E}}^{(0)}[\alpha(t),\alpha]_D &= \hat{\mathbb{U}}^{-1}\left[\exp\left(\frac{\hat{\gamma}^{(0)T}}{b}\ln\frac{\alpha}{\alpha(t)}\right)\right]\hat{\mathbb{U}} = \\ &= \left[\frac{\alpha}{\alpha(t)}\right]^{\frac{\hat{\gamma}_D^{(0)}}{b}}\end{aligned} \tag{2.41}$$

where $\vec{\gamma}^{(0)}$ is the vector whose components are the eigenvalues of $\hat{\gamma}^{(0)T}$.

In this basis the previous equation reads:

$$\mathbb{W}^{(1)} + \left[\frac{\hat{\gamma}_D^{(0)}}{b}, \mathbb{W}^{(1)}\right] = 4\pi\left(-\frac{\hat{\mathbb{G}}^{(1)}}{b} + \hat{\gamma}_D^{(0)}\frac{b'}{b}\right) \tag{2.42}$$

from which it is possible to find the $\hat{\mathbb{W}}^{(1)}$ matrix elements explicitly:

$$\mathbb{W}_{ij}^{(1)} = 4\pi\frac{b'}{b}\delta_{ij}\gamma_i^{(0)} - 4\pi\frac{\mathbb{G}_{ij}^{(1)}}{b + \gamma_{Dii}^{(0)} - \gamma_{Djj}^{(0)}} \tag{2.43}$$

In order to derive the final form for the evolution of $\vec{C}$, let us fix the initial and final mass scales to be M_W^2 and μ. As we have seen at **Step 1**, in order to have the complete evolution from $\vec{C}(M_W^2)$ to $\vec{C}(\mu)$, we need an extra input, i.e. the initial conditions $\vec{C}(M_W^2)$. The calculation of $\vec{C}(M_W^2)$ is strictly analogous to the simpler case explained before. at **Step 1** for a single operator ET. The vector $\vec{C}(M_W^2)$ is still given by the matching conditions between the full theory at the larger scale and the ET at the lower scale, when both the theories have been renormalized in the same renormalization scheme. The matching, generalized to the vector case, works as in

(2.22) and (2.24): the logarithms combine to give a final $\ln \frac{M_W^2}{\mu^2}$ dependence from the initial and final state mass scale, while the finite parts match as in (2.24).

The direct calculation of the matching on the finite parts has now to account for the operator mixing. The one-loop contribution of the full theory will be of the form[2]:

$$T = \left[\vec{T}^{(0)} + \frac{\alpha}{4\pi}\vec{T}^{(1)}\right] \langle \vec{Q}^{(0)} \rangle \tag{2.44}$$

where $\langle \vec{Q}^{(0)} \rangle$ are the tree level matrix elements of the operator of the basis. The analogous one-loop contribution in the ET will read:

$$\vec{A} = \langle \vec{Q}[\alpha(M_W)] \rangle = \left[\hat{\mathbb{I}} + \frac{\alpha}{4\pi}\hat{r}\right] \langle \vec{Q}^{(0)} \rangle \tag{2.45}$$

where $\langle \vec{Q}[\alpha(M_W)] \rangle$ are the set of the one-loop matrix elements, renormalized at a given scale. The matrix $\hat{r}$ is the matrix of the finite parts of the one-loop diagrams in the Effective Theory, for a given choice of the external momenta and a given subtraction scheme. The matrix $\hat{r}$ accounts for the mixing between the operators of the basis as well as the anomalous dimension matrix does (with respect to the pole part contributions).

Using (2.44) and (2.45), from the definition of the coefficient function:

$$T = \vec{C}[\alpha(M_W)]^T \langle \vec{Q}[\alpha(M_W)] \rangle \tag{2.46}$$

we get:

$$\vec{C}(M_W) = \vec{T}^{(0)} + \frac{\alpha(M_W)}{4\pi}\left[\vec{T}^{(1)} - \hat{r}^T \vec{T}^{(0)}\right] \tag{2.47}$$

We have finally all the ingredients to obtain the complete expression for the evolution of the coefficient function vector. From (2.47), (2.37) and (2.28) we get:

$$\begin{aligned} \vec{C}(\mu) &= \left(\hat{\mathbb{I}} + \frac{\alpha(\mu)}{4\pi}\hat{\mathbb{V}}^{(1)}\right) \hat{\mathbb{E}}^{(0)}[\mu, M_W] \left(\hat{\mathbb{I}} - \frac{\alpha(M_W)}{4\pi}\hat{\mathbb{V}}^{(1)}\right) \left(\vec{C}^{(0)T} + \frac{\alpha(M_W)}{4\pi}\vec{C}^{(1)T}\right) \\ &= \left(\hat{\mathbb{I}} + \frac{\alpha(\mu)}{4\pi}\hat{\mathbb{V}}^{(1)}\right) \hat{\mathbb{E}}^{(0)}[\mu, M_W] \left(\vec{T}^{(0)} + \frac{\alpha(M_W)}{4\pi}\vec{T}^{(1)} - \frac{\alpha(M_W)}{4\pi}\left[r^T + \hat{\mathbb{V}}^{(1)}\right]\vec{T}^{(0)}\right) \end{aligned} \tag{2.48}$$

An important observation is necessary at this point. Many terms appearing in eq. (2.48) depend on the number of flavours active at a given scale between M_W and μ. The one-loop and the two-loop anomalous dimension matrices as well as the $\hat{r}$ matrix are flavour-dependent. In order to compute $\vec{C}(\mu)$ from (2.48) one has to take into account that some heavy flavours are integrated out and different Effective Theories are considered. Every time one crosses the threshold between two different Effective Theories, matching conditions have to be imposed and this plays a fundamental role in the numerical implementation of (2.48) of the final result.

[2]We drop here the explicit dependence on the reference mass scales, because it is already given for the simpler case of only one operator(/coefficient) in (2.22) and (2.24)

Finally, let us remember that in a NLO calculation both the one-loop coefficient function and the two-loop anomalous dimension are renormalization scheme dependent. Nevertheless the RS-dependence cancels out between them. Thus, if we change f.i. the renormalization prescription for the operators $\{O_i\}$, defining a new operator set [3] as:

$$\vec{O}'^T[\alpha] = \vec{O}^T[\alpha]\hat{\tau}[\alpha] \simeq \vec{O}^T[\alpha]\left[\hat{\mathbb{I}} + \alpha\hat{\tau}^{(1)} + \cdots\right] \tag{2.49}$$

then the evolution matrix and the initial conditions for the coefficient functions will change according to:

$$\begin{aligned} & \vec{O}^T[\alpha]\hat{\mathbb{E}}[\alpha,\alpha(t)]\vec{C}[\alpha(t)] \qquad (2.50)\\ = \; & \vec{O}^T[\alpha]\hat{\tau}[\alpha]\hat{\tau}^{-1}[\alpha]\hat{\mathbb{E}}[\alpha,\alpha(t)]\hat{\tau}[\alpha(t)]\hat{\tau}^{-1}[\alpha(t)]\vec{C}[\alpha(t)] \\ = \; & \vec{O}'^T[\alpha]\hat{\mathbb{E}}'[\alpha,\alpha(t)]\vec{C}'[\alpha(t)] \end{aligned}$$

where we see that the initial condition vector and the evolution matrix transform as:

$$\vec{C}'[\alpha] = \vec{C}[\alpha]\hat{\tau}^{-1}[\alpha] \tag{2.51}$$

$$\hat{\mathbb{E}}'[\alpha,\alpha(t)] = \hat{\tau}[\alpha]\hat{\mathbb{E}}[\alpha,\alpha(t)]\hat{\tau}^{-1}[\alpha] \tag{2.52}$$

We will have the possibility to verify calculations defined by different renormalization prescriptions in the two-loop computation of the vertex+penguin anomalous dimension matrix.

Step 3

We will consider here the same ET as in **Step 2** but with both QCD and EW-corrections[4]. In spite of the smallness of the EW coupling constant[5], EW-corrections can be relevant either because of the particular physical quantity of interest or because of non-perturbative enhancement. Due to their different chiral structure, EW-operators can be enhanced or suppressed in a complete independent way with respect to the QCD ones.

If this is the case, the EH for a given weak process should be modified in order to take care of $O(\alpha_{em})$ corrections. $O(\alpha_{em}^2)$ corrections are obviously neglected to a very good approximation. The analysis at **Step 2** is still valid and needs only to be generalized to the case of a theory with two coupling constants. Let us denote the two couplings as α_s and α_e. The RG equation (2.26) has an obvious generalization to:

$$\left\{-\frac{\partial}{\partial t} + \beta_s(\alpha_s)\frac{\partial}{\partial\alpha_s} + \beta_e(\alpha_e)\frac{\partial}{\partial\alpha_e} - \hat{\tilde{\gamma}}_s(\alpha_s) - \hat{\tilde{\gamma}}_e(\alpha_e)\right\}\vec{C}(t,\alpha_s,\alpha_e) = 0 \tag{2.53}$$

where we can imagine for $\beta_e(\alpha_e)$ and $\hat{\tilde{\gamma}}_e(\alpha_e)$ analogous definitions and analogous expansions as the ones given for $\beta_s(\alpha_s)$ and $\hat{\tilde{\gamma}}_s(\alpha_s)$ in (2.5)-(2.8). The calculation of the

[3] where we have supposed that the definitions for the two operator sets coincide at the tree level

[4] Electro-Weak corrections, i. e. both photon and Z^0 boson corrections

[5] we will chose it to be the QED coupling constant, α_{em}.

one-loop and two-loop coefficients of the expansion of $\hat{\vec{\gamma}}_s(\alpha_s)$ and $\hat{\vec{\gamma}}_e(\alpha_e)$ will be given in detail in section (2.2) and in the next chapter. In a theory with two coupling constants, more diagrams contribute to a given physical process and the operator basis is enlarged. The solution of equations (2.53) will be analogous to (2.28), modified in order to account for $O(\alpha_e)$ effects:

$$\vec{C}^T(t,\vec{\alpha}) = \hat{\mathbb{E}}'[\vec{\alpha},\vec{\alpha}(t)]\vec{C}^T[\vec{\alpha}(t)] \tag{2.54}$$

where:

$$\hat{\mathbb{E}}'[\vec{\alpha}(t),\vec{\alpha}] = T\exp\int_0^t dt'\left(\hat{\vec{\gamma}}_s(\alpha_s)+\hat{\vec{\gamma}}_e(\alpha_e)\right) \tag{2.55}$$

and

$$\vec{C}^T[\vec{\alpha}(t)] = \vec{C}^T[0,\vec{\alpha}(t)] \tag{2.56}$$

with a straightforward modification of (2.31) and (2.28), and $\vec{\alpha}$ is a shorthand notation to indicate the set of the two coupling constants:

$$\vec{\alpha} = (\alpha_s,\alpha_e) \tag{2.57}$$

The new evolution matrix $\hat{\mathbb{E}}'[\vec{\alpha},\vec{\alpha}(t)]$ is very complicated. It greatly simplifies if we consider only $O(\alpha_e \ln(M_W^2/\mu^2))$ corrections, while keeping all orders in $\alpha_s \ln(M_W^2/\mu^2))$, as explained in ref. [41, 42] and [14] (where only the LLA case was considered).

In the LLA case, with both $O(\alpha_s)$ and $O(\alpha_e)$ corrections taken into account, the evolution matrix results to be of the form:

$$\hat{\mathbb{E}}'^{(0)} = \left(\hat{\mathbb{I}} + \frac{\alpha_e}{\alpha_s(\mu)}\hat{\mathbb{P}}\right)\hat{\mathbb{E}}_s^{(0)} \tag{2.58}$$

where the running of α_e is completely neglected,because it turns out to have very slight relevance (about 1%). In (2.58) $\hat{\mathbb{E}}_s^{(0)}$ is the strong LO evolution matrix in eq.(2.33) and $\hat{\mathbb{P}}$ can be determined as follows. Using eq.(2.54) and (2.55), in the LLA we get that:

$$\vec{C}^T(t,\vec{\alpha}) = \hat{\mathbb{E}}^{(0)}[\vec{\alpha},\vec{\alpha}(t)]\vec{C}^T[\vec{\alpha}(t)] \tag{2.59}$$

and

$$\frac{d\vec{C}^T(t,\vec{\alpha})}{d\alpha(t)} = \left\{\frac{\hat{\gamma}_s^{(0)}\alpha_s + \hat{\gamma}_e^{(0)}\alpha_e}{2b\alpha_s^2}\right\}\vec{C}^T(t,\vec{\alpha}) \tag{2.60}$$

Keeping only the leading terms in the perturbative expansion, we get for $\hat{\mathbb{P}}$ the following equation:

$$\hat{\mathbb{P}} + \left[\hat{\mathbb{P}}, \frac{\hat{\gamma}_s^{(0)}}{2b}\right] = \frac{\hat{\gamma}_e^{(0)}}{2b} \tag{2.61}$$

In the basis where $\hat{\gamma}_s^{(0)}$ is diagonal, the explicit solution for (2.61) is given by:

$$\hat{\mathbb{P}}_{ij} = \frac{\hat{\gamma}_{e_{ij}}^{(0)}}{2b + \hat{\gamma}_{Ds_{jj}}^{(0)} - \hat{\gamma}_{Ds_{ii}}^{(0)}} \tag{2.62}$$

On the other hand, at NLO in the strong interactions, but always at $O\left(\alpha_e \ln \frac{M_W^2}{\mu^2}\right)$ in the EW interactions, the expression of the evolution matrix is a little more involved. It turns out to be of the form:

$$\begin{aligned}&\hat{\mathbb{E}}'[\vec{\alpha}(t),\vec{\alpha}] = \\ &\left(\hat{\mathbb{I}}+\frac{\alpha_s(t)}{4\pi}\hat{\mathbb{V}}^{(1)}\right)\left(\hat{\mathbb{I}}+\frac{\alpha_e}{\alpha_s(t)}\hat{\mathbb{K}}\right)\hat{\mathbb{E}}_s^{(0)}[\alpha_s(t),\alpha_s]\left(\hat{\mathbb{I}}-\frac{\alpha_e}{\alpha_s}\hat{\mathbb{K}}\right)\left(\hat{\mathbb{I}}-\frac{\alpha_s}{4\pi}\hat{\mathbb{V}}^{(1)}\right) \\ &+\int_0^t d\alpha_s'(t)\hat{\mathbb{E}}_s^{(0)}[\alpha_s(t),\alpha_s'(t)]\frac{\alpha_e\alpha_s'(t)}{(4\pi)^2}\hat{\mathbb{E}}_s^{(0)}[\alpha_s'(t),\alpha_s]\end{aligned} \tag{2.63}$$

where $\hat{\mathbb{K}}$ is a matrix to be determined applying the same methods explained for the one-loop case, i.e. using again eq.(2.54) and (2.55), but keeping this time NLO terms in the perturbative expansion.

2.2 Effective Hamiltonian for $\Delta S = 1$ and $\Delta B = 1$ non-leptonic-decays in the NLO approximation

The aim of this section is to specialize the general discussion outlined in section 2.1 to $\Delta S = 1$ and $\Delta B = 1$ non-leptonic-decays. We have studied the Effective Hamiltonian (EH) for these decays in the NLO approximation including QCD and to $O(\alpha_e \ln(M_W^2/\mu^2))$ corrections. This is precisely the case considered in **Step 3** of section 2.1: multi-operator basis + QCD-corrections at NLO approximation + EW-corrections at $O(\alpha_e)$. To be more specific we will articulate the discussion into many different points:

- the operator basis which defines the EH: which are the operators involved and how they appear;
- the initial conditions for the coefficient functions;
- the mixing between different operators under renormalization: how it works at one-loop and at two-loops, in presence of both QCD and QED corrections;
- structure and results for the one-loop and two-loop anomalous dimension matrices.

2.2.1 Operator basis

$\Delta S=1$ and $\Delta B=1$ non-leptonic decays can be described in the EH formalism on a basis of *vertex+penguin* operators. *Vertex*-operators are the usual four-fermion operators of

the Fermi-interaction (see fig.(2.1)) and they already appear at the tree level. On the other side, *Penguin*-operators are a one-loop effect (see fig.(2.2)) and can be expressed as a sum over flavours of vertex operators, as it is clear from their formal expression in (2.66).

The complete basis of operators in the EH depends on the kind of corrections considered for a given weak process. QCD-penguins arise from gluon-corrections, while QED-penguins or Z^0-penguins from photon or Z^0-corrections.

The operator basis has already been given in the discussion of ϵ'/ϵ. Here we will give it in a more explicit form and in a more general context. Greek indices $\alpha, \beta, \ldots$ denote the colour charge, latin indices denote the flavour, while $_{(V\mp A)}$ indicates the chiral structure of each fermion line, where we adopt the usual convention:

$$(\bar{q}_i q_j)_{(V\mp A)} = \bar{q}_i \gamma^\mu (1 \mp \gamma_5) q_j \tag{2.64}$$

Here following the standard basis necessary for $\Delta S = 1$ decays is reported, following for instance ref. [14]:

$$\begin{aligned}
\text{Vertex-type} \;\rightarrow\; & \begin{cases} O_1 = (\bar{s}_\alpha u_\beta)_{(V-A)} (\bar{u}_\beta d_\alpha)_{(V-A)} \\ O_2 = (\bar{s}u)_{(V-A)} (\bar{u}d)_{(V-A)} \end{cases} \\
\text{QCD-Penguins} \;\rightarrow\; & \begin{cases} O_3 = (\bar{s}d)_{(V-A)} \sum_q (\bar{q}q)_{(V-A)} \\ O_4 = (\bar{s}_\alpha d_\beta)_{(V-A)} \sum_q (\bar{q}_\beta q_\alpha)_{(V-A)} \\ O_5 = (\bar{s}d)_{(V-A)} \sum_q (\bar{q}q)_{(V+A)} \\ O_6 = (\bar{s}_\alpha d_\beta)_{(V-A)} \sum_q (\bar{q}_\beta q_\alpha)_{(V+A)} \end{cases} \\
\text{QED-Penguins} \;\rightarrow\; & \begin{cases} O_7 = \frac{3}{2} (\bar{s}d)_{(V-A)} \sum_q e_q (\bar{q}q)_{(V+A)} \\ O_8 = \frac{3}{2} (\bar{s}_\alpha d_\beta)_{(V-A)} \sum_q e_q (\bar{q}_\beta q_\alpha)_{(V+A)} \\ O_9 = \frac{3}{2} (\bar{s}d)_{(V-A)} \sum_q e_q (\bar{q}q)_{(V-A)} \\ O_{10} = \frac{3}{2} (\bar{s}_\alpha d_\beta)_{(V-A)} \sum_q e_q (\bar{q}_\beta q_\alpha)_{(V-A)} \end{cases}
\end{aligned} \tag{2.65}$$

For $\Delta B = 1$ decays one needs only to modify the external fields. from $(\bar{s}d)$ to $(\bar{b}d)$ or $(\bar{b}s)$.

There are two main features that should be stressed at this point.

- There is an evident dependence on active flavours in the basis and this is the reason why it can be used to describe many different physical situations. The real point is that different physical processes correspond to different mass scales, i.e. to different Effective Theories, with different number of flavours. For instance, all the penguin operators have the same structure at every mass scale, but not the same explicit expression: they are summed over different number of flavours in different Effective Theories. Thus, the previous set of operators (provided the modification on the initial states) describes a $\Delta B = 1$ non-leptonic decay at $\mu \sim m_b$, where the range of the summation index q goes from u-quark till b-quark included, and also a $\Delta S = 1$ non-leptonic decay at $\mu \sim m_s$, where the sums in the penguin-type operators extend only over u-,d- and s-quarks.

- The physical meaning of the previous set of operators is also understood in terms of related Feynman diagrams (see fig.(2.1) and (2.2) for vertex- and penguin-diagrams respectively). However, the basis $\{O_i\}$ presents more structures than those coming from the basic diagrams. This is essentially due to the action of radiative corrections on the Dirac- and colour-structure of the original operators and we consider in detail both the one-loop and the two-loop cases.

We will put particular emphasis on the evolution of the effective hamiltonian at different mass scales, starting from $\mu \sim m_t, M_W$, i.e. in the full theory comprehensive of all the physical particles, till low energies scales, where, depending on the number of *active* flavours, some particular ET holds.

At the tree level, the EH for a generic $\Delta F=1$ process can be written as[6]:

$$\mathcal{H}_{eff}^{(0)} = \lambda_u^* \frac{G_F}{\sqrt{2}} \left[(1-\tau)\left(O_2^{0(u)} - O_2^{0(c)}\right) + \tau\left(O_2^{0(u)} - O_2^{0(t)}\right)\right] = \mathcal{H}_c^{(0)} + \mathcal{H}_t^{(0)} \tag{2.66}$$

where the unitarity of the CKM matrix ($\hat{\mathbb{V}}$) has already been used and the notation for the CKM parameters is the standard one:

$$\lambda_i = \mathbb{V}_{is}^* \mathbb{V}_{id} \quad , \quad \tau = -\frac{\mathbb{V}_{ts}^* \mathbb{V}_{td}}{\mathbb{V}_{us}^* \mathbb{V}_{ud}} \tag{2.67}$$

Only one operator is present in the theory, the *physical* four-fermion vertex operator $O_2^{0(q_i)}$, given by:

$$O_2^{(q_i)} = (\bar{s}q_i)_{(V-A)}(\bar{q}_i d)_{(V-A)} \quad \text{for} \quad \Delta S=1 \text{ decays} \tag{2.68}$$

$$O_2^{(q_i)} = (\bar{b}q_i)_{(V-A)}(\bar{q}_i d)_{(V-A)} \quad \text{for} \quad \Delta B=1 \text{ decays} \tag{2.69}$$

where the given $O_2^{(q_i)}$ in the $\Delta B=1$ case corresponds to the B_d case. The analogous operator for the B_s case is obtained by replacing the d-quark with an s-quark in the expression for $O_2^{(q_i)}$.

In absence of QCD or EW corrections there is no way of generating new operators from the original one. Only the four-quark effective vertex is present and both the chiral and colour structure of $O_2^{(q_i)}$ are conserved. Rescaling the theory from higher to lower scales, corresponds to the elimination of the heavy degrees of freedom (i.e. heavy quarks). Starting at the M_W-scale[7], we first remove $O_2^{(t)}$, because of the explicit dependence on the top quark, and second we match the full theory with the $N_f=5$ Effective Theory under the W-thresholds. Then we evolve to m_b-scale: for $\Delta B=1$ processes we already get the *physical* scale, while for $\Delta S=1$ nothing changes at this threshold, because there is no explicit b-dependence. Proceeding in the evolution, at

[6]The index zero above the EH and the $O_2^{(q)}$ operators denotes that we are considering the tree level approximation: no QCD- or QED-corrections taken into account

[7]We always assume to integrate out the W, the top and whatever other very heavy particle at the M_W-scale. This is allowed in view of the of the smallness of the strong-coupling constant in that region, such that there are only very small running-effects.

the m_c-scale, also $O_2^{(c)}$ is dropped and we are finally left with the usual $N_f = 3$ Effective Theory for K-physics.

With the introduction of QCD and/or EW corrections new diagrams like those in fig.(1.6) and (2.4) appear and contribute to $\Delta S = 1$ and $\Delta B = 1$ amplitudes. The presence of new colour structures (due to gluon-exchange) and the isospin-breaking, due to photon exchanges, allow the mixing between O_2 and O_1 and generate penguin-operators and their mixing with vertex operators. QCD-corrections are responsible for $O_3 \dots O_6$ operators while EW-corrections for $O_7 \dots O_{10}$ operators. This mixing is already present at the one-loop level and is enhanced by two-loop corrections.

We now consider the one loop evolution in presence of QCD and EW corrections. At $\mu \gg M_W$, all the diagrams in fig.(1.6) contribute: all the operators in (2.66) are present plus those originating from box diagrams, namely:

$$O_{11} = (\bar{s}d)_{(V-A)}(\bar{b}b)_{(V-A)} \quad \text{and} \quad O_{12} = (\bar{s}b)_{(V-A)}(\bar{b}d)_{(V-A)} \tag{2.70}$$

O_{11} and O_{12} contribute only in the range between M_W and m_b. Due to the smallness of the strong coupling constant and of its running in this region, their contribution is negligible and they are not included in the operator basis from the beginning.

In principle, we should also account for diagrams with physical Higgs particles (f.i. penguin diagrams with H^0 exchanged in place of Z^0). Their presence would correspond to the introduction of a new operator of the form:

$$O_H = (\bar{s}(1-\gamma_5)d)(\bar{b}b) \tag{2.71}$$

plus similar ones where the b-quark is replaced by c, s, d or u quarks. The last ones can be immediately neglected because the Higgs coupling to fermions is proportional to their mass. O_H on the contrary could even give a relevant contribution, if not for two main features: first it does not mix at all with QCD-penguins; second its mixing with EW-penguins is already $O(\alpha_e^2)$ and we neglect it. Moreover, every other heavy particle in the theory should be considered at this level, as it is the case for extended version of the Standard Model (Two-doublets Higgs models, etc.) This means the introduction of new operators and it has been extensively studied in literature, for different extensions of the Standard Model. Nevertheless it goes beyond the spirit of the present calculation and we will not consider these cases at all.

From the above considerations, we see that it is enough to consider the diagrams in fig.(1.6) and the operators in (2.66).

The vertex-diagram contribution is finite. The the colour structure of the diagrams where a gluon in exchanged between the two quark lines is responsible for O_1-O_2 mixing. On the other hand QCD-penguins introduce in the theory a new Dirac-structure. Indeed, they have a $\gamma^\mu(1-\gamma_5)\otimes\gamma_\mu$ chiral structure, which can be decomposed in a Left-Left plus a Left-Right piece, that is:

$$\begin{aligned} \gamma^\mu(1-\gamma_5)\otimes\gamma_\mu &= \frac{1}{2}\gamma^\mu(1-\gamma_5)\otimes\gamma_\mu(1-\gamma_5) + \frac{1}{2}\gamma^\mu(1-\gamma_5)\otimes\gamma_\mu(1+\gamma_5) \\ &= \frac{1}{2}\gamma^\mu_L \otimes \gamma_{\mu L} + \frac{1}{2}\gamma^\mu_L \otimes \gamma_{\mu R} \end{aligned} \tag{2.72}$$

This explains the presence of *pairs* of operators with the same contractions on the colour indices, but with different chiral structure, precisely a Left-Right one for each Left-Left one (f.i. $(O_3,\ O_5)$, (O_4,O_6), etc.) The penguin-diagram contribution is not finite by itself, but as long as quarks are not distinguished by any mass isospin-breaking (f.i., at very high energy scale, where all quarks can be considered massless), the total contribution of penguin-diagrams cancels by GIM mechanism. The same observation holds also for the box-diagrams in (1.6).

Let us see how the previous ingredients combine in the evolution of the one-loop Hamiltonian for $\Delta F = 1$ weak non-leptonic decays. Remember the tree level approximation for the EH given in (2.66). $\mathcal{H}^{(0)}_{eff}$ is there expressed in terms of:

$$\mathcal{H}^{(0)}_c = (O_2^{0(u)} - O_2^{0(c)}) \quad \text{and} \quad \mathcal{H}^{(0)}_t = (O_2^{0(u)} - O_2^{0(t)}) \tag{2.73}$$

It is very useful and natural to consider the evolution of the EH in terms of these two combinations of $O_2^{0(q)}$-type operators. Indeed, they rescale in a quite independent way and we will suppose that, in presence of one-loop QCD+EW corrections, the mixing of the $O_2^{0(q)}$-type operators with all the other operators in (2.66) can be given as:

$$(O_2^{0(u)} - O_2^{0(c)}) \ \rightarrow \ \sum_{i=1}^{10} z_i(\mu) O_i(\mu) \tag{2.74}$$

$$(O_2^{0(u)} - O_2^{0(t)}) \ \rightarrow \ \sum_{i=1}^{10} y_i(\mu) O_i(\mu) \tag{2.75}$$

where the μ-dependence of the OPE is what we would like to clarify in the present discussion.

At scales $\mu \gg M_W$ or $\mu \gg m_t$, the only contribution comes from the mixing of the vertex operators, while penguin-diagram and box-diagram contributions cancel via GIM mechanism, as explained before. But at $\mu \sim M_W, m_t$ the isospin symmetry between quark is broken, because the top quark becomes much heavier than all the other quarks in the theory. The two parts of the EH, $\mathcal{H}^{(0)}_c$ and $\mathcal{H}^{(0)}_t$, start evolving in a quite different way. Indeed, the *light* sector $\mathcal{H}^{(0)}_c$ is not affected at all by the rescaling, because both u- and c-quark can still be considered as massless and their contribute is still given only in terms of vertex operator renormalization mixing. On the other hand, in the *heavy* sector $\mathcal{H}^{(0)}_t$ the GIM cancellation fails and all the diagrams in fig.(1.6) start contributing.

The W, the top quark as well as all other heavy particles present in the theory (i.e. the Z^0 or the heavy charged Higgses in extended models) are integrated out below the M_W threshold and a new $N_f = 5$ ET develops. Below M_W, only a subset of the original Feynman diagrams (see fig.(2.4)) will contribute to the EH. In particular we see that the Z^0-penguin contribution and the box-diagram contribution are present only in the full theory.

At $\mu \sim m_b$ also the explicit dependence on the b-quark is dropped (f.i. in the sum over flavours which define penguin-type operators), but no particular new features arise.

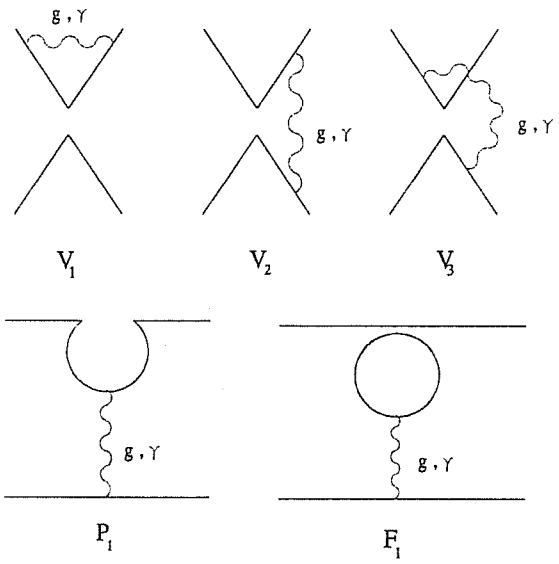

Figure 2.4: Diagrams contributing to the Effective Theory Hamiltonian at one loop

The operators related to the two box-diagrams in fig.((1.6), i.e. O_{11} and O_{12}, disappear below the b-threshold. Thus they would mix with other operators and contribute to the evolution of the EH in the $m_b \leq \mu \leq M_W$ region only. Due to the smallness of the strong coupling constant at these scales, we can safely neglect them[8]. On the contrary, at $\mu \sim m_c$, GIM mechanism is broken also in the *light* sector: the charm quark mass cannot be neglected anymore and the c-penguins need to be included in the EH. Moreover, the Effective Theory has now $N_f = 3$.

We note that the discussion of the one-loop mixing and of the one-loop evolution of the EH is important in the calculation of the one-loop initial condition for the coefficient functions, which will be treated in detail in paragraph (2.2.2).

The two-loop generalization of the previous arguments is straightforward. The mixing "dynamics" is much more complicated both in the full and in the effective theory. Nevertheless one does not need a complete evaluation of the two-loop EH in the full theory.

The two-loop form of the the EH requires the knowledge of some well-determined coefficients, as $\beta^{(0)}$, $\beta^{(1)}$ and $\hat{\vec{\gamma}}^{(0)}$ plus the two-loop anomalous dimension $\hat{\vec{\gamma}}^{(1)}$ and the one-loop coefficient-function $\vec{C}^{(1)}$, see sec.2.1. A good choice is to evaluate $\hat{\vec{\gamma}}^{(1)}$ in a five-quark ET just below M_W (so that all quarks are still massless) and to match it at $\mu \sim M_W$ with the full theory. The contributions of the full theory diagrams will only enter the evaluation of the coefficient functions $\vec{C}^{(1)}(M_W)$ at one-loop.

On the other hand, the evaluation of $\hat{\vec{\gamma}}^{(1)}$ is the real two-loop step. The Feynman diagrams present in the Effective Theory are given in fig.(2.5) for the vertex-diagram corrections and in fig.(2.6) for the penguin-diagram corrections. The colour and the

[8]It would correspond to a $\sim 0.5\%$ more uncertainty.

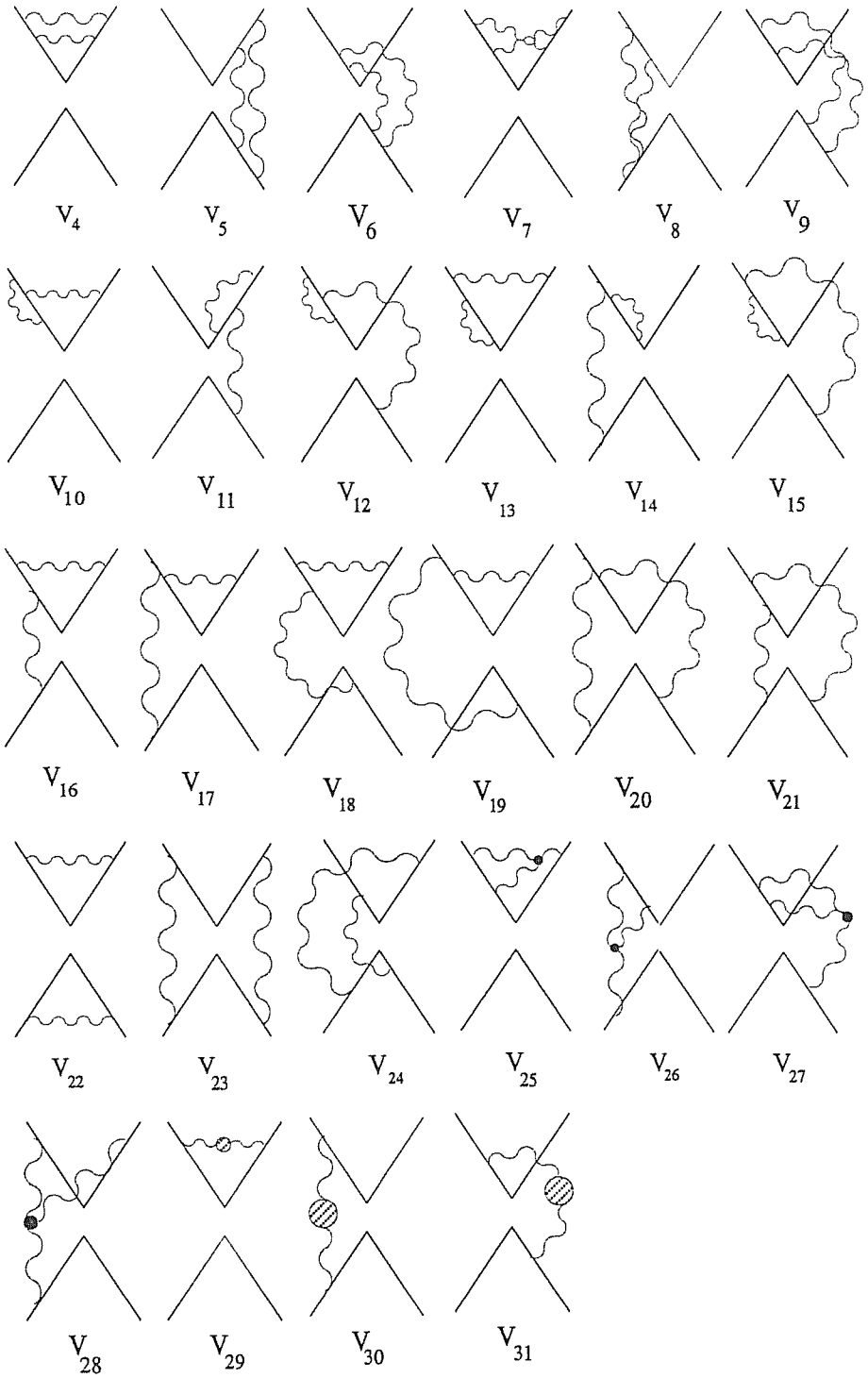

Figure 2.5: Vertex diagrams contributing to the Effective Theory Hamiltonian at two loops

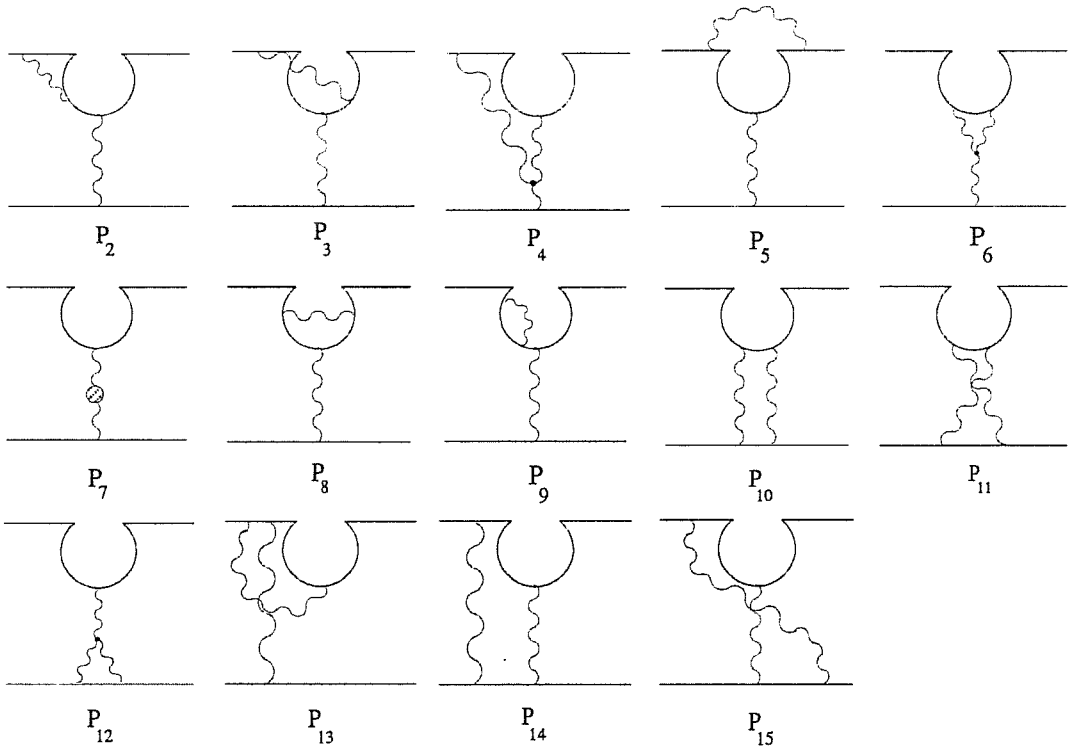

Figure 2.6: P-type Penguins diagrams contributing to the Effective Theory Hamiltonian at two loops

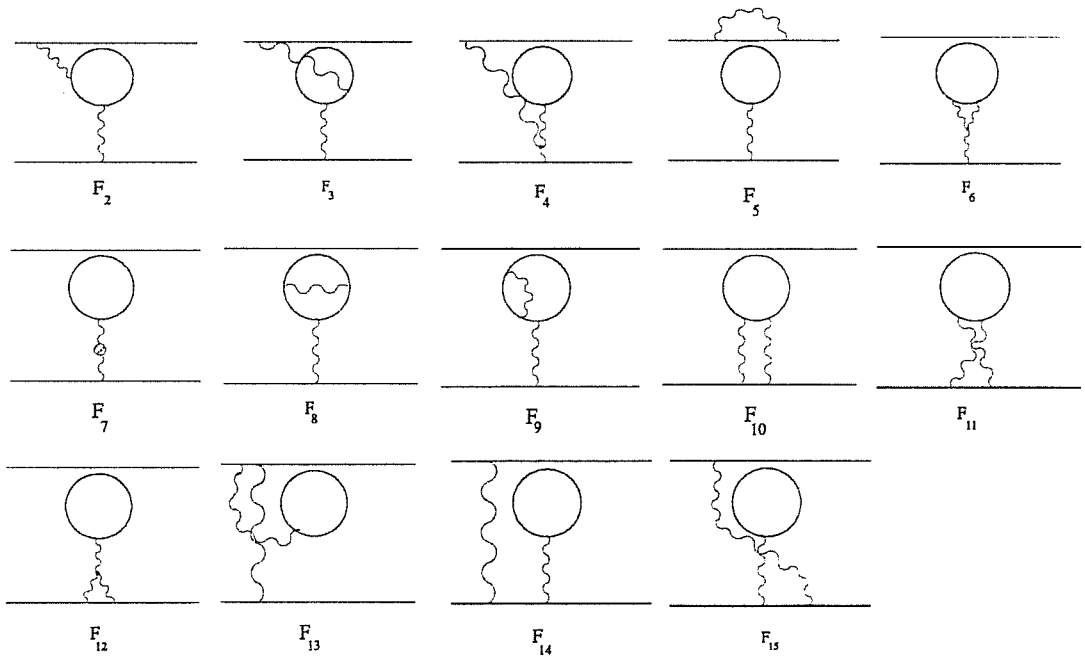

Figure 2.7: F-type Penguins diagrams contributing to the Effective Theory Hamiltonian at two loops

Dirac structure of each diagram is more complicated, but no new structure appears and the operator basis is still given by (2.66).

2.2.2 Initial conditions for the coefficient function

In the previous section we have explained the construction of the Effective Theory from $\mu \gg M_{\rm W}, m_t$ to $\mu \sim M_{\rm W}$. This is the region ($\mu \sim M_{\rm W}$) where we start the evolution of the coefficient functions (CF). Here we consider the problem of the determination of the initial conditions for the evolution of the CF.

We integrate out the W-boson and the top quark simultaneously [9]. Due to the smallness of the strong coupling constant and its poor running in this region, the effect of distinct thresholds is negligible. Below the thresholds, weak decays are described by a $N_f = 5$ Effective Theory. The full and the effective theory need to be renormalized in the same regularization scheme and the CF are finally obtained by matching the finite parts, as computed by (2.47). The determination of $\vec{T}^{(0)}$ does not present any problem: the only operator present at the tree level is O_2. On the other hand we need the expression of :

$$\vec{T}^{(1)} - r^T \vec{T}^{(0)} \tag{2.76}$$

where we have used the notation of section 2.2. The most "intuitive" way to understand the results of the one-loop coefficient functions is to show the matching at work diagram by diagram. Let us consider the tree level Hamiltonian in (2.66), expressed as the sum of two independent pieces:

$$\mathcal{H}_{eff}^{(0)} = \mathcal{H}_c^{(0)} + \mathcal{H}_t^{(0)} \tag{2.77}$$

As we have already seen in the previous subsection, the two terms $\mathcal{H}_c^{(0)}$ and $\mathcal{H}_t^{(0)}$ have a completely independent evolution, just because they concern two different physical sectors: the *light* and the *heavy* one respectively. Thus, when we consider QCD+EW one loop corrections, we can still write the Hamiltonian as:

$$\mathcal{H}_{eff} = \mathcal{H}_c + \mathcal{H}_t \tag{2.78}$$

Let us consider first $\mathcal{H}_t$. At $\mu \sim M_{\rm W}$ or m_t, the top mass is the UV cut-off of the theory and the flavour symmetry is broken by its mass term. Thus t- and u-contributions do not cancel anymore in penguin and box diagrams, fig.(1.6). We will have different contributions besides the vertex-diagrams. The one-loop corrected Hamiltonian will be constructed starting from:

- vertex diagrams;
- QCD-penguin diagrams;
- QED-penguin diagram (photon ones);

[9] For this reason, instead of "$M_{\rm W}$ threshold" we could also have said "m_t threshold".

Vertex-Type	*Coefficient*
$\mathrm{Box}(T_3=-1/2)$	$\lambda_t \frac{G_F}{\sqrt{2}} \frac{\alpha_e}{2\pi \sin^2\vartheta_W} B(x_t)(\gamma_L^\mu \otimes \gamma_{\mu L})$
$\mathrm{Box}(T_3=1/2)$	$\lambda_t \frac{G_F}{\sqrt{2}} \frac{\alpha_e}{2\pi \sin^2\vartheta_W} [-4B(x_t)](\gamma_L^\mu \otimes \gamma_{\mu L})$
$\bar{s}Zd$	$\lambda_t \frac{G_F}{\sqrt{2}} \frac{e}{2\pi^2 \sin^2\vartheta_W} C(x_t)\gamma_L^\mu$
$\bar{s}\gamma d$	$-\lambda_t \frac{G_F}{\sqrt{2}} \frac{e}{8\pi^2} D(x_t)\gamma^\mu$
$\bar{s}Gd$	$\lambda_t \frac{G_F}{\sqrt{2}} \frac{g_s}{2\pi^2} E(x_t) T^a \gamma_\mu$

Table 2.1: Basic coupling coefficients for diagrams in fig.(1.6)

- Z^0-penguin diagrams;
- $\Delta S=1$ or $\Delta B=1$ box diagrams.

Below the threshold all the EW-penguins but the photon one are shrunk to a point, because W- and Z-bosons are integrated out. The same is also true for the box diagram, which reduces to a single vertex operator. We are left with vertex and penguin diagrams shown in fig.(2.4), and the relative gluon and photon corrections. Thus, the computation of Z^0-penguin and of the two box diagrams in fig.(2.4) at $\mu \sim M_W$ will simply give their contribution to the initial condition for the coefficient functions. On the other hand, for vertex, QCD- and QED-penguins we have to match with the analogous ET contribution, below the threshold. Moreover, being the top quark completely absent below the threshold, we will drop any operator with an explicit t-dependence from the beginning.

All the heaviest particles present in the theory contribute only at the very high energy scale, i.e. in the evaluation of the one-loop initial condition for the CF only. This is typical of a NLO calculation, because in the LLA only the tree-level initial conditions for the CF are required and they do not depend on the "heavy sector" of the theory. This is the only indirect way we have to "probe" the hadronic sector of the theory.

The contribution of each diagram in fig.(2.4) will be given in terms of the Inami-Lim functions reported in (1.3). A summary of the coefficients which appear in the calculation of the relevant diagrams is given in table (2.1) for the $\Delta S=1$ case[10].

Let us consider now the matching dynamics diagram by diagram, in order to determine all the single contributions to the CF.

[10]The generalization to the $\Delta B=1$ case is straightforward.

1. *Vertex Diagrams*

The one-loop CF for vertex-diagrams in presence of only QCD-corrections has been known for a long time in literature [5, 13]. It is obtained as a simple matching between the full theory result and the Effective Theory one. The same procedure has a straightforward generalization to the QED case. We only have to account for the electric charge, which will assign different "weights" to QCD-equivalent diagrams. The final result can be easily derived using the corresponding tables for coefficients and finite parts. The final result will be of the form:

$$\begin{aligned} C_V^{(1)}(M_W) &= \frac{\alpha_s^{(5)}(M_W)}{4\pi} B_s^{(1)} + \frac{\alpha_e(M_W)}{4\pi} B_e^{(1)} \\ C_V^{(2)}(M_W) &= \frac{\alpha_s^{(5)}(M_W)}{4\pi} B_s^{(2)} + \frac{\alpha_e(M_W)}{4\pi} B_e^{(2)} \end{aligned} \tag{2.79}$$

where:

$$B_s^{(1)} = \frac{7}{2} \quad B_e^{(1)} = \frac{7}{2} e_u e_d, \quad B_s^{(2)} = \frac{-7}{6} \quad B_s^{(2)} = \frac{-7}{6} e_u e_d \tag{2.80}$$

where e_u and e_d are the charges of type-u and type-d quarks. The V-index indicates that this is the vertex-diagram contribution to the initial conditions for the coefficients of O_1 and O_2. Moreover we have explicitly pointed out that the value for α_s has now to be taken from the $N_f=5$ effective theory and evaluated at the M_W-scale.

2. *QCD-Penguins Diagrams*

In the full theory, the QCD-penguin diagram contribution to $\mathcal{H}_t$ is computed as the difference between the t-penguin and the u-penguin. Being the u-quark approximately massless at this scale, this difference coincide exactly with the original Inami-Lim function [34]. In the ET, only the u-penguin survives. Considering the $x_i \ll 1$ limit of the correspondent Inami-Lim function, we see that the u-contribution exactly cancels across the threshold. Thus, the QCD-penguin contributes to the CF with a slightly modified Inami-Lim function, what we have called here $E(x_t)$ (see (1.3)). More explicitly it gives:

$$\begin{aligned} P_{QCD} &= \lambda_t \frac{G_F}{\sqrt{2}} \frac{\alpha_s^{(5)}(M_W)}{2\pi} E(x_t)(\bar{s}T^a\gamma_L^\mu d)\sum_q(\bar{q}\gamma_\mu T^a q) = \\ &\lambda_t \frac{G_F}{\sqrt{2}} \frac{\alpha_s^{(5)}(M_W)}{2\pi} E(x_t)(\bar{s}T^a\gamma_L^\mu d)\frac{1}{2}\sum_q((\bar{q}T^a\gamma_{\mu L}q) + (\bar{q}T^a\gamma_{\mu R}q)) = \\ &\lambda_t \frac{G_F}{\sqrt{2}} \frac{\alpha_s^{(5)}(M_W)}{2\pi} E(x_t)\left((O_4+O_6) - \frac{1}{3}(O_3+O_5)\right) \end{aligned} \tag{2.81}$$

where γ_L^μ and γ_R^μ denoted respectively the $\gamma^\mu(1\mp\gamma_5)$ chiral structure. Summarizing, the single operator coefficients get the following contribution from QCD-penguins:

$$\begin{aligned} C_3^{(g)}(M_W) &= C_5^{(g)}(M_W) = -\frac{\alpha_s^{(5)}}{24\pi} E(x_t) \\ C_4^{(g)}(M_W) &= C_6^{(g)}(M_W) = \frac{\alpha_s^{(5)}}{8\pi} E(x_t) \end{aligned} \tag{2.82}$$

3. *QED-Penguin Diagrams*

QED- or photon-penguin diagrams consist of two different terms as can be realized looking at fig.(2.4): the first one completely equivalent to the QCD-penguin plus a second non-abelian penguin. This last one, being $O(\alpha_e)$ is indeed of the same order of the other photon-corrections. This would not be the case for a non-abelian QCD-penguin, which is already an $O(\alpha_s^2)$ effect. Also in this case, the $\mathcal{H}_t$ part of full theory hamiltonian, contains the difference between the t- and the u-penguins and this coincides with the original Inami-Lim function [34]. On the other hand, the u-contribution is cancelled by the matching with the ET at $\mu \ll M_W$ and the left function, namely $D(x_t)$ is given in (1.3). Looking at table (2.1), we find the following global contribution for QED-penguin diagrams:

$$\begin{aligned} P_{QED} &= \lambda_t \frac{G_F}{\sqrt{2}} \frac{\alpha_e}{2\pi} D(x_t)(\bar{s}\gamma_L^\mu d) \sum_q e_q(\bar{q}\gamma_\mu q) = \\ & \lambda_t \frac{G_F}{\sqrt{2}} \frac{\alpha_e}{6\pi} D(x_t)(\bar{s}\gamma_L^\mu d) \left\{ \frac{3}{2} \sum_q e_q(\bar{q}\gamma_{\mu L} q) + \frac{3}{2} \sum_q e_q(\bar{q}\gamma_{\mu R} q) \right\} = \\ & \lambda_t \frac{G_F}{\sqrt{2}} \frac{\alpha_e}{6\pi} D(x_t) \{O_7 + O_9\} \end{aligned} \tag{2.83}$$

Only the O_7 and the O_9 CF are modified by these diagrams as follows:

$$\begin{aligned} C_7^{(\gamma)}(M_W) &= \frac{\alpha_e}{6\pi} D(x_t) \\ C_9^{(\gamma)}(M_W) &= \frac{\alpha_e}{6\pi} D(x_t) \end{aligned} \tag{2.84}$$

4. *Z-penguin Diagrams*

These penguin diagrams are $O(\alpha_e)$ effects as the photon-penguins and consists of both an abelian and a non-abelian part too. The Z^0-boson id removed from the theory below the M_W-threshold and we have no contributions from the Effective Theory. The CF will be given by the full theory diagrams only and also in this case $\mathcal{H}_t$ consists of the difference between the t- and the u-penguins. The corresponding Inami-Lim function [34] behaves as $(x_j \ln x_j)$ for $x_j \ll 1$ and we can reasonably assume that the u-contribution can be neglected. Remembering that the Z^0-coupling to fermions is of the form:

$$\bar{q} Z q \to \frac{1}{2} \sum_q \{ g_L^{(q)} (\bar{q}q)_L + g_R^{(q)} (\bar{q}q)_R \} \tag{2.85}$$

where:

$$\begin{aligned} g_L^{(q)} &= T_3(q_L) - e_q \sin^2 \vartheta_w \\ g_R^{(q)} &= T_3(q_R) - e_q \sin^2 \vartheta_w \end{aligned}$$

we can rewrite it in the following form:

$$\begin{aligned} P_Z &= -\frac{1}{3}\{O_7+O_9\}\sin^2\vartheta_W+\frac{1}{2}(\bar{s}\gamma_L^\mu d)\cdot \\ &\quad \cdot\left\{\frac{1}{2}((\bar{u}\gamma_{\mu L}u)+\cdots)-\frac{1}{2}\left((\bar{d}\gamma_{\mu L}d)+\cdots\right)\right\}= \\ &= -\frac{1}{3}\{O_7+O_9\}\sin^2\vartheta_W-\frac{1}{12}\{O_3-4O_9\} \end{aligned} \tag{2.86}$$

Using as $(\bar{s}Zd)$-vertex the one in Table (2.1) we finally get:

$$P_Z=\lambda_t\frac{G_F}{\sqrt{2}}\frac{\alpha_e}{6\pi}C(x_t)\left\{4(O_7+O_9)+\frac{1}{\sin^2\vartheta_W}(O_3-4O_9)\right\} \tag{2.87}$$

or for the single coefficients:

$$\begin{aligned} C_3^{(Z)}(M_W) &= \frac{\alpha_e}{6\pi}C(x_t) \\ C_7^{(Z)}(M_W) &= \frac{\alpha_e}{6\pi}4C(x_t) \\ C_9^{(Z)}(M_W) &= \frac{\alpha_e}{6\pi}\left\{4C(x_t)-\frac{1}{\sin^2\vartheta_W}4C(x_t)\right\} \end{aligned} \tag{2.88}$$

where $C(x_t)$ is given in (1.3).

5. *Box Diagrams*

In the case of the two box diagrams of fig.(1.6) we have to make some important remarks. First of all one has to fix the initial and final external states, depending on the process of interest. This means that for a $\Delta S=1$ decay one will have $(\bar{s}d)$ as initial state and only $\Delta F=0$ final states. On the other hand for a $\Delta B=1$ decay the initial state could be $(\bar{b}s)$ or $(\bar{b}d)$ and again only $\Delta F=0$ final states are allowed. In this case, while on the left-hand side of the boxes GIM mechanism is effective, the right-hand sides, having identical external flavours, are not subject to the GIM mechanism. But a great simplification could be introduced if one set to zero quark masses on the right-hand side propagator. This is not obvious in principle, but we can argue that it is indeed the case. If we did not make this approximation, the final effect would be the presence of some more operators of the type of O_{11} and O_{12} in (2.70), with light quarks too. Most of them would be suppressed by CKM factors. The only surviving ones would be O_{11} and O_{12} themselves, but, as we have already explained, their effect is negligible, because confined to a region where the running of α_s is really small.

In the approximation of zero-mass propagator on the right-hand side, summing all the analogous boxes with different $\Delta F=0$ final states, dropping the explicit t-dependence and applying the unitarity of the CKM matrix, one can reduce the whole problem in terms of the $\Delta T_3=1/2$ and $\Delta T_3=-1/2$ boxes in the original Inami-Lim classification [34] (i.e. $B(x_t)$ function in (1.3)). Thus, the

final contribution will be:

$$\begin{aligned}
\text{Box} &= \lambda_t \frac{G_F}{\sqrt{2}} \frac{\alpha_e}{2\pi \sin^2\vartheta_W} B(x_t)(\bar{s}\gamma_L^\mu d)\cdot \\
&\quad \cdot \Big\{(1)\left[(\bar{d}\gamma_{\mu L} d) + \cdots\right] + (-4)\left[(\bar{u}\gamma_L^\mu u) + \cdots\right]\Big\} \qquad (2.89)\\
&= \lambda_t \frac{G_F}{\sqrt{2}} \frac{\alpha_e}{6\pi} \frac{1}{\sin^2\vartheta_W} B(x_t)(\bar{s}\gamma_L^\mu d) 2 \sum_q \left(1 + 5\cdot\frac{3}{2}e_q\right)(\bar{q}\gamma_L^\mu q) = \\
&= \lambda_t \frac{G_F}{\sqrt{2}} \frac{\alpha_e}{6\pi} \frac{1}{\sin^2\vartheta_W} B(x_t)\left[2O_3 + 10O_9\right]
\end{aligned}$$

or in terms of single coefficients:

$$\begin{aligned}
C_3^{(\Box)}(M_W) &= \frac{\alpha_e}{6\pi}\frac{1}{\sin^2\vartheta_W} 2B(x_t) \qquad (2.90)\\
C_9^{(\Box)}(M_W) &= \frac{\alpha_e}{6\pi}\frac{1}{\sin^2\vartheta_W} 10B(x_t)
\end{aligned}$$

We can now summarize all the found contributions to obtain the components of the complete CF vector:

$$C_1(M_W) = \frac{\alpha_s^{(5)}(M_W)}{4\pi}\frac{7}{2} + \frac{\alpha_e}{4\pi}\frac{7}{2}e_u e_d \qquad (2.91)$$

$$C_2(M_W) = \frac{\alpha_s^{(5)}(M_W)}{4\pi}\frac{-7}{6} + \frac{\alpha_e}{4\pi}\frac{-7}{6}e_u e_d \qquad (2.92)$$

$$C_3(M_W) = -\frac{\alpha_s^{(5)}(M_W)}{24\pi}E(x_t) + \frac{\alpha_e}{6\pi}\frac{1}{\sin^2\vartheta_W}\left[2B(x_t) + C(x_t)\right] \qquad (2.93)$$

$$C_4(M_W) = \frac{\alpha_s^{(5)}(M_W)}{8\pi}E(x_t) \qquad (2.94)$$

$$C_5(M_W) = -\frac{\alpha_s^{(5)}(M_W)}{24\pi}E(x_t) \qquad (2.95)$$

$$C_6(M_W) = \frac{\alpha_s^{(5)}(M_W)}{8\pi}E(x_t) \qquad (2.96)$$

$$C_7(M_W) = \frac{\alpha_e}{6\pi}\left[4C(x_t) + D(x_t)\right] \qquad (2.97)$$

$$C_8(M_W) = 0 \qquad (2.98)$$

$$C_9(M_W) = \frac{\alpha_e}{6\pi}\left[4C(x_t) + D(x_t) + \frac{1}{\sin^2\vartheta_W}\left(10B(x_t) - 4C(x_t)\right)\right] \qquad (2.99)$$

$$C_{10}(M_W) = 0 \qquad (2.100)$$

Let us now consider the other part of the EH, $\mathcal{H}_c$ which we have neglected up to now. Indeed, involving only u- and c-quarks, it does not influence the physics of processes related to much higher scales and its evolution can be considered starting from the charm thresholds. Thus at $\mu \sim m_c$ we have to compute new initial conditions for the CF vector of $\mathcal{H}_c$. Nevertheless, the case here is much simpler, because only the Effective Theory penguin diagrams in fig.(2.4) contribute, that is the gluon and

the photon-penguin. Their contribution can be found by simply computing the generic penguin-diagram of the ET in the massive and in the massless case, matching the two results at the m_c threshold. Both the QCD- and the QED-case will be proportional to a common function, call it $F(x_c)$, given by:

$$F(x_c) = -4C_2(m_c)^{l.o.} \int_0^1 dx x(1-x) \ln\left[1 + x(1-x)\right] \tag{2.101}$$

where $C_2(m_c)^{l.o.}$ is the leading order expression for the coefficient of O_2, evaluated at $\mu = m_c$. Thus, the CF of the $\mathcal{H}_c$ part of the original hamiltonian, at $\mu \sim m_c$ is given by:

$$\begin{aligned}
C_1(m_c) &= \frac{\alpha_s^{(3)}(m_c)}{4\pi}\frac{7}{2} + \frac{\alpha_e}{4\pi}\frac{7}{2}e_u e_d && (2.102)\\
C_2(m_c) &= \frac{\alpha_s^{(3)}(m_c)}{4\pi}\frac{-7}{6} + \frac{\alpha_e}{4\pi}\frac{-7}{6}e_u e_d && (2.103)\\
C_3(m_c) &= -\frac{\alpha_s^{(3)}(m_c)}{24\pi}F(x_c) && (2.104)\\
C_4(m_c) &= \frac{\alpha_s^{(3)}(m_c)}{8\pi}F(x_c) && (2.105)\\
C_5(m_c) &= -\frac{\alpha_s^{(3)}(m_c)}{24\pi}F(x_c) && (2.106)\\
C_6(m_c) &= \frac{\alpha_s^{(3)}(m_c)}{8\pi}F(x_c) && (2.107)\\
C_7(m_c) &= \frac{\alpha_e}{6\pi}F(x_c) && (2.108)\\
C_8(m_c) &= 0 && (2.109)\\
C_9(m_c) &= \frac{\alpha_e}{6\pi}F(x_c) && (2.110)\\
C_{10}(m_c) &= 0 && (2.111)
\end{aligned}$$

where $\mu = m_c$ and the index (3) indicate the new framework of an $N_f = 3$ Effective Theory.

2.2.3 Operator mixing

One of the most important ingredients in the evaluation of the Anomalous Dimension Matrix is the operator mixing among the operator in the EH basis (2.66).

At a given order in perturbation theory (one-loop, two-loop. etc.) different sets of Feynman diagrams contribute to the EH (see fig.(2.4)-(2.7)). Each diagram consists of a Dirac+colour structure and a numerical coefficient obtained from the analytical calculation of the integral on the momentum space and from the reduction of the Dirac algebra. The operator mixing depends only on the Dirac and colour structures of the Feynman diagrams present in the theory. On the other hand the amount of mixing is given by the direct computation of the divergent part of the diagrams. We will explain

the analytic calculation of the two-loop contribution of each diagram to the anomalous dimension matrix $\hat{\hat{\gamma}}^{(1)}$ in the next chapter. Here we will concentrate on the mixing mechanism.

Our method in determining the mixing of each operator can be summarized in few simple points:

- identification of the Dirac+colour[11] structure of each operator in the basis (2.66);
- identification, for a chosen operator, of the diagrams (at a given order) where the operator can be inserted;
- determination of the Dirac+colour structure of each of the previous diagrams (tables of the results will be given);
- recognition in the final Dirac+colour decomposition of the operator of the different structures corresponding to the operators in the original (2.66) basis.

In what follow we will apply the above "recipe" first at one-loop in presence of both QCD and QED corrections, then to the two-loop case. The same method applies to the one-loop and to the two-loop cases with very slight differences. For this reason, we will treat in great detail the one-loop case here following.

One-loop mixing: vertex-operators O_1 and O_2 only

The explicit Dirac+colour structure of the vertex operators[12] O_1 and O_2 can be explicitly given as follows:

$$\begin{aligned} O_1 &= (\bar{s}_\alpha d_\beta)_{(V-A)}(\bar{u}_\gamma u_\delta)_{(V-A)}\,\delta_{\alpha\beta}\otimes\delta_{\gamma\delta} \\ O_2 &= (\bar{s}_\alpha d_\beta)_{(V-A)}(\bar{u}_\gamma u_\delta)_{(V-A)}\,\delta_{\alpha\delta}\otimes\delta_{\gamma\beta} \end{aligned} \tag{2.112}$$

A more schematic notation can be introduced if we fix the ordering of the external fermions as for O_1, drop the external spinors and denote the operators only as a product of Dirac and colour matrices. Introducing the following short-hand notations:

$$\gamma_{LL} = \gamma^\mu(1-\gamma_5)\otimes\gamma_\mu(1-\gamma_5) \tag{2.113}$$

for the Dirac structure, and:

$$\begin{aligned} \mathbb{I}_{\alpha\beta,\gamma\delta} &= \delta_{\alpha\beta}\otimes\delta_{\gamma\delta} \\ \tilde{\mathbb{I}}_{\alpha\beta,\gamma\delta} &= \delta_{\alpha\delta}\otimes\delta_{\gamma\beta} \end{aligned} \tag{2.114}$$

[11] With colour structure we denote both the proper colour coefficient and the charge-dependent coefficient when QED corrections are present.

[12] Here O_i denotes a generic $O_i^{(q)}$ operator. We drop the distinction between different q's, because it is not relevant for vertex operator in the present context.

for the two possible colour combinations (2.113). We write:

$$O_1 = \mathbb{I}\gamma_{LL} \quad , \quad O_2 = \tilde{\mathbb{I}}\gamma_{LL} \tag{2.115}$$

QCD corrections, introducing new colour structures (as we can read in Table (2.2)), mix O_1 and O_2. Let us develop the case of O_1 and O_2 as a detailed example. Consider diagrams V_1, V_2 and V_3 in fig.(2.4) plus the one-loop self-energy in fig.(2.8). They are the only diagrams which contribute to the one-loop renormalization of O_1 and O_2 in the present case. We can read the colour structure of V_1, V_2 and V_3 in Table (2.2) and their numerical contribution in Table (2.14). The analogous quantities for the self-energy are given in Table (2.15). In presence of vertex-type interactions only, the Dirac structure of given operator can not be changed by one-loop interactions. On the other hand, the exchange of a gluon might modify the original colour structure. For instance, V_2 and V_3 have a $\mathbb{T}$-colour structure, where:

$$\mathbb{T}_{\alpha\beta,\gamma\delta} = \sum_a T^a_{\alpha\beta} T^a_{\gamma\delta} \tag{2.116}$$

being T^a the SU(N) colour matrices in the quark (fundamental) representation with the normalization:

$$Tr(T^a T^b) = \frac{1}{2}\delta^{ab} \tag{2.117}$$

The following equality:

$$\mathbb{T} = \frac{1}{2}\left(\tilde{\mathbb{I}} - \frac{1}{N}\mathbb{I}\right) \tag{2.118}$$

is the origin of mixing. Indeed, if we insert O_1 in diagrams V_2 and V_3 we will get:

$$\begin{aligned} O_1 \quad \rightarrow \quad & -6 \cdot \mathbb{T} = -6 \cdot \left(\frac{1}{2}\tilde{\mathbb{I}} - \frac{1}{2N}\mathbb{I}\right) = \\ & -6 \cdot \left(\frac{1}{2}O_2 - \frac{1}{2N}O_1\right) \end{aligned} \tag{2.119}$$

Thus, when QCD-corrections generate a $\mathbb{T}$-structure starting from an O_1-type operator, they reproduce the original operator plus a new O_2 term. In particular, in the O_1 case, eq.(2.119) gives the whole mixing of the operator, because diagram V_1 cancels with the self-energy contribution.

The mixing of O_2 is quite similar, but some more remarks are in order. With respect to the colour structure, we might describe the operators O_1 and O_2 projecting on the $\{\mathbb{I}, \tilde{\mathbb{I}}\}$ basis or on the $\{\mathbb{I}, \mathbb{T}\}$ basis, where the following equality holds:

$$\tilde{\mathbb{I}} = \frac{1}{N} \cdot \mathbb{I} + 2 \cdot \mathbb{T} \tag{2.120}$$

or, expliciting the colour indices:

$$\delta_{\alpha\delta} \otimes \delta_{\gamma\beta} = \frac{1}{N} \cdot \delta_{\alpha\beta} \otimes \delta_{\gamma\delta} + 2 \cdot \sum_a T^a_{\alpha\beta} T^a_{\gamma\delta} \tag{2.121}$$

We adopt the $\{\mathbb{I}, \mathbb{T}\}$ basis because more convenient for colour factor evaluation. In the $\{\mathbb{I}, \mathbb{T}\}$ basis all the operators with a $\mathbb{I}$ colour structure (O_1) are not modified, while those with a $\tilde{\mathbb{I}}$ structure (O_2) are modified. They practically undergo a Fierz transformation on the colour indices and, for consistency, also the Dirac indices has to be Fierz-transformed. In the O_2 case, the Dirac structure γ_{LL} is not modified by the Fierz transformation, thus O_2 can be written as:

$$O_2 = \left(\frac{1}{N}\mathbb{I} + 2\mathbb{T}\right) \cdot \gamma_{LL} \tag{2.122}$$

The insertion of O_2 in diagrams $\hat{\mathbb{V}}_1$, $\hat{\mathbb{V}}_2$, $\hat{\mathbb{V}}_3$ and in the external leg self-energy diagrams consists now of two parts. We have to account both for the insertion of the $\mathbb{I}$-structure and of the $\mathbb{T}$ one. The numerical coefficient for each diagram is clearly the same in both cases and can be read in Table (2.14). On the other hand the colour factors for the $\mathbb{I}$ and $\mathbb{T}$-vertex insertion are given in Table (2.2). The final result for the insertion of O_2 is:

$$O_2 \to \left\{\frac{1}{N}(-6\mathbb{T}) + 2\left(-\frac{3}{2}\frac{(N^2-1)}{2N^2}\mathbb{I} + \frac{6}{N}\mathbb{T}\right)\right\} \cdot \gamma_{LL} \tag{2.123}$$

In order to recover the structure of the original operators O_1 and O_2, one has to move back in (2.123) to the $\{\mathbb{I}, \tilde{\mathbb{I}}\}$ basis. This corresponds to another Fierz transformation on the colour structure, which must be followed by a Fierz rearrangement of the Dirac structure. $\gamma_L^\mu \otimes \gamma_{\mu L}$ is not modified by the Fierz-symmetry and we finally obtain:

$$O_2 \to -6 \cdot \frac{1}{2}\left(\mathbb{I} - \frac{1}{N}\tilde{\mathbb{I}}\right) = -6 \cdot \left(\frac{1}{2}O_1 - \frac{1}{2N}O_2\right) \tag{2.124}$$

From (2.119) and (2.124) the one-loop anomalous dimension results to be a symmetric matrix of the form:

$$\gamma_s^{(0)} = \begin{pmatrix} -6/N & 6 \\ 6 & -6/N \end{pmatrix} \tag{2.125}$$

where some normalization factor has been taken into account. It is also well-known that the mixing problem can be "diagonalized" considering the basis:

$$O_\pm = \frac{1}{2}(\mathbb{I} \pm \tilde{\mathbb{I}})\gamma_{LL} \tag{2.126}$$

The $O_\pm$ operators undergo a multiplicative renormalization[13] and their anomalous dimension reads[14]:

$$\gamma_\pm^{(0)} = \pm 12\frac{(N \mp 1)}{2N} \tag{2.127}$$

Let us now consider the same mixing problem when QED corrections are introduced. The possible diagrams are always the one-loop vertex-diagrams in fig.(2.4) plus

[13] Look: at one-loop only!

[14] It would be in fact a diagonal matrix.

diagram	QCD		QED	
	$\mathbb{I}$	$\mathbb{T}$	$\mathbb{I}$	$\mathbb{T}$
V_1	$\frac{N^2-1}{2N}\mathbb{I}$	$-\frac{1}{2N}\mathbb{T}$	$\mathbb{I}$	$\mathbb{T}$
V_2	$\mathbb{T}$	$-\frac{1}{N}\mathbb{T}+\frac{N^2-1}{4N^2}\mathbb{I}$	$\mathbb{I}$	$\mathbb{T}$
V_3	$\mathbb{T}$	$\frac{N^2-2}{2N}\mathbb{T}+\frac{N^2-1}{4N^2}\mathbb{I}$	$\mathbb{I}$	$\mathbb{T}$
P_1	$\mathbb{T}$	$-\frac{1}{2N}$	$\mathbb{I}$	$\frac{N^2-1}{2N}$
F_1	0	$\frac{1}{2}\mathbb{T}$	$N\mathbb{I}$	0

Table 2.2: Colour factors for diagrams in fig.(2.4) with either QCD or QED corrections

the self-energy ones, but with a photon in the wavy line. Due to the isospin breaking on the charge, different flavours are "weighted" with different electromagnetic charges. The colour structure is also different, because no gluons are present. We will account here for the charges, while the colour factors and the numerical coefficients are given in Tables (2.2) and (2.14).

The insertion of O_1 proceeds as in the QCD case: V_1 cancels with the external leg self-energy diagrams and the final result is given by V_2 and V_3 only:

$$O_1 \to -6e_u e_d \cdot \mathbb{I} \cdot \gamma_{LL} = \frac{4}{3} O_1 \tag{2.128}$$

where e_u and e_d denotes the charges of a u- and a d-type quark respectively ($e_u = 2/3$, $e_d = -1/3$). Eq.(2.128) tells us that O_1 renormalizes multiplicatively in presence of QED corrections only.

In the O_2 case, we project on the $\{\mathbb{I}, \mathbb{T}\}$ basis using (2.120) and we insert the $\mathbb{I}$ and the $\mathbb{T}$-structure separately into the one-loop diagrams. The contribution of V_1 always cancels with the self-energy one and the sum of V_2 and V_3 now gives:

$$O_2 \to \left\{ \frac{1}{N} \cdot (-6e_u e_d \mathbb{I}) + 2 \cdot (-6e_u e_d \mathbb{T}) \right\} \cdot \gamma_{LL} = \frac{4}{3} \cdot \tilde{\mathbb{I}} = \frac{4}{3} O_2 \tag{2.129}$$

Also O_2 is multiplicatively renormalized by QED interactions. The QED Anomalous Dimension Matrix, analogous to the QCD one in (2.125), will be a diagonal matrix of the form:

$$\gamma_e^{(0)} = \begin{pmatrix} 4/3 & 0 \\ 0 & 4/3 \end{pmatrix} \tag{2.130}$$

One-loop mixing: the complete basis $\{O_i\}_{i=1,\dots 10}$ case

Let us consider first the pure QCD case. O_1 and O_2 mixing is modified by the presence of new diagrams: the penguin diagrams P_1 and F_1. We can read the necessary colour factors and numerical coefficients from Tables (2.2) and (2.14). As before, we start projecting on the $\{\mathbb{I}, \mathbb{T}\}$ basis, while the final result will be written in the $\{\mathbb{I}, \tilde{\mathbb{I}}\}$ basis, in order to recover the structure of the original operators in (2.66).

With respect to the Dirac structure, the following "rules" can be summarized:

- whatever chiral structure is conserved by vertex-type diagrams;
- the insertion of a $\gamma_L^\mu \otimes \gamma_{\mu L}$ or a $\gamma_L^\mu \otimes \gamma_{\mu R}$ structure in penguin-type diagrams gives always the sum of a $\gamma_L^\mu \otimes \gamma_{\mu L}$ plus a $\gamma_L^\mu \otimes \gamma_{\mu R}$ structure, as explained in eq.(2.72)[15];
- if the colour structure has been Fierz transformed, going from the $\{\mathbb{I}, \tilde{\mathbb{I}}\}$ to the $\{\mathbb{I}, \mathbb{T}\}$ basis or viceversa, also the Dirac structure of each diagram must be Fierz-rearranged. We have to remember that :

$$\begin{aligned} \gamma_L^\mu \otimes \gamma_{\mu L} &\xrightarrow{\text{Fierz}} \gamma_L^\mu \otimes \gamma_{\mu L} \\ \gamma_L^\mu \otimes \gamma_{\mu R} &\xrightarrow{\text{Fierz}} (1+\gamma_5) \otimes (1-\gamma_5) \end{aligned} \tag{2.131}$$

O_1, due to its colour structure, can be inserted in the Fierz-rearranged penguin diagram F_1[16] (call it F-penguin-diagram). Nevertheless the insertion of a $\mathbb{I}$ structure in diagram F_1 gives a zero colour coefficient. This is the reason why O_1 does not mix with penguin-operators.

On the other hand, O_2 can be inserted only in the normal penguin P_1 (call it P-penguin diagram). Using the (2.122) Fierzed colour structure for O_2, we have to Fierz the Dirac structure of the F_1 penguin too. Thus the insertion of a $\tilde{\mathbb{I}}$-vertex in P_1 turns out to be equivalent to the insertion of given combination of a $\mathbb{I}$ and a $\mathbb{T}$-verteces in F_1. Being zero the $\mathbb{I}$-part contribution, the final result is given only by the $\mathbb{T}$-vertex insertion in F_1:

$$\begin{aligned} O_2 \;\to\; & -\frac{4}{3}\mathbb{T} \cdot \frac{1}{2}\left(\gamma_L^\mu \otimes \gamma_{\mu L} + \gamma_L^\mu \otimes \gamma_{\mu R}\right) = \\ & -\frac{4}{3}\left(\frac{1}{2}\tilde{\mathbb{I}} - \frac{1}{2N}\mathbb{I}\right) \cdot \frac{1}{2}\left(\gamma_L^\mu \otimes \gamma_{\mu L} + \gamma_L^\mu \otimes \gamma_{\mu R}\right) = \\ & \frac{1}{9}\left(O_3 + O_5\right) - \frac{1}{3}\left(O_4 + O_6\right) \end{aligned} \tag{2.132}$$

In order to extend our discussion to the whole set of operators, it will be useful to introduce a more general formalism. In this new formalism the global mixing of the

[15] This is the origin of mixing between vertex and penguin operators.

[16] We do not distinguish now the case of a gluon or a photon penguin: our present aim is only to give the very general description of the problem.

two vertex operators O_1 and O_2 can be summarized as follows:

$$\begin{aligned} O_1 &\rightarrow (F^{(1)} + O_u^{(1)}) \\ O_2 &\rightarrow (P^{(\bar{1})} + O_u^{(\bar{1})}) = \frac{1}{N}(F^{(1)} + O_u^{(1)}) + 2(F^{(T)} + O_u^{(T)}) \end{aligned} \tag{2.133}$$

with the following understanding of the notation:

- $F^{(1)}$ and $F^{(T)}$ are the contributions of the F-penguin diagrams, when a $\mathbb{1}$-type or a $\mathbb{T}$-type colour structure is inserted in the upper vertex;
- $P^{(\bar{1})}$ is the contribution of the P-penguin diagrams, when a $\bar{\mathbb{1}}$-type colour structure is inserted in the upper vertex;
- $O_u^{(1)}$ and $O_u^{(T)}$ are the contributions of the vertex-diagrams, when a $\mathbb{1}$-type or a $\mathbb{1}$-type colour structure are inserted in the vertex. We specified the presence of the only u-quark as external state, in order to distinguish this case from the case in which a penguin operator itself is inserted in a vertex diagram, generating a sum over flavour of vertex operators with that flavour as external state.

The expressions in (2.133) consist of the sum over all diagrams of a given type (vertex, F-penguins, P-penguins). Each terms in the sum as the sum itself is the product of a numerical coefficient and a Dirac+colour structure. For instance, the O_1-O_2 mixing due to vertex diagrams only is now summarized by $O_u^{(1)}$ and $O_u^{(\bar{1})}$. The structure of $O_u^{(1)}$ and $O_u^{(\bar{1})}$ might be directly deduced from eq.(2.119) and (2.124). The analogous penguin quantities have been obtained before, when considering the insertion of O_1 and O_2 in diagrams P_1 and F_1.

In the same spirit, let us consider the mixing of QCD-penguin operators. Penguin operators, being a sum over flavours of vertex-type operators, can be described for their Dirac and colour structure using the same notation introduced for O_1 and O_2. Nevertheless, their flavour structure has to be carefully considered. Let us illustrate the case of O_3 and O_4 in the $\Delta S=1$ basis:

$$\begin{aligned} O_3 &= (\bar{s}_\alpha d_\beta)\sum_q(\bar{q}_\gamma q_\delta)\cdot \mathbb{1}_{\alpha\beta,\gamma\delta}\cdot\gamma_{LL} \\ O_4 &= (\bar{s}_\alpha d_\beta)\sum_q(\bar{q}_\gamma q_\delta)\cdot \bar{\mathbb{1}}_{\alpha\beta,\gamma\delta}\cdot\gamma_{LL} \end{aligned} \tag{2.134}$$

The mixing of these operators is computed from those diagrams of fig.(2.4) which can contribute. O_3, can be inserted in a F-penguin diagram, in a vertex-type diagram and even in a P-penguin diagram. This last insertion is due, to the $(\bar{d}d)$ and the $(\bar{s}s)$ terms in the sum, which reproduces the right structures to be inserted in a P-penguin-diagram, namely:

$$(\bar{s}\gamma_L^\mu d)(\bar{d}\gamma_{\mu L}d) \quad \text{and} \quad (\bar{s}\gamma_L^\mu d)(\bar{s}\gamma_{\mu L}s) \tag{2.135}$$

The same holds for O_4, provided the $\tilde{\mathbb{I}}$ is treated as in (2.120. Thus, all together the structures of O_3 and O_4 can be decomposed as follows:

$$\begin{aligned} O_3 &\rightarrow (N_f F^{(1)} + 2P^{(1)} + O^{(1)}) \\ O_4 &\rightarrow \frac{1}{N}(N_f F^{(1)} + 2P^{(1)} + O^{(1)}) + 2(N_f F^{(T)} + 2P^{(T)} + O^{(T)}) \end{aligned} \tag{2.136}$$

where N_f is the number of active flavours and the general formalism introduced for O_1 and O_2 mixing is used. The insertion of a penguin-type operator in a F-penguin diagram generate N_f equal contributions, because QCD-interactions are isospin-conserving and do not distinguish different flavours. Moreover, the insertion in a vertex diagram O_i has no flavour index now. Indeed, the insertion of a penguin-type operator in a vertex diagram reproduce a sum over flavours of vertex operators with the summed flavour as external state, i.e. a penguin operator. Thus, the insertion of a penguin operator can never reproduce a vertex operator, because the sum over flavours is always present.

The case of operators O_5 and O_6 is strictly analogous: the colour decomposition is the same, but we have to account for the different Dirac structure $\gamma_L^\mu \otimes \gamma_{\mu R}$ with its own Fierz-symmetry properties. The final mixing of O_5 and O_6 differs from the one of the analogous $\gamma_L^\mu \otimes \gamma_{\mu L}$ operators because of the different analytic contribution of $\gamma_L^\mu \otimes \gamma_{\mu R}$ diagrams with respect to the correspondent $\gamma_L^\mu \otimes \gamma_{\mu L}$ ones.

The QED-penguins have the same structure of QCD-penguins, except for the isospin breaking in the charge. When a QED-penguin operator is inserted both in F-penguin and in P-penguin diagrams different flavours enter the sum of flavours at the upper vertex with different coefficients, i.e. "weighted" by the electric charge. In the case of vertex-diagrams a sum over the external flavour charge will be generated. For instance, O_9 and O_{10} turn out to have the following decomposition:

$$\begin{aligned} O_9 &\rightarrow ((e_u N_u + e_d N_d)F^{(1)} + 2e_d P^{(1)} + e_q O^{(1)})) \\ O_{10} &\rightarrow \frac{1}{N}((e_u N_u + e_d N_d)F^{(1)} + 2e_d P^{(1)} + e_q O^{(1)}) + \\ &\quad 2((e_u N_u + e_d N_d)F^{(T)} + 2e_d P^{(T)} + e_q O^{(T)}) \end{aligned} \tag{2.137}$$

where N_u and N_d are respectively the number of flavours of type u (charge e_u) and of type d (charge e_d), while e_q denotes the charge of the generic summed flavour. The same can be said for O_7 and O_8, which only differs for the Dirac structure. This ends up the discussion of the one-loop mixing in presence of only QCD corrections.

We should now introduce QED interactions (one-loop diagrams in fig.(2.4) with a photon in the wavy line) and analyze if new mixing features arise. The basic structures, i.e. $F^{(1)}$, $P^{(1)}$, $O^{(1)}$,... will be substituted now by $F_\gamma^{(1)}$, $P_\gamma^{(1)}$, $O_\gamma^{(1)}$,..., which differ from the previous one by the colour factors only[17]. The new colour factors for each diagram are given in the third and fourth column of Table (2.2). Moreover, the new structures $F_\gamma^{(1)}$, $P_\gamma^{(1)}$, $O_\gamma^{(1)}$,... will appear in the decomposition of each operator with

[17]Here the index γ has been chosen to indicate QED contributions

new coefficients, proportional to the charge of the external or internal loop quarks. The important features of the one-loop case is that it is always possible to factorize a one charge coefficient and one colour coefficient for each diagram. This allows us to account here for the charge dependence and to report the colour coefficient in Table (2.2). The same features will not survive in the two loop calculation. After the previous detailed discussion for the pure QCD case, it will be easy to recognize the origin of each coefficient in the the following global operator decomposition:

$$
\begin{aligned}
O_1 &\rightarrow \left(e_u e_q F_\gamma^{(1)} + e_d e_u O_{\gamma,u}^{(1)}\right) \\
O_2 &\rightarrow \frac{1}{N}\left(e_u e_q F_\gamma^{(1)} + e_d e_u O_{\gamma,u}^{(1)}\right) + 2\left(e_u e_q F_\gamma^{(T)} + e_d e_u O_{\gamma,u}^{(T)}\right) \mathbb{T}\gamma_{LL} \\
O_3 &\rightarrow \left((e_u N_u + e_d N_d) e_q F_\gamma^{(1)} + 2 e_d e_q P_\gamma^{(1)} + e_d e_q O_\gamma^{(1)}\right) \\
O_4 &\rightarrow \frac{1}{N}\left((e_u N_u + e_d N_d) e_q F_\gamma^{(1)} + 2 e_d e_q P_\gamma^{(1)} + e_d e_q O_\gamma^{(1)}\right) + \\
&\quad +2\left((e_u N_u + e_d N_d) e_q F_\gamma^{(T)} + 2 e_d e_q P_\gamma^{(T)} + e_d e_q O_\gamma^{(T)}\right) \\
&\vdots \\
O_7 &\rightarrow \left((e_u^2 N_u + e_d^2 N_d) e_q F_\gamma^{(1)} + 2 e_d^2 e_q P_\gamma^{(1)} + e_d \frac{2}{9}\left(1 + \frac{3}{2} e_q\right) O_\gamma^{(1)}\right) \\
O_8 &\rightarrow \frac{1}{N}\left((e_u^2 N_u + e_d^2 N_d) e_q F_\gamma^{(1)} + 2 e_d^2 e_q P_\gamma^{(1)} + e_d \frac{2}{9}\left(1 + \frac{3}{2} e_q\right) O_\gamma^{(1)}\right) + \\
&\quad +2\left((e_u^2 N_u + e_d^2 N_d) e_q F_\gamma^{(T)} + 2 e_d^2 e_q P_\gamma^{(T)} + e_d \frac{2}{9}\left(1 + \frac{3}{2} e_q\right) O_\gamma^{(T)}\right) \\
&\vdots
\end{aligned}
\tag{2.138}
$$

where the dots indicates operators whose decompositions can be easily argued from the ones given, f.i. with a slight modification in the colour or Dirac structure.

Two-loop mixing

The two-loop mixing is substantially analogous to the one-loop case, provided some important remarks. Again, it is better to distinguish the pure QCD case from the QCD+QED case, because the operator mixing presents some different features in the two cases. In both cases all the diagrams in fig.(2.5), (2.6) and (2.7) contribute, with two gluons or one gluon+one photon in the two wavy lines respectively. This difference will be manifest in the different colour+charge coefficients. The method used in finding the operator decomposition will be the usual one. Knowing the colour+Dirac structure of each operator, we have only to update the penguin and vertex contributions and to compute the new charge+colour coefficients very carefully. The final mixing of each operator will be now a sum over a much greater number of terms, one for each contributing diagram. As before, the single diagram contribution will be the product of a numerical coefficient, a Dirac structure and a colour/charge factor.

In the pure QCD case ($O(\alpha_s^2)$-corrections), the $\{O_i\}_{i=1\ldots10}$ have exactly the same

diagram	$\mathbb{I}$	$\mathbb{T}$
V_4	$\frac{(N^2-1)^2}{4N^2}\mathbb{I}$	$\frac{1}{4N^2}\mathbb{T}$
V_5	$\frac{(N^2-1)}{4N^2}\mathbb{I} - \frac{1}{N}\mathbb{T}$	$-\frac{(N^2-1)}{4N^3}\mathbb{I} + \frac{(N^2+3)}{4N^2}\mathbb{T}$
V_6	$\frac{(N^2-1)}{4N^2}\mathbb{I} + \frac{(N^2-2)}{2N}\mathbb{T}$	$\frac{(N^2-2)(N^2-1)}{8N^3}\mathbb{I} + \frac{(N^4-3N^2+3)}{4N^2}\mathbb{T}$
V_7	$-\frac{(N^2-1)}{4N^2}\mathbb{I}$	$\frac{(N^2+1)}{4N^2}\mathbb{T}$
V_8	$\frac{(N^2-1)}{4N^2}\mathbb{I} + \frac{(N^2-2)}{2N}\mathbb{T}$	$\frac{(N^2-2)(N^2-1)}{8N^3}\mathbb{I} + \frac{(N^2-3)}{4N^2}\mathbb{T}$
V_9	$\frac{(N^2-1)}{4N^2}\mathbb{I} - \frac{1}{N}\mathbb{T}$	$-\frac{(N^2-1)}{4N^3}\mathbb{I} - \frac{(N^2-3)}{4N^2}\mathbb{T}$
V_{10}	$-\frac{(N^2-1)}{4N^2}\mathbb{I}$	$\frac{1}{4N^2}\mathbb{T}$
V_{11}	$-\frac{1}{2N}\mathbb{I}$	$-\frac{(N^2-1)}{8N^3}\mathbb{I} + \frac{1}{2N^2}\mathbb{T}$
V_{12}	$-\frac{1}{2N}\mathbb{I}$	$-\frac{(N^2-1)}{8N^3}\mathbb{I} - \frac{(N^2-2)}{4N^2}\mathbb{T}$
V_{13}	$\frac{(N^2-1)^2}{4N^2}\mathbb{I}$	$-\frac{(N^2-1)}{4N^2}\mathbb{T}$
V_{14}	$\frac{(N^2-1)}{2N}\mathbb{T}$	$\frac{(N^2-1)^2}{8N^3}\mathbb{I} - \frac{(N^2-1)}{2N^2}\mathbb{T}$
V_{15}	$\frac{(N^2-1)}{2N}\mathbb{T}$	$\frac{(N^2-1)^2}{8N^3}\mathbb{I} + \frac{(N^2-2)(N^2-1)}{4N^2}\mathbb{T}$
V_{16}	$-\frac{1}{2N}\mathbb{I}$	$\frac{(N^2-1)^2}{8N^3}\mathbb{I} + \frac{1}{2N^2}\mathbb{T}$
V_{17}	$\frac{(N^2-1)}{2N}\mathbb{T}$	$-\frac{(N^2-1)}{8N^3}\mathbb{I} + \frac{1}{2N^2}\mathbb{T}$
V_{18}	$-\frac{1}{2N}\mathbb{I}$	$\frac{(N^2-1)^2}{8N^3}\mathbb{I} - \frac{(N^2-2)}{4N^2}\mathbb{T}$
V_{19}	$\frac{(N^2-1)}{2N}\mathbb{T}$	$-\frac{(N^2-1)}{8N^3}\mathbb{I} - \frac{(N^2-2)}{4N^2}\mathbb{T}$
V_{20}	$\frac{(N^2-1)}{4N^2}\mathbb{I} - \frac{1}{N}\mathbb{T}$	$\frac{(N^2-2)(N^2-1)}{8N^3}\mathbb{I} + \frac{(N^2-3)}{4N^2}\mathbb{T}$
V_{21}	$\frac{(N^2-1)}{4N^2}\mathbb{I} + \frac{(N^2-2)}{2N}\mathbb{T}$	$-\frac{(N^2-1)}{4N^3}\mathbb{I} - \frac{(N^2-3)}{4N^2}\mathbb{T}$
V_{22}	$\frac{(N^2-1)^2}{4N^2}\mathbb{I}$	$\frac{1}{4N^2}\mathbb{T}$
V_{23}	$\frac{(N^2-1)}{4N^2}\mathbb{I} - \frac{1}{N}\mathbb{T}$	$-\frac{(N^2-1)}{4N^3}\mathbb{I} + \frac{(N^2+3)}{4N^2}\mathbb{T}$
V_{24}	$\frac{(N^2-1)}{4N^2}\mathbb{I} + \frac{(N^2-2)}{2N}\mathbb{T}$	$\frac{(N^2-2)(N^2-1)}{8N^3}\mathbb{I} + \frac{(N^4-3N^2+3)}{4N^2}\mathbb{T}$
V_{25}	$-\frac{(N^2-1)}{4}\mathbb{I}$	$\frac{1}{4}\mathbb{T}$
V_{26}	$-\frac{N}{2}\mathbb{T}$	$-\frac{(N^2-1)}{8N}\mathbb{I} + \frac{1}{2}\mathbb{T}$
V_{27}	$-\frac{N}{2}\mathbb{T}$	$-\frac{(N^2-1)}{8N}\mathbb{I} - \frac{(N^2-2)}{4}\mathbb{T}$
V_{28}	$-\frac{N}{2}\mathbb{T}$	$\frac{(N^2-1)}{8N}\mathbb{I}$
V_{29}	$\frac{(N^2-1)}{2N}\mathbb{I}$	$-\frac{1}{2N}\mathbb{I}$
V_{30}	$\mathbb{T}$	$\frac{(N^2-1)}{4N^2}\mathbb{I} - \frac{1}{N}\mathbb{T}$
V_{31}	$\mathbb{T}$	$\frac{(N^2-1)}{4N^2}\mathbb{I} + \frac{(N^2-2)}{2N}\mathbb{T}$

Table 2.3: Colour factors for diagrams in fig.(2.5) with $O(\alpha_s^2)$ QCD-corrections.

diagram	$\mathbb{I}$	$\mathbb{T}$
P_2	$\frac{(N^2-1)}{2N}\mathbb{T}$	$\frac{1}{4N^2}\mathbb{T}$
P_3	$-\frac{1}{2N}\mathbb{T}$	$\frac{(N^2+1)}{4N^2}\mathbb{T}$
P_4	$\frac{N}{2}\mathbb{T}$	$-\frac{1}{4}\mathbb{T}$
P_5	$-\frac{1}{2N}\mathbb{T}$	$\frac{1}{4N^2}\mathbb{T}$
P_6	$\frac{N}{2}\mathbb{T}$	$-\frac{1}{4}\mathbb{T}$
P_7	$N\mathbb{T}, \frac{N_f}{2}\mathbb{T}$	$\frac{1}{2}\mathbb{T}, -\frac{1}{4}\frac{N_f}{N}\mathbb{T}$
P_8	$-\frac{1}{2N}\mathbb{T}$	$\frac{1}{4N^2}\mathbb{T}$
P_9	$\frac{(N^2-1)}{2N}\mathbb{T}$	$-\frac{(N^2-1)}{4N^2}\mathbb{T}$
P_{10}	$\frac{(N^2-1)}{4N^2}\mathbb{I} - \frac{1}{N}\mathbb{T}$	$\frac{(N^2-1)^2}{8N^3}\mathbb{I} + \frac{1}{2N^2}\mathbb{T}$
P_{11}	$\frac{(N^2-1)}{4N^2}\mathbb{I} + \frac{(N^2-2)}{2N}\mathbb{T}$	$\frac{(N^2-1)^2}{8N^3}\mathbb{I} - \frac{(N^2-2)}{4N^2}\mathbb{T}$
P_{12}	$\frac{N}{2}\mathbb{T}$	$-\frac{1}{4}\mathbb{T}$
P_{13}	$-\frac{1}{2N}\mathbb{T}$	$\frac{1}{4N^2}\mathbb{T}$
P_{14}	$\frac{(N^2-1)}{4N^2}\mathbb{I} - \frac{1}{N}\mathbb{T}$	$-\frac{(N^2-1)}{8N^3}\mathbb{I} + \frac{1}{2N^2}\mathbb{T}$
P_{15}	$\frac{(N^2-1)}{4N^2}\mathbb{I} + \frac{(N^2-2)}{2N}\mathbb{T}$	$-\frac{(N^2-1)}{8N^3}\mathbb{I} - \frac{(N^2-2)}{4N^2}\mathbb{T}$

Table 2.4: Colour factors for diagrams in fig.(2.6) with $O(\alpha_s^2)$ QCD-corrections.

decomposition seen in the one-loop case in terms of $F^{(1)}$, $F^{(T)}$, $P^{(1)}$,etc., but each of these terms now include the contribution of a much larger set of diagrams. The new two-loop colour coefficients are responsible for some new mixing, like the mixing of O_1 with penguin operators, not present at the one-loop level. We summarize all the charge+colour coefficients, diagram by diagram in Tables (2.3)-(2.5) for vertex, F-penguin and P-penguin diagrams respectively.

For the QCD+QED case ($O(\alpha_s\alpha_e)$-corrections) the previous decomposition is not valid anymore, because much more different charge+colour structures are present. We have to introduce different notations for the insertion of vertex operators like O_1 or O_2, QCD-penguin operators like O_3-O_6 or QED-penguin operators like O_7-O_{10} in the different classes of diagrams of the theory. The global mixing can be summarized as follows:

$$
\begin{aligned}
O_1 &\rightarrow \left(F^{(1)}_{\gamma,u} + O^{(1)}_{\gamma,u}\right) \\
O_2 &\rightarrow \frac{1}{N}\left(F^{(1)}_{\gamma,u} + O^{(1)}_{\gamma,u}\right) + 2\left(F^{(T)}_{\gamma,u} + O^{(T)}_{\gamma,u}\right) \\
O_3 &\rightarrow \left(F^{(1)}_{\gamma} + 2P^{(1)}_{\gamma} + O^{(1)}_{\gamma}\right) \\
O_4 &\rightarrow \frac{1}{N}\left(F^{(1)}_{\gamma} + 2P^{(1)}_{\gamma} + O^{(1)}_{\gamma}\right) + 2\left(F^{(T)}_{\gamma} + 2P^{(T)}_{\gamma} + O^{(T)}_{\gamma}\right) \\
&\vdots \\
O_7 &\rightarrow \left(F^{(1)}_{\gamma,e_q} + 2P^{(1)}_{\gamma,e_q} + O^{(1)}_{\gamma,e_q}\right) \\
O_8 &\rightarrow \frac{1}{N}\left(F^{(1)}_{\gamma,e_q} + 2P^{(1)}_{\gamma,e_q} + O^{(1)}_{\gamma,e_q}\right) + 2\left(F^{(T)}_{\gamma,e_q} + 2P^{(T)}_{\gamma,e_q} + O^{(T)}_{\gamma,e_q}\right) \\
&\vdots
\end{aligned}
\tag{2.139}
$$

where it has not been possible to factorize any colour or charge dependence. Moreover, for each class of diagrams, the introduction of three different symbols for each colour structure, as $O^{(1)}_{\gamma,u}$, $O^{(1)}_{\gamma}$ and $O^{(1)}_{\gamma,e_q}$, etc., is needed in view of the previous observation. In Tables (2.6)-(2.13) we report for each diagram the charge factor plus the colour factors for the case of a $\mathbb{I}$-structure and of a $\mathbb{T}$-structure in the weak vertex respectively.

Concerning the Dirac-structure, on the other side, no relevant differences are present and what we observed in the one-loop case is still valid.

Having the one-loop and the two-loop operator decomposition at hand, we would be ready to find the final one-loop and two-loop mixing. The last step of our procedure was indeed the identification of pairs of colour(charge)+Dirac structure with given operators. This is a quite easy task and we will see a direct implementation of that in the next subsection, where the final expressions for the one-loop and two-loop anomalous dimension matrices will be given, both in the pure QCD and in the QCD+QED case.

diagram	$\mathbb{I}$	$\mathbb{T}$
F_2	$\frac{1}{2}\mathbb{T}$	$\frac{(N^2-2)}{4N}\mathbb{T}$
F_3	$\frac{1}{2}\mathbb{T}$	$-\frac{1}{2N}\mathbb{T}$
F_4	0	$\frac{N}{4}\mathbb{T}$
F_5	0	$-\frac{1}{4N}\mathbb{T}$
F_6	0	$\frac{N}{4}\mathbb{T}$
F_7	0	$\frac{N}{2}\mathbb{T}, \frac{N_f}{4}\mathbb{T}$
F_8	0	$-\frac{1}{4N}\mathbb{T}$
F_9	0	$\frac{(N^2-1)}{4N}\mathbb{T}$
F_{10}	$\frac{(N^2-1)}{4N}\mathbb{I}$	$-\frac{1}{2N}\mathbb{T}$
F_{11}	$\frac{(N^2-1)}{4N}\mathbb{I}$	$\frac{(N^2-2)}{4N}\mathbb{T}$
F_{12}	0	$\frac{N}{4}\mathbb{T}$
F_{13}	0	$-\frac{1}{4N}\mathbb{T}$
F_{14}	0	$\frac{(N^2-1)}{8N^3}\mathbb{I}-\frac{1}{2N}\mathbb{T}$
F_{15}	0	$\frac{(N^2-1)}{8N^3}\mathbb{I}+\frac{(N^2-2)}{4N}\mathbb{T}$

Table 2.5: Colour factors for diagrams in fig.(2.7) with $O(\alpha_s^2)$ QCD-corrections.

diagram	$\mathbb{I}$	$\mathbb{T}$
V_4	$(e_u^2+e_d^2)\frac{(N^2-1)}{2N}\mathbb{I}$	$(e_u^2+e_d^2)(-\frac{1}{2N})\mathbb{T}$
V_5	$2e_ue_d\mathbb{T}$	$2e_ue_d(-\frac{1}{N}\mathbb{T}+\frac{(N^2-1)}{4N^2}\mathbb{I})$
V_6	$2e_ue_d\mathbb{T}$	$2e_ue_d(\frac{(N^2-2)}{2N}\mathbb{T}+\frac{(N^2-1)}{4N^2}\mathbb{I})$
V_7	$(e_u^2+e_d^2)\frac{(N^2-1)}{2N}\mathbb{I}$	$(e_u^2+e_d^2)(-\frac{1}{2N})\mathbb{T}$
V_8	$2e_ue_d\mathbb{T}$	$2e_ue_d(-\frac{1}{N}\mathbb{T}+\frac{(N^2-1)}{4N^2}\mathbb{I})$
V_9	$2e_ue_d\mathbb{T}$	$2e_ue_d(\frac{(N^2-2)}{2N}\mathbb{T}+\frac{(N^2-1)}{4N^2}\mathbb{I})$
V_{10}	$(e_u^2+e_d^2)\frac{(N^2-1)}{2N}\mathbb{I}$	$(e_u^2+e_d^2)\frac{(N^2-2)}{4N}\mathbb{T}$
V_{11}	$e_ue_d\frac{(N^2-1)}{2N}\mathbb{I}+\frac{(e_u^2+e_d^2)}{2}\mathbb{T}$	$\frac{(e_u^2+e_d^2)}{2}(-\frac{1}{N}\mathbb{T}+\frac{(N^2-1)}{4N^2}\mathbb{I})+e_ue_d\frac{(N^2-1)}{2N}\mathbb{T}$
V_{12}	$e_ue_d\frac{(N^2-1)}{2N}\mathbb{I}+\frac{(e_u^2+e_d^2)}{2}\mathbb{T}$	$\frac{(e_u^2+e_d^2)}{2}(\frac{(N^2-2)}{2N}\mathbb{T}+\frac{(N^2-1)}{4N^2}\mathbb{I})+e_ue_d\frac{(N^2-1)}{2N}\mathbb{T}$
V_{13}	$(e_u^2+e_d^2)\frac{(N^2-1)}{2N}\mathbb{I}$	$(e_u^2+e_d^2)\frac{(N^2-2)}{4N}\mathbb{T}$
V_{14}	$e_ue_d\frac{(N^2-1)}{2N}\mathbb{I}+\frac{(e_u^2+e_d^2)}{2}\mathbb{T}$	$\frac{(e_u^2+e_d^2)}{2}(-\frac{1}{N}\mathbb{T}+\frac{(N^2-1)}{4N^2}\mathbb{I})+e_ue_d\frac{(N^2-1)}{2N}\mathbb{T}$
V_{15}	$e_ue_d\frac{(N^2-1)}{2N}\mathbb{I}+\frac{(e_u^2+e_d^2)}{2}\mathbb{T}$	$\frac{(e_u^2+e_d^2)}{2}(\frac{(N^2-2)}{2N}\mathbb{T}+\frac{(N^2-1)}{4N^2}\mathbb{I})+e_ue_d\frac{(N^2-1)}{2N}\mathbb{T}$
V_{16}	$e_ue_d\frac{(N^2-1)}{2N}\mathbb{I}+\frac{(e_u^2+e_d^2)}{2}\mathbb{T}$	$\frac{(e_u^2+e_d^2)}{2}(-\frac{1}{N}\mathbb{T}+\frac{(N^2-1)}{4N^2}\mathbb{I})+e_ue_d\frac{-1}{2N}\mathbb{T}$
V_{17}	$e_ue_d\frac{(N^2-1)}{2N}\mathbb{I}+\frac{(e_u^2+e_d^2)}{2}\mathbb{T}$	$\frac{(e_u^2+e_d^2)}{2}(-\frac{1}{N}\mathbb{T}+\frac{(N^2-1)}{4N^2}\mathbb{I})+e_ue_d\frac{-1}{2N}\mathbb{T}$
V_{18}	$e_ue_d\frac{(N^2-1)}{2N}\mathbb{I}+\frac{(e_u^2+e_d^2)}{2}\mathbb{T}$	$\frac{(e_u^2+e_d^2)}{2}(\frac{(N^2-2)}{2N}\mathbb{T}+\frac{(N^2-1)}{4N^2}\mathbb{I})+e_ue_d\frac{-1}{2N}\mathbb{T}$
V_{19}	$e_ue_d\frac{(N^2-1)}{2N}\mathbb{I}+\frac{(e_u^2+e_d^2)}{2}\mathbb{T}$	$\frac{(e_u^2+e_d^2)}{2}(\frac{(N^2-2)}{2N}\mathbb{T}+\frac{(N^2-1)}{4N^2}\mathbb{I})+e_ue_d\frac{-1}{2N}\mathbb{T}$
V_{20}	$2e_ue_d\mathbb{T}$	$\frac{(N^2-1)}{4N^2}\mathbb{I}+e_ue_d(\frac{(N^2-4)}{2N}\mathbb{T})$
V_{21}	$2e_ue_d\mathbb{T}$	$\frac{(N^2-1)}{4N^2}\mathbb{I}+e_ue_d(\frac{(N^2-4)}{2N}\mathbb{T})$
V_{22}	$(e_u^2+e_d^2)\frac{(N^2-1)}{2N}\mathbb{I}$	$(e_u^2+e_d^2)\frac{-1}{2N}\mathbb{I}$
V_{23}	$2e_ue_d\mathbb{T}$	$2e_ue_d(-\frac{1}{N}\mathbb{T}+\frac{(N^2-1)}{4N^2}\mathbb{I})$
V_{24}	$2e_ue_d\mathbb{T}$	$2e_ue_d(\frac{(N^2-2)}{2N}\mathbb{T}+\frac{(N^2-1)}{4N^2}\mathbb{I})$

Table 2.6: Colour+charge factors for diagrams in fig.(2.5) with $O(\alpha_s\alpha_e)$ QCD+QED corrections, when O_1 and O_2 are inserted.

diagram	$\mathbb{I}$	$\mathbb{T}$
V_4	$(e_q^2+e_d^2)\frac{(N^2-1)}{2N}\mathbb{I}$	$(e_q^2+e_d^2)(-\frac{1}{2N})\mathbb{T}$
V_5	$2e_qe_d\mathbb{T}$	$2e_qe_d(-\frac{1}{N}\mathbb{T}+\frac{(N^2-1)}{4N^2}\mathbb{I})$
V_6	$2e_qe_d\mathbb{T}$	$2e_qe_d(\frac{(N^2-2)}{2N}\mathbb{T}+\frac{(N^2-1)}{4N^2}\mathbb{I})$
V_7	$(e_q^2+e_d^2)\frac{(N^2-1)}{2N}\mathbb{I}$	$(e_q^2+e_d^2)(-\frac{1}{2N})\mathbb{T}$
V_8	$2e_qe_d\mathbb{T}$	$2e_qe_d(-\frac{1}{N}\mathbb{T}+\frac{(N^2-1)}{4N^2}\mathbb{I})$
V_9	$2e_qe_d\mathbb{T}$	$2e_qe_d(\frac{(N^2-2)}{2N}\mathbb{T}+\frac{(N^2-1)}{4N^2}\mathbb{I})$
V_{10}	$(e_q^2+e_d^2)\frac{(N^2-1)}{2N}\mathbb{I}$	$(e_q^2+e_d^2)\frac{(N^2-2)}{4N}\mathbb{T}$
V_{11}	$e_qe_d\frac{(N^2-1)}{2N}\mathbb{I}+\frac{(e_q^2+e_d^2)}{2}\mathbb{T}$	$\frac{(e_q^2+e_d^2)}{2}(-\frac{1}{N}\mathbb{T}+\frac{(N^2-1)}{4N^2}\mathbb{I})+e_qe_d\frac{(N^2-1)}{2N}\mathbb{T}$
V_{12}	$e_qe_d\frac{(N^2-1)}{2N}\mathbb{I}+\frac{(e_q^2+e_d^2)}{2}\mathbb{T}$	$\frac{(e_q^2+e_d^2)}{2}(\frac{(N^2-2)}{2N}\mathbb{T}+\frac{(N^2-1)}{4N^2}\mathbb{I})+e_qe_d\frac{(N^2-1)}{2N}\mathbb{T}$
V_{13}	$(e_q^2+e_d^2)\frac{(N^2-1)}{2N}\mathbb{I}$	$(e_q^2+e_d^2)\frac{(N^2-2)}{4N}\mathbb{T}$
V_{14}	$e_qe_d\frac{(N^2-1)}{2N}\mathbb{I}+\frac{(e_q^2+e_d^2)}{2}\mathbb{T}$	$\frac{(e_q^2+e_d^2)}{2}(-\frac{1}{N}\mathbb{T}+\frac{(N^2-1)}{4N^2}\mathbb{I})+e_qe_d\frac{(N^2-1)}{2N}\mathbb{T}$
V_{15}	$e_qe_d\frac{(N^2-1)}{2N}\mathbb{I}+\frac{(e_q^2+e_d^2)}{2}\mathbb{T}$	$\frac{(e_q^2+e_d^2)}{2}(\frac{(N^2-2)}{2N}\mathbb{T}+\frac{(N^2-1)}{4N^2}\mathbb{I})+e_qe_d\frac{(N^2-1)}{2N}\mathbb{T}$
V_{16}	$e_qe_d\frac{(N^2-1)}{2N}\mathbb{I}+\frac{(e_q^2+e_d^2)}{2}\mathbb{T}$	$\frac{(e_q^2+e_d^2)}{2}(-\frac{1}{N}\mathbb{T}+\frac{(N^2-1)}{4N^2}\mathbb{I})+e_qe_d\frac{-1}{2N}\mathbb{T}$
V_{17}	$e_qe_d\frac{(N^2-1)}{2N}\mathbb{I}+\frac{(e_q^2+e_d^2)}{2}\mathbb{T}$	$\frac{(e_q^2+e_d^2)}{2}(-\frac{1}{N}\mathbb{T}+\frac{(N^2-1)}{4N^2}\mathbb{I})+e_qe_d\frac{-1}{2N}\mathbb{T}$
V_{18}	$e_qe_d\frac{(N^2-1)}{2N}\mathbb{I}+\frac{(e_q^2+e_d^2)}{2}\mathbb{T}$	$\frac{(e_q^2+e_d^2)}{2}(\frac{(N^2-2)}{2N}\mathbb{T}+\frac{(N^2-1)}{4N^2}\mathbb{I})+e_qe_d\frac{-1}{2N}\mathbb{T}$
V_{19}	$e_qe_d\frac{(N^2-1)}{2N}\mathbb{I}+\frac{(e_q^2+e_d^2)}{2}\mathbb{T}$	$\frac{(e_q^2+e_d^2)}{2}(\frac{(N^2-2)}{2N}\mathbb{T}+\frac{(N^2-1)}{4N^2}\mathbb{I})+e_qe_d\frac{-1}{2N}\mathbb{T}$
V_{20}	$2e_qe_d\mathbb{T}$	$\frac{(N^2-1)}{4N^2}\mathbb{I}+e_qe_d(\frac{(N^2-4)}{2N}\mathbb{T})$
V_{21}	$2e_qe_d\mathbb{T}$	$\frac{(N^2-1)}{4N^2}\mathbb{I}+e_qe_d(\frac{(N^2-4)}{2N}\mathbb{T})$
V_{22}	$(e_q^2+e_d^2)\frac{(N^2-1)}{2N}\mathbb{I}$	$(e_q^2+e_d^2)\frac{-1}{2N}\mathbb{I}$
V_{23}	$2e_qe_d\mathbb{T}$	$2e_qe_d(-\frac{1}{N}\mathbb{T}+\frac{(N^2-1)}{4N^2}\mathbb{I})$
V_{24}	$2e_qe_d\mathbb{T}$	$2e_qe_d(\frac{(N^2-2)}{2N}\mathbb{T}+\frac{(N^2-1)}{4N^2}\mathbb{I})$

Table 2.7: Colour+charge factors for diagrams in fig.(2.5) with $O(\alpha_s\alpha_e)$ QCD+QED corrections, when QCD-penguin operators O_3-O_6 are inserted.

diagram	$\mathbb{I}$	$\mathbb{T}$
V_4	$e_q(e_q^2+e_d^2)\frac{(N^2-1)}{2N}\mathbb{I}$	$e_q(e_q^2+e_d^2)(-\frac{1}{2N})\mathbb{T}$
V_5	$2e_q^2e_d\mathbb{T}$	$2e_q^2e_d(-\frac{1}{N}\mathbb{T}+\frac{(N^2-1)}{4N^2}\mathbb{I})$
V_6	$2e_q^2e_d\mathbb{T}$	$2e_q^2e_d(\frac{(N^2-2)}{2N}\mathbb{T}+\frac{(N^2-1)}{4N^2}\mathbb{I})$
V_7	$e_q(e_q^2+e_d^2)\frac{(N^2-1)}{2N}\mathbb{I}$	$e_q(e_q^2+e_d^2)(-\frac{1}{2N})\mathbb{T}$
V_8	$2e_q^2e_d\mathbb{T}$	$2e_q^2e_d(-\frac{1}{N}\mathbb{T}+\frac{(N^2-1)}{4N^2}\mathbb{I})$
V_9	$2e_q^2e_d\mathbb{T}$	$2e_q^2e_d(\frac{(N^2-2)}{2N}\mathbb{T}+\frac{(N^2-1)}{4N^2}\mathbb{I})$
V_{10}	$e_q(e_q^2+e_d^2)\frac{(N^2-1)}{2N}\mathbb{I}$	$e_q(e_q^2+e_d^2)\frac{(N^2-2)}{4N}\mathbb{T}$
V_{11}	$e_q^2e_d\frac{(N^2-1)}{2N}\mathbb{I}+\frac{e_q(e_q^2+e_d^2)}{2}\mathbb{T}$	$\frac{e_q(e_q^2+e_d^2)}{2}(-\frac{1}{N}\mathbb{T}+\frac{(N^2-1)}{4N^2}\mathbb{I})+e_q^2e_d\frac{(N^2-1)}{2N}\mathbb{T}$
V_{12}	$e_q^2e_d\frac{(N^2-1)}{2N}\mathbb{I}+\frac{e_q(e_q^2+e_d^2)}{2}\mathbb{T}$	$\frac{e_q(e_q^2+e_d^2)}{2}(\frac{(N^2-2)}{2N}\mathbb{T}+\frac{(N^2-1)}{4N^2}\mathbb{I})+e_q^2e_d\frac{(N^2-1)}{2N}\mathbb{T}$
V_{13}	$e_q(e_q^2+e_d^2)\frac{(N^2-1)}{2N}\mathbb{I}$	$e_q(e_q^2+e_d^2)\frac{(N^2-2)}{4N}\mathbb{T}$
V_{14}	$e_q^2e_d\frac{(N^2-1)}{2N}\mathbb{I}+\frac{e_q(e_q^2+e_d^2)}{2}\mathbb{T}$	$\frac{e_q(e_q^2+e_d^2)}{2}(-\frac{1}{N}\mathbb{T}+\frac{(N^2-1)}{4N^2}\mathbb{I})+e_q^2e_d\frac{(N^2-1)}{2N}\mathbb{T}$
V_{15}	$e_q^2e_d\frac{(N^2-1)}{2N}\mathbb{I}+\frac{e_q(e_q^2+e_d^2)}{2}\mathbb{T}$	$\frac{e_q(e_q^2+e_d^2)}{2}(\frac{(N^2-2)}{2N}\mathbb{T}+\frac{(N^2-1)}{4N^2}\mathbb{I})+e_q^2e_d\frac{(N^2-1)}{2N}\mathbb{T}$
V_{16}	$e_q^2e_d\frac{(N^2-1)}{2N}\mathbb{I}+\frac{e_q(e_q^2+e_d^2)}{2}\mathbb{T}$	$\frac{e_q(e_q^2+e_d^2)}{2}(-\frac{1}{N}\mathbb{T}+\frac{(N^2-1)}{4N^2}\mathbb{I})+e_q^2e_d\frac{-1}{2N}\mathbb{T}$
V_{17}	$e_q^2e_d\frac{(N^2-1)}{2N}\mathbb{I}+\frac{e_q(e_q^2+e_d^2)}{2}\mathbb{T}$	$\frac{e_q(e_q^2+e_d^2)}{2}(-\frac{1}{N}\mathbb{T}+\frac{(N^2-1)}{4N^2}\mathbb{I})+e_q^2e_d\frac{-1}{2N}\mathbb{T}$
V_{18}	$e_q^2e_d\frac{(N^2-1)}{2N}\mathbb{I}+\frac{e_q(e_q^2+e_d^2)}{2}\mathbb{T}$	$\frac{e_q(e_q^2+e_d^2)}{2}(\frac{(N^2-2)}{2N}\mathbb{T}+\frac{(N^2-1)}{4N^2}\mathbb{I})+e_q^2e_d\frac{-1}{2N}\mathbb{T}$
V_{19}	$e_q^2e_d\frac{(N^2-1)}{2N}\mathbb{I}+\frac{e_q(e_q^2+e_d^2)}{2}\mathbb{T}$	$\frac{e_q(e_q^2+e_d^2)}{2}(\frac{(N^2-2)}{2N}\mathbb{T}+\frac{(N^2-1)}{4N^2}\mathbb{I})+e_q^2e_d\frac{-1}{2N}\mathbb{T}$
V_{20}	$2e_q^2e_d\mathbb{T}$	$\frac{(N^2-1)}{4N^2}\mathbb{I}+e_q^2e_d(\frac{(N^2-4)}{2N}\mathbb{T})$
V_{21}	$2e_q^2e_d\mathbb{T}$	$\frac{(N^2-1)}{4N^2}\mathbb{I}+e_q^2e_d(\frac{(N^2-4)}{2N}\mathbb{T})$
V_{22}	$e_q(e_q^2+e_d^2)\frac{(N^2-1)}{2N}\mathbb{I}$	$e_q(e_q^2+e_d^2)\frac{-1}{2N}\mathbb{I}$
V_{23}	$2e_q^2e_d\mathbb{T}$	$2e_q^2e_d(-\frac{1}{N}\mathbb{T}+\frac{(N^2-1)}{4N^2}\mathbb{I})$
V_{24}	$2e_q^2e_d\mathbb{T}$	$2e_q^2e_d(\frac{(N^2-2)}{2N}\mathbb{T}+\frac{(N^2-1)}{4N^2}\mathbb{I})$

Table 2.8: Colour+charge factors for diagrams in fig.(2.5) with $O(\alpha_s\alpha_e)$ QCD+QED corrections, when QED-penguin operators O_7-O_{10} are inserted.

diagram	$\mathbb{I}$	$\mathbb{T}$
P_2	$e_d e_q \frac{(N^2-1)}{2N}\mathbb{I} + e_d^2\mathbb{T}$	$e_d e_q(-\frac{(N^2-1)}{4N^2}\mathbb{I}) + e_d^2(-\frac{1}{2N}\mathbb{T})$
P_3	$e_d e_q \frac{(N^2-1)}{2N}\mathbb{I} + e_d^2\mathbb{T}$	$e_d e_q(-\frac{(N^2-1)}{4N^2}\mathbb{I}) + e_d^2(-\frac{1}{2N}\mathbb{T})$
P_5	$\frac{(N^2-1)}{2N} e_d e_q\mathbb{I} + e_d^2\mathbb{T}$	$e_d e_q(\frac{(N^2-1)^2}{4N^2}\mathbb{I}) + e_d^2(-\frac{1}{2N}\mathbb{T})$
P_8	$e_d e_q \frac{(N^2-1)}{2N}\mathbb{I} + e_d^2\mathbb{T}$	$e_d e_q(\frac{(N^2-1)^2}{4N^2}\mathbb{I}) + e_d^2(-\frac{1}{2N}\mathbb{T})$
P_9	$e_d e_q \frac{(N^2-1)}{2N}\mathbb{I} + e_d^2\mathbb{T}$	$e_d e_q(\frac{(N^2-1)^2}{4N^2}\mathbb{I}) + e_d^2(-\frac{1}{2N}\mathbb{T})$
P_{10}	$e_d e_q\mathbb{T}$	$e_d e_q(-\frac{1}{2N}\mathbb{T})$
P_{11}	$e_d e_q\mathbb{T}$	$e_d e_q(-\frac{1}{2N}\mathbb{T})$
P_{13}	$e_d e_q \frac{(N^2-1)}{2N}\mathbb{I} + e_d^2\mathbb{T}$	$e_d e_q(-\frac{(N^2-1)}{4N^2}\mathbb{I} + e_d^2\frac{(N^2-1)}{2N}\mathbb{T})$
P_{14}	$e_d e_q\mathbb{T}$	$e_d e_q \frac{(N^2-1)}{2N}\mathbb{T})$
P_{15}	$e_d e_q\mathbb{T}$	$e_d e_q(-\frac{1}{2N}\mathbb{T})$

Table 2.9: Colour factors for diagrams in fig.(2.6) with $O(\alpha_s\alpha_e)$ QCD+QED corrections, when QCD-penguin operators O_3-O_6 are inserted.

diagram	$\mathbb{I}$	$\mathbb{T}$
P_2	$e_d^2 e_q \frac{(N^2-1)}{2N}\mathbb{I} + e_d^3\mathbb{T}$	$e_d^2 e_q(-\frac{(N^2-1)}{4N^2}\mathbb{I}) + e_d^3(-\frac{1}{2N}\mathbb{T})$
P_3	$e_d^2 e_q \frac{(N^2-1)}{2N}\mathbb{I} + e_d^3\mathbb{T}$	$e_d^2 e_q(-\frac{(N^2-1)}{4N^2}\mathbb{I}) + e_d^3(-\frac{1}{2N}\mathbb{T})$
P_5	$e_d^2 e_q \frac{(N^2-1)}{2N}\mathbb{I} + e_d^3\mathbb{T}$	$e_d^2 e_q(-\frac{(N^2-1)^2}{4N^2}\mathbb{I}) + e_d^3(-\frac{1}{2N}\mathbb{T})$
P_8	$e_d^2 e_q \frac{(N^2-1)}{2N}\mathbb{I} + e_d^3\mathbb{T}$	$e_d^2 e_q(-\frac{(N^2-1)^2}{4N^2}\mathbb{I}) + e_d^3(-\frac{1}{2N}\mathbb{T})$
P_9	$e_d^2 e_q \frac{(N^2-1)}{2N}\mathbb{I} + e_d^3\mathbb{T}$	$e_d^2 e_q(-\frac{(N^2-1)^2}{4N^2}\mathbb{I}) + e_d^3(-\frac{1}{2N}\mathbb{T})$
P_{10}	$e_d^2 e_q\mathbb{T}$	$e_d^2 e_q(-\frac{1}{2N}\mathbb{T})$
P_{11}	$e_d^2 e_q\mathbb{T}$	$e_d^2 e_q(-\frac{1}{2N}\mathbb{T})$
P_{13}	$e_d^2 e_q \frac{(N^2-1)}{2N}\mathbb{I} + e_d^3\mathbb{T}$	$e_d^2 e_q(-\frac{(N^2-1)}{4N^2}\mathbb{I} + e_d^3\frac{(N^2-1)}{2N}\mathbb{T})$
P_{14}	$e_d^2 e_q\mathbb{T}$	$e_d^2 e_q\frac{(N^2-1)}{2N}\mathbb{T})$
P_{15}	$e_d^2 e_q\mathbb{T}$	$e_d^2 e_q(-\frac{1}{2N}\mathbb{T})$

Table 2.10: Colour factors for diagrams in fig.(2.6) with $O(\alpha_s\alpha_e)$ QCD+QED corrections, when QED-penguin operators O_7-O_{10} are inserted.

diagram	$\mathbb{I}$	$\mathbb{T}$
F_2	0	$\frac{1}{2}e_u e_d \frac{(N^2-1)}{2N}\mathbb{I} + \frac{1}{2}e_u e_d \mathbb{T}$
F_3	0	$\frac{1}{2}e_u e_d \frac{(N^2-1)}{2N}\mathbb{I} + \frac{1}{2}e_u e_d \mathbb{T}$
F_5	$e_u e_q \frac{(N^2-1)}{2}\mathbb{I}$	$\frac{1}{2}e_d^2 \mathbb{T}$
F_8	$e_u e_q \frac{(N^2-1)}{2}\mathbb{I}$	$\frac{1}{2}e_u^2 \mathbb{T}$
F_9	$e_u e_q \frac{(N^2-1)}{2}\mathbb{I}$	$\frac{1}{2}e_u^2 \mathbb{T}$
F_{10}	0	$e_u e_q \mathbb{T}$
F_{11}	0	$e_u e_q \mathbb{T}$
F_{13}	$e_u e_d N \mathbb{T}$	$\frac{1}{2}e_d e_q \frac{(N^2-1)}{2N}\mathbb{I}$
F_{14}	$e_u e_q N \mathbb{T}$	$\frac{1}{2}e_d e_q \mathbb{T}$
F_{15}	$e_u e_q N \mathbb{T}$	$\frac{1}{2}e_d e_q \mathbb{T}$

Table 2.11: Colour factors for diagrams in fig.(2.7) with $O(\alpha_s\alpha_e)$ QCD+QED corrections, when vertex operators O_1 and O_2 are inserted.

diagram	$\mathbb{I}$	$\mathbb{T}$
F_2	0	$\frac{1}{2}(e_u N_u + e_d N_d)e_d \frac{(N^2-1)}{2N}\mathbb{I} + \frac{1}{2}(e_u N_u + e_d N_d)e_d \mathbb{T}$
F_3	0	$\frac{1}{2}(e_u N_u + e_d N_d)e_d \frac{(N^2-1)}{2N}\mathbb{I} + \frac{1}{2}(e_u N_u + e_d N_d)e_d \mathbb{T}$
F_5	$(e_u N_u + e_d N_d)e_q \frac{(N^2-1)}{2N}\mathbb{I}$	$\frac{1}{2}e_d^2 \mathbb{T}$
F_8	$(e_u N_u + e_d N_d)e_q \frac{(N^2-1)}{2N}\mathbb{I}$	$\frac{1}{2}(e_u^2 N_u + e_d^2 N_d)\mathbb{T}$
F_9	$(e_u N_u + e_d N_d)e_q \frac{(N^2-1)}{2N}\mathbb{I}$	$\frac{1}{2}(e_u^2 N_u + e_d^2 N_d)\mathbb{T}$
F_{10}	0	$(e_u N_u + e_d N_d)e_q \mathbb{T}$
F_{11}	0	$(e_u N_u + e_d N_d)e_q \mathbb{T}$
F_{13}	$(e_u N_u + e_d N_d)e_d N \mathbb{T}$	$\frac{1}{2}e_d e_q N_f \frac{(N^2-1)}{2N}\mathbb{I}$
F_{14}	$(e_u N_u + e_d N_d)e_q N \mathbb{T}$	$\frac{1}{2}e_d e_q N_f \mathbb{T}$
F_{15}	$(e_u N_u + e_d N_d)e_q N \mathbb{T}$	$\frac{1}{2}e_d e_q N_f \mathbb{T}$

Table 2.12: Colour factors for diagrams in fig.(2.7) with $O(\alpha_s\alpha_e)$ QCD+QED corrections, when QCD-penguin operators O_3-O_6 are inserted.

diagram	$\mathbb{I}$	$\mathbb{T}$
F_2	0	$\frac{1}{2}(e_u^2 N_u + e_d^2 N_d) e_d \frac{(N^2-1)}{2N}\mathbb{I} + \frac{1}{2}(e_u^2 N_u + e_d^2 N_d) e_d \mathbb{T}$
F_3	0	$\frac{1}{2}(e_u^2 N_u + e_d^2 N_d) e_d \frac{(N^2-1)}{2N}\mathbb{I} + \frac{1}{2}(e_u^2 N_u + e_d^2 N_d) e_d \mathbb{T}$
F_5	$(e_u^2 N_u + e_d^2 N_d) e_q \frac{(N^2-1)}{2}\mathbb{I}$	$\frac{1}{2}(e_u N_u + e_d N_d) e_d^2 \mathbb{T}$
F_8	$(e_u^2 N_u + e_d^2 N_d) e_q \frac{(N^2-1)}{2}\mathbb{I}$	$\frac{1}{2}(e_u^3 N_u + e_d^3 N_d) \mathbb{T}$
F_9	$(e_u N_u + e_d N_d) e_q \frac{(N^2-1)}{2}\mathbb{I}$	$\frac{1}{2}(e_u^3 N_u + e_d^3 N_d) \mathbb{T}$
F_{10}	0	$(e_u^2 N_u + e_d^2 N_d) e_q \mathbb{T}$
F_{11}	0	$(e_u^2 N_u + e_d^2 N_d) e_q \mathbb{T}$
F_{13}	$(e_u^2 N_u + e_d^2 N_d) e_d N \mathbb{T}$	$\frac{1}{2}(e_u N_u + e_d N_d) e_d e_q \frac{(N^2-1)}{2N}\mathbb{I}$
F_{14}	$(e_u^2 N_u + e_d^2 N_d) e_q N \mathbb{T}$	$\frac{1}{2}(e_u N_u + e_d N_d) e_d e_q \mathbb{T}$
F_{15}	$(e_u^2 N_u + e_d^2 N_d) e_q N \mathbb{T}$	$\frac{1}{2}(e_u N_u + e_d N_d) e_d e_q \mathbb{T}$

Table 2.13: Colour factors for diagrams in fig.(2.7) with $O(\alpha_s \alpha_e)$ QCD+QED corrections, when QED-penguin operators O_7-O_{10} are inserted.

2.2.4 Anomalous dimension matrix

Operator mixing in the renormalization of the EH gives the Anomalous Dimension Matrix. All the necessary ingredients, see 2.2.1 and 2.2.3, have been already introduced. The one-loop Anomalous Dimension Matrix [14, 41] gives already a complete implementation of the formalism explained in the previous section, where all the main characteristics of the mixing phenomenon can be are present.Here we will report the final expression for the $O(\alpha_{QCD})$ and for the $O(\alpha_{QED})$ matrices, denoting them as $\hat{\gamma}_s^{(0)}$ and $\hat{\gamma}_e^{(0)}$ respectively. The singular terms for each one-loop diagram are reported in table (2.14).

For convenience, we will split the (10×10) each Anomalous Dimension Matrices in four sub-matrices, defined as:

$$\hat{\gamma}_s^{(0)} = \begin{pmatrix} \hat{\gamma}_s^{(0)(ss)} & \hat{\gamma}_s^{(0)(se)} \\ \hat{\gamma}_s^{(0)(es)} & \hat{\gamma}_s^{(0)(ee)} \end{pmatrix} \tag{2.140}$$

for $\hat{\gamma}_s^{(0)}$ and as:

$$\hat{\gamma}_e^{(0)} = \begin{pmatrix} \hat{\gamma}_e^{(0)(ss)} & \hat{\gamma}_e^{(0)(se)} \\ \hat{\gamma}_e^{(0)(es)} & \hat{\gamma}_e^{(0)(ee)} \end{pmatrix} \tag{2.141}$$

for $\hat{\gamma}_e^{(0)}$. Moreover, with respect to the notation used in Section 2.2.3, we will replace:

- $N_f \longrightarrow f$,

- $N_u \longrightarrow u$,
- $N_d \longrightarrow d$,

Among the eight sum-matrices in (2.140) and (2.141), $\hat{\gamma}_s^{(0)(se)} = 0$ and the other seven are given by [30, 41]:

$$\hat{\gamma}_s^{(0)(ss)} = \begin{pmatrix} -2 & 6 & 0 & 0 & 0 & 0 \\ 6 & -2 & -\frac{2}{9} & \frac{2}{3} & -\frac{2}{9} & \frac{2}{3} \\ 0 & 0 & -\frac{22}{9} & \frac{22}{3} & -\frac{4}{9} & \frac{4}{3} \\ 0 & 0 & 6-\frac{2}{9}f & -2+\frac{2}{3}f & -\frac{2}{9}f & \frac{2}{3} \\ 0 & 0 & 0 & 0 & 2 & -6 \\ 0 & 0 & -\frac{2}{9}f & \frac{2}{3}f & -\frac{2}{9}f & -16+\frac{2}{3}f \end{pmatrix} \tag{2.142}$$

$$\hat{\gamma}_s^{(0)(es)} = \begin{pmatrix} 0 & 0 & 0 & 0 & 0 & 0 \\ 0 & 0 & \left(-\frac{2}{9}u+\frac{1}{9}d\right) & \left(\frac{2}{3}u-\frac{1}{3}d\right) & \left(-\frac{2}{9}u+\frac{1}{9}d\right) & \left(\frac{2}{3}u-\frac{1}{3}d\right) \\ 0 & 0 & \frac{2}{9} & -\frac{2}{3} & \frac{2}{9} & -\frac{2}{3} \\ 0 & 0 & \left(-\frac{2}{9}u+\frac{1}{9}d\right) & \left(\frac{2}{3}u-\frac{1}{3}d\right) & \left(-\frac{2}{9}u+\frac{1}{9}d\right) & \left(\frac{2}{3}u-\frac{1}{3}d\right) \end{pmatrix} \tag{2.143}$$

$$\hat{\gamma}_s^{(0)(ee)} = \begin{pmatrix} 2 & -6 & 0 & 0 \\ 0 & -16 & 0 & 0 \\ 0 & 0 & -2 & 6 \\ 0 & 0 & 6 & -2 \end{pmatrix} \tag{2.144}$$

$$\hat{\gamma}_e^{(0)(ss)} = \begin{pmatrix} -\frac{8}{3} & 0 & 0 & 0 & 0 & 0 \\ 0 & -\frac{8}{3} & 0 & 0 & 0 & 0 \\ 0 & 0 & 0 & 0 & 0 & 0 \\ 0 & 0 & 0 & 0 & 0 & 0 \\ 0 & 0 & 0 & 0 & 0 & 0 \\ 0 & 0 & 0 & 0 & 0 & 0 \end{pmatrix} \tag{2.145}$$

$$\hat{\gamma}_e^{(0)(se)} = \begin{pmatrix} \frac{16}{9} & 0 & \frac{16}{9} & 0 \\ \frac{16}{27} & 0 & \frac{16}{27} & 0 \\ \left(-\frac{16}{27}+\frac{16}{9}u-\frac{8}{9}d\right) & 0 & \left(-\frac{88}{27}+\frac{16}{9}u-\frac{8}{9}d\right) & 0 \\ \left(-\frac{16}{9}+\frac{16}{27}u-\frac{8}{27}d\right) & 0 & \left(-\frac{16}{9}+\frac{16}{27}u-\frac{8}{27}d\right) & 0 \\ \left(\frac{8}{3}+\frac{16}{9}u-\frac{8}{9}d\right) & 0 & \left(\frac{16}{9}u-\frac{8}{9}d\right) & 0 \\ \left(\frac{16}{27}u-\frac{8}{27}d\right) & 0 & \left(\frac{16}{27}u-\frac{8}{27}d\right) & 0 \end{pmatrix} \tag{2.146}$$

$$\hat{\gamma}_e^{(0)(es)} = \begin{pmatrix} 0 & 0 & 0 & 0 & \frac{4}{3} & 0 \\ 0 & 0 & 0 & 0 & 0 & \frac{4}{3} \\ 0 & 0 & -\frac{4}{3} & 0 & 0 & 0 \\ 0 & 0 & 0 & -\frac{4}{3} & 0 & 0 \end{pmatrix} \tag{2.147}$$

diagram	$\gamma_L^\mu \otimes \gamma_{\mu L}$		$\gamma_L^\mu \otimes \gamma_{\mu R}$	
	$(1/\epsilon)$	$O(1)$	$(1/\epsilon)$	$O(1)$
V_1	2	5	2	5
V_2	-8	-19	8	-3
V_3	2	5	-2	20
P_1	-4/3	-20/9	0	0
F_1	-4/3	-20/9	-4/3	-20/9

Table 2.14: Singular and finite terms for diagrams in fig.(2.4), with $\gamma_L^\mu \otimes \gamma_{\mu L}$ or $\gamma_L^\mu \otimes \gamma_{\mu R}$ Dirac structure.

$$\hat{\hat{\gamma}}_e^{(0)(ee)} = \begin{pmatrix} \left(\frac{4}{3} + \frac{16}{9}u + \frac{4}{9}d\right) & 0 & \left(\frac{16}{9}u + \frac{4}{9}d\right) & 0 \\ \left(\frac{16}{27}u + \frac{4}{27}d\right) & 0 & \left(\frac{16}{27}u + \frac{4}{27}d\right) & 0 \\ \left(\frac{8}{27} + \frac{16}{9}u + \frac{4}{9}d\right) & 0 & \left(-\frac{28}{27} + \frac{16}{9}u + \frac{4}{9}d\right) & 0 \\ \left(\frac{8}{9} + \frac{16}{27}u + \frac{4}{27}d\right) & 0 & \left(\frac{8}{9} + \frac{16}{27}u + \frac{4}{27}d\right) & -\frac{4}{3} \end{pmatrix} \tag{2.148}$$

On the other hand, we have not given yet all the elements to evaluate the two-loop Anomalous Dimension Matrix because the details of the analytical calculation will be the argument of the next chapter. Nevertheless we can anticipate our final result for completeness. Also in this case we will give two matrices: the pure QCD one $\hat{\hat{\gamma}}_s^{(1)}$ (two gluon insertions) and the mixed QCD+QED one $\hat{\hat{\gamma}}_e^{(1)}$ (one gluon and one photon insertion), splitting each of them in four sub-matrices as we have done in the one-loop case, i.e.:

$$\hat{\hat{\gamma}}_s^{(1)} = \begin{pmatrix} \hat{\hat{\gamma}}_s^{(1)(ss)} & \hat{\hat{\gamma}}_s^{(1)(se)} \\ \hat{\hat{\gamma}}_s^{(1)(es)} & \hat{\hat{\gamma}}_s^{(1)(ee)} \end{pmatrix} \tag{2.149}$$

for $\hat{\hat{\gamma}}_s^{(1)}$ and as:

$$\hat{\hat{\gamma}}_e^{(1)} = \begin{pmatrix} \hat{\hat{\gamma}}_e^{(1)(ss)} & \hat{\hat{\gamma}}_e^{(1)(se)} \\ \hat{\hat{\gamma}}_e^{(1)(es)} & \hat{\hat{\gamma}}_e^{(1)(ee)} \end{pmatrix} \tag{2.150}$$

for $\hat{\hat{\gamma}}_e^{(1)}$. Among the eight sum-matrices in (2.149) and (2.150), again $\hat{\hat{\gamma}}_s^{(1)(se)} = 0$ and the other seven are given by:

$$\hat{\tilde{\gamma}}_s^{(1)(ss)} =$$

$$\begin{pmatrix}
\frac{553}{6}-\frac{58}{9}f & \frac{95}{2}-2f & \frac{23}{3} & 1 & -\frac{25}{3} & 1 \\
\frac{95}{2}-2f & \frac{553}{6}-\frac{58}{9}f & -\frac{400}{243} & \frac{832}{81} & -\frac{1192}{243} & \frac{472}{81} \\
0 & 0 & \frac{43193}{486}+\frac{11}{9}f & \frac{11-23}{162}-f & -\frac{2384}{243}-\frac{25}{3}f & \frac{944}{81}+f \\
0 & 0 & \frac{377}{6}+\frac{11}{9}f & \frac{565}{6}+\frac{310}{81}f & -\frac{50}{3}-\frac{1192}{243}f & 2+\frac{472}{81}f \\
0 & 0 & -\frac{73}{9}f & \frac{f}{3} & 121+f & -39-\frac{f}{3} \\
0 & 0 & -\frac{1228}{243}f & \frac{364}{81}f & \frac{95}{2}-\frac{562}{243}f & -\frac{85}{2}+\frac{418}{81}f
\end{pmatrix} \tag{2.151}$$

The first two columns of $\hat{\tilde{\gamma}}_s^{(1)(es)}$ are always zero and we will report here following only the last four columns:

$$\hat{\tilde{\gamma}}_s^{(1)(es)} =$$

$$\begin{pmatrix}
-\frac{73}{9}u+\frac{73}{18}d & \frac{1}{3}u-\frac{1}{6}d & -\frac{71}{9}u+\frac{71}{18}d & \frac{1}{3}u-\frac{1}{6}d \\
-\frac{1228}{243}u+\frac{614}{243}d & \frac{364}{81}u-\frac{182}{81}d & -\frac{238}{243}u+\frac{119}{243}d & \frac{814}{81}u-\frac{407}{81}d \\
\frac{400}{243}+\frac{23}{3}u-\frac{26}{3}d & -\frac{832}{81}+u-\frac{1}{2}d & \frac{1192}{243}-\frac{25}{3}u+\frac{25}{6}d & -\frac{472}{81}+u-\frac{1}{2}d \\
-\frac{23}{3}-\frac{400}{243}u-\frac{200}{243}d & -1+\frac{832}{81}u-\frac{416}{81}d & \frac{25}{3}-\frac{1192}{243}u+\frac{596}{243}d & -1+\frac{472}{81}u-\frac{236}{81}d
\end{pmatrix} \tag{2.152}$$

$$\hat{\tilde{\gamma}}_s^{(1)(ee)} = \begin{pmatrix}
121-\frac{62}{9}f & -39-\frac{2}{3}f & 0 & 0 \\
\frac{95}{2}-\frac{4}{3}f & -\frac{85}{2}-\frac{44}{9}f & 0 & 0 \\
0 & 0 & \frac{553}{6}-\frac{58}{9}f & \frac{95}{2}-2f \\
0 & 0 & \frac{95}{2}-2f & \frac{553}{6}-\frac{58}{9}f
\end{pmatrix} \tag{2.153}$$

$$\hat{\tilde{\gamma}}_e^{(1)(ss)} =$$

$$\begin{pmatrix}
\frac{194}{9} & -\frac{2}{3} & -\frac{88}{243} & \frac{88}{81} & -\frac{88}{243} & \frac{88}{81} \\
\frac{25}{3} & -\frac{49}{9} & -\frac{340}{729} & \frac{430}{243} & -\frac{340}{729} & \frac{430}{243} \\
0 & 0 & \frac{1258}{729} - \frac{88}{243}u + \frac{44}{243}d & -\frac{1258}{243} + \frac{88}{81}u - \frac{44}{81}d & -\frac{200}{729} - \frac{88}{243}u + \frac{44}{243}d & \frac{200}{243} + \frac{88}{81}u - \frac{44}{81}d \\
0 & 0 & -\frac{641}{243} - \frac{340}{729}u - \frac{100}{729}d & -\frac{655}{81} + \frac{340}{243}u + \frac{100}{243}d & \frac{88}{243} - \frac{340}{729}u - \frac{100}{729}d & -\frac{88}{81} + \frac{340}{243}u + \frac{100}{243}d \\
0 & 0 & -\frac{88}{243}u + \frac{44}{243}d & \frac{88}{81}u - \frac{44}{81}d & -2 - \frac{88}{243}u + \frac{44}{243}d & 6 + \frac{88}{81}u - \frac{44}{81}d \\
0 & 0 & -\frac{412}{729}u - \frac{64}{729}d & \frac{412}{243}u + \frac{64}{243}d & -3 - \frac{412}{729}u - \frac{64}{729}d & 7 + \frac{412}{243}u + \frac{64}{243}d
\end{pmatrix} \tag{2.154}$$

$$\hat{\tilde{\gamma}}_e^{(1)(se)} =$$

$$\begin{pmatrix}
\frac{328}{27} & -\frac{8}{9} & \frac{344}{27} & -\frac{8}{3} \\
\frac{6644}{729} & -\frac{148}{27} & \frac{4124}{729} & \frac{44}{9} \\
-\frac{4640}{729} + \frac{328}{27}u - \frac{164}{27}d & \frac{160}{27} - \frac{8}{9}u + \frac{4}{9}d & \frac{11920}{729} + \frac{344}{27}u - \frac{172}{27}d & \frac{16}{9} - \frac{8}{3}u + \frac{4}{3}d \\
-\frac{328}{27} + \frac{6664}{729}u - \frac{2320}{729}d & \frac{8}{9} - \frac{148}{27}u + \frac{80}{27}d + \frac{4}{27}f & -\frac{38}{27} + \frac{4124}{729}u - \frac{1168}{729}d & \frac{38}{9} + \frac{44}{9}u - \frac{16}{9}d \\
-\frac{232}{9} + \frac{328}{27}u - \frac{164}{27}d & \frac{40}{3} - \frac{8}{9}u + \frac{4}{9}d & \frac{344}{27}u - \frac{172}{27}d & -\frac{8}{3}u + \frac{4}{3}d \\
-2 + \frac{2900}{729}u - \frac{448}{729}d & \frac{182}{9} + \frac{140}{27}u - \frac{64}{27}d & \frac{5564}{729}u - \frac{1888}{729}d & -\frac{52}{9}u + \frac{32}{9}d
\end{pmatrix} \tag{2.155}$$

The first two columns of $\hat{\hat{\gamma}}_e^{(1)(es)}$ are always zero and we will report here following only the last four columns:

$$\hat{\hat{\gamma}}_e^{(1)(es)} =$$

$$\begin{pmatrix} -\frac{88}{243}u - \frac{22}{243}d & \frac{88}{81}u + \frac{22}{81}d & -\frac{116}{9} - \frac{88}{243}u - \frac{22}{243}d & \frac{20}{3} + \frac{88}{81}u + \frac{22}{81}d \\ -\frac{412}{729}u + \frac{32}{729}d & \frac{412}{243}u - \frac{32}{243}d & -1 - \frac{412}{729}u + \frac{32}{729}d & \frac{91}{9} + \frac{412}{243}u - \frac{32}{243}d \\ \frac{7228}{729} - \frac{88}{243}u - \frac{22}{243}d & \frac{548}{243} + \frac{88}{81}u + \frac{22}{81}d & \frac{100}{729} - \frac{88}{243}u - \frac{22}{243}d & -\frac{100}{243} + \frac{88}{81}u + \frac{22}{81}d \\ \frac{1333}{243} - \frac{340}{729}u + \frac{50}{729}d & \frac{107}{81} + \frac{340}{243}u - \frac{50}{243}d & -\frac{44}{243} - \frac{340}{729}u + \frac{50}{729}d & \frac{44}{81} + \frac{340}{243}u - \frac{50}{243}d \end{pmatrix} \tag{2.156}$$

$$\hat{\hat{\gamma}}_e^{(1)(ee)} =$$

$$\begin{pmatrix} -\frac{134}{9} + \frac{328}{27}u + \frac{82}{27}d & \frac{38}{3} - \frac{8}{9}u - \frac{2}{9}d & \frac{344}{27}u + \frac{86}{27}d & -\frac{8}{3} - \frac{2}{3}d \\ 2 + \frac{2900}{729}u + \frac{224}{729}d & \frac{154}{9} + \frac{140}{27}u + \frac{32}{27}d & \frac{5564}{729}u + \frac{944}{729}d & -\frac{52}{9}u - \frac{16}{9}d \\ \frac{2320}{729} + \frac{328}{27}u + \frac{82}{27}d & -\frac{80}{27} - \frac{8}{9}u - \frac{2}{9}d & \frac{9754}{729} + \frac{344}{27}u + \frac{86}{27}d & -\frac{14}{9} - \frac{8}{3} - \frac{2}{3}d \\ \frac{164}{27} + \frac{6644}{729}u + \frac{1160}{729}d & -\frac{4}{9} - \frac{148}{27}u - \frac{40}{27}d & \frac{244}{27} + \frac{4124}{729}u + \frac{584}{729}d & -\frac{68}{9} + \frac{44}{9} + \frac{8}{9}d \end{pmatrix} \tag{2.157}$$

The numerical contribution of each diagram can be found in Tables (2.16)-(2.19), for vertex and penguin diagrams respectively.

Moreover, at two loops we have to consider also the non-zero anomalous dimension of the weak current. In the HV scheme, $\gamma_J = \frac{16}{3}b$, with b the $O(\alpha_s^2)$ coefficient of the QCD β-function.

Finally, we should remark that both the one-loop and the two-loop Anomalous Dimension Matrix are comprehensive of the self-energy contributions. The corresponding diagrams are shown in fig.(2.8) and their colour+charge factors, pole coefficients and finite parts are given in Table (2.15). We report finite parts in the one-loop case only because it is the only case in which we need to know them, dealing with the Coefficient Function one-loop computation.

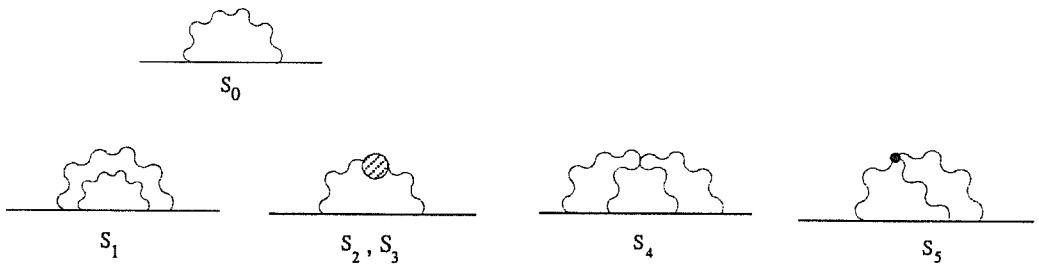

Figure 2.8: One-loop and two-loop self-energy diagrams.

Diagram	QCD	QED	$(1/\epsilon)$	$O(1)$
S_0	$\frac{N^2-1}{2N}\mathbb{I}$	$\mathbb{I}\, e_q^2$	-2	-2
S_1	$\frac{(N^2-1)^2}{4N^2}\mathbb{I}$	$\frac{N^2-1}{N}\mathbb{I}\, e_q^2$	-1	-
S_2	$\frac{N_f}{2}\frac{N^2-1}{2N}\mathbb{I}$	-	-4	-
S_3	$\frac{N^2-1}{2}\mathbb{I}$	-	5	-
S_4	$-\frac{1}{2N}\frac{N^2-1}{2N}\mathbb{I}$	$\frac{N^2-1}{N}\mathbb{I}\, e_q^2$	-2	-
S_5	$\frac{N^2-1}{2}\mathbb{I}$	-	11	-

Table 2.15: Colour+charge coefficients and singular+finite parts for the one-loop and two-loop self energy diagrams in fig.(2.8). For the two loop case the finite part is neglected, because of no relevance in the calculation. We denote the generic quark charge by e_q.

diagram	M	$G^{(0)}$	G_{CT}	$G_{CT}^{(EV)}$	$G^{(R)}$
V_4	2	$\left(\frac{1}{2}\frac{1}{\epsilon^2}+\frac{15}{4}\frac{1}{\epsilon}\right)$	$\left(\frac{1}{\epsilon^2}+\frac{5}{2}\frac{1}{\epsilon}\right)$	—	$\left(-\frac{1}{2}\frac{1}{\epsilon^2}+\frac{5}{4}\frac{1}{\epsilon}\right)$
V_5	2	$\left(\frac{8}{\epsilon^2}+\frac{37}{\epsilon}\right)$	$\left(\frac{16}{\epsilon^2}+\frac{22}{\epsilon}\right)$	$-\frac{7}{\epsilon}$	$\left(-\frac{8}{\epsilon^2}+\frac{8}{\epsilon}\right)$
V_6	2	$\left(\frac{1}{2}\frac{1}{\epsilon^2}+\frac{15}{4}\frac{1}{\epsilon}\right)$	$\left(\frac{1}{\epsilon^2}+\frac{5}{2}\frac{1}{\epsilon}\right)$	—	$\left(-\frac{1}{2}\frac{1}{\epsilon^2}+\frac{5}{4}\frac{1}{\epsilon}\right)$
V_7	2	$\left(-\frac{2}{\epsilon}\right)$	—	—	$\left(-\frac{2}{\epsilon}\right)$
V_8	2	$\left(-\frac{2}{\epsilon}\right)$	—	—	$\left(-\frac{2}{\epsilon}\right)$
V_9	2	$\left(-\frac{2}{\epsilon}\right)$	—	—	$\left(-\frac{2}{\epsilon}\right)$
V_{10}	4	$\left(\frac{1}{2}\frac{1}{\epsilon^2}+\frac{9}{4}\frac{1}{\epsilon}\right)$	$\left(\frac{1}{\epsilon^2}+\frac{5}{2}\frac{1}{\epsilon}\right)$	—	$\left(-\frac{1}{2}\frac{1}{\epsilon^2}-\frac{1}{4}\frac{1}{\epsilon}\right)$
V_{11}	4	$\left(-\frac{2}{\epsilon^2}-\frac{11}{2}\frac{1}{\epsilon}\right)$	$\left(-\frac{4}{\epsilon^2}-\frac{9}{\epsilon}\right)$	—	$\left(\frac{2}{\epsilon^2}+\frac{7}{2}\frac{1}{\epsilon}\right)$
V_{12}	4	$\left(\frac{1}{2}\frac{1}{\epsilon^2}+\frac{9}{4}\frac{1}{\epsilon}\right)$	$\left(\frac{1}{\epsilon^2}+\frac{5}{2}\frac{1}{\epsilon}\right)$	—	$\left(-\frac{1}{2}\frac{1}{\epsilon^2}-\frac{1}{4}\frac{1}{\epsilon}\right)$
V_{13}	4	$\left(-\frac{1}{2}\frac{1}{\epsilon^2}-\frac{9}{4}\frac{1}{\epsilon}\right)$	$\left(-\frac{1}{\epsilon^2}-\frac{5}{2}\frac{1}{\epsilon}\right)$	—	$\left(\frac{1}{2}\frac{1}{\epsilon^2}+\frac{1}{4}\frac{1}{\epsilon}\right)$
V_{14}	4	$\left(\frac{2}{\epsilon^2}+\frac{17}{2}\frac{1}{\epsilon}\right)$	$\left(\frac{4}{\epsilon^2}+\frac{9}{\epsilon}\right)$	—	$\left(-\frac{2}{\epsilon^2}-\frac{1}{2}\frac{1}{\epsilon}\right)$
V_{15}	4	$\left(-\frac{1}{2}\frac{1}{\epsilon^2}-\frac{9}{4}\frac{1}{\epsilon}\right)$	$\left(-\frac{1}{\epsilon^2}-\frac{5}{2}\frac{1}{\epsilon}\right)$	—	$\left(\frac{1}{2}\frac{1}{\epsilon^2}+\frac{1}{4}\frac{1}{\epsilon}\right)$
V_{16}	4	$\left(-\frac{2}{\epsilon^2}-\frac{17}{2}\frac{1}{\epsilon}\right)$	$\left(-\frac{4}{\epsilon^2}-\frac{8}{\epsilon}\right)$	$\frac{1}{\epsilon}$	$\left(\frac{2}{\epsilon^2}+\frac{1}{2}\frac{1}{\epsilon}\right)$
V_{17}	4	$\left(-\frac{2}{\epsilon^2}-\frac{19}{2}\frac{1}{\epsilon}\right)$	$\left(-\frac{4}{\epsilon^2}-\frac{9}{\epsilon}\right)$	—	$\left(\frac{2}{\epsilon^2}+\frac{1}{2}\frac{1}{\epsilon}\right)$
V_{18}	4	$\left(\frac{1}{2}\frac{1}{\epsilon^2}+\frac{17}{4}\frac{1}{\epsilon}\right)$	$\left(\frac{1}{\epsilon^2}+\frac{9}{2}\frac{1}{\epsilon}\right)$	$\frac{2}{\epsilon}$	$\left(-\frac{1}{2}\frac{1}{\epsilon^2}+\frac{3}{4}\frac{1}{\epsilon}\right)$
V_{19}	4	$\left(\frac{1}{2}\frac{1}{\epsilon^2}+\frac{13}{4}\frac{1}{\epsilon}\right)$	$\left(\frac{1}{\epsilon^2}+\frac{5}{2}\frac{1}{\epsilon}\right)$	—	$\left(-\frac{1}{2}\frac{1}{\epsilon^2}+\frac{3}{4}\frac{1}{\epsilon}\right)$
V_{20}	4	$\left(-\frac{2}{\epsilon^2}-\frac{17}{2}\frac{1}{\epsilon}\right)$	$\left(-\frac{4}{\epsilon^2}-\frac{7}{\epsilon}\right)$	$\frac{1}{\epsilon}$	$\left(\frac{2}{\epsilon^2}-\frac{1}{2}\frac{1}{\epsilon}\right)$
V_{21}	4	$\left(-\frac{2}{\epsilon^2}-\frac{19}{2}\frac{1}{\epsilon}\right)$	$\left(-\frac{4}{\epsilon^2}-\frac{10}{\epsilon}\right)$	—	$\left(\frac{2}{\epsilon^2}+\frac{1}{2}\frac{1}{\epsilon}\right)$
V_{22}	1	$\left(\frac{1}{\epsilon^2}+\frac{5}{\epsilon}\right)$	$\left(\frac{2}{\epsilon^2}+\frac{5}{\epsilon}\right)$	—	$-\frac{1}{\epsilon^2}$
V_{23}	1	$\left(\frac{16}{\epsilon^2}+\frac{74}{\epsilon}\right)$	$\left(\frac{32}{\epsilon^2}+\frac{76}{\epsilon}\right)$	$\frac{2}{\epsilon}$	$-\frac{16}{\epsilon^2}$
V_{24}	1	$\left(-\frac{1}{\epsilon^2}+\frac{5}{\epsilon}\right)$	$\left(\frac{2}{\epsilon^2}+\frac{5}{\epsilon}\right)$	—	$-\frac{1}{\epsilon^2}$

Table 2.16: Two loop pole contributions for the $\gamma_L^\mu \otimes \gamma_{\mu L}$ four-quark type diagrams in fig.(2.5), in the HV scheme.(Continue)

diagram	M	$G^{(0)}$	G_{CT}	$G_{CT}^{(EV)}$	$G^{(R)}$
V_{25}	4	$\left(\frac{3}{2}\frac{1}{\epsilon^2} - \frac{29}{4}\frac{1}{\epsilon}\right)$	$\left(-\frac{3}{\epsilon^2} - \frac{15}{2}\frac{1}{\epsilon}\right)$	–	$\left(\frac{3}{2}\frac{1}{\epsilon^2} + \frac{1}{4}\frac{1}{\epsilon}\right)$
V_{26}	4	$\left(\frac{6}{\epsilon^2} + \frac{55}{2}\frac{1}{\epsilon}\right)$	$\left(\frac{12}{\epsilon^2} + \frac{27}{\epsilon}\right)$	–	$\left(-\frac{6}{\epsilon^2} + \frac{1}{2}\frac{1}{\epsilon}\right)$
V_{27}	4	$\left(\frac{3}{2}\frac{1}{\epsilon^2} - \frac{29}{4}\frac{1}{\epsilon}\right)$	$\left(-\frac{3}{\epsilon^2} - \frac{15}{2}\frac{1}{\epsilon}\right)$	–	$\left(\frac{3}{2}\frac{1}{\epsilon^2} + \frac{1}{4}\frac{1}{\epsilon}\right)$
V_{28}	4	–	–	–	–
V_{29}	2	$\left(\frac{35}{12}N - \frac{7}{6}N_f\right)\frac{1}{\epsilon}$	$\left(\frac{10}{3}N - \frac{4}{3}N_f\right)\frac{1}{\epsilon}$	–	$\left(-\frac{5}{12}N + \frac{1}{6}N_f\right)\frac{1}{\epsilon}$
V_{30}	2	$\left(-\frac{5}{2}N + \frac{1}{2}N_f\right)\frac{1}{\epsilon^2}$	$(-5N + 2N_f)\frac{1}{\epsilon^2}$	–	$\left(\frac{5}{2}N - N_f\right)\frac{1}{\epsilon^2}$
		$+\left(-\frac{27}{2}N + 5N_f\right)\frac{1}{\epsilon}$	$+\left(-\frac{35}{3}N + \frac{14}{3}N_f\right)\frac{1}{\epsilon}$		$+\left(-\frac{11}{6}N + \frac{1}{3}N_f\right)\frac{1}{\epsilon}$
V_{31}	2	$\left(\frac{35}{12}N - \frac{7}{6}N_f\right)\frac{1}{\epsilon}$	$\left(\frac{10}{3}N - \frac{4}{3}N_f\right)\frac{1}{\epsilon}$	–	$\left(-\frac{5}{12}N + \frac{1}{6}N_f\right)\frac{1}{\epsilon}$

Table 2.16: (Continued) Two loop pole contributions for the $\gamma_L^\mu \otimes \gamma_{\mu L}$ four-quark type diagrams in fig.(2.5), in the HV scheme. For each diagram is given: the multiplicity (M), the value of the bare diagram ($G^{(0)}$), the value of the $\gamma_L^\mu \otimes \gamma_{\mu L}$-type counter-diagram ($G_{CT}$), the value of the evanescent operators counter-diagram ($G_{CT}^{(EV)}$) and the value of the renormalized diagram ($G^{(R)}$). All the results are not comprehensive of the multiplicity.

diagram	M	$G^{(0)}$	G_{CT}	$G_{CT}^{(EV)}$	$G^{(R)}$
V_4	2	$\left(\frac{1}{2}\frac{1}{\epsilon^2}+\frac{15}{4}\frac{1}{\epsilon}\right)$	$\left(\frac{1}{\epsilon^2}+\frac{5}{2}\frac{1}{\epsilon}\right)$	$-$	$\left(-\frac{1}{2}\frac{1}{\epsilon^2}+\frac{5}{4}\frac{1}{\epsilon}\right)$
V_5	2	$\left(\frac{1}{2}\frac{1}{\epsilon^2}+\frac{7}{4}\frac{1}{\epsilon}\right)$	$\left(\frac{1}{\epsilon^2}-\frac{1}{2}\frac{1}{\epsilon}\right)$	$-\frac{1}{\epsilon}$	$\left(-\frac{1}{2}\frac{1}{\epsilon^2}+\frac{5}{4}\frac{1}{\epsilon}\right)$
V_6	2	$\left(\frac{8}{\epsilon^2}+\frac{48}{\epsilon}\right)$	$\left(\frac{16}{\epsilon^2}+\frac{40}{\epsilon}\right)$	$-$	$\left(-\frac{8}{\epsilon^2}+\frac{8}{\epsilon}\right)$
V_7	2	$\left(-\frac{2}{\epsilon}\right)$	$-$	$-$	$\left(-\frac{2}{\epsilon}\right)$
V_8	2	$\left(-\frac{2}{\epsilon}\right)$	$-$	$-$	$\left(-\frac{2}{\epsilon}\right)$
V_9	2	$\left(-\frac{2}{\epsilon}\right)$	$-$	$-$	$\left(-\frac{2}{\epsilon}\right)$
V_{10}	4	$\left(\frac{1}{2}\frac{1}{\epsilon^2}+\frac{9}{4}\frac{1}{\epsilon}\right)$	$\left(\frac{1}{\epsilon^2}+\frac{5}{2}\frac{1}{\epsilon}\right)$	$-$	$\left(-\frac{1}{2}\frac{1}{\epsilon^2}-\frac{1}{4}\frac{1}{\epsilon}\right)$
V_{11}	4	$\left(-\frac{1}{2}\frac{1}{\epsilon^2}-\frac{7}{4}\frac{1}{\epsilon}\right)$	$\left(-\frac{1}{\epsilon^2}-\frac{3}{2}\frac{1}{\epsilon}\right)$	$-$	$\left(\frac{1}{2}\frac{1}{\epsilon^2}-\frac{1}{4}\frac{1}{\epsilon}\right)$
V_{12}	4	$\left(\frac{2}{\epsilon^2}\frac{6}{\epsilon}\right)$	$\left(\frac{4}{\epsilon^2}+\frac{10}{\epsilon}\right)$	$-$	$\left(-\frac{2}{\epsilon^2}-\frac{4}{\epsilon}\right)$
V_{13}	4	$\left(-\frac{1}{2}\frac{1}{\epsilon^2}-\frac{9}{4}\frac{1}{\epsilon}\right)$	$\left(-\frac{1}{\epsilon^2}-\frac{5}{2}\frac{1}{\epsilon}\right)$	$-$	$\left(\frac{1}{2}\frac{1}{\epsilon^2}+\frac{1}{4}\frac{1}{\epsilon}\right)$
V_{14}	4	$\left(\frac{1}{2}\frac{1}{\epsilon^2}+\frac{7}{4}\frac{1}{\epsilon}\right)$	$\left(\frac{1}{\epsilon^2}+\frac{3}{2}\frac{1}{\epsilon}\right)$	$-$	$\left(-\frac{1}{2}\frac{1}{\epsilon^2}-\frac{1}{4}\frac{1}{\epsilon}\right)$
V_{15}	4	$\left(-\frac{2}{\epsilon^2}-\frac{9}{\epsilon}\right)$	$\left(-\frac{4}{\epsilon^2}-\frac{10}{\epsilon}\right)$	$-$	$\left(\frac{2}{\epsilon^2}+\frac{1}{\epsilon}\right)$
V_{16}	4	$\left(-\frac{1}{2}\frac{1}{\epsilon^2}-\frac{7}{4}\frac{1}{\epsilon}\right)$	$\left(-\frac{1}{\epsilon^2}-\frac{1}{2}\frac{1}{\epsilon}\right)$	$\frac{1}{\epsilon}$	$\left(\frac{1}{2}\frac{1}{\epsilon^2}-\frac{1}{4}\frac{1}{\epsilon}\right)$
V_{17}	4	$\left(-\frac{1}{2}\frac{1}{\epsilon^2}-\frac{11}{4}\frac{1}{\epsilon}\right)$	$\left(-\frac{1}{\epsilon^2}-\frac{3}{2}\frac{1}{\epsilon}\right)$	$-$	$\left(\frac{1}{2}\frac{1}{\epsilon^2}-\frac{5}{4}\frac{1}{\epsilon}\right)$
V_{18}	4	$\left(\frac{2}{\epsilon^2}+\frac{11}{\epsilon}\right)$	$\left(\frac{4}{\epsilon^2}+\frac{12}{\epsilon}\right)$	$\frac{2}{\epsilon}$	$\left(-\frac{2}{\epsilon^2}\right)$
V_{19}	4	$\left(\frac{2}{\epsilon^2}+\frac{10}{\epsilon}\right)$	$\left(\frac{4}{\epsilon^2}+\frac{10}{\epsilon}\right)$	$-$	$\left(-\frac{2}{\epsilon^2}\right)$
V_{20}	4	$\left(-\frac{2}{\epsilon^2}-\frac{7}{\epsilon}\right)$	$\left(-\frac{4}{\epsilon^2}-\frac{4}{\epsilon}\right)$	$\frac{1}{\epsilon}$	$\left(\frac{2}{\epsilon^2}-\frac{2}{\epsilon}\right)$
V_{21}	4	$\left(-\frac{2}{\epsilon^2}-\frac{8}{\epsilon}\right)$	$\left(-\frac{4}{\epsilon^2}-\frac{10}{\epsilon}\right)$	$-$	$\left(\frac{2}{\epsilon^2}+\frac{2}{\epsilon}\right)$
V_{22}	1	$\left(\frac{1}{\epsilon^2}+\frac{5}{\epsilon}\right)$	$\left(\frac{2}{\epsilon^2}+\frac{5}{\epsilon}\right)$	$-$	$-\frac{1}{\epsilon^2}$
V_{23}	1	$\left(\frac{1}{\epsilon^2}+\frac{5}{\epsilon}\right)$	$\left(\frac{2}{\epsilon^2}+\frac{7}{\epsilon}\right)$	$\frac{2}{\epsilon}$	$-\frac{1}{\epsilon^2}$
V_{24}	1	$\left(\frac{16}{\epsilon^2}+\frac{80}{\epsilon}\right)$	$\left(\frac{32}{\epsilon^2}+\frac{80}{\epsilon}\right)$	$-$	$-\frac{16}{\epsilon^2}$

Table 2.17: Two loop pole contributions for the $\gamma_L^\mu \otimes \gamma_{\mu R}$ four-quark type diagrams in fig.(2.5), in the HV scheme.(Continue)

diagram	M	$G^{(0)}$	G_{CT}	$G_{CT}^{(EV)}$	$G^{(R)}$
V_{25}	4	$\left(\frac{3}{2}\frac{1}{\epsilon^2} - \frac{29}{4}\frac{1}{\epsilon}\right)$	$\left(-\frac{3}{\epsilon^2} - \frac{15}{2}\frac{1}{\epsilon}\right)$	–	$\left(\frac{3}{2}\frac{1}{\epsilon^2} + \frac{1}{4}\frac{1}{\epsilon}\right)$
V_{26}	4	$\left(\frac{3}{2}\frac{1}{\epsilon^2} + \frac{23}{4}\frac{1}{\epsilon}\right)$	$\left(\frac{3}{\epsilon^2} + \frac{9}{2}\frac{1}{\epsilon}\right)$	–	$\left(-\frac{3}{2}\frac{1}{\epsilon^2} + \frac{5}{4}\frac{1}{\epsilon}\right)$
V_{27}	4	$\left(-\frac{6}{\epsilon^2} - \frac{29}{\epsilon}\right)$	$\left(-\frac{12}{\epsilon^2} - \frac{30}{\epsilon}\right)$	–	$\left(\frac{6}{\epsilon^2} + \frac{1}{\epsilon}\right)$
V_{28}	4	–	–	–	–
V_{29}	2	$\left(\frac{35}{12}N - \frac{7}{6}N_f\right)\frac{1}{\epsilon}$	$\left(\frac{10}{3}N - \frac{4}{3}N_f\right)\frac{1}{\epsilon}$	–	$\left(-\frac{5}{12}N + \frac{1}{6}N_f\right)\frac{1}{\epsilon}$
V_{30}	2	$\left(-\frac{25}{12}N + \frac{5}{6}N_f\right)\frac{1}{\epsilon}$	$\left(-\frac{5}{3}N + \frac{2}{3}N_f\right)\frac{1}{\epsilon}$	–	$\left(-\frac{5}{12}N + \frac{1}{6}N_f\right)\frac{1}{\epsilon}$
V_{31}	2	$\left(\frac{5}{2}N - N_f\right)\frac{1}{\epsilon^2}$ $+\left(\frac{43}{3}N - \frac{16}{3}N_f\right)\frac{1}{\epsilon}$	$(5N - 2N_f)\frac{1}{\epsilon^2}$ $+\left(\frac{40}{3}N - \frac{16}{3}N_f\right)\frac{1}{\epsilon}$	–	$\left(-\frac{5}{2}N + N_f\right)\frac{1}{\epsilon^2}$ $+N\frac{1}{\epsilon}$

Table 2.17: (Continued) Two loop pole contributions for the $\gamma_L^\mu \otimes \gamma_{\mu R}$ four-quark type diagrams in fig.(2.5), in the HV scheme. For each diagram is given: the multiplicity (M), the value of the bare diagram ($G^{(0)}$), the value of the $\gamma_L^\mu \otimes \gamma_{\mu L}$-type counter-diagram ($G_{CT}$), the value of the evanescent operators counter-diagram ($G_{CT}^{(EV)}$) and the value of the renormalized diagram ($G^{(R)}$). All the results are not comprehensive of the multiplicity.

diagram	$G^{(0)}$	G_{CT}	$G_{CT}^{(EV)}$	$G^{(R)}$
P_2	$-\frac{26}{9}\frac{1}{\epsilon}$	$-\frac{8}{9}\frac{1}{\epsilon}$	–	$-\frac{34}{9}\frac{1}{\epsilon}$
P_3	$\left(\frac{4}{\epsilon^2}+\frac{128}{9}\frac{1}{\epsilon}\right)$	$\left(-\frac{8}{\epsilon^2}-\frac{112}{9}\frac{1}{\epsilon}\right)$	–	$\left(-\frac{4}{\epsilon^2}+\frac{16}{9}\frac{1}{\epsilon}\right)$
P_4	$\left(-\frac{23}{9}\frac{1}{\epsilon^2}-\frac{611}{54}\frac{1}{\epsilon}\right)$	$\left(\frac{46}{9}\frac{1}{\epsilon^2}+\frac{308}{27}\frac{1}{\epsilon}\right)$	–	$\left(\frac{23}{9}\frac{1}{\epsilon^2}+\frac{5}{54}\frac{1}{\epsilon}\right)$
P_4^{bg}	$\left(-\frac{22}{9}\frac{1}{\epsilon^2}-\frac{305}{27}\frac{1}{\epsilon}\right)$	$\left(\frac{44}{9}\frac{1}{\epsilon^2}+\frac{292}{27}\frac{1}{\epsilon}\right)$	–	$\left(\frac{22}{9}\frac{1}{\epsilon^2}+\frac{13}{27}\frac{1}{\epsilon}\right)$
P_6	$\left(\frac{8}{3}\frac{1}{\epsilon^2}+\frac{26}{3}\frac{1}{\epsilon}\right)$	$\left(-\frac{16}{3}\frac{1}{\epsilon^2}-\frac{100}{9}\frac{1}{\epsilon}\right)$	–	$\left(-\frac{8}{3}\frac{1}{\epsilon^2}-\frac{22}{9}\frac{1}{\epsilon}\right)$
P_6^{bg}	$\left(\frac{1}{9}\frac{1}{\epsilon^2}-\frac{59}{54}\frac{1}{\epsilon}\right)$	$\left(-\frac{2}{9}\frac{1}{\epsilon^2}-\frac{52}{27}\frac{1}{\epsilon}\right)$	–	$\left(-\frac{1}{9}\frac{1}{\epsilon^2}-\frac{163}{54}\frac{1}{\epsilon}\right)$
P_8	$\left(-\frac{4}{3}\frac{1}{\epsilon^2}-\frac{22}{3}\frac{1}{\epsilon}\right)$	$\left(\frac{8}{3}\frac{1}{\epsilon^2}+\frac{16}{9}\frac{1}{\epsilon}\right)$	$-\frac{4}{3}\frac{1}{\epsilon}$	$\left(\frac{4}{3}\frac{1}{\epsilon^2}-\frac{38}{9}\frac{1}{\epsilon}\right)$
P_9	$\left(\frac{4}{3}\frac{1}{\epsilon^2}+\frac{8}{3}\frac{1}{\epsilon}\right)$	$\left(-\frac{8}{9}\frac{1}{\epsilon^2}-\frac{40}{9}\frac{1}{\epsilon}\right)$	–	$\left(-\frac{4}{3}\frac{1}{\epsilon^2}+\frac{8}{9}\frac{1}{\epsilon}\right)$
P_{10}	$\left(-\frac{2}{\epsilon^2}-\frac{6}{\epsilon}\right)\cdot$LV+	$\left(\frac{4}{\epsilon^2}+\frac{16}{3}\frac{1}{\epsilon}\right)\cdot$LV	–	$\left(\frac{2}{\epsilon^2}\frac{1}{\epsilon^2}-\frac{2}{3}\frac{1}{\epsilon}\right)\cdot$LV+
	$\left(\frac{3}{\epsilon}\right)\cdot$LA	–	–	$\left(\frac{3}{\epsilon}\right)\cdot$LA
P_{11}	$\left(\frac{2}{\epsilon^2}+\frac{6}{\epsilon}\right)\cdot$LV+	$\left(-\frac{4}{\epsilon^2}-\frac{16}{3}\frac{1}{\epsilon}\right)\cdot$LV	–	$\left(-\frac{2}{\epsilon^2}\frac{1}{\epsilon^2}+\frac{2}{3}\frac{1}{\epsilon}\right)\cdot$LV+
	$\left(\frac{3}{\epsilon}\right)\cdot$LA	–	–	$\left(\frac{3}{\epsilon}\right)\cdot$LA
P_{13}	$\left(\frac{8}{9}\frac{1}{\epsilon^2}+\frac{139}{27}\frac{1}{\epsilon}\right)$	$\left(-\frac{16}{9}\frac{1}{\epsilon^2}-\frac{95}{27}\frac{1}{\epsilon}\right)$	–	$\left(-\frac{8}{9}\frac{1}{\epsilon^2}+\frac{44}{27}\frac{1}{\epsilon}\right)$
P_{14}	$\left(\frac{2}{\epsilon^2}+\frac{27}{3}\frac{1}{\epsilon}\right)\cdot$LV+	$\left(-\frac{4}{\epsilon^2}-\frac{22}{3}\frac{1}{\epsilon}\right)\cdot$LV+	–	$\left(-\frac{2}{\epsilon^2}\frac{1}{\epsilon^2}+\frac{5}{3}\frac{1}{\epsilon}\right)\cdot$LV+
	$\left(-\frac{1}{\epsilon^2}-\frac{31}{3}\frac{1}{\epsilon}\right)\cdot$LA	$\left(\frac{4}{\epsilon^2}+\frac{10}{\epsilon}\right)\cdot$LA	–	$\left(\frac{2}{\epsilon^2}-\frac{1}{3}\frac{1}{\epsilon}\right)\cdot$LA
P_{15}	$\left(-\frac{2}{\epsilon^2}-\frac{31}{3}\frac{1}{\epsilon}\right)\cdot$LV+	$\left(\frac{4}{\epsilon^2}+\frac{10}{\epsilon}\right)\cdot$LV+	–	$\left(\frac{2}{\epsilon^2}\frac{1}{\epsilon^2}-\frac{1}{3}\frac{1}{\epsilon}\right)\cdot$LV+
	$\left(-\frac{2}{\epsilon^2}-\frac{31}{3}\frac{1}{\epsilon}\right)\cdot$LA	$\left(\frac{4}{\epsilon^2}+\frac{10}{\epsilon}\right)\cdot$LA	–	$\left(\frac{2}{\epsilon^2}-\frac{1}{3}\frac{1}{\epsilon}\right)\cdot$LA

Table 2.18: Two loop pole contributions for the P-type penguin diagrams in fig.(2.6), when a $\gamma_L^\mu\otimes\gamma_{\mu L}$ structure is inserted in the upper vertex. For each diagram is given: the value of the bare diagram ($G^{(0)}$), the value of the counter-diagrams (G_{CT}), the value of the evanescent operators counter-diagrams ($G_{CT}^{(EV)}$) and the value of the renormalized diagram ($G^{(R)}$). All the results are comprehensive of the multiplicity. All penguin diagrams have a $\gamma_L^\mu\otimes\gamma_\mu$ structure, except P_{10}, P_{11}, P_{14} and P_{15}, for which we explicitly give the $\gamma_L^\mu\otimes\gamma_\mu$ (LV) and the $\gamma_L^\mu\otimes\gamma_\mu\gamma_5$ (LA) part. For P_4 and P_6 both the normal Feynman gauge and the background gauge results are reported. Diagrams F_5, F_7 and F_{12} are not included, because their simple pole coefficient is zero and they do not contribute to the two-loop anomalous dimension.

diagram	$G^{(0)}$	G_{CT}	$G_{CT}^{(EV)}$	$G^{(R)}$
F_2	$\left(-\frac{4}{\epsilon^2}-\frac{134}{9}\frac{1}{\epsilon}\right)$	$\left(\frac{8}{\epsilon^2}+\frac{100}{9}\frac{1}{\epsilon}\right)$	$\frac{2}{3}\frac{1}{\epsilon}$	$\left(\frac{4}{\epsilon^2}-\frac{28}{9}\frac{1}{\epsilon}\right)$
F_3	$\frac{20}{9}\frac{1}{\epsilon}$	$-\frac{4}{9}\frac{1}{\epsilon}$	$\frac{2}{3}\frac{1}{\epsilon}$	$\frac{22}{9}\frac{1}{\epsilon}$
F_4	$\left(-\frac{23}{9}\frac{1}{\epsilon^2}-\frac{611}{54}\frac{1}{\epsilon}\right)$	$\left(\frac{46}{9}\frac{1}{\epsilon^2}+\frac{308}{27}\frac{1}{\epsilon}\right)$	–	$\left(\frac{23}{9}\frac{1}{\epsilon^2}+\frac{5}{54}\frac{1}{\epsilon}\right)$
F_4^{bg}	$\left(-\frac{22}{9}\frac{1}{\epsilon^2}-\frac{305}{27}\frac{1}{\epsilon}\right)$	$\left(\frac{44}{9}\frac{1}{\epsilon^2}+\frac{292}{27}\frac{1}{\epsilon}\right)$	–	$\left(\frac{22}{9}\frac{1}{\epsilon^2}+\frac{13}{27}\frac{1}{\epsilon}\right)$
F_6	$\left(\frac{8}{3}\frac{1}{\epsilon^2}+\frac{26}{3}\frac{1}{\epsilon}\right)$	$\left(-\frac{16}{3}\frac{1}{\epsilon^2}-\frac{100}{9}\frac{1}{\epsilon}\right)$	–	$\left(-\frac{8}{3}\frac{1}{\epsilon^2}-\frac{22}{9}\frac{1}{\epsilon}\right)$
F_6^{bg}	$\left(\frac{1}{9}\frac{1}{\epsilon^2}-\frac{59}{54}\frac{1}{\epsilon}\right)$	$\left(-\frac{2}{9}\frac{1}{\epsilon^2}-\frac{52}{27}\frac{1}{\epsilon}\right)$	–	$\left(-\frac{1}{9}\frac{1}{\epsilon^2}-\frac{163}{54}\frac{1}{\epsilon}\right)$
F_8	$\left(-\frac{4}{3}\frac{1}{\epsilon^2}-\frac{22}{3}\frac{1}{\epsilon}\right)$	$\left(\frac{8}{3}\frac{1}{\epsilon^2}+\frac{16}{9}\frac{1}{\epsilon}\right)$	$-\frac{4}{3}\frac{1}{\epsilon}$	$\left(\frac{4}{3}\frac{1}{\epsilon^2}-\frac{38}{9}\frac{1}{\epsilon}\right)$
F_9	$\left(\frac{4}{3}\frac{1}{\epsilon^2}+\frac{8}{3}\frac{1}{\epsilon}\right)$	$\left(-\frac{8}{9}\frac{1}{\epsilon^2}-\frac{40}{9}\frac{1}{\epsilon}\right)$	–	$\left(-\frac{4}{3}\frac{1}{\epsilon^2}+\frac{8}{9}\frac{1}{\epsilon}\right)$
F_{10}	$\left(-\frac{2}{\epsilon^2}-\frac{6}{\epsilon}\right)\cdot$LV+	$\left(\frac{4}{\epsilon^2}+\frac{16}{3}\frac{1}{\epsilon}\right)\cdot$LV	–	$\left(\frac{2}{\epsilon^2}\frac{1}{\epsilon^2}-\frac{2}{3}\frac{1}{\epsilon}\right)\cdot$LV+
	$\left(-\frac{3}{\epsilon}\right)\cdot$LA	–	–	$\left(-\frac{3}{\epsilon}\right)\cdot$LA
F_{11}	$\left(\frac{2}{\epsilon^2}+\frac{6}{\epsilon}\right)\cdot$LV+	$\left(-\frac{4}{\epsilon^2}-\frac{16}{3}\frac{1}{\epsilon}\right)\cdot$LV	–	$\left(-\frac{2}{\epsilon^2}\frac{1}{\epsilon^2}+\frac{2}{3}\frac{1}{\epsilon}\right)\cdot$LV+
	$\left(-\frac{3}{\epsilon}\right)\cdot$LA	–	–	$\left(-\frac{3}{\epsilon}\right)\cdot$LA
F_{13}	$\left(\frac{8}{9}\frac{1}{\epsilon^2}+\frac{139}{27}\frac{1}{\epsilon}\right)$	$\left(-\frac{16}{9}\frac{1}{\epsilon^2}-\frac{95}{27}\frac{1}{\epsilon}\right)$	–	$\left(-\frac{8}{9}\frac{1}{\epsilon^2}+\frac{44}{27}\frac{1}{\epsilon}\right)$
F_{14}	$\left(\frac{2}{\epsilon^2}+\frac{27}{3}\frac{1}{\epsilon}\right)\cdot$LV+	$\left(-\frac{4}{\epsilon^2}-\frac{22}{3}\frac{1}{\epsilon}\right)\cdot$LV+	–	$\left(-\frac{2}{\epsilon^2}\frac{1}{\epsilon^2}+\frac{5}{3}\frac{1}{\epsilon}\right)\cdot$LV+
	$\left(-\frac{1}{\epsilon^2}-\frac{31}{3}\frac{1}{\epsilon}\right)\cdot$LA	$\left(\frac{4}{\epsilon^2}+\frac{10}{\epsilon}\right)\cdot$LA	–	$\left(\frac{2}{\epsilon^2}-\frac{1}{3}\frac{1}{\epsilon}\right)\cdot$LA
F_{15}	$\left(-\frac{2}{\epsilon^2}-\frac{31}{3}\frac{1}{\epsilon}\right)\cdot$LV+	$\left(\frac{4}{\epsilon^2}+\frac{10}{\epsilon}\right)\cdot$LV+	–	$\left(\frac{2}{\epsilon^2}\frac{1}{\epsilon^2}-\frac{1}{3}\frac{1}{\epsilon}\right)\cdot$LV+
	$\left(-\frac{2}{\epsilon^2}-\frac{31}{3}\frac{1}{\epsilon}\right)\cdot$LA	$\left(\frac{4}{\epsilon^2}+\frac{10}{\epsilon}\right)\cdot$LA	–	$\left(\frac{2}{\epsilon^2}-\frac{1}{3}\frac{1}{\epsilon}\right)\cdot$LA

Table 2.19: Two loop pole contributions for the F-type penguin diagrams in fig.(2.6), when a $\gamma_L^\mu\otimes\gamma_{\mu R}$ structure is inserted in the upper vertex. For each diagram is given: the value of the bare diagram ($G^{(0)}$), the value of the counter-diagrams (G_{CT}), the value of the evanescent operators counter-diagrams ($G_{CT}^{(EV)}$) and the value of the renormalized diagram ($G^{(R)}$). All the results are comprehensive of the multiplicity. All penguin diagrams have a $\gamma_L^\mu\otimes\gamma_\mu$ structure, except F_{10}, F_{11}, F_{14} and F_{15}, for which we explicitly give the $\gamma_L^\mu\otimes\gamma_\mu$ (LV) and the $\gamma_L^\mu\otimes\gamma_\mu\gamma_5$ (LA) part. For F_4 and F_6 both the normal Feynman gauge and the background gauge results are reported. Diagrams F_5, F_7 and F_{12} are not included, because their simple pole coefficient is zero and they do not contribute to the two-loop anomalous dimension.

Chapter 3

Two loop analytic calculation: methods and results

The determination of the initial conditions for the Coefficient Function and the operator mixing via QCD and QED radiative corrections have been discussed in detail in the previous chapter. As a final application, the two loop anomalous dimension matrices $\hat{\hat{\gamma}}_s^{(1)}$ and $\hat{\hat{\gamma}}_e^{(1)}$ for vertex+penguin operators have been given.

Each two-loop diagram can be thought as composed by the integration over loop-momenta plus the Dirac structure. In order to get rid of the singularities in the momentum-integration we need to regularize the theory and the choice of the regularization scheme influences the Dirac algebra. The regularization procedure may introduce new unphysical operators. These unphysical operators are an artifact of the regularization procedure and disappear in the final physical matrix which governs the evolution of the coefficient of the OPE. However, in the intermediate steps of the calculation their mixing with the operators of the $\{O_i\}_{1,\ldots,10}$ basis has to be taken into account. To fix the ideas we will work with different schemes of Dimensional Regularization. In this case several operators which arise in $N > 4$ dimensions are present. We will denote them as "*evanescent*" operators.

The aim of the present chapter is to explain in detail the analytic aspects of the calculation. We will emphasize the following aspects:

- choice of the regularization scheme;
- presence of evanescent operators and mixing with the 4-dimensional ones;
- choice of the subtraction scheme and counterterms in presence of $(N-4)$-dimensional operators;
- IR regularization, external momenta, masses, etc.;
- gauge choice and independence of the final result from this choice;

- on-shell or off-shell basis;
- results and comments.

The context of the present chapter is not essential to the understanding of the structure of the final matrices and for this reason $\hat{\hat{\gamma}}_s^{(1)}$ and $\hat{\hat{\gamma}}_e^{(1)}$ have been given in the previous chapter. Nevertheless the points mentioned before are very important from a technical point of view, and we report them in order to make the calculation more explicit and available for future comparisons or implementations.

3.1 Regularization schemes and N-dimensional extension of the operator basis

We have to regularize the UV (and eventually IR) divergencies of the theory. With the choice of Dimensional Regularization, i.e. by working in $N = (4-2\epsilon)$ dimensions and one immediately finds inconsistencies in the algebra of the γ-matrices. In a theory with fermion field and spinor structures, odd parity fermion loops, as for instance $Tr(\gamma_5\gamma_\mu\gamma_\nu\gamma_\rho\gamma_\sigma)$, are not well-defined in N-dim. Three schemes to handle the algebra of γ-matrices are very often quoted in literature : Naive Dimensional Regularization (NDR), Dimensional Reduction (DRED) and t'Hooft-Veltman (HV) regularization. We have decided to perform the calculation in the HV scheme, because of it is theoretically well-founded (the calculation in NDR, as a check of the results, will be done in a separate study). In any case we will list the peculiar features of both the NDR and HV schemes.

1. *Naive Dimensional Regularization* (NDR)

   In NDR γ-matrices are N-dimensional and only the N-dimensional metric tensor is introduced, following the convention:

   $$g_{\mu\nu} = g_{\nu\mu} \ , \quad g_\mu^\rho g_\rho^\nu = g_\mu^\nu \ , \quad g_\mu^\mu = N \ , \quad Tr(\mathbb{I}) = 4 \tag{3.1}$$

   The N-dimensional Dirac matrices obey the usual algebra:

   $$\{\gamma_\mu, \gamma_\nu\} = 2g_{\mu\nu} \tag{3.2}$$

   and γ_5 is taken to be anticommuting with the whole algebra, as if the γ's were 4-dimensional:

   $$\{\gamma_5, \gamma_\mu\} = 0 \tag{3.3}$$

   It si precisely here that the previous γ_5-ambiguity arises and the scheme fails to reproduce, f.i., the axial anomaly. Nevertheless it is maybe the most used scheme in literature and non rigorous proofs exist of its compatibility with more consistent and well-defined prescriptions.

2. *t'Hooft-Veltman Regularization* (HV)

With respect to NDR and DRED, the HV regularization scheme has a more solid theoretical background and has been proved not to reproduce ambiguities or inconsistencies in the γ-algebra [3, 11, 54]. The fundamental assumption is that the N-dimensional γ-matrices γ^μ are considered as the sum of two terms, a 4-dimensional one $\tilde{\gamma}^\mu$ and a $(N-4)$-dimensional one $\hat{\gamma}^\mu$, i.e.:

$$\gamma^\mu = \tilde{\gamma}^\mu + \hat{\gamma}_\mu \tag{3.4}$$

and different algebraic properties with respect to γ_5 are assumed for the 4-dim. and for the (-2ϵ)-dim. algebras. In both sector the usual Dirac algebra holds and two metric tensor are introduced, the 4-dim. one $\tilde{g}_{\mu\nu}$ and the (-2ϵ)-dim. one $\hat{g}_{\mu\nu}$:

$$\{\tilde{\gamma}_\mu, \tilde{\gamma}_\nu\} = 2\tilde{g}_{\mu\nu} \quad , \quad \{\hat{\gamma}_\mu, \hat{\gamma}_\nu\} = 2\hat{g}_{\mu\nu} \quad , \quad \{\hat{\gamma}_\mu, \tilde{\gamma}_\nu\} = 0 \tag{3.5}$$

with the following "mixed" contraction properties:

$$\tilde{g}^\mu_\mu = 4 \ , \quad \hat{g}^\mu_\mu = -2\epsilon \ , \quad \tilde{g}^\rho_\mu \hat{g}_{\rho\nu} = 0 \tag{3.6}$$

and

$$\tilde{g}^\rho_\mu g_{\rho\nu} = \tilde{g}^\nu_\mu \quad , \quad \hat{g}^\rho_\mu g_{\rho\nu} = \hat{g}^\nu_\mu \tag{3.7}$$

With respect to γ_5, the 4-dim. algebra anticommutes, while the (-2ϵ)-dim. one commutes, i.e.:

$$\{\tilde{\gamma}_\mu, \gamma_5\} = 0 \quad , \quad [\hat{\gamma}_\mu, \gamma_5] = 0 \tag{3.8}$$

The rigorousness of the method is precisely due to the splitting of the algebra and the price to be paid for that is a less straightforward analytic implementation of the algebra, due to the breaking of N-dim Lorentz invariance. One has to pay much more attention when dealing with some algebraic manipulation program, in order to clearly specify the right range for each index saturated on a γ-matrix.

A convenient assumption is to take, on one hand, 4-dim. external momenta but N-dim. loop momenta. On the other hand we will consider the renormalization of operators made by 4-dim. γ's, i.e.:

$$\tilde{\gamma}^\mu(1-\gamma_5) \otimes \tilde{\gamma}_\mu(1-\gamma_5) \quad \text{or} \quad \tilde{\gamma}^\mu(1-\gamma_5) \otimes \tilde{\gamma}_\mu(1+\gamma_5) \tag{3.9}$$

In order to fulfill this property, we have adopted the notation originally proposed in ref. [13] and write the weak vertex as:

$$\frac{1}{4}(1+\gamma_5)\gamma^\mu(1-\gamma_5) \otimes (1+\gamma_5)\gamma_\mu(1-\gamma_5) \tag{3.10}$$

and analogously for the $\gamma^\mu_L \otimes \gamma_{\mu R}$ case.

Both NDR and HV schemes provides some rules to handle, with or without inconsistencies, the problem of Dirac algebra in N-dimension. When we extend the usual 4-dim. basis of operators to the N-dimensional case many more independent

operators appear. They are operators which leave in $(N-4)$-dimensions and make sense only in the N-dimensional extension of the theory. The problem however seems to be much more complicated than in the case of the usual 4-dim. algebra. Indeed, in the 4-dim. case we can easily construct a basis for the γ-algebra, by identifying the sixteen independent antisymmetrized products out of the elements of the algebra. On the other hand in the N-dimensional case there exists an infinite number of such antisymmetrized products and an infinite number of independent operator seems to be required. Nevertheless the operator product expansion is still possible and we can get rid of such (-2ϵ)-dimensional operators as we will explain in the following.

The (-2ϵ)-dimensional operators are not present in the 4-dim. theory, i.e. we can image that they are somehow projected away at the end of the renormalization procedure. We can even take this as a definition of the "*evanescent*" operators, requiring their projection to the 4-dim. space to be exactly zero [13]. Either they are $\hat{\gamma}^\mu$-type structures or they are $O(\epsilon)$ contributions. In the former case they do not exist at all in the 4-dim. theory, in the latter case either they go to zero in the $\epsilon = 0$ limit or they can be reabsorbed in some finite parts of the 4-dim. operators. With this definition, we see that the calculation of the one-loop anomalous dimension will not be affected by the presence of evanescent operators, but they will be present in the two-loop calculation. Indeed, also if they do not appear by definition in the final result, their contribution appears at one-loop and, by insertion in a two-loop counter-diagram, this can modify the pole coefficient of the final two-loop result. More details will be given in section (3.2), when dealing with the construction of the counterterms.

3.2 Renormalization and counterterms in N-dimensions

In the HV or NDR regularization schemes we can succeed in computing the singular terms of each two-loop diagram. The next step will be to chose a renormalization prescription. We have chosen the modified minimal subtraction ($\overline{\text{MS}}$) prescription, i.e. each counterterm will subtract only the pole part (i.e. the $O(1/\epsilon)$ part) of the corresponding one-loop sub-diagram. Nevertheless the presence of evanescent "unphysical" operator adds some new features to the subtraction procedure.

To fix the ideas, let us denote the basis of the bare operators as $\{O_i^{(0)}\}_{i=1,\ldots,10}$ and the basis of the renormalized ones as $\{O_i\}_{i=1,\ldots,10}$. The relation between renormalized and bare operators is given through the operator renormalization constant (a matrix in the case of a multi-operator basis):

$$O_i = (\hat{\mathbb{Z}}_{\vec{\sigma}}^{-1})_{ij} O_j^{(0)} \tag{3.11}$$

The computation consists in evaluating all the renormalized one-loop and two-loop diagrams in fig.(2.4)-(2.7) for the subtracted four-quark Green functions with the in-

sertion of the operators $\{O_i\}_{i=1,\dots,10}$. In the same formalism, we will denote[1] by $\Gamma_4^{(0)}(\vec{O})$ the bare four-quark Green function and by $\Gamma_4(\vec{O})$ the renormalized one. The relation between bare and renormalized Green function is given by:

$$\Gamma_4(\vec{O}) = \hat{\mathbb{Z}}_{\vec{O}}^{-1}\hat{\mathbb{Z}}_{\psi}^{2}\Gamma_4^{(0)}(\vec{O}) \tag{3.12}$$

where $\hat{\mathbb{Z}}_{\psi}$ denotes the wave function renormalization function, obtained up to the two-loop level by computing the diagrams in fig.(2.8) and defined as the relation between bare and renormalized quark wave function:

$$\psi = \hat{\mathbb{Z}}_{\psi}^{-1/2}\psi^{(0)} \tag{3.13}$$

Defining the Anomalous Dimension Matrix for the four-quark Green function to be:

$$\hat{\gamma} = \mu\frac{\partial}{\partial\mu}\ln\hat{\mathbb{Z}} = \hat{\mathbb{Z}}^{-1}\frac{\partial}{\partial\mu}\hat{\mathbb{Z}} \tag{3.14}$$

the Anomalous Dimension Matrix for the operators in $\vec{O}$ will be obtained by adding the wave function contribution:

$$\hat{\gamma}_{\vec{O}} = \hat{\gamma} + 2\gamma_{\psi} \tag{3.15}$$

The self-energy contribution can be read off Table (2.15) and will be added at the end as: $2\gamma_{\psi}\cdot\mathbb{I}$ where $\mathbb{I}$ denotes the unit matrix in the operator vector space. By the way, we note here that in computing $\hat{\tilde{\gamma}} = \hat{\gamma} - 2\gamma_j$ we will have to account for γ_j in the same way, i.e. including the wave-function anomalous dimension there too. We will give γ_j, the two-loop anomalous dimension, in section 3.3. Indeed, while the one-loop current anomalous dimension is zero, the two-loop one depends on the regularization prescription: it vanishes in NDR but not in HV scheme.

For the time being, let us concentrate on $\hat{\gamma}$. We can also rewrite (3.14) as:

$$\hat{\gamma} = \mu\frac{\partial}{\partial\mu}\ln\hat{\mathbb{Z}} = \hat{\mathbb{Z}}^{-1}\left(-\epsilon g + \beta(g)\right)\frac{\partial}{\partial g}\hat{\mathbb{Z}} \tag{3.16}$$

being g the generic renormalized coupling constant of the theory. It means that the same general discussion could be applied both to pure QCD and to QCD+QED interactions. Remembering the $\beta(g)$ and $\hat{\gamma}$ perturbative expansions in (2.7) and (2.8) and giving an analogous expansion for the renormalization matrix:

$$\hat{\mathbb{Z}} = 1 + \frac{g^2}{16\pi^2}\hat{\mathbb{Z}}^{(1)} + \frac{g^4}{(16\pi^2)^2}\hat{\mathbb{Z}}^{(2)} + \cdots \tag{3.17}$$

from (3.16) we can derive the following relations:

$$\hat{\gamma}^{(0)} = -2\epsilon\hat{\mathbb{Z}}^{(1)} \tag{3.18}$$

[1] We introduce the more compact notation $\vec{O}$ in order to indicate the insertion of a generic operator of the basis.

and

$$\hat{\gamma}^{(1)} = -4\epsilon\hat{\mathbb{Z}}^{(2)} - 2b\hat{\mathbb{Z}}^{(1)} + 2\epsilon\hat{\mathbb{Z}}^{(1)}\hat{\mathbb{Z}}^{(1)} \tag{3.19}$$

Each term in the previous expansion of the renormalization coupling constant is indeed an expansion in powers of ϵ, i.e.:

$$\hat{\mathbb{Z}}^{(i)} = \sum_{j=0}^{i} \left(\frac{1}{\epsilon}\right)^{j} \hat{\mathbb{Z}}_{j}^{(i)} \tag{3.20}$$

while the anomalous dimension should be finite. This means that pole contribution mutually cancel. In particular:

$$4\hat{\mathbb{Z}}_{2}^{2} + 2b\hat{\mathbb{Z}}_{1}^{(1)} - 2\hat{\mathbb{Z}}_{1}^{(1)}\hat{\mathbb{Z}}_{1}^{(1)} = 0 \tag{3.21}$$

and we finally explicitly obtain for the two-loop Anomalous Dimension Matrix:

$$\hat{\gamma}^{(1)} = -4\hat{\mathbb{Z}}_{1}^{(2)} - 2b\hat{\mathbb{Z}}_{0}^{(1)} + 2(\hat{\mathbb{Z}}_{1}^{(1)}\hat{\mathbb{Z}}_{0}^{(1)} + \hat{\mathbb{Z}}_{0}^{(1)}\hat{\mathbb{Z}}_{1}^{(1)}) \tag{3.22}$$

Many comments are in order at this point. First of all we see that $\hat{\gamma}^{(1)}$ is determined by only the $O(1/\epsilon)$ contributions. This means that we have to consider all the diagrams contributing to a given order, to renormalize them in the MS scheme as we fixed in the beginning and to pick out the single pole term.

Nevertheless we would have expected only the two-loop term to appear in (3.22). This is indeed the case if we suppose that no evanescent operator is present in the theory. But this would not be correct just in view of the fact that it is precisely the simple pole contribution the one which gives the anomalous dimension. The presence of an evanescent operator at one loop certainly gives a zero contribution to the one-loop anomalous dimension, but, if inserted in a two-loop diagram, it could in principle contribute to the single pole of the two-loop result. From (3.18), we see that $\hat{\mathbb{Z}}_{0}^{(1)}$ is zero for the physical operators, but not for the evanescent ones. They could be present with "dressed" finite contribution, that is with $O(1)$ contributions hidden in some simple pole of a $\hat{\gamma}$-operator structure. Such a structure is indeed something like an $O(\epsilon)$ contribution, because it vanishes in 4-dim., even though it cannot be eliminated in the intermediate steps.

All the previous observations are extremely important when we start computing the one-loop counterterms to be subtracted from the two-loop diagrams. Let us recall that the general two-loop diagram subtracted of its counterterms will be of the form:

$$G - G_{CT} = (q^2)^{-2\epsilon}\left(\frac{A^{(1)}}{\epsilon^2} + \frac{A^{(0)}}{\epsilon} + \cdots\right) - (q^2)^{-\epsilon}\left(\frac{A_{CT}^{(1)}}{\epsilon^2} + \frac{A_{CT}^{(0)}}{\epsilon} + \cdots\right) \tag{3.23}$$

where q is the scale of a given external momentum. Applying the In order to cancel the dependence on external momentum, the pole coefficients in (3.23) have to satisfy certain given relations. These relations are obtainable from the Renormalization Group equation for the renormalized Green function and are summarized by:

$$\begin{aligned} A_{CT}^{(1)} &= 2A^{(1)} \\ A_{CT}^{(0)} &= B^{(1)}B^{(0)} + bB^{(0)} - b_{\lambda}B_{\lambda}^{(0)} \end{aligned} \tag{3.24}$$

where $B^{(1)}$ and $B^{(0)}$ correspond to the pole and to the finite part of the unrenormalized one-loop sub-diagrams; b is the $O(\alpha^2)$ coefficient of the β-function and $B^{(0)}_\lambda$ is defined give the dependence of $B^{(0)}$ from the gauge parameter λ:

$$B^{(0)}_\lambda = \lambda \frac{\partial}{\partial \lambda} B^{(0)} \tag{3.25}$$

The conditions in (3.25) correspond to the cancellation of linear and constant terms in $\ln(-q^2/\mu^2)$ respectively. They have to be verified by each diagram or set of diagrams.

The counterterm diagrams are computed by inserting the pole part of a given divergent sub-diagram at one-loop in the corresponding two-loop diagram. Evanescent operators arise at the one-loop level and their pole terms should be accounted for in the one-loop counterterms. They are identified from the definition of evanescent operator, as an operator which should disappear by projection on 4-dim. space-time. With this definition one can select it out of the one-loop result for a given diagram. We will show by explicit examples that this often has the effect to add a further $O(\epsilon)$ contribution to the single pole contribution of the physical operator (i.e. a globally finite contribution).

Our strategy will be as follows: first we will pick out the one-loop counterterms needed in the renormalization of the theory at NLO. Then we will consider case by case the possible presence of evanescent operators. Finally, we will give the prescription we have used to account for the counterterms.

In order to identify the one-loop counterterms to be inserted in the theory, let us think to the structure of the composite operators of dimension not greater than six which could be present [4, 27, 55]. In particular operators with dimension five or less are not relevant, because either they are magnetic type operators (dim. five) and vanishes for massless quark, or they are mass-term and elementary vertex operators of which mass and coupling constant renormalization already take care. The six dimensional operators of the theory are only of the form:

$$\bar{\psi}\psi\,\bar{\psi}\psi \quad \text{and} \quad \bar{\psi} D^\mu D^\nu D^\rho \psi \tag{3.26}$$

where the covariant indices can be contracted in many ways giving origin to a complete off-shell operator basis. This basis is completely equivalent to the on-shell basis we adopted. Applying the equations of motion and some algebraic manipulation, indeed, the various terms with covariant derivatives transform in four-fermion or magnetic type operators. Neglecting the latter for massless quarks, we get the on-shell basis [32, 33, 20]. Nevertheless, in order to identify the counterterms, it is better to think in terms of the operators given in (3.26). Up to $O(\alpha_s^2)$ or $O(\alpha_s\alpha_e)$ (3.26) operators give origin to three possible effective vertices:

- four-fermion vertex,
- two-fermion and one-gluon(/photon) vertex,
- two-fermion and two-gluon(/one-gluon and one-photon) vertex.

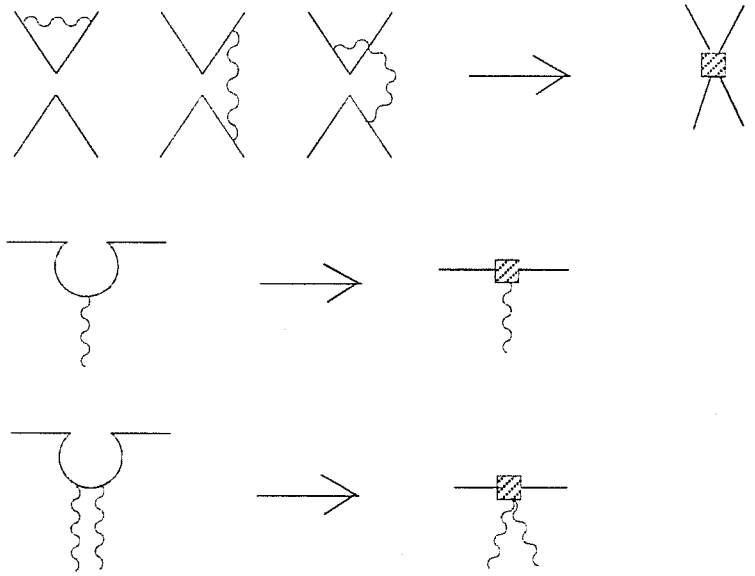

Figure 3.1: One loop counterterms.

These are the basic one-loop vertices for which we have to compute a counterterm, looking at the presence of evanescent operator contributions.

1. **Four-fermion vertex.**

   Let us consider the first three diagram in fig.(2.4), in which the wavy line could be a gluon or a photon. The Dirac structure could be $\gamma_L^\mu \otimes \gamma_{\mu L}$ or $\gamma_L^\mu \otimes \gamma_{\mu R}$ and we have to account for the two different cases.

   For both $\gamma_L^\mu \otimes \gamma_{\mu L}$ and $\gamma_L^\mu \otimes \gamma_{\mu R}$ vertices, after the loop integration but without having performed the Dirac algebra, the three diagrams have the following analytical structure:

$$
\begin{aligned}
G^{(1)}_{L(L,R)} &= C^{(1)}\frac{1}{4\epsilon}\left(\gamma^\mu\gamma^\rho\Gamma_L^\mu\gamma_\rho\gamma_\mu \otimes \Gamma_{\mu L,R} + \Gamma_L^\mu \otimes \gamma^\mu\gamma^\rho\Gamma_{\mu L,R}\gamma_\rho\gamma_\mu\right) \\
G^{(2)}_{L(L,R)} &= -C^{(2)}\frac{1}{4\epsilon}\left(\gamma^\mu\gamma^\rho\Gamma_L^\mu \otimes \gamma_\mu\gamma_\rho\Gamma_{\mu L,R} + \Gamma_L^\mu\gamma^\mu\gamma^\rho \otimes \Gamma_{\mu L,R}\gamma^\mu\gamma^\rho\right) \qquad (3.27) \\
G^{(3)}_{L(L,R)} &= C^{(3)}\frac{1}{4\epsilon}\left(\gamma^\mu\gamma^\rho\Gamma_L^\mu \otimes \Gamma_{\mu L,R}\gamma_\rho\gamma_\mu + \Gamma_L^\mu\gamma^\rho\gamma^\mu \otimes \gamma_\mu\gamma_\rho\Gamma_{\mu L,R}\right)
\end{aligned}
$$

$$
(3.28)
$$

   where $C^{(1)}$, $C^{(2)}$ and $C^{(3)}$ are coefficient which summarize the colour/charge dependence of each diagram and can be read in Table(2.2). On the other hand, Γ_L^μ and Γ_R^μ denote the weak vertex structure, given in NDR and in HV respectively by:

$$
\Gamma_L^\mu = \begin{cases} \gamma^\mu(1-\gamma_5), & \text{NDR} \\ \tilde{\gamma}^\mu(1-\gamma_5), & \text{HV} \end{cases} \qquad \Gamma_R^\mu = \begin{cases} \gamma^\mu(1+\gamma_5), & \text{NDR} \\ \tilde{\gamma}^\mu(1+\gamma_5), & \text{HV} \end{cases} \qquad (3.29)
$$

Reducing the γ-algebra in (3.28) we can factorize the 4-dim. vertex operator contribution from the evanescent one. By definition, we assume something to be evanescent if its projection on the 4-dim. operator is zero. Thus we have to define a projection too. There is no particular reason for choosing one projector with respect to the other. Being the physical 4-dim. operators $\gamma_L^\mu \otimes \gamma_{\mu L}$ or $\gamma_L^\mu \otimes \gamma_{\mu R}$, it is important only to chose a projector which reproduces $\gamma_L^\mu \otimes \gamma_{\mu L}$ or $\gamma_L^\mu \otimes \gamma_{\mu R}$. Then, the final definition of the evanescent operators and the ϵ-dependent coefficient of the physical operator will depend on the choice of the projector itself. Moreover, they will depend on this choice in such a way that the evanescent part is always projected to zero, rescaling finite terms in the coefficient of the physical operator. Therefore, depending on the choice of the projection also the definition of the evanescent counterterms will be modified. The final result is invariant under any choice of projection, as we explicitly verified. In particular we will use the following projectors:

- for $\gamma_L^\mu \otimes \gamma_{\mu L} \longrightarrow \mathbb{P}_{LL} = \gamma_R^\mu \otimes \gamma_{\mu R}$
- for $\gamma_L^\mu \otimes \gamma_{\mu R} \longrightarrow \mathbb{P}_{LR} = (1-\gamma_5) \otimes (1+\gamma_5)$

The projection methods is standard: in order to project $\gamma_L^\mu \otimes \gamma_{\mu L}$ with $\gamma_R^\mu \otimes \gamma_{\mu R}$ one has to take the following trace:

$$\mathbb{P}_{LL}(\gamma_L^\mu \otimes \gamma_{\mu L}) = \sum_{\alpha,\beta,\gamma,\delta} (\gamma^\mu(1-\gamma_5))_{\alpha\beta}(\gamma^\nu(1+\gamma_5))_{\beta\gamma}(\gamma_\mu(1-\gamma_5))_{\gamma\delta}(\gamma_\nu(1+\gamma_5))_{\delta\alpha} \tag{3.30}$$

while in order to project $\gamma_L^\mu \otimes \gamma_{\mu R}$ with $(1-\gamma_5) \otimes (1+\gamma_5)$:

$$\mathbb{P}_{LR}(\gamma_L^\mu \otimes \gamma_{\mu R}) = \sum_{\alpha,\beta,\gamma,\delta} (\gamma^\mu(1-\gamma_5))_{\alpha\beta}(1-\gamma_5)_{\beta\gamma}(\gamma_\mu(1+\gamma_5))_{\gamma\delta}(1+\gamma_5)_{\delta\alpha} \tag{3.31}$$

When projecting a string of γ-matrices or a linear combination of given operators on $\gamma_L^\mu \otimes \gamma_{\mu L}$ (with $\gamma_R^\mu \otimes \gamma_{\mu R}$) or on $\gamma_L^\mu \otimes \gamma_{\mu R}$ (with $(1-\gamma_5) \otimes (1+\gamma_5)$), the values of the traces in (3.31) and (3.32) are taken as normalization factors.

With this method [13] we obtain the following decomposition for the one-loop vertex diagrams in (3.28):

$$\begin{aligned} G^{(1)}_{L(L,R)} &= C^{(1)} \frac{1}{2\epsilon} \left(F^{(1)}_{L(L,R)}(\epsilon) \gamma_L^\mu \otimes \gamma_{\mu L,R} + E^{(1)}_{L(L,R)} \right) \\ G^{(2)}_{L(L,R)} &= C^{(2)} \frac{1}{4\epsilon} \left(F^{(2)}_{L(L,R)}(\epsilon) \gamma_L^\mu \otimes \gamma_{\mu L,R} + E^{(2)}_{L(L,R)} \right) \\ G^{(3)}_{L(L,R)} &= C^{(3)} \frac{1}{4\epsilon} \left(F^{(3)}_{L(L,R)}(\epsilon) \gamma_L^\mu \otimes \gamma_{\mu L,R} + E^{(3)}_{L(L,R)} \right) \end{aligned} \tag{3.32}$$

where the ϵ-dependent coefficient are given by:

$$F^{(1)}_{LL}(\epsilon) = F^{(3)}_{LL}(\epsilon) = \begin{cases} 4(1-\epsilon)^2 & \text{NDR} \\ 4(1+\epsilon^2) & \text{HV} \end{cases} \tag{3.33}$$

$$F^{(2)}_{LL}(\epsilon) = \begin{cases} -4(4-\epsilon-\epsilon^2) & \text{NDR} \\ -4(4-\epsilon-\epsilon^2) & \text{HV} \end{cases} \tag{3.34}$$

and:

$$F_{LR}^{(1)}(\epsilon) = \begin{cases} 4(1-2\epsilon+\frac{3}{4}\epsilon^2) & \text{NDR} \\ 4(1+\epsilon^2) & \text{HV} \end{cases} \tag{3.35}$$

$$F_{LR}^{(2)}(\epsilon) = \begin{cases} 4(4+\epsilon+\frac{5}{4}\epsilon^2) & \text{NDR} \\ -4(1-\epsilon-\epsilon^2) & \text{HV} \end{cases} \tag{3.36}$$

$$F_{LR}^{(3)}(\epsilon) = \begin{cases} 16(1-\epsilon) & \text{NDR} \\ 4(4+\epsilon^2) & \text{HV} \end{cases} \tag{3.37}$$

On the other hand, $E_{L(L,R)}^{(i)}$ are the evanescent operator contribution. They are different diagram by diagram and depend on the $\gamma_L^\mu \otimes \gamma_{\mu L}$ or $\gamma_L^\mu \otimes \gamma_{\mu R}$ structure and on the regularization prescription, i.e. if HV or NDR. In the **HV scheme**, the evanescent operators derived from a $\gamma_L^\mu \otimes \gamma_{\mu L}$ structure are respectively:

$$\begin{aligned} E_{LL}^{(1)(HV)} &= R_{LL}^{(a)(HV)} \\ E_{LL}^{(2)(HV)} &= R_{LL}^{(a)(HV)} + R_{LL}^{(b)(HV)} + R_{LL}^{(c)(HV)} \\ E_{LL}^{(3)(HV)} &= R_{LL}^{(a)(HV)} + R_{LL}^{(c)(HV)} \end{aligned} \tag{3.38}$$

where:

$$\begin{aligned} R_{LL}^{(a)(HV)} &= -4\epsilon\left(\Gamma_L^\mu \otimes \Gamma_{\mu R} + \Gamma_R^\mu \otimes \Gamma_{\mu L}\right) \\ R_{LL}^{(b)(HV)} &= -2\left(\hat{\gamma}^\rho\tilde{\gamma}^\nu\tilde{\gamma}^\mu\gamma_5 \otimes \hat{\gamma}_\rho\tilde{\gamma}_\nu\tilde{\gamma}_\mu\gamma_5 + 4\hat{\gamma}^\mu \otimes \hat{\gamma}_\mu - 4\hat{\gamma}^\mu\gamma_5 \otimes \hat{\gamma}_\mu\gamma_5\right) \\ R_{LL}^{(c)(HV)} &= -2\epsilon\Gamma_L^\mu \otimes \Gamma_{\mu L} - \frac{1}{2}\hat{\gamma}^\nu\hat{\gamma}^\rho\Gamma_L^\mu \otimes \Gamma_{\mu L}\hat{\gamma}_\nu\hat{\gamma}_\rho + \\ &\quad + \left(\hat{\gamma}^\rho\tilde{\gamma}^\nu\tilde{\gamma}^\mu \otimes \hat{\gamma}_\rho\tilde{\gamma}_\mu\tilde{\gamma}_\nu - \hat{\gamma}^\rho\tilde{\gamma}^\nu\tilde{\gamma}^\mu\gamma_5 \otimes \hat{\gamma}_\rho\tilde{\gamma}_\mu\tilde{\gamma}_\nu\gamma_5\right) \end{aligned} \tag{3.39}$$

while in the **NDR scheme**, with respect to the same decomposition we have:

$$\begin{aligned} R_{LL}^{(a)(NDR)} &= 0 \\ R_{LL}^{(b)(NDR)} &= 0 \\ R_{LL}^{(c)(NDR)} &= -2\epsilon\Gamma_L^\mu \otimes \Gamma_{\mu L} - \frac{1}{2}\hat{\gamma}^\nu\hat{\gamma}^\rho\Gamma_L^\mu \otimes \Gamma_{\mu L}\hat{\gamma}_\nu\hat{\gamma}_\rho + \\ &\quad + \left(\hat{\gamma}^\rho\gamma^\nu\gamma^\mu \otimes \hat{\gamma}_\rho\gamma_\mu\gamma_\nu - \hat{\gamma}^\rho\gamma^\nu\gamma^\mu\gamma_5 \otimes \hat{\gamma}_\rho\gamma_\mu\gamma_\nu\gamma_5\right) \end{aligned} \tag{3.40}$$

For the $\gamma_{\mathbf{L}}^\mu \otimes \gamma_{\mu\mathbf{R}}$ structure on the other hand we have in the **HV scheme**:

$$\begin{aligned} E_{LR}^{(1)(HV)} &= R_{LR}^{(a)(HV)} \\ E_{LR}^{(2)(HV)} &= R_{LR}^{(a)(HV)} + R_{LR}^{(c)(HV)} \\ E_{LR}^{(3)(HV)} &= R_{LR}^{(a)(HV)} + R_{LR}^{(b)(HV)} + R_{LR}^{(c)(HV)} \end{aligned} \tag{3.41}$$

where now:

$$\begin{aligned} R_{LR}^{(a)(HV)} &= -4\epsilon\left(\Gamma_L^\mu \otimes \Gamma_{\mu L} + \Gamma_R^\mu \otimes \Gamma_{\mu R}\right) \\ R_{LR}^{(b)(HV)} &= -2\left(\hat{\gamma}^\rho\tilde{\gamma}^\nu\tilde{\gamma}^\mu\gamma_5 \otimes \hat{\gamma}_\rho\tilde{\gamma}_\nu\tilde{\gamma}_\mu\gamma_5 - 4\hat{\gamma}^\mu \otimes \hat{\gamma}_\mu - 4\hat{\gamma}^\mu\gamma_5 \otimes \hat{\gamma}_\mu\gamma_5\right) \\ R_{LR}^{(c)(HV)} &= -2\epsilon\Gamma_L^\mu \otimes \Gamma_{\mu R} - \frac{1}{2}\hat{\gamma}^\nu\hat{\gamma}^\rho\Gamma_L^\mu \otimes \Gamma_{\mu L,R}\hat{\gamma}_\nu\hat{\gamma}_\rho + \\ &\quad - \left(\hat{\gamma}^\rho\tilde{\gamma}^\nu\tilde{\gamma}^\mu \otimes \hat{\gamma}_\rho\tilde{\gamma}_\nu\tilde{\gamma}_\mu - \hat{\gamma}^\rho\tilde{\gamma}^\nu\tilde{\gamma}^\mu\gamma_5 \otimes \hat{\gamma}_\rho\tilde{\gamma}_\nu\tilde{\gamma}_\mu\gamma_5\right) \end{aligned} \tag{3.42}$$

and in **NDR scheme**:

$$\begin{aligned} R_{LR}^{(a)(NDR)} &= 0 \\ R_{LR}^{(b)(NDR)} &= 0 \\ R_{LR}^{(c)(NDR)} &= -2\epsilon\Gamma_L^\mu \otimes \Gamma_{\mu R} - \frac{1}{2}\hat{\gamma}^\nu\hat{\gamma}^\rho\Gamma_L^\mu \otimes \Gamma_{\mu L,R}\hat{\gamma}_\nu\hat{\gamma}_\rho + \\ &\quad - (\hat{\gamma}^\rho\gamma^\nu\gamma^\mu \otimes \hat{\gamma}_\rho\gamma_\nu\gamma_\mu - \hat{\gamma}^\rho\gamma^\nu\gamma^\mu\gamma_5 \otimes \hat{\gamma}_\rho\gamma_\nu\gamma_\mu\gamma_5) \end{aligned} \tag{3.43}$$

On one hand, using the projectors defined in (3.31) and (3.32) one can explicitly verify that the all the evanescent operators in (3.40) and (3.43) for the HV case or in (3.41) and (3.44) for the NDR case are projected away in 4-dim. On the other hand, looking at the ϵ-dependent coefficient in (3.34) and (3.37) one can realize that the pole coefficient of the physical 4-dim. operator has now acquired some finite contributions, of the form $\frac{1}{\epsilon}\cdot O(\epsilon) \simeq O(1)$. This corresponds exactly to the reshuffling mechanism explained before: the projection of the evanescent operators is maintained to be zero, whatever the projector, but the coefficient of the physical operator get some finite contributions.

We are now ready to define our renormalization procedure for the vertex operators. We will have two counterterms:

- the counterterm for the insertion of the $\gamma_L^\mu \otimes \gamma_{\mu L}$ or $\gamma_L^\mu \otimes \gamma_{\mu R}$ operator;
- the counterterm for the insertion of the evanescent operators.

as shown in fig.(3.1). In both cases, $\overline{\text{MS}}$ tell us to subtract only the pole coefficient. Thus we use the following algorithm for a generic subtracted two-loop diagram containing a vertex-type subdiagram:

$$\begin{aligned} \left(D^{(i)}_{L(L,R)}\right)_{Sub} &= D^{(i)}_{L(L,R)} - G^{(i)}_{L(L,R)}\cdot F^{(i)-1}_{L(L,R)}(\epsilon)\gamma_L^\mu \otimes \gamma_{\mu L,R} + \\ &+\frac{1}{2}\left(G^{(i)}_{L(L,R)}\cdot F^{(i)-1}_{L(L,R)}(\epsilon)\gamma_L^\mu \otimes \gamma_{\mu L,R} - \frac{1}{2\epsilon}F^{(i)}_{L(L,R)}(\epsilon=0)\gamma_L^\mu \otimes \gamma_{\mu L,R}\right) \end{aligned} \tag{3.44}$$

which can be better understood from eq.(3.21).

Let us make some comments. The generic diagram $D^{(i)}_{L(L,R)}$ appears on the right hand side in its subtracted form, while on the left hand side in the bare one. About counterterms, the second and third term on the right hand side should be interpreted has the insertion of the given expression in a two-loop diagram, i.e. as the corresponding two-loop counter-diagram. The first subtraction corresponds to the pole coefficient of the $\gamma_L^\mu \otimes \gamma_{\mu L,R}$ operator, without $O(\epsilon)$ terms (this is the reason of the multiplication for $F^{(i)-1}_{L(L,R)}(\epsilon)$). This is true only because when $F^{(i)-1}_{L(L,R)}(\epsilon)$) multiplies the evanescent operator contribution, no other finite contribution arises. This first term correspond to the $\hat{Z}_1^{(2)}$ contribution in (3.21). The second subtraction is the evanescent operator counterterm. Its structure is simply the difference between the counterterm computed in N-dim. and in 4-dim. It corresponds to the third term in (3.21). Moreover, it is easy to verify that this

second subtraction term is exactly projected to zero in 4-dim. Finally, the second term in (3.21), proportional to the β-function coefficient is absent, because $\hat{\mathbb{Z}}_0^{(1)}$ vanishes with our subtraction prescription.

This ends our discussion of the four-fermion vertex counterterms. In Tables (2.16) and (2.17) we give the value of each two loop counterterm for vertex diagrams, specifying also the value of the effervescent operator counterterm whenever present.

2. **One-gluon/photon vertex.**

The computation of this counterterms will be much easier, due to the absence of evanescent operator contributions at the one-loop level. We have to isolate the singular part of penguin diagrams in fig.(2.4). By direct computation one gets both in the HV and in the NDR scheme:

$$(\text{Penguin})_{\text{pole}} = -\frac{4}{3}\frac{1}{\epsilon}(q^2\Gamma_L^\mu - q^\mu \not{q}_L) \tag{3.45}$$

where q^μ is the incoming momentum of the gluon/photon (see fig.(3.1)) and Γ_L^μ is to be thought in 4-dim. or in N-dim. respectively in the HV or in the NDR case. It is clear that there is no way to get an evanescent operator out of (3.45). In the HV scheme, indeed, the algebra is automatically projected in 4-dim by the structure of the penguin diagram itself, because (3.45) is derived by:

$$(\text{Penguin})_{\text{pole}}^{(HV)} = \frac{1}{3}\frac{1}{\epsilon}\tilde{\gamma}_L^\alpha(q^2\gamma_L^\mu - q^\mu \not{q})\tilde{\gamma}_{\alpha L} \tag{3.46}$$

where the inner structure of the penguin is forced to be in 4-dim.

On the other side also in NDR, one would have:

$$(\text{Penguin})_{\text{pole}}^{(NDR)} = \frac{1}{3}\frac{1}{\epsilon}\gamma_L^\alpha(q^2\gamma_L^\mu - q^\mu \not{q})\gamma_{\alpha L} \tag{3.47}$$

where the N-dim. γ_L^μ vertex is reproduced multiplied by the pole part in (3.45) plus some finite part not relevant at all in the $\overline{\text{MS}}$ scheme. Thus, the only penguin counterterm is the one in (3.45).

3. **Two-gluon or one-gluon+one-photon vertex.**

The presence of this counterterm is a typical feature of the two-loop calculation. It is in fact a "penguin-like" contribution and it retains the previous property not to have evanescent terms at the one-loop level. Referring to fig.(3.1), for k_1^μ and k_2^ν incoming momenta, its pole part results to be [58]:

$$\frac{4}{3}\frac{1}{\epsilon}(g^{\mu\nu}(\not{k}_1 - \not{k}_2)_L - (2k_1 + k_2)^\nu\gamma_L^\mu + (k_1 + 2k_2)\gamma_L^\nu) \tag{3.48}$$

Also in this case the γ-structure of the vertex is 4-dim. in HV while N-dim. in NDR and no room is left for evanescent operators. The previous expression already give the counterterm to be inserted into two-loop counter-diagrams. It is interesting to note [58] that by applying the equation of motion the previous structure of the two-gluon penguin-like vertex reduces to a sum over four- quarks operators.

3.3 Diagram calculation, methods and results

With definite regularization and renormalization prescriptions, we are now in the condition to give the result for each single diagram. In order to perform the two-loop diagram calculation some observations are still needed. Let analyze the case of vertex-type diagrams and penguin-diagrams separately.

1. **Vertex-type diagrams.**

   As we have already stressed in discussing the CF initial conditions, we calculate the ADM just below the M_W-scale, i.e. with all massless quarks. This clearly greatly simplifies the loop integrations, but in order to avoid IR divergencies we should chose non zero external momenta whenever necessary. In the case of vertex-type diagrams we take the same p-momentum for all the external legs. This is enough to preserve from IR divergencies and p-dependence in the final result is cancelled by counterterms. The two-loop anomalous dimension for four-quark operators is known in literature [6, 13]. In reference [6] it is computed in DRED scheme only while in reference [13] the whole calculation has been checked in all the three prescriptions: NDR, DRED and HV, proving the equivalence of the three schemes and thus confirming the previous DRED result. For our aims, we have checked the HV and NDR results for the $\gamma_L^\mu \otimes \gamma_{\mu L}$ case and extended the calculation to the $\gamma_L^\mu \otimes \gamma_{\mu R}$ case.

   The results for vertex diagrams, with both $\gamma_L^\mu \otimes \gamma_{\mu L}$ and $\gamma_L^\mu \otimes \gamma_{\mu R}$ chiral structures, are given in Tables (2.16) and (2.17).

2. **Penguin diagrams.**

   In the case of penguin-type diagrams on the other hand it is often necessary to consider both the incoming gluon/photon and the incoming fermion momenta different from zero. One can still use the equations of motion [51] in order to simplify the external-momenta dependence in the calculation. This is connected to the choice of the operator basis we have already discussed. We have used the equations of motion because we are interested in physical quantities like the $\mathbb{S}$-matrix elements, for which the equations of motions can be applied.

   To fix the point, consider a diagram like the one reported in detail in fig.(3.2), where the closed diagram corresponds to P_2 in our classification. It represents a typical two-loop correction to a penguin-type vertex. We work both in the Feynman and in the back-ground gauge [2], in order to verify the transversality of the penguin vertex, as we will point out later on.

   About P_2, one might perform the integration retaining all the momenta and the final result would be of the form:

$$G_{P_2} = \frac{G_F}{\sqrt{2}} \cdot C_{(c,e)} \int \frac{d^n k}{(2\pi)^n} \int \frac{d^n l}{(2\pi)^n} \frac{N_{P_2}}{\Delta_{P_2}} \tag{3.49}$$

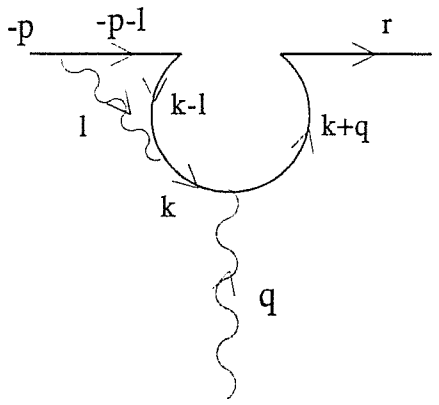

Figure 3.2: Momentum-structure of the P_2 penguin diagram.

where k and l are the loop momenta and $C_{(c,e)}$ is a coefficient which accounts for all the charges and/or colour dependences. N_{P_2} and P_{P_2} gives the numerator and the denominator of the integrand and are explicitly given by:

$$\begin{aligned} N_{P_2} &= \gamma_L^\mu(\not{k}+\not{q})\gamma^\lambda\not{k}\gamma^\rho(\not{k}-\not{l})\gamma_{\mu L}(-\not{p}-\not{l})\gamma_\rho \\ P_{P_2} &= k^2(k+q)^2(k-l)^2l^2(p+l)^2 \end{aligned} \tag{3.50}$$

Introducing Feynman parameters and performing the first integration over l, the integral in (3.49) becomes of the form:

$$\begin{aligned} G_{P_2} &= F_{(c,e)} \cdot \Gamma(3+\epsilon)\int_0^1 dx x^{-\epsilon}(1-x)^{-1-\epsilon}\int_0^1 dy\int_0^1 dt t^{1+\epsilon}\int_0^1 dv v^\epsilon \cdot \\ &\quad \cdot \int \frac{d^nK}{(2\pi)^n}\frac{G(x,y,t,v,p,q,K)}{[K^2-\Omega^2]} \end{aligned} \tag{3.51}$$

where $F_{(c,e)}$ is now a coefficient which summarizes the original $C_{(c,e)}$ and all other terms deriving from the integration procedure. Big-K is the shifted loop momentum corresponding to small-k, i.e.:

$$K^\mu = k^\mu + ytvp^\mu + (1-t)q^\mu \tag{3.52}$$

and Ω is given by:

$$\Omega = -\left[tvy\left(\frac{1-xy}{1-x} - ytv\right)p^2 - t(1-t)q^2 - 2ytv(1-t)p\cdot q\right] \tag{3.53}$$

Finally, $G(x,y,t,v,p,q,K)$ gives the numerator expression after the introduction of the Feynman parameters and the shifts on the integration variables. This G-function and the Ω-part in the denominator give the dependence on the external momenta in the final result.

In the case of diagrams P_2, we have to subtract two counter-diagrams: one for the four-quark vertex subdiagram and an other for the two-gluons (or one gluon+one

photon) subdiagram. They are easily obtainable from section 3.2 and the relative tables of results. The main feature of this subtraction is that all the dependence on logarithms of the external momenta cancels and the relation between the double pole of the bare diagram and of the counter-diagrams (sum of) is fulfilled.

The final result for the subtracted diagram is of the form:

$$\alpha_i^{(1)} q^2 \gamma_L^\mu + \alpha_i^{(2)} q^\mu \not{q}_L + \alpha_i^{(3)} p^\mu \not{q}_L + \alpha_i^{(4)} q^\mu \not{p}_L + \alpha_i^{(5)} p^\mu \not{p}_L \tag{3.54}$$

where the $\alpha_i^{(j)}$'s are the coefficients of each tensorial structure j in the result for the diagram i. When saturating with the lower leg some dot-product appears. Using the equations of motion one could put:

$$p^2 = 0 \quad \text{and} \quad p \cdot q = \frac{q^2}{2} \tag{3.55}$$

greatly simplifying the previous expression and obtaining a results expressed only in terms of q^2 and $q^\mu \not{q}_L$. The same result could also have been obtained using on-shell external momenta from the beginning, provided no IR divergencies arise. This would have meant to use (3.55) in (3.53),factorizing the q^2-dependence in the integration. Clearly in this way it would not have been possible anymore to verify the correct cancellation between the bare diagram and the counter-diagram with respect to logarithms of the external momenta. In non-ambiguous cases this cancellation have been really helpful as a check of the calculation.

Finally we should note that in all this game, the only stable coefficient is $\alpha_i^{(1)}$ i.e. the coefficient of the $q^2\gamma_L^\mu$ tensorial structure. Thus, in the final bookkeeping of the results, we will give for each diagram the $\alpha_i^{(1)}$ coefficient.

Applying the equations of motion and reducing the result in terms of q^2 and $q^\mu \not{q}_L$ only, the transversality of the penguin diagram vertex is verified by single diagrams or set of gauge invariant diagrams. To accomplish this task we have performed our calculation in the back-ground gauge too and we have finally verified the gauge invariance of the results. In practice, the only gauge-dependent diagrams are P_4, P_6 and P_7. Being P_7 not 1PI (One-Particle Irreducible) it will not be considered and the only gauge dependence is left in P_4 and P_6. For these two diagrams we will give both the results (F and BG).

More in detail the subset of diagrams which explicitly verify the transversality condition are:

- $(P_2 + P_3)$ and $(P_2 + P_4)$ separately, because the colour coefficient of P_2 makes it combining both with P_3 and with P_4;
- P_8 by itself;
- $(P_6 + P_9)$ and $(P_8 + P_9)$ separately, always due to colour coefficients;
- P_{13} by itself.

where the notation is the same used in the Table compilation.

All the results for two-loop penguin diagrams[2] are given in Tables (2.18)-(2.19). There we specify for each diagram: the bare result (pole contributions only), the counterterms (both the 4-dim. and the evanescent one) and the subtracted result (always pole contributions). Moreover we note that:

- $\gamma_L^\mu \otimes \gamma_{\mu R}$ P-penguin diagrams are always zero, because the chiral structure of the weak vertex is incompatible with the γ- structure of the upper quark-line;
- $\gamma_L^\mu \otimes \gamma_{\mu L}$ F-penguin and P-penguins give the same result, due to Fierz symmetry.

Thus, for penguin diagrams we will report two Tables only: one common table for the $\gamma_L^\mu \otimes \gamma_{\mu L}$ penguins and one Table for the $\gamma_L^\mu \otimes \gamma_{\mu R}$ F-penguins.All the results are given in Tables (2.18) and (2.19).

[2]We neglect diagrams which are not 1PI or diagrams whose single pole is zero, i.e. P_5, P_7 and P_{12}.

Chapter 4

Numerical results for $\Delta B=1$ and $\Delta S=1$ Effective Hamiltonians beyond the Leading Order.

In this chapter the explicit expression for $\Delta B=1$ and $\Delta S=1$ Effective Hamiltonian will be given, considering the two different cases:

- only NLO pure QCD corrections are taken into account;
- both NLO QCD and LO QED corrections are considered.

The general expression for the tree level $\Delta F=1$ Hamiltonian has been give in section 2.2.1:

$$\mathcal{H}_{eff}^{(0)\Delta F=1} = \mathcal{H}_c + \mathcal{H}_t = \lambda_u^* \frac{G_F}{\sqrt{2}} \left[(1-\tau) \left(O_2^{(0)u} - O_2^{(0)c} \right) + \tau \left(O_2^{(0)u} - O_2^{(0)t} \right) \right] \tag{4.1}$$

where in the $\Delta S=1$ case:

$$\lambda_i = \mathbb{V}_{is}^* \mathbb{V}_{id} \quad , \quad \tau = -\frac{\mathbb{V}_{ts}^* \mathbb{V}_{td}}{\mathbb{V}_{us}^* \mathbb{V}_{ud}} \tag{4.2}$$

while in the $\Delta B=1$ case, for a B_d meson:

$$\lambda_i = \mathbb{V}_{ib}^* \mathbb{V}_{id} \quad , \quad \tau = -\frac{\mathbb{V}_{tb}^* \mathbb{V}_{td}}{\mathbb{V}_{ub}^* \mathbb{V}_{ud}} \tag{4.3}$$

and the generalization to the B_s meson case is obvious. The tree level four-quark operator is respectively given by:

$$\begin{aligned} O_2^{(0)q_i} &= (\bar{s} q_i)_{(V-A)} (\bar{q}_i d)_{(V-A)} \text{ for } \Delta S=1 \text{ decays} \\ O_2^{(0)q_i} &= (\bar{b} q_i)_{(V-A)} (\bar{q}_i d)_{(V-A)} \text{ for } \Delta B_d=1 \text{ decays} \\ O_2^{(0)q_i} &= (\bar{b} q_i)_{(V-A)} (\bar{q}_i s)_{(V-A)} \text{ for } \Delta B_d=1 \text{ decays} \end{aligned} \tag{4.4}$$

From Chapt.2 and Chapt.3 we know how to derive from (4.1) the expression of the $\Delta B = 1$ and $\Delta S = 1$ Effective Hamiltonian taking into account QCD corrections at NLO and electro-weak corrections at LO. This means that at any scale μ (in particular: $\mu = m_b$ and $\mu = m_c$) we know:

(i) the set of operators present in the Effective Hamiltonian at that scale $\{O_i(\mu)\}$;

(ii) the initial conditions for the evolution of the correspondent Wilson coefficients;

(iii) the evolution matrix to be used in order to derive the expression of the Wilson coefficients at the given scale μ.

$\Delta B = 1$ and $\Delta S = 1$ decays will be studied in sections 4.1 and 4.2 respectively. Both in the $\Delta B = 1$ and in the $\Delta S = 1$ case, we will give two series of Tables, for barred and unbarred Wilson coefficients respectively. Indeed, the authors of ref. [15] observed that the expression:

$$\hat{r}^T + \hat{\mathbb{V}}^{(1)} \tag{4.5}$$

in the evolution equation (2.48) is renormalization scheme independent. In order to write (2.48) in terms of this particular combination of the $\hat{r}$ and $\hat{\mathbb{V}}^{(1)}$ matrices, they shifted both the Wilson coefficients and the operators in the Effective Hamiltonian by $\hat{r}$, defining the barred quantities:

$$\overline{\vec{O}}(\mu) \equiv \left[\mathbb{I} - \frac{\alpha_s(\mu)}{4\pi}\hat{r}\right]\vec{O}(\mu) \quad \text{and} \quad \overline{\vec{C}}(\mu) \equiv \left[\mathbb{I} + \frac{\alpha_s(\mu)}{4\pi}\hat{r}^T\right]\vec{C}(\mu) \tag{4.6}$$

in such a way that:

$$\mathcal{H}_{eff} = \frac{G_F}{\sqrt{2}}\vec{O}^T(\mu)\vec{C}(\mu) = \frac{G_F}{\sqrt{2}}\overline{\vec{O}}^T(\mu)\overline{\vec{C}}(\mu) \tag{4.7}$$

They obtained in this way a renormalization scheme independent evolution equation, which however depends on the choice of the external states. Indeed, $\hat{\mathbb{V}}^{(1)}$ does not depend on the choice of the external momenta, while $\hat{r}$ does. This dependence cancels in the combination[1]:

$$\vec{T}^{(1)} - \hat{r}^T\vec{T}^{(0)} \tag{4.8}$$

and the final evolution equation is independent of the choice of the external states. In this way the matching with the non-perturbative calculation of the matrix elements will be easier, because it will be not necessary to specify the details of the analytic calculation. The perturbative and the non-perturbative calculation will be completely independent and we only require their matching at a give scale.

Thus we will report, for each set of Wilson coefficients $\vec{C}(\mu)$, in different Tables:

[1] This is indeed the one-loop term in the coefficient function expression (2.47), where the dependence on the external states cancels in the matching between the full and the effective theory.

- the barred $\overline{\vec{C}}(\mu)$ values, in presence of NLO QCD corrections only, in order to compare our results with those of ref. [15]. In particular, we will use the same $\hat{r}$ matrix, in the HV scheme:

$$\hat{r}_{HV} = \begin{pmatrix} 7 & -5 & 0 & 0 & 0 & 0 \\ -5 & 7 & \frac{5}{27} & -\frac{5}{9} & \frac{5}{27} & -\frac{5}{9} \\ 0 & 0 & \frac{199}{27} & -\frac{55}{9} & \frac{10}{27} & -\frac{10}{9} \\ 0 & 0 & -5+\frac{5}{27}N_f & 7-\frac{5}{9}N_f & \frac{5}{27}N_f & -\frac{5}{9}N_f \\ 0 & 0 & 0 & 0 & 3 & 7 \\ 0 & 0 & \frac{5}{27}N_f & -\frac{5}{9}N_f & 1+\frac{5}{27}N_f & 21-\frac{5}{9}N_f \end{pmatrix} \tag{4.9}$$

  Had we computed our own $\hat{r}_{HV}$ matrix, with our external state convention, a different result would be obtained and no meaningful comparison with ref. [15] would be possible. possible meaningful comparison.

- the unbarred $\vec{C}$ Wilson coefficients, with no $\hat{r}^T$-shift, both in the case of NLO pure QCD corrections and in the case of QED+QCD corrections.

The numerical implementation of the NLO results for the $\Delta F=1$ Effective Hamiltonian involves many other technical points. For instance, the correct implementation of mass thresholds present in the evolution is necessary. Indeed, the evolution of the Wilson coefficients of the Effective Hamiltonian from the initial scale $\mu = M_W$ to a general lower scale $\mu = \mu_0$ might cross one or more thresholds. In crossing a mass threshold, we switch between two different Effective Theories, corresponding to N_f and (N_f-1) flavours. Many quantities in our evolution prescription are N_f-dependent and one has to require that they correctly match at the threshold. We remember that a NLO calculation requires a NLO matching at each threshold. Some more comments will be present in the following sections.

Finally, the last section will contain an updated analysis of CP-violation (and quark-mixing) on the basis of the new $\Delta S=1$ Hamiltonian. The analysis will reproduce a set of figures given originally in ref. [43] where the LO QCD+QED Effective Hamiltonian was used. Now we are in the condition to improve it including the NLO of strong interactions.

4.1 $\Delta B=1$ Effective Hamiltonian beyond the Leading Order

When we consider $\Delta B=1$ weak non-leptonic decays, (4.1) has to be evolved to a scale $\mu = m_b$. We have seen that at $\mu = m_b$ the $\mathcal{H}_{eff}^{(0)c}$ part of the Effective Hamiltonian in (4.1) follows the usual four-fermion operator renormalization, while in the $\mathcal{H}_{eff}^{(0)t}$ part the explicit dependence on the t-quark is dropped and penguins operators are generated, due to the failure of the GIM mechanism (breaking of the isospin in the mass spectrum).

	Λ_4	$\overline{C}_1$	$\overline{C}_2$	$\overline{C}_3$	$\overline{C}_4$	$\overline{C}_5$	$\overline{C}_6$
l.o.	0.15	-0.237	1.102	0.011	-0.024	0.007	-0.030
$(\text{n.l.})_S$	0.15	-0.254	1.112	0.013	-0.030	0.009	-0.036
l.o.	0.20	-0.255	1.111	0.011	-0.026	0.008	-0.032
$(\text{n.l.})_S$	0.20	-0.274	1.123	0.014	-0.032	0.009	-0.039
l.o.	0.25	-0.271	1.119	0.012	-0.028	0.008	-0.034
$(\text{n.l.})_S$	0.25	-0.292	1.133	0.015	-0.034	0.010	-0.042
l.o.	0.30	-0.285	1.127	0.013	-0.029	0.008	-0.037
$(\text{n.l.})_S$	0.30	-0.309	1.143	0.016	-0.036	0.010	-0.045
l.o.	0.35	-0.299	1.134	0.014	-0.030	0.009	-0.039
$(\text{n.l.})_S$	0.35	-0.325	1.152	0.017	-0.038	0.011	-0.047
l.o.	0.40	-0.312	1.141	0.014	-0.031	0.009	-0.041
$(\text{n.l.})_S$	0.40	-0.340	1.161	0.018	-0.040	0.011	-0.050

Table 4.1: $\overline{C}_1(\mu),\ldots,\overline{C}_6(\mu)$ Wilson coefficients for the $\Delta B=1$ Effective Hamiltonian at $\mu=m_b=4.8$ GeV: LO and NLO results with QCD corrections only.

Thus the Effective Hamiltonian evolved to $\mu=m_b$ will be of the form:

$$\mathcal{H}_{eff}^{\Delta B=1} = \frac{G_F}{\sqrt{2}}\Big\{ \lambda_c\,(C_1(\mu)O_1^c + C_2(\mu)O_2^c) + \lambda_u\,(C_1(\mu)O_1^u + C_2(\mu)O_2^u) + \sum_i C_i(\mu)O_i \Big\} \tag{4.10}$$

where the first two terms represent the evolution of the four-quark vertex operators and the last one the new contribution due to penguin operators. The sum over penguin operators will run from 3 to 6 in presence of only QCD penguin operators or from 3 to 10 when also QED penguin opertors are taken into account.

The Wilson coefficients at scale $\mu=m_b$ are obtained as:

$$\vec{C}(m_b) = \hat{\mathbb{E}}_5(m_b, M_W)\vec{C}(M_W) \tag{4.11}$$

where $\vec{C}(M_W)$ are the initial conditions given in (2.100) and $\hat{\mathbb{E}}_5(m_b, M_W)$ is the evolution matrix derived in section 2.1, defined in a $N_f=5$ Effective Theory. The case of the

	Λ_4	C_1	C_2	C_3	C_4	C_5	C_6
l.o.	0.15	-0.237	1.102	0.011	-0.024	0.007	-0.030
$(\text{n.l.})_S$	0.15	-0.159	1.994	0.008	-0.021	0.007	-0.022
$(\text{n.l.})_{S+E}$	0.15	-0.160	1.002	0.008	-0.021	0 007	-0.022
l.o.	0.20	-0.255	1.111	0.011	-0.026	0.008	-0.032
$(\text{n.l.})_S$	0.20	-0.170	0.994	0.009	-0.022	0.007	-0.024
$(\text{n.l.})_{S+E}$	0.20	-0.171	1.119	0.012	-0.028	0.008	-0.035
l.o.	0.25	-0.271	1.119	0.012	-0.028	0.008	-0.035
$(\text{n.l.})_S$	0.25	-0.179	0.993	0.009	-0.023	0.007	-0.026
$(\text{n.l.})_{S+E}$	0.25	-0.180	1.002	0.010	-0.023	0.007	-0.026
l.o.	0.30	-0.285	1.127	0.013	-0.029	0.008	-0.037
$(\text{n.l.})_S$	0.30	-0.188	0.993	0.010	-0.024	0.008	-0.027
$(\text{n.l.})_{S+E}$	0.30	-0.189	1. 002	0.010	-0.025	0.008	-0.027
l.o.	0.35	-0.299	1.134	0.014	-0.030	0.009	-0.039
$(\text{n.l.})_S$	0.35	-0.196	0.993	0.011	-0.025	0.008	-0.028
$(\text{n.l.})_{S+E}$	0.35	-0.197	1.002	0.011	-0.026	0.008	-0.029
l.o.	0.40	-0.312	1.141	0.014	-0.031	0.009	-0.041
$(\text{n.l.})_S$	0.40	-0.204	0.993	0.011	-0.026	0.008	-0.029
$(\text{n.l.})_{S+E}$	0.4	-0.201	1.002	0.011	-0.027	0.008	-0.030

Table 4.2: $C_1(\mu),\ldots,C_6(\mu)$ Wilson coefficients for the $\Delta B=1$ Effective Hamiltonian at $\mu=m_b=4.8$ GeV: LO and NLO results with QCD and QCD+QED corrections.

Λ_4	C_7	C_8	C_9	C_{10}
0.15	$-5.48 \cdot 10^{-5}$	$1.40 \cdot 10^{-4}$	$-9.45 \cdot 10^{-3}$	$1.69 \cdot 10^{-3}$
0.20	$-4.47 \cdot 10^{-5}$	$1.53 \cdot 10^{-4}$	$-9.59 \cdot 10^{-3}$	$1.81 \cdot 10^{-3}$
0.25	$-3.97 \cdot 10^{-5}$	$1.64 \cdot 10^{-4}$	$-9.64 \cdot 10^{-3}$	$1.90 \cdot 10^{-3}$
0.30	$-3.34 \cdot 10^{-5}$	$1.74 \cdot 10^{-4}$	$-9.68 \cdot 10^{-3}$	$2.00 \cdot 10^{-3}$
0.35	$-2.74 \cdot 10^{-5}$	$1.84 \cdot 10^{-4}$	$-9.72 \cdot 10^{-3}$	$2.10 \cdot 10^{-3}$
0.40	$-2.19 \cdot 10^{-5}$	$1.94 \cdot 10^{-4}$	$-9.75 \cdot 10^{-3}$	$2.18 \cdot 10^{-3}$

Table 4.3: $C_7(\mu), \ldots, C_{10}(\mu)$ Wilson coefficients for the $\Delta B = 1$ Effective Hamiltonian at $\mu = m_b = 4.8$ GeV: NLO results with QCD+QED corrections.

$\Delta B = 1$ Hamiltonian is quite simple, because the evolution goes only from $\mu = M_W$ to $\mu = m_b$ without crossing any mass threshold. No product of different evolution matrices is present and the perturbative theory is consistent as it is.

We give our numerical results in Tables (4.1),(4.2) and (4.3) for the "barred" and "unbarred" cases respectively. In order to have a direct comparison with the result given in ref. [15], we have used: $M_W = 81$ GeV, $m_t = 150$ GeV and $m_b = 4.8$ GeV. Indeed, there is no reason to vary m_t, because the result is very weakly dependent on it. The impact of NLO corrections either in the presence of QED corrections or not is more relevant for the penguin sector than for the vertex-operator sector. This has important consequences in the study of the asymmetries of the B-system, as explained in section 1.1. Among the $\Delta B = 1$ weak non-leptonic decays, the penguin-type decays are enhanced and this will be a very interesting field to be investigated.

4.2 $\Delta S = 1$ Effective Hamiltonian beyond the Leading Order

The $\mathcal{H}_{eff}^{(0)t}$ part of the Effective Hamiltonian generates penguin operators below the M_W threshold and evolve as in the $\Delta B = 1$ case till $\mu = m_b$. Then the evolution of the present operators is performed as in the first region (from M_W to m_b), but in different Effective Theories: with $N_f = 4$ from $\mu = m_b$ to $\mu = m_c$ and with $N_f = 3$ for $\mu < m_c$. On the other hand, the $\mathcal{H}_{eff}^{(0)c}$ part of the Effective Hamiltonian does not generate new operators till the charm threshold. Below m_c again the GIM mechanism of the $N_f = 4$ Effective Theory fails and penguin operators are generated. The detailed initial conditions and operator mixing are discussed in sections 2.2.2 and 2.2.3. It is better to distinguish the evolution of $\mathcal{H}_{eff}^{(0)t}$ and $\mathcal{H}_{eff}^{(0)c}$, introducing two different sets of Wilson coefficients, z_i and

v_i, defined as follows:

$$\begin{aligned}(O_2^{(0)u} - O_2^{(0)c}) &\longrightarrow \vec{z}(\mu)\vec{O}^T(\mu) = \sum_i z_i(\mu)O_i(\mu) \\ (O_2^{(0)u} - O_2^{(0)t}) &\longrightarrow \vec{v}(\mu)\vec{O}^T(\mu) = \sum_i v_i(\mu)O_i(\mu)\end{aligned} \tag{4.12}$$

with $\vec{z}(\mu)$ and $\vec{v}(\mu)$ given by:

$$\vec{z}(\mu) = \hat{\mathbb{E}}_3(\mu, m_c)\vec{C}(m_c) \tag{4.13}$$

$$\vec{v}(\mu) = \hat{\mathbb{E}}_3(\mu, m_c)\hat{\mathbb{E}}_4(m_c, m_b)\hat{\mathbb{E}}_5(m_b, M_W)\vec{C}(M_W) \tag{4.14}$$

$$\tag{4.15}$$

$\vec{C}(M_W)$ and $\vec{C}(m_c)$ are given in (2.100) and (2.111) respectively. $\hat{\mathbb{E}}_3(\mu, m_c)$, $\hat{\mathbb{E}}_4(m_c, m_b)$ and $\hat{\mathbb{E}}_5(m_b, M_W)$ are the flavour-dependent evolution matrices. In the product of different evolution matrices many terms of higher order in α_s and α_e are generated. In principle we could also consider them as negligible higher order contributions, always present in a truncated perturbative expansion. On the other hand, the optimization of the numerical program require their elimination and our program account for that.

We maintain here the same notation of ref. [15] in order to make the numerical comparison as easier as possible. Thus we will rewrite the Effective Hamiltonian in the following form:

$$\mathcal{H}_{eff}^{\Delta S=1} = \frac{G_F}{\sqrt{2}}\lambda_u \sum_i [z_i(\mu) + \tau y_i(\mu)] \tag{4.16}$$

where the $\{y_i(\mu)\}$ are only a linear combination of the previous coefficient, i.e.:

$$y_i(\mu) = v_i(\mu) - z_i(\mu) \tag{4.17}$$

We observe that, since the evolution for $\vec{z}(\mu)$ and $\vec{v}(\mu)$ is governed by the same matrix, $\hat{\mathbb{E}}_3(\mu, m_c)$, for $\mu < m_c$ the first two components of the $\vec{y}(\mu)$ will be always zero.

The value of the $\Delta S = 1$ Wilson coefficients, a part from the Λ_{QCD}^f, strongly depends on μ and m_t. In this section we will analyze the μ-dependence of the NLO Wilson coefficients, both in the case of QCD and of QCD+QED corrections. In the next section, on the other hand, for fixed μ we will study the m_t-dependence of the NLO coefficients. This dependence will be evident in the analysis of CP-violation at different values of m_t and it is summarized in Table (4.22) for $\mu = 2.$ GeV

In the present numerical analysis we have used: $M_W = 81$ GeV, $m_t = 150$ GeV and $m_c = 1.35$ GeV. The numerical results are reported in Tables (4.4)-(4.21), where the same logic of section 4.1 is followed. There are two principal sets of Tables: for $\vec{z}(\mu)$ and $\vec{y}(\mu)$coefficient respectively. Then, for each set of coefficients we give, at scales $\mu = 1.$ GeV, $\mu = 0.8$ GeV and $\mu = 0.6$ GeV:

- a Table of barred coefficients, with only LO and NLO QCD results, for comparison with ref. [15];

	Λ_4	$\bar{z}_1$	$\bar{z}_2$	$\bar{z}_3$	$\bar{z}_4$	$\bar{z}_5$	$\bar{z}_6$
l.o.	0.15	-0.521	1.268	0.003	-0.007	0.002	-0.008
$(\text{n.l.})_S$	0.15	-0.581	1.313	0.010	-0.026	0.008	-0.027
l.o.	0.20	-0.584	1.311	0.003	-0.009	0.003	-0.009
$(\text{n.l.})_S$	0.20	-0.675	1.378	0.012	-0.031	0.009	-0.033
l.o.	0.25	-0.647	1.354	0.004	-0.010	0.003	-0.011
$(\text{n.l.})_S$	0.25	-0.778	1.453	0.016	-0.038	0.011	-0.041
l.o.	0.30	-0.711	1.399	0.005	-0.012	0.004	-0.013
$(\text{n.l.})_S$	0.30	-0.897	1.543	0.020	-0.047	0.013	-0.051
l.o.	0.35	-0.777	1.448	0.005	-0.014	0.005	-0.015
$(\text{n.l.})_S$	0.35	-1.042	1.655	0.026	-0.058	0.015	-0.064
l.o.	0.40	-0.849	1.501	0.006	-0.017	0.005	-0.018
$(\text{n.l.})_S$	0.40	-1.224	1.800	0.034	-0.073	0.017	-0.082

Table 4.4: $\bar{z}_1(\mu), \ldots, \bar{z}_6(\mu)$ Wilson coefficients for the $\Delta S = 1$ Effective Hamiltonian at $\mu = 1.0$ GeV, for $m_t = 150$ GeV: LO and NLO results with QCD corrections only.

	Λ_4	z_1	z_2	z_3	z_4	z_5	z_6
l.o.	0.15	-0.521	1.268	0.003	-0.007	0.002	-0.008
$(\text{n.l.})_S$	0.15	-0.360	1.055	0.003	-0.008	0.002	-0.008
$(\text{n.l.})_{S+E}$	0.15	-0.365	1.071	0.003	-0.009	0.002	-0.008
l.o.	0.20	-0.584	1.311	0.003	-0.009	0.003	-0.009
$(\text{n.l.})_S$	0.20	-0.399	1.060	0.004	-0.010	0.003	-0.010
$(\text{n.l.})_{S+E}$	0.20	-0.405	1.076	0.004	-0.011	0.003	-0.010
l.o.	0.25	-0.647	1.354	0.004	-0.010	0.003	-0.011
$(\text{n.l.})_S$	0.25	-0.436	1.064	0.005	-0.013	0.003	-0.012
$(\text{n.l.})_{S+E}$	0.25	-0.443	1.080	0.005	-0.013	0.003	-0.018
l.o.	0.30	-0.711	1.399	0.005	-0.012	0.004	-0.013
$(\text{n.l.})_S$	0.30	-0.473	1.064	0.007	-0.016	0.004	-0.014
$(\text{n.l.})_{S+E}$	0.30	-0.480	1.082	0.007	-0.016	0.004	-0.014
l.o.	0.35	-0.777	1.448	0.005	-0.014	0.005	-0.015
$(\text{n.l.})_S$	0.35	-0.509	1.060	0.009	-0.019	0.004	-0.017
$(\text{n.l.})_{S+E}$	0.35	-0.517	1.079	0.009	-0.019	0.004	-0.017
l.o.	0.40	-0.849	1.501	0.006	-0.017	0.005	-0.018
$(\text{n.l.})_S$	0.40	-0.542	1.048	0.012	-0.024	0.004	-0.021
$(\text{n.l.})_{S+E}$	0.40	-0.552	1.068	0.012	-0.024	0.004	-0.021

Table 4.5: $z_1(\mu),\ldots,z_6(\mu)$ Wilson coefficients for the $\Delta S=1$ Effective Hamiltonian at $\mu=1.0$ GeV, for $m_t=150$ GeV: LO and NLO results with QCD and QCD+QED corrections.

Λ_4	z_7	z_8	z_9	z_{10}
0.15	$0.35 \cdot 10^{-5}$	$0.21 \cdot 10^{-5}$	$0.49 \cdot 10^{-5}$	$-0.20 \cdot 10^{-5}$
0.20	$1.91 \cdot 10^{-5}$	$0.33 \cdot 10^{-5}$	$2.13 \cdot 10^{-5}$	$-0.31 \cdot 10^{-5}$
0.25	$3.64 \cdot 10^{-5}$	$0.49 \cdot 10^{-5}$	$3.96 \cdot 10^{-5}$	$-0.46 \cdot 10^{-5}$
0.30	$5.61 \cdot 10^{-5}$	$0.73 \cdot 10^{-5}$	$6.08 \cdot 10^{-5}$	$-0.67 \cdot 10^{-5}$
0.35	$7.90 \cdot 10^{-5}$	$1.07 \cdot 10^{-5}$	$8.57 \cdot 10^{-5}$	$-0.97 \cdot 10^{-5}$
0.40	$1.05 \cdot 10^{-4}$	$1.57 \cdot 10^{-5}$	$1.15 \cdot 10^{-4}$	$-1.41 \cdot 10^{-5}$

Table 4.6: $z_7(\mu), \ldots, z_{10}(\mu)$ Wilson coefficients for the $\Delta B = 1$ Effective Hamiltonian at $\mu = m_b = 1.0$ GeV: NLO results with QCD+QED corrections.

	Λ_4	$\bar{y}_3$	$\bar{y}_4$	$\bar{y}_5$	$\bar{y}_6$
l.o.	0.15	0.025	-0.045	0.011	-0.071
$(\text{n.l.})_S$	0.15	0.026	-0.042	0.008	-0.073
l.o.	0.20	0.028	-0.050	0.012	-0.083
$(\text{n.l.})_S$	0.20	0.030	-0.047	0.009	-0.089
l.o.	0.25	0.032	-0.054	0.012	-0.094
$(\text{n.l.})_S$	0.25	0.036	-0.052	0.008	-0.107
l.o.	0.30	0.035	-0.058	0.013	-0.107
$(\text{n.l.})_S$	0.30	0.042	-0.057	0.008	-0.130
l.o.	0.35	0.039	-0.062	0.013	-0.121
$(\text{n.l.})_S$	0.35	0.049	-0.062	0.007	-0.161
l.o.	0.40	0.043	-0.066	0.013	-0.137
$(\text{n.l.})_S$	0.40	0.058	-0.068	0.006	-0.202

Table 4.7: $\bar{y}_3(\mu), \ldots, \bar{y}_6(\mu)$ Wilson coefficients for the $\Delta S = 1$ Effective Hamiltonian at $\mu = 1.0$ GeV, for $m_t = 150$ GeV: LO and NLO results with QCD corrections only.

	Λ_4	y_3	y_4	y_5	y_6
l.o.	0.15	0.025	-0.045	0.011	-0.071
$(\text{n.l.})_S$	0.15	0.019	-0.036	0.010	-0.049
$(\text{n.l.})_{S+E}$	0.15	0.020	-0.037	0.010	-0.050
l.o.	0.20	0.028	-0.050	0.012	-0.083
$(\text{n.l.})_S$	0.20	0.021	-0.039	0.011	-0.055
$(\text{n.l.})_{S+E}$	0.20	0.022	-0.041	0.011	-0.057
l.o.	0.25	0.032	-0.054	0.012	-0.094
$(\text{n.l.})_S$	0.25	0.024	-0.042	0.012	-0.062
$(\text{n.l.})_{S+E}$	0.25	0.025	-0.044	0.012	-0.064
l.o.	0.30	0.035	-0.058	0.013	-0.107
$(\text{n.l.})_S$	0.30	0.027	-0.045	0.013	-0.069
$(\text{n.l.})_{S+E}$	0.30	0.028	-0.047	0.013	-0.071
l.o.	0.35	0.039	-0.062	0.013	-0.121
$(\text{n.l.})_S$	0.35	0.030	-0.048	0.014	-0.077
$(\text{n.l.})_{S+E}$	0.35	0.031	-0.049	0.014	-0.079
l.o.	0.40	0.043	-0.066	0.013	-0.137
$(\text{n.l.})_S$	0.40	0.032	-0.050	0.015	-0.086
$(\text{n.l.})_{S+E}$	0.40	0.034	-0.051	0.015	-0.088

Table 4.8: $y_3(\mu),\ldots,y_6(\mu)$ Wilson coefficients for the $\Delta S=1$ Effective Hamiltonian at $\mu=1.0$ GeV, for $m_t=150$ GeV: LO and NLO results with QCD and QCD+QED corrections.

Λ_4	y_7	y_8	y_9	y_{10}
0.15	$-2.52 \cdot 10^{-4}$	$3.40 \cdot 10^{-4}$	-0.011	$3.76 \cdot 10^{-3}$
0.20	$-2.23 \cdot 10^{-4}$	$4.08 \cdot 10^{-4}$	-0.011	$4.25 \cdot 10^{-3}$
0.25	$-1.96 \cdot 10^{-4}$	$4.85 \cdot 10^{-4}$	-0.011	$4.75 \cdot 10^{-3}$
0.30	$-1.70 \cdot 10^{-4}$	$5.77 \cdot 10^{-4}$	-0.012	$5.31 \cdot 10^{-3}$
0.35	$-1.44 \cdot 10^{-4}$	$6.90 \cdot 10^{-4}$	-0.012	$5.93 \cdot 10^{-3}$
0.40	$-1.17 \cdot 10^{-4}$	$8.33 \cdot 10^{-4}$	-0.013	$6.67 \cdot 10^{-3}$

Table 4.9: $y_7(\mu), \ldots, y_{10}(\mu)$ Wilson coefficients for the $\Delta B = 1$ Effective Hamiltonian at $\mu = m_b = 1.0$ GeV: NLO results with QCD+QED corrections.

	Λ_4	$\bar{z}_1$	$\bar{z}_2$	$\bar{z}_3$	$\bar{z}_4$	$\bar{z}_5$	$\bar{z}_6$
l.o.	0.15	-0.588	1.314	0.005	-0.014	0.004	-0.015
$(\text{n.l.})_S$	0.15	-0.678	1.381	0.015	-0.036	0.010	-0.040
l.o.	0.20	-0.669	1.370	0.007	-0.017	0.005	-0.019
$(\text{n.l.})_S$	0.20	-0.814	1.480	0.020	-0.047	0.012	-0.053
l.o.	0.25	-0.752	1.429	0.008	-0.021	0.006	-0.023
$(\text{n.l.})_S$	0.25	-0.980	1.606	0.028	-0.061	0.015	-0.070
l.o.	0.30	-0.840	1.495	0.010	-0.025	0.008	-0.028
$(\text{n.l.})_S$	0.30	-1.198	1.780	0.040	-0.081	0.018	-0.097
l.o.	0.35	-0.937	1.569	0.012	-0.029	0.009	-0.034
$(\text{n.l.})_S$	0.35	-1.504	2.033	0.059	-0.111	0.021	-0.140
l.o.	0.40	-1.047	1.655	0.015	-0.035	0.011	-0.042
$(\text{n.l.})_S$	0.40	-1.966	2.430	0.092	-0.158	0.025	-0.216

Table 4.10: $\bar{z}_1(\mu), ldots, \bar{z}_6(\mu)$ Wilson coefficients for the $\Delta S = 1$ Effective Hamiltonian at $\mu = 0.8$ GeV, for $m_t = 150$ GeV: LO and NLO results with QCD corrections only.

	Λ_4	z_1	z_2	z_3	z_4	z_5	z_6
l.o.	0.15	-0.588	1.314	0.005	-0.014	0.004	-0.015
$(\text{n.l.})_S$	0.15	-0.406	1.068	0.006	-0.015	0.004	-0.014
$(\text{n.l.})_{S+E}$	0.15	-0.413	1.085	0.006	-0.015	0.004	-0.014
l.o.	0.20	-0.669	1.370	0.007	-0.017	0.005	-0.019
$(\text{n.l.})_S$	0.20	-0.455	1.073	0.009	-0.019	0.005	-0.018
$(\text{n.l.})_{S+E}$	0.20	-0.462	1.090	0.009	-0.019	0.005	-0.018
l.o.	0.25	-0.752	1.429	0.008	-0.021	0.006	-0.023
$(\text{n.l.})_S$	0.25	-0.503	1.072	0.012	-0.025	0.006	-0.023
$(\text{n.l.})_{S+E}$	0.25	-0.511	1.091	0.012	-0.025	0.006	-0.023
l.o.	0.30	-0.840	1.495	0.010	-0.025	0.008	-0.028
$(\text{n.l.})_S$	0.30	-0.547	1.061	0.017	-0.032	0.006	-0.029
$(\text{n.l.})_{S+E}$	0.30	-0.557	1.081	0.017	-0.032	0.006	-0.030
l.o.	0.35	-0.937	1.569	0.012	-0.029	0.009	-0.034
$(\text{n.l.})_S$	0.35	-0.580	1.027	0.024	-0.041	0.006	-0.037
$(\text{n.l.})_{S+E}$	0.35	-0.592	1.049	0.024	-0.041	0.006	-0.036
l.o.	0.40	-1.047	1.655	0.015	-0.035	0.011	-0.042
$(\text{n.l.})_S$	0.40	-0.580	0.941	0.036	-0.053	0.005	-0.045
$(\text{n.l.})_{S+E}$	0.40	-0.595	0.966	0.036	-0.053	0.005	-0.045

Table 4.11: $z_1(\mu),\ldots,z_6(\mu)$ Wilson coefficients for the $\Delta S=1$ Effective Hamiltonian at $\mu=0.8$ GeV, for $m_t=150$ GeV: LO and NLO results with QCD and QCD+QED corrections.

Λ_4	z_7	z_8	z_9	z_{10}
0.15	$1.96 \cdot 10^{-5}$	$0.80 \cdot 10^{-5}$	$2.46 \cdot 10^{-5}$	$-0.72 \cdot 10^{-5}$
0.20	$5.24 \cdot 10^{-5}$	$1.32 \cdot 10^{-5}$	$6.07 \cdot 10^{-5}$	$-1.18 \cdot 10^{-5}$
0.25	$9.03 \cdot 10^{-5}$	$2.13 \cdot 10^{-5}$	$1.03 \cdot 10^{-4}$	$-1.85 \cdot 10^{-5}$
0.30	$1.35 \cdot 10^{-4}$	$3.41 \cdot 10^{-5}$	$1.56 \cdot 10^{-4}$	$-2.89 \cdot 10^{-5}$
0.35	$1.87 \cdot 10^{-4}$	$5.47 \cdot 10^{-5}$	$2.20 \cdot 10^{-4}$	$-4.47 \cdot 10^{-5}$
0.40	$2.49 \cdot 10^{-4}$	$8.86 \cdot 10^{-5}$	$2.30 \cdot 10^{-4}$	$-6.49 \cdot 10^{-5}$

Table 4.12: $z_7(\mu), \ldots, z_{10}(\mu)$ Wilson coefficients for the $\Delta B = 1$ Effective Hamiltonian at $\mu = m_b = 0.8$ GeV: NLO results with QCD+QED corrections.

	Λ_4	$\bar{y}_3$	$\bar{y}_4$	$\bar{y}_5$	$\bar{y}_6$
l.o.	0.15	0.027	-0.045	0.010	-0.078
$(\text{n.l.})_S$	0.15	0.028	-0.042	0.008	-0.084
l.o.	0.20	0.031	-0.050	0.011	-0.093
$(\text{n.l.})_S$	0.20	0.034	-0.047	0.007	-0.106
l.o.	0.25	0.035	-0.054	0.011	-0.109
$(\text{n.l.})_S$	0.25	0.041	-0.052	0.007	-0.137
l.o.	0.30	0.039	-0.058	0.011	-0.126
$(\text{n.l.})_S$	0.30	0.050	-0.058	0.005	-0.181
l.o.	0.35	0.044	-0.063	0.011	-0.147
$(\text{n.l.})_S$	0.35	0.060	-0.063	0.003	-0.251
l.o.	0.40	0.049	-0.067	0.011	-0.172
$(\text{n.l.})_S$	0.40	0.074	-0.068	0.001	-0.372

Table 4.13: $\bar{y}_3(\mu), \ldots, \bar{y}_6(\mu)$ Wilson coefficients for the $\Delta S = 1$ Effective Hamiltonian at $\mu = 0.8$ GeV, for $m_t = 150$ GeV: LO and NLO results with QCD corrections only.

	Λ_4	y_3	y_4	y_5	y_6
l.o.	0.15	0.027	-0.045	0.011	-0.078
$(\text{n.l.})_S$	0.15	0.020	-0.036	0.010	-0.053
$(\text{n.l.})_{S+E}$	0.15	0.021	-0.037	0.009	-0.045
l.o.	0.20	0.031	-0.050	0.011	-0.093
$(\text{n.l.})_S$	0.20	0.023	-0.039	0.011	-0.061
$(\text{n.l.})_{S+E}$	0.20	0.024	-0.040	0.011	-0.062
l.o.	0.25	0.035	-0.054	0.011	-0.109
$(\text{n.l.})_S$	0.25	0.026	-0.041	0.012	-0.070
$(\text{n.l.})_{S+E}$	0.25	0.027	-0.042	0.012	-0.071
l.o.	0.30	0.039	-0.058	0.011	-0.126
$(\text{n.l.})_S$	0.30	0.028	-0.043	0.013	-0.079
$(\text{n.l.})_{S+E}$	0.30	0.030	-0.044	0.013	-0.081
l.o.	0.35	0.044	-0.063	0.011	-0.147
$(\text{n.l.})_S$	0.35	0.030	-0.043	0.016	-0.089
$(\text{n.l.})_{S+E}$	0.35	0.032	-0.045	0.016	-0.092
l.o.	0.40	0.049	-0.067	0.011	-0.172
$(\text{n.l.})_S$	0.40	0.030	-0.041	0.022	-0.097
$(\text{n.l.})_{S+E}$	0.40	0.032	-0.043	0.022	-0.100

Table 4.14: $y_3(\mu),\ldots,y_6$ Wilson coefficients for the $\Delta S=1$ Effective Hamiltonian at $\mu = 0.8$ GeV, for $m_t = 150$ GeV: LO and NLO results with QCD and QCD+QED corrections.

Λ_4	y_7	y_8	y_9	y_{10}
0.15	$-2.62 \cdot 10^{-4}$	$4.02 \cdot 10^{-4}$	-0.011	$4.31 \cdot 10^{-3}$
0.20	$-2.35 \cdot 10^{-4}$	$5.02 \cdot 10^{-4}$	-0.012	$4.98 \cdot 10^{-3}$
0.25	$-2.10 \cdot 10^{-4}$	$6.26 \cdot 10^{-4}$	-0.012	$5.75 \cdot 10^{-3}$
0.30	$-1.86 \cdot 10^{-4}$	$7.91 \cdot 10^{-4}$	-0.013	$6.66 \cdot 10^{-3}$
0.35	$-1.61 \cdot 10^{-4}$	$1.02 \cdot 10^{-3}$	-0.014	$7.79 \cdot 10^{-3}$
0.40	$-1.36 \cdot 10^{-4}$	$1.36 \cdot 10^{-3}$	-0.015	$9.25 \cdot 10^{-3}$

Table 4.15: $y_7(\mu), \ldots, y_{10}(\mu)$ Wilson coefficients for the $\Delta B = 1$ Effective Hamiltonian at $\mu = m_b = 0.8$ GeV: NLO results with QCD+QED corrections.

- a Table of unbarred coefficient for vertex and QCD-penguin operators (i.e. the first six entries of each ten dimensional $\vec{z}(\mu)$ and $\vec{y}(\mu)$ vector), with LO and NLO QCD results plus NLO QCD+QED results;

- a Table of unbarred coefficients for EW-penguin operators (i.e. the last four entries of each ten dimensional $\vec{z}(\mu)$ and $\vec{y}(\mu)$ vector), with NLO QCD+QED corrections only.

Our main conclusions are:

- considerable corrections with respect to the LO values are found for z_1, z_2;

- among the QCD-penguin coefficients y_6 receives the greatest enhancement from NLO corrections;

- all the QED-penguins are greatly enhanced;

- at very low scales we find very large corrections which indicate the failure of perturbation theory for $\mu < 0.8$ GeV. Bad news for all the non-perturbative methods (like $1/N$-expansions, etc) which should match the perturbative theory at scales of order $\mu = 0.6$ GeV.

- there is a strong m_t-dependence for the QED penguin coefficients and this will have a great relevance in the CP-violation analysis, as it will be shown in Section 4.3.

	Λ_4	$\bar{z}_1$	$\bar{z}_2$	$\bar{z}_3$	$\bar{z}_4$	$\bar{z}_5$	$\bar{z}_6$
l.o.	0.15	-0.699	1.391	0.010	-0.025	0.008	-0.029
$(\text{n.l.})_S$	0.15	-0.861	1.515	0.027	-0.057	0.014	-0.067
l.o.	0.20	-0.815	1.476	0.013	-0.031	0.009	-0.037
$(\text{n.l.})_S$	0.20	-1.121	1.718	0.042	-0.082	0.018	-0.103
l.o.	0.25	-0.945	1.575	0.017	-0.039	0.011	-0.048
$(\text{n.l.})_S$	0.25	-1.524	2.050	0.070	-0.123	0.022	-0.169
l.o.	0.30	-1.097	1.695	0.022	-0.049	0.014	-0.063
$(\text{n.l.})_S$	0.30	-2.243	2.675	0.129	-0.202	0.026	-0.317
l.o.	0.35	-1.285	1.850	0.030	-0.062	0.017	-0.085
$(\text{n.l.})_S$	0.35	-3.796	4.089	0.278	-0.381	0.026	-0.723
l.o.	0.40	-1.539	2.066	0.041	-0.081	0.021	-0.119
$(\text{n.l.})_S$	0.40	-8.180	8.234	0.749	-0.894	0.006	-2.270

Table 4.16: $\bar{z}_1(\mu),\ldots,\bar{z}_6(\mu)$ Wilson coefficients for the $\Delta S=1$ Effective Hamiltonian at $\mu=0.6$ GeV, for $m_t=150$ GeV: LO and NLO results with QCD corrections only.

	Λ_4	z_1	z_2	z_3	z_4	z_5	z_6
l.o.	0.15	-0.699	1.391	0.010	-0.025	0.008	-0.029
$(\text{n.l.})_S$	0.15	-0.480	1.085	0.012	-0.027	0.007	-0.026
$(\text{n.l.})_{S+E}$	0.15	-0.488	1.104	0.012	-0.02719	0.007	-0.026
l.o.	0.20	-0.815	1.476	0.013	-0.031	0.009	-0.037
$(\text{n.l.})_S$	0.20	-0.545	1.080	0.019	-0.036	0.008	-0.035
$(\text{n.l.})_{S+E}$	0.20	-0.556	1.101	0.019	-0.036	0.008	-0.035
l.o.	0.25	-0.945	1.575	0.017	-0.039	0.011	-0.048
$(\text{n.l.})_S$	0.25	-0.595	1.041	0.030	-0.050	0.008	-0.048
$(\text{n.l.})_{S+E}$	0.25	-0.609	1.065	0.030	-0.050	0.008	-0.048
l.o.	0.30	-1.097	1.695	0.022	-0.049	0.014	-0.063
$(\text{n.l.})_S$	0.30	-0.575	1.896	0.050	-0.069	0.007	-0.063
$(\text{n.l.})_{S+E}$	0.30	-0.593	0.923	0.050	-0.069	0.007	-0.062
l.o.	0.35	-1.285	1.850	0.030	-0.062	0.017	-0.085
$(\text{n.l.})_S$	0.35	-0.256	2.066	0.092	-0.095	0.002	-0.062
$(\text{n.l.})_{S+E}$	0.35	-0.281	0.415	0.091	-0.094	-0.002	-0.061
l.o.	0.40	-1.539	2.066	0.041	-0.081	0.021	-0.119
$(\text{n.l.})_S$	0.40	1.442	-1.675	0.183	-0.112	-0.023	0.093
$(\text{n.l.})_{S+E}$	0.40	1.403	-1.603	0.181	-0.108	-0.024	-0.097

Table 4.17: $z_1(\mu), \ldots, z_6(\mu)$ Wilson coefficients for the $\Delta S = 1$ Effective Hamiltonian at $\mu = 0.6$ GeV, for $m_t = 150$ GeV: LO and NLO results with QCD and QCD+QED corrections.

Λ_4	z_7	z_8	z_9	z_{10}
0.15	$6.53\cdot10^{-5}$	$2.78\cdot10^{-5}$	$8.21\cdot10^{-5}$	$-0.20\cdot10^{-5}$
0.20	$1.35\cdot10^{-4}$	$5.18\cdot10^{-5}$	$1.65\cdot10^{-4}$	$-0.31\cdot10^{-5}$
0.25	$2.20\cdot10^{-4}$	$9.67\cdot10^{-5}$	$2.75\cdot10^{-4}$	$-0.46\cdot10^{-5}$
0.30	$3.22\cdot10^{-4}$	$1.85\cdot10^{-4}$	$4.21\cdot10^{-4}$	$-0.67\cdot10^{-5}$
0.35	$4.36\cdot10^{-4}$	$3.71\cdot10^{-4}$	$6.19\cdot10^{-4}$	$-0.97\cdot10^{-5}$
0.40	0.054	$8.06\cdot10^{-4}$	$8.96\cdot10^{-4}$	$-1.41\cdot10^{-5}$

Table 4.18: $z_7(\mu),\ldots,z_{10}(\mu)$ Wilson coefficients for the $\Delta B=1$ Effective Hamiltonian at $\mu=m_b=0.6$ GeV: NLO results with QCD+QED corrections.

	Λ_4	$\bar{y}_3$	$\bar{y}_4$	$\bar{y}_5$	$\bar{y}_6$
l.o.	0.15	0.030	-0.046	0.009	-0.091
$(\text{n.l.})_S$	0.15	0.032	-0.043	0.006	-0.106
l.o.	0.20	0.035	-0.051	0.009	-0.112
$(\text{n.l.})_S$	0.20	0.041	-0.048	0.005	-0.151
l.o.	0.25	0.040	-0.055	0.009	-0.137
$(\text{n.l.})_S$	0.25	0.052	-0.053	0.002	-0.234
l.o.	0.30	0.046	-0.059	0.008	-0.170
$(\text{n.l.})_S$	0.30	0.067	-0.056	-0.002	-0.412
l.o.	0.35	0.053	-0.063	0.007	-0.214
$(\text{n.l.})_S$	0.35	0.082	-0.042	-0.012	-0.898
l.o.	0.40	0.062	-0.065	0.004	-0.280
$(\text{n.l.})_S$	0.40	0.048	-0.076	-0.035	-2.739

Table 4.19: $\bar{y}_3(\mu), ldots, \bar{y}_6(\mu)$ Wilson coefficients for the $\Delta S=1$ Effective Hamiltonian at $\mu=0.6$ GeV, for $m_t=150$ GeV: LO and NLO results with QCD corrections only.

	Λ_4	y_3	y_4	y_5	y_6
l.o.	0.15	0.030	-0.046	0.009	-0.091
$(\text{n.l.})_S$	0.15	0.021	-0.035	0.010	-0.059
$(\text{n.l.})_{S+E}$	0.15	0.023	-0.036	0.010	-0.061
l.o.	0.20	0.035	-0.051	0.009	-0.112
$(\text{n.l.})_S$	0.20	0.024	-0.037	0.011	-0.071
$(\text{n.l.})_{S+E}$	0.20	0.026	-0.038	0.011	-0.073
l.o.	0.25	0.040	-0.055	0.009	-0.137
$(\text{n.l.})_S$	0.25	0.026	-0.036	0.014	-0.083
$(\text{n.l.})_{S+E}$	0.25	0.028	-0.038	0.015	-0.086
l.o.	0.30	0.046	-0.059	0.008	-0.170
$(\text{n.l.})_S$	0.30	0.023	-0.031	0.024	-0.091
$(\text{n.l.})_{S+E}$	0.30	0.025	-0.033	0.024	-0.095
l.o.	0.35	0.053	-0.063	0.007	-0.214
$(\text{n.l.})_S$	0.35	0.003	-0.014	0.057	-0.060
$(\text{n.l.})_{S+E}$	0.35	0.006	-0.018	0.057	-0.067
l.o.	0.40	0.062	-0.065	0.004	-0.280
$(\text{n.l.})_S$	0.40	-0.090	0.032	0.210	0.239
$(\text{n.l.})_{S+E}$	0.40	-0.084	0.025	0.210	0.223

Table 4.20: $y_3(\mu), \ldots, y_6(\mu)$ Wilson coefficients for the $\Delta S = 1$ Effective Hamiltonian at $\mu = 0.6$ GeV, for $m_t = 150$ GeV: LO and NLO results with QCD and QCD+QED corrections.

Λ_4	y_7	y_8	y_9	y_{10}
0.15	$-2.75 \cdot 10^{-4}$	$5.19 \cdot 10^{-4}$	-0.012	$5.28 \cdot 10^{-3}$
0.20	$-2.49 \cdot 10^{-4}$	$7.06 \cdot 10^{-4}$	-0.013	$6.45 \cdot 10^{-3}$
0.25	$-2.24 \cdot 10^{-4}$	$9.94 \cdot 10^{-4}$	-0.014	$7.99 \cdot 10^{-3}$
0.30	$-1.99 \cdot 10^{-4}$	$1.49 \cdot 10^{-3}$	-0.015	0.010
0.35	$-1.70 \cdot 10^{-4}$	$2.46 \cdot 10^{-3}$	-0.018	0.014
0.40	-0.014	$4.70 \cdot 10^{-3}$	-0.023	0.019

Table 4.21: $y_7(\mu), \ldots, y_{10}(\mu)$ Wilson coefficients for the $\Delta B = 1$ Effective Hamiltonian at $\mu = m_b = 0.6$ GeV: NLO results with QCD+QED corrections.

4.3 NLO analysis of CP-violation in the three generation Standard Model

In ref. [43] we presented a global analysis of CP-violation in the three generation Standard Model, derived from the available theoretical and experimental informations coming from K- and B-physics. We showed that, in spite of the large non-perturbative uncertainties, the space of parameters relevant for the description of CP-violation could be greatly constrained if we used simultaneously the informations coming from:

- $K^0 - \bar{K}^0$ mixing $\longrightarrow$ ϵ parameter;
- $B^0 - \bar{B}^0$ mixing $\longrightarrow$ x_d parameter;
- ϵ'/ϵ ratio.

On one hand we had very precise perturbative determination of the coefficients for the $\Delta F = 2$ sector of the problem, because the NLO Effective Hamiltonian was already known [21, 15]. On the other hand, we used the LLA values for the Wilson coefficients of the $\Delta F = 1$ Effective hamiltonian [41]. We are now in the condition to improve our previous analysis, applying the present NLO results to the determination of ϵ'/ϵ. In this respect, the inclusion of QED corrections is fundamental. The results in [15] could not be used in this case, because comprehensive of the QCD sector only.

In ref. [43], we work in the three generation Standard Model. The theoretical expression of $|\epsilon|_{\xi=0}$ is given by[2]:

$$|\epsilon|_{\xi=0} = C_\epsilon B_K 2A^2\lambda^6\rho \sin\delta \left[F(x_c, x_t) + A^2\lambda^4(1-\rho\cos\delta)F(x_t) - F(x_c)\right] \qquad (4.18)$$

[2]The Inami-Lim function $F(x_i, x_j)$ and $F(x_i)$ are here the NLO evolved expressions. We refer to section 1.3 for a more detailed discussion.

	Λ_4	$m_t = 100$	$m_t = 140$	$m_t = 180$	$m_t = 200$
	0.10	-0.232	-0.232	-0.232	-0.232
C_1	0.20	-0.276	-0.276	-0.276	-0.276
	0.30	-0.315	-0.315	-0.315	-0.315
	0.10	1.032	1.032	1.032	1.032
C_2	0.20	1.037	1.037	1.037	1.037
	0.30	1.041	1.041	1.041	1.041
	0.10	$1.21 \cdot 10^{-2}$	$1.29 \cdot 10^{-2}$	$1.34 \cdot 10^{-2}$	$1.41 \cdot 10^{-2}$
C_3	0.20	$1.53 \cdot 10^{-2}$	$1.62 \cdot 10^{-2}$	$1.70 \cdot 10^{-2}$	$1.75 \cdot 10^{-2}$
	0.30	$1.82 \cdot 10^{-2}$	$1.92 \cdot 10^{-2}$	$2.01 \cdot 10^{-2}$	$2.05 \cdot 10^{-2}$
	0.10	$-2.83 \cdot 10^{-2}$	$-2.90 \cdot 10^{-2}$	$-2.96 \cdot 10^{-2}$	$-2.98 \cdot 10^{-2}$
C_4	0.20	$-3.40 \cdot 10^{-2}$	$-3.49 \cdot 10^{-2}$	$-3.55 \cdot 10^{-2}$	$-3.58 \cdot 10^{-2}$
	0.30	$-3.89 \cdot 10^{-2}$	$-3.99 \cdot 10^{-2}$	$-4.06 \cdot 10^{-2}$	$-4.09 \cdot 10^{-2}$
	0.10	$8.70 \cdot 10^{-3}$	$8.80 \cdot 10^{-3}$	$8.89 \cdot 10^{-3}$	$9.01 \cdot 10^{-3}$
C_5	0.20	$1.02 \cdot 10^{-2}$	$1.04 \cdot 10^{-2}$	$1.05 \cdot 10^{-2}$	$1.06 \cdot 10^{-2}$
	0.30	$1.15 \cdot 10^{-2}$	$1.16 \cdot 10^{-2}$	$1.17 \cdot 10^{-2}$	$1.18 \cdot 10^{-2}$
	0.10	$-3.22 \cdot 10^{-2}$	$-3.32 \cdot 10^{-2}$	$-3.38 \cdot 10^{-2}$	$-3.41 \cdot 10^{-2}$
C_6	0.20	$-3.99 \cdot 10^{-2}$	$-4.11 \cdot 10^{-2}$	$-4.19 \cdot 10^{-2}$	$-4.21 \cdot 10^{-2}$
	0.30	$-4.67 \cdot 10^{-2}$	$-4.82 \cdot 10^{-2}$	$-4.91 \cdot 10^{-2}$	$-4.93 \cdot 10^{-2}$
	0.10	$2.64 \cdot 10^{-4}$	$-2.88 \cdot 10^{-4}$	$5.15 \cdot 10^{-5}$	$2.82 \cdot 10^{-4}$
C_7	0.20	$3.01 \cdot 10^{-4}$	$-2.42 \cdot 10^{-4}$	$9.20 \cdot 10^{-5}$	$3.18 \cdot 10^{-4}$
	0.30	$3.31 \cdot 10^{-4}$	$-2.05 \cdot 10^{-4}$	$1.25 \cdot 10^{-4}$	$3.49 \cdot 10^{-4}$
	0.10	$3.80 \cdot 10^{-4}$	$1.68 \cdot 10^{-4}$	$2.99 \cdot 10^{-4}$	$3.87 \cdot 10^{-4}$
C_8	0.20	$4.89 \cdot 10^{-4}$	$2.19 \cdot 10^{-4}$	$3.85 \cdot 10^{-4}$	$4.98 \cdot 10^{-4}$
	0.30	$5.92 \cdot 10^{-4}$	$2.68 \cdot 10^{-4}$	$4.67 \cdot 10^{-4}$	$6.03 \cdot 10^{-4}$
	0.10	$-5.39 \cdot 10^{-3}$	$-9.26 \cdot 10^{-3}$	$-1.24 \cdot 10^{-2}$	$-1.41 \cdot 10^{-2}$
C_9	0.20	$-5.47 \cdot 10^{-3}$	$-9.47 \cdot 10^{-3}$	$-1.27 \cdot 10^{-2}$	$-1.45 \cdot 10^{-2}$
	0.30	$-5.56 \cdot 10^{-3}$	$-9.66 \cdot 10^{-3}$	$-1.30 \cdot 10^{-2}$	$-1.48 \cdot 10^{-2}$
	0.10	$1.18 \cdot 10^{-3}$	$2.16 \cdot 10^{-3}$	$2.95 \cdot 10^{-3}$	$3.37 \cdot 10^{-3}$
C_{10}	0.20	$1.43 \cdot 10^{-3}$	$2.62 \cdot 10^{-3}$	$3.58 \cdot 10^{-3}$	$4.09 \cdot 10^{-3}$
	0.30	$1.65 \cdot 10^{-3}$	$3.01 \cdot 10^{-3}$	$4.13 \cdot 10^{-3}$	$4.72 \cdot 10^{-3}$

Table 4.22: $c_1(\mu), \ldots, c_{10}(\mu)$ Wilson coefficients for the $\Delta S = 1$ Effective Hamiltonian at $\mu = m_b = 2.0$ GeV: NLO results with QCD+QED corrections, for $\Lambda^4_{QCD} = 0.1$, 0.2 , 0.3 and $m_t = 100$, 140 , 180 , 200 GeV.

where:

$$C_\epsilon = \left[\frac{G_F^2 M_W^2 M_K f_K^2}{12\sqrt{2}\pi^2 \Delta M}\right] \tag{4.19}$$

is given in Table (4.24). When fitted to the experimental value $|\epsilon|^{exp}_{\xi=0} = (2.258 \pm 0.018)\cdot 10^{-3}$, (4.18) fixes the CP-violating angle δ (i.e. the complex phases in the CKM matrix). Depending on the value of the top mass, we can have for large values of m_t ($m_t > 140\text{GeV}$) two distinct solutions for $\cos\delta$, which merge for lower values of m_t (see fig.(4.1)-(4.3)). The present experimental results would suggest a large value of m_t, so that we are left with a definite ambiguity in $\cos\delta$. For both the solutions ($\cos\delta < 0$ and $\cos\delta > 0$) we can derive a value of f_B from the x_d mixing parameter

$$f_B^2 = x_B C_B^{-1} \left[\tau_B A^2 (1+\rho^2 - 2\rho\cos\delta) F(x_t)\right]^{-1} \tag{4.20}$$

where:

$$C_B = \left[\frac{G_F^2 M_W^2 M_B \lambda^6}{6\pi^2}\right] \tag{4.21}$$

and a value of ϵ'/ϵ from (1.37) and (1.38). We rewrite eq.(1.37) in the following form:

$$\epsilon' = \frac{e^{i\pi/4}}{\sqrt{2}} \frac{\omega}{\text{Re}A_0} \left[\omega^{-1}(\text{Im}A_2)' - (1-\Omega_{IB})\,\text{Im}A_0\right] \tag{4.22}$$

The meaning of the different quantities appearing in eq.(4.22) has been explained in section 1.3. The numerical values of all the experimental inputs are given in Table (4.24). We only introduce the new convention:

$$\text{Im}A_2 = (\text{Im}A_2)' + \Omega_{IB}(\omega\,\text{Im}A_0) \tag{4.23}$$

$(\text{Im}A_2)'$ and $\text{Im}A_0$ are quantities construct in terms of the coefficient and the operator matrix elements of the $\Delta F = 1$ Effective Hamiltonian. In particular, in the vacuum insertion approximation, the matrix elements of all the operators $O_1, \ldots, O_{10}$ are given in terms of the three quantities:

$$X = f_\pi (M_K^2 - M_\pi^2) \tag{4.24}$$

$$Y = f_\pi \left(\frac{M_K^2}{m_s(\mu) + m_d(\mu)}\right)^2 \sim 12\,X \left(\frac{0.15\text{GeV}}{m_s(\mu)}\right)^2 \tag{4.25}$$

$$Z = 4\left(\frac{f_K}{f_\pi} - 1\right) Y \tag{4.26}$$

and a set $\{B_i\}$ of B-parameters. We give the values of the B-parameters in Table (4.23). They are part of the non-perturbative inputs in the evaluation of ϵ'/ϵ and are subject to a large uncertainty. We refer to ref. [43] for the discussion of the chosen values for the B-parameters.

B_K	B_B	B^c_{1-2}	$B_{3,4}$	$B_{5,6}$	$B^{(1/2)}_{7-8-9}$	$B^{(3/2)}_{7-8}$	$B^{(3/2)}_9$
0.8 ± 0.2	$1^{(*)}$	$0 \div 0.15^{(*)}$	$1 \div 6^{(*)}$	1.0 ± 0.2	$1^{(*)}$	1.0 ± 0.2	0.8 ± 0.2

Table 4.23: Used values of the B-parameters. Entries with a $^{(*)}$ are educated guesses; the others are taken from lattice QCD calculations.

In terms of X, Y, Z, the operator B-parameters and Wilson coefficients, $(\mathrm{Im}A_2)'$ and $\mathrm{Im}A_0$ are given by:

$$\begin{aligned}\mathrm{Im}A_0 \;=\; & -\frac{G_F}{\sqrt{2}}\mathbb{V}^*_{ts}\mathbb{V}_{td}\left\{-\left(C_6B_6+\frac{1}{3}C_5B_5\right)Z+\left(C_4B_4+\frac{1}{3}C_3B_3\right)X+\right.\\ & C_7B_7^{1/2}\left(\frac{2Y}{3}+\frac{Z}{6}-\frac{X}{2}\right)+C_8B_8^{1/2}\left(2Y+\frac{Z}{2}+\frac{X}{6}\right)-\\ & \left.C_9B_9^{1/2}\frac{X}{3}+\left(\frac{C_1B_1^c}{3}+C_2B_2^c\right)V\right\} \qquad (4.27)\end{aligned}$$

and

$$\begin{aligned}(\mathrm{Im}A_2)' \;=\; & -G_F\mathrm{Im}\lambda_t\left\{C_7B_7^{3/2}\left(\frac{Y}{3}-\frac{X}{2}\right)+\right. \qquad (4.28)\\ & \left.C_8B_8^{3/2}\left(Y-\frac{X}{6}\right)+C_9B_9^{3/2}\frac{2X}{3}\right\}\end{aligned}$$

Good estimates of f_B and ϵ'/ϵ are crucial in selecting one of the possible solutions for $\cos\delta$.

The latest indications from lattice calculations, now confirmed by QCD-sum rules, suggest a large value of f_B (see Table (1.3)). This would select the solution corresponding to $\cos\delta > 0$. A definite proof that CP-violation arises from the CKM matrix with six flavours relies on ϵ'/ϵ. The experimental determination of ϵ'/ϵ is still rather poor (see the values in (1.40)) and we also need improvement on the theoretical side.

We have inserted our new NLO $\Delta F = 1$ Wilson coefficients in (4.22), i.e. in the evaluation of $(\mathrm{Im}A_0)$ and $(\mathrm{Im}A_2)'$ in (4.27) and (4.29). The value of the coefficients for different Λ^I_{QCD} and different m_t are given in Table (4.22). We observe that in eq.(4.22) only nine coefficients are appear, because we have used the relation:

$$O_{10} = -O_3 + O_4 + O_9 \qquad (4.29)$$

which slightly modifies C_3, C_4 and C_9. The results are shown in fig.(4.4)-(4.7) for different values of the top mass ($m_t = 100$, 140, 180 GeV). It is quite interesting to note that our theoretical predictions now coincide with the new experimental determination

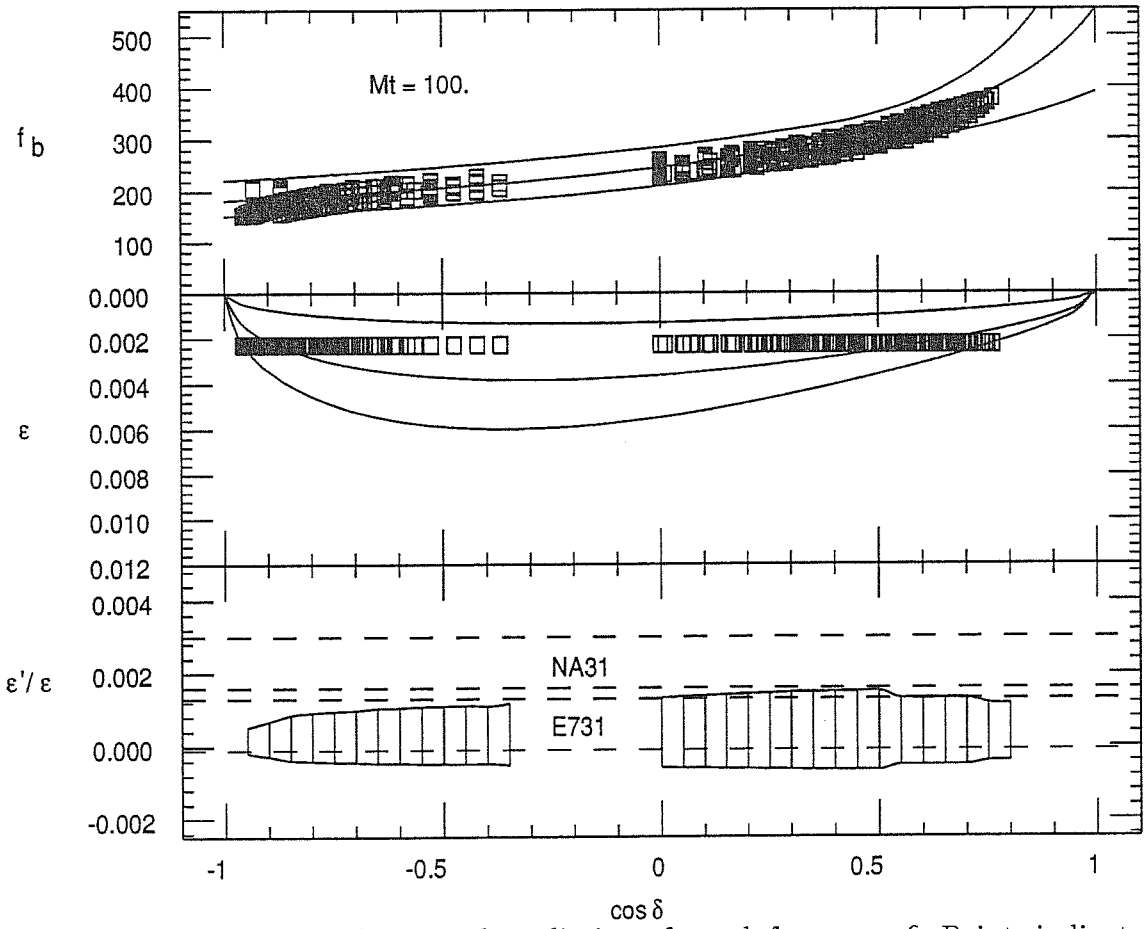

Figure 4.1: $m_t = 100$ GeV: theoretical prediction of ϵ and f_B vs. $\cos\delta$. Points indicate values compatible with both ϵ and x_d, with input parameters within 1-σ from the central value. The allowed regions of ϵ'/ϵ are reported in the lowest section.

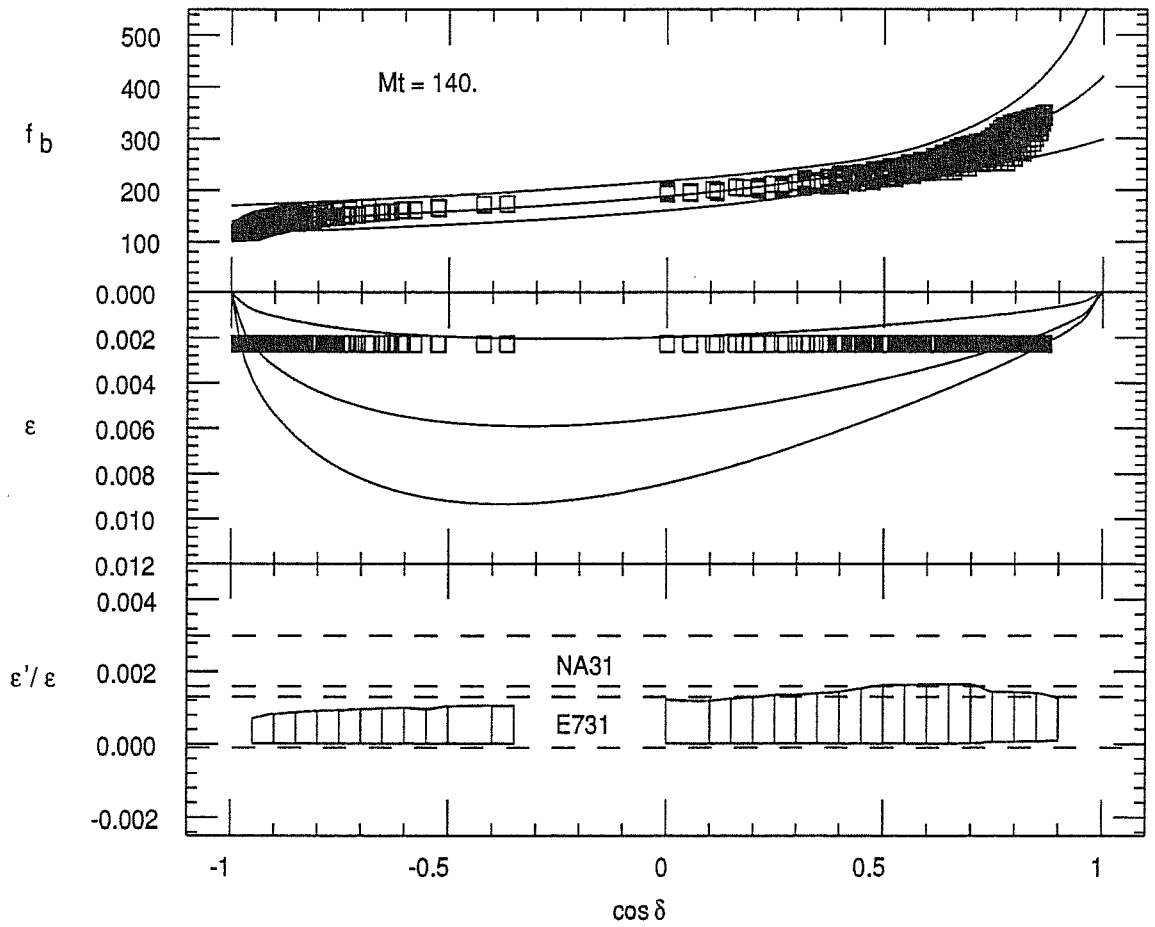

Figure 4.2: $m_t = 140$ GeV: theoretical prediction of ϵ and f_B vs. $\cos\delta$. Points indicate values compatible with both ϵ and x_d, with input parameters within 1-σ from the central value. The allowed regions of ϵ'/ϵ are reported in the lowest section.

of E731. This was not the case of ref. [43], where the LO approximation for the coefficients and the old experimental values for NA31 and E731 (NA31:$(2.7 \pm 0.9)\cdot 10^{-3}$, E731:$(-0.4 \pm 1.4)\cdot 10^{-3}$), were used. The NLO values of the coefficients seem to lower the value of ϵ'/ϵ and to make it more stable.

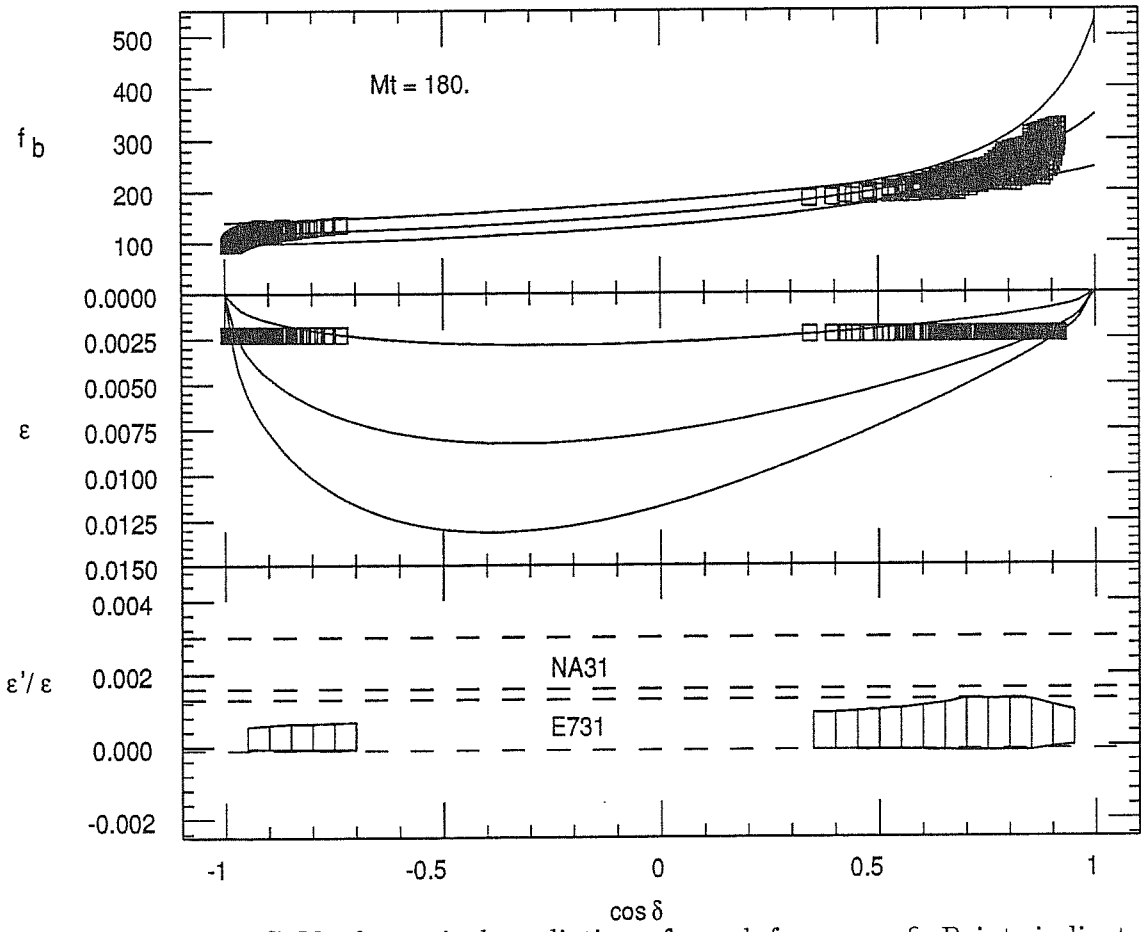

Figure 4.3: $m_t = 180$ GeV: theoretical prediction of ϵ and f_B vs. $\cos\delta$. Points indicate values compatible with both ϵ and x_d, with input parameters within 1-σ from the central value. The allowed regions of ϵ'/ϵ are reported in the lowest section.

parameter	*value*
$\frac{G_F}{\sqrt{2}}$	$1.16634 \cdot 10^{-5}$ GeV^{-2}
Λ_{QCD}	200 ± 100 GeV
m_s	(170 ± 30) MeV
$m_c(2\,\mathrm{GeV})$	1.5 GeV
$m_b(2\,\mathrm{GeV})$	4.5 GeV
$M_W(2\,\mathrm{GeV})$	80.6 GeV
M_π	139.56 MeV
M_K	0.49 GeV
M_B	5.287 GeV
ΔM	$3.521 \cdot 10^{-15}$
f_π	0.132 GeV
f_K	0.160 GeV
$\lambda = \sin\theta_c$	0.221 ± 0.002
τ_B	$(1.18 \pm 0.11) \cdot 10^{-12}$ sec
$\rho = \frac{\mathrm{V}_{ub}}{\lambda \mathrm{V}_{cb}}$	0.50 ± 0.14
x_B	0.67 ± 0.10
ϵ_{exp}	$2.28 \cdot 10^{-3}$
$C_\epsilon = \left(\frac{G_F^2 M_W^2 M_K^2 f_K^2}{6\sqrt{2}\pi^2 \Delta m}\right)$	$4.00 \cdot 10^{-4}$
$C_B = \left(\frac{G_F^2 M_W^2 M_B^2}{6\pi^2}\right)$	$4.15\ 10^{-7}$
$\mathrm{Re}A_0$	$2.7 \cdot 10^{-7}$
$\omega = \frac{\mathrm{Re}A_2}{\mathrm{Re}A_0}$	0.45
Ω_{IB}	0.25 ± 0.1

Table 4.24: Used values of the fixed parameters.

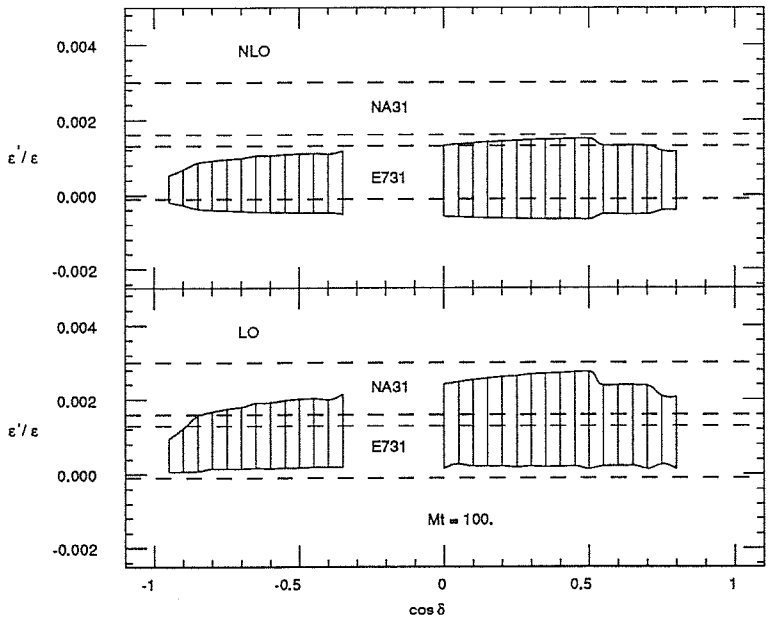

Figure 4.4: $m_t = 100$ GeV: allowed values of ϵ'/ϵ corresponding to the variation of input parameters given in Tables (4.23) and (4.24). 1-σ bands from the most recent experiments are indicated: $\epsilon'/\epsilon = (2.3 \pm 0.7)10^{-3}$(NA31), $\epsilon'/\epsilon = (0.6 \pm 0.7)10^{-3}$ (E731).

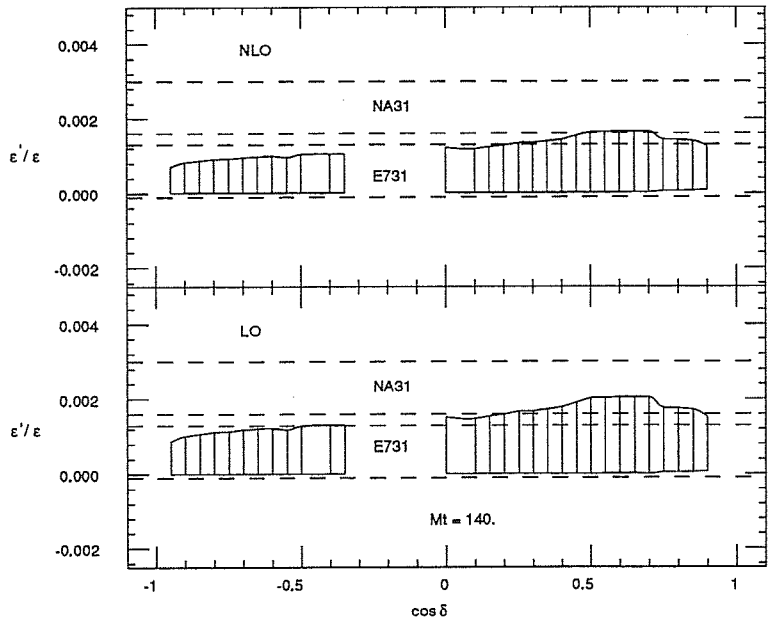

Figure 4.5: $m_t = 140$ GeV: allowed values of ϵ'/ϵ corresponding to the variation of input parameters given in Tables (4.23) and (4.24). 1-σ bands from the most recent experiments are indicated: $\epsilon'/\epsilon = (2.3 \pm 0.7)10^{-3}$(NA31), $\epsilon'/\epsilon = (0.6 \pm 0.7)10^{-3}$ (E731).

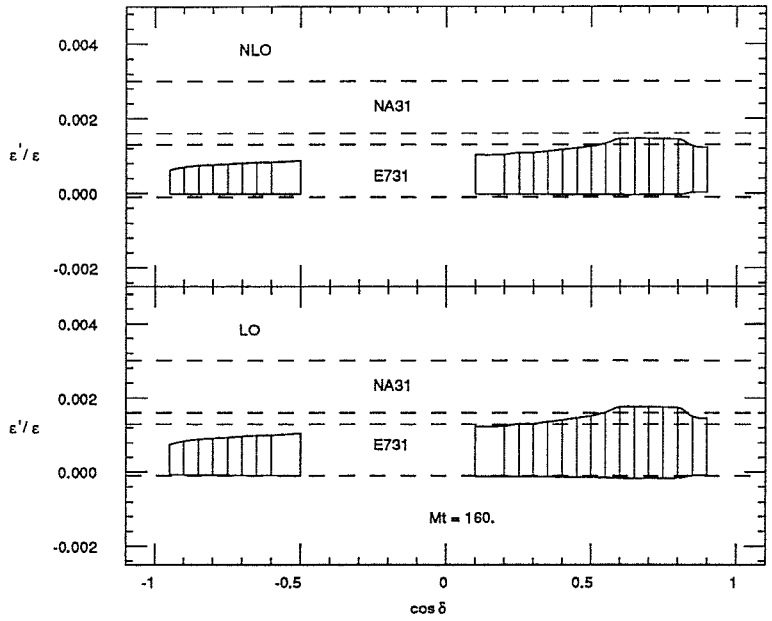

Figure 4.6: $m_t = 160$ GeV: allowed values of ϵ'/ϵ corresponding to the variation of input parameters given in Tables (4.23) and (4.24). 1-σ bands from the most recent experiments are indicated: $\epsilon'/\epsilon = (2.3 \pm 0.7)10^{-3}$(NA31), $\epsilon'/\epsilon = (0.6 \pm 0.7)10^{-3}$ (E731).

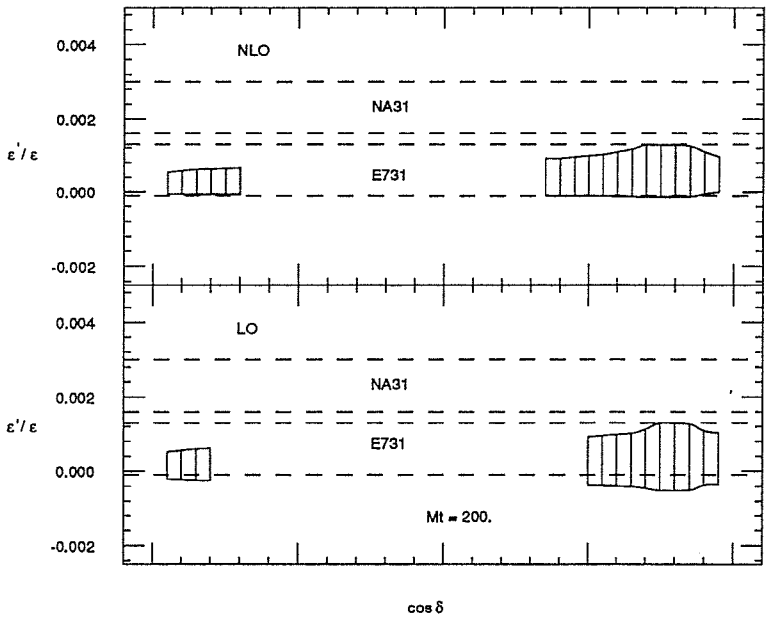

Figure 4.7: $m_t = 200$ GeV: allowed values of ϵ'/ϵ corresponding to the variation of input parameters given in Tables (4.23) and (4.24). 1-σ bands from the most recent experiments are indicated: $\epsilon'/\epsilon = (2.3 \pm 0.7)10^{-3}$(NA31), $\epsilon'/\epsilon = (0.6 \pm 0.7)10^{-3}$ (E731).

Conclusions

The main result of the present work is the calculation of the Effective Hamiltonian for $\Delta S = 1$ and $\Delta B = 1$ processes at NLO in the strong interactions and at LO in the electro-weak ones. This represents a substantial improvement in the theoretical description of K- and B-meson physics. With this calculation, we have now an accurate perturbative evaluation of the coefficient functions of the Effective Hamiltonian. This will be essential when future improvements in the non-perturbative calculation of the hadronic matrix elements of the relevant operators will be available. Moreover, the results presented here have an important phenomenological impact, because we are now in the condition of studying $\Delta S = 1$ and $\Delta B = 1$ physics in terms of a complete NLO Effective Hamiltonian.

Our aims for the near future are ::

- to generalize the present results by including electro-weak corrections to NLO. he essential ingredients for this generalization are already given in this thesis. We believe that the NLO electro-weak terms still to be included will give only a small contribution, but they are necessary for consistency with the perturbative expansion.
- to reproduce the whole calculation in a different regularization scheme, for instance the NDR one.

This concludes the analytical work. Obviously, many extensions "beyond the Standard Model" are easy to be studied beyond the leading logarithmic approximation, using the results of the present work. The big effort made in the understanding of the theoretical aspects of a complete NLO calculation and the techniques developed in the particular case of $\Delta F = 1$ processes in the three generation Standard Model could be applied, with some slight modifications, to many different physical kaon and heavy meson decays.

Nevertheless, we think that a complete and updated phenomenological analysis of the present status of CP-violation and flavour-mixing physics is more urgent. This was the initial aim we started with and we hope that the phenomenological study of the problem can provide new interesting indications for the Standard Model physics.

Acknowledgements

I am extremely grateful to the people with whom I spent my last four years here at S.I.S.S.A.

I would like to express particular thanks to my supervisor G. Martinelli, who suggested to me the subject of my thesis. He introduced me to the many aspects of the problem and I enjoied very much my scientific collaboration with him.

Finally I have a special thank for E. Franco and M. Ciuchini, for their constant collaboration and encouragement.

Bibliography

[1] A. Abada et al. (European Lattice Collaboration): I.N.F.N. Roma preprint 823

[2] L.F. Abbott: Nucl. Phys. **B185** (1981) 189

[3] D.A. Akyeampong, R. Delbourgo Nuovo Cimento **17A** (1973) 578; **18A** (1973) 94;**19A** (1974) 219

[4] G. Altarelli, L. Maiani: Phys. Lett. **52B** (1974) 351

[5] G. Altarelli, G. Curci, G. Martinelli, S. Petrarca Nucl. Phys. **B187** (1981) 461

[6] G. Altarelli Phys. Rep. **81** (1982) 1

[7] E. Bagan, P. Ball, V.M. Braun, H.G. Dosh: HD-THEP-91-36

[8] W.A. Bardeen, A.J. Buras, J.-M. Gérard: Phys. Lett. **211B** (1988) 343

[9] C. Bernard, A. Soni: Proc. of Lattice 89, eds. N. Cabibbo et al., Nucl. Phys. **B** (Proc. Suppl.) **17** (1990) 495

[10] J. Bijnenes, M.B. Wise: Phys. Lett. **137 B** (1984) 245

[11] P. Brietenlohner, D. Maison Commun. Math. Phys. **52** (1977) 11,39,55

[12] F.R. Brown et al., Columbia Collaboration: presented at lattice Workshop in Tallahassee, September 1990

[13] A.J. Buras, P.H. Weisz: Nucl. Phys. **B333** (1990) 66

[14] G. Buchalla, A.J. Buras, M.K. Harlander: Nucl. Phys. **B337** (1990) 313

[15] A.J. Buras, M. Jamin, P.H. Weisz: Nucl. Phys. **B347** (1990) 491

[16] A.J. Buras, M.K. Harlander: MPI-PAE/PTh 1/92, TUM-T31-25/92

[17] S. Capstick, S. Godfrey: Phys. Rev. **D 41** (1990) 2856; P.J. O'Donnell: Univ. of Toronto Report

[18] G. Cella, G. Ricciardi, A. Vicerè: IFUP-TH 40/90

[19] P. Colangelo, G. Nardulli, M. Pietroni: Phys. Rev. **D 43** (1991) 3002

[20] G. Cella, G. Curci, G. Ricciardi, A. Viceré: Phys Lett. **248B** (1990) 181

[21] A. Datta, J. Fröhlich, E.A. Paschos: Z. Phys. C - Particles and Fields **46** (1990) 63-70

[22] R. Decker: Proceedings of the Ringberg Workshop, Nucl. Phys. **B** (Proc. Suppl.) **7A** (1989)

[23] J.F. Donoghue, E. Golowich, B.R. Holstein: Phys. Lett. **119B** (1982) 412

[24] J.M. Flynn, L. Randall: Phys. Lett. **224B** (1989) 221

[25] J.M. Flynn: RAL-89-093 (Sept. 1989)

[26] J.M. Frére, W.A. Kaufman, Y.P. Yao: Phys. Rev. **D36** (1987) 809

[27] M.K. Gaillard, B.W. Lee: Phys. Rev. Lett. **33** (1974) 108

[28] M.B. Gavela et al.: Phys. Lett. **206B** (1988) 113; Nucl. Phys. **B306** (1988) 677

[29] J.-M. Gérard: Proc. XXIV Int. Conf. on High Energy Physics, Munich, 1988, eds. R. Kotthaus and J.H. Kühn, p.840

[30] F.J. Gilman, M. Wise: Phys. Rev. **D27** (1983) 1128

[31] M. Gronau: Phys. Rev. Lett. **63** (1989) 1451, Phys. Lett. **223 B** (1989) 479

[32] R. Grigjanis, P.J. O'Donnell, M. Sutherland, H. Navelet: Phys. Lett. **213B** (1988) 355

[33] B. Grinstein, R. Springer, M.B. Wise: Phys. Lett. **202B** (1988) 138

[34] T. Inami, C.S. Lim: Prog. Theor. Phys. **65** (1981) 297; Erratum **65**, 1772

[35] C. Jarslkog, R.Stora: Phys. Lett. **208B** (1988) 268

[36] W.A. Kaufman, H. Steger, Y.P. Yao: Mod. Phys. Lett. **A**, Vol. 3, No. 15 (1988) 1479

[37] W.A. Kaufman, Y.P.Yao: UM-TH-88-04 (1988)

[38] G.W. Kilcup, S.R. Sharpe, R. Gupta, A. Patel: Phys. Rev. Lett. **64** (1990) 25

[39] J.Kobayashi, M. Maskawa: Prog. Theor. Phys. **49** (1973) 652

[40] P. Krawczyk, D. London, R.D. Peccei, H. Steger: Nucl. Phys. **B307** (1988) 19

[41] M. Lusignoli: Nucl. Phys. **B325** (1989) 33

[42] S. Bellucci, L. Lusignoli, L. Maiani: Nucl. Phys. **B189** (1981) 329

[43] L. Lusignoli, L. Maiani, G. Martinelli, L. Reina: Nucl. Phys. **B369** (1992) 139

[44] *Proceedings of the Int. Symposium on Lepton and Photon Interactions at High Energies*, Hamburg (1977)

[45] M. Neubert: SLAC-PUB-5712 (1991)

[46] V.A. Novikov, M.A. Shifman, A.I. Vainshtein, V.I.Zakharov: Phys. Rev. **16D** (1977) 223

[47] Particle Data Group: Phys. Lett. **239 B** (1990) 1

[48] A. Pich, E. de Rafael: Phys. Lett. **158B** (1985) 477

[49] A. Pich, E. de Rafael: Nucl. Phys. **B358** (1991) 311

[50] A. Pich: Phys. Lett. **206B** (1988) 322

[51] H. David Politzer: Nucl. Phys. **B172** (1980) 349

[52] J. Prades, C.A. Dominguez, J.A. Peñarrocha, A. Pich, E. de Rafael: CERN-TH 6015/91

[53] R. Sommer, C. Alexandrou, F. Jegerlehner, S. Güsken, K. Schilling: CERN-TH 6113/91; Nucl. Phys. **B** (Proc. Suppl.) (1992)

[54] G. t'Hooft, M. Veltman: Nucl. Phys. **B44** (1972) 189

[55] A.J. Vaĭnshteĭn, V.I. Zakharov, M.A. Shifman: Sov. Phys. JEPT **45**(4), Apr.1977

[56] A.J. Vaĭnshteĭn, V.I. Zakharov, V.A. Novikov, M.A. Shifman: Sov. J. Nucl. Phys., vol. **23**, no. 5 (1976) 540

[57] M.I. Vysotskij: Sov. J. Nucl. Phys. **31**(6) (1980),797

[58] M.B. Wise, E. Witten: Phys. Rev. **D20** (5) (1979) 1216

[59] L. Wolfenstein: Phys. Rev. Lett. **13** (1964) 562

[60] L. Wolfenstein: Nuovo Cimento **42** (1966) 17

[61] L. Wolfenstein: Phys. Rev. Lett. **51** (1983) 1945